

Octavian Adrian Postolache
Subhas Chandra Mukhopadhyay
Krishanthi P. Jayasundera
Akshya K. Swain *Editors*

Sensors for Everyday Life

Healthcare Settings

Smart Sensors, Measurement and Instrumentation

Volume 22

Series editor

Subhas Chandra Mukhopadhyay
Department of Engineering, Faculty of Science and Engineering
Macquarie University
Sydney, NSW
Australia
e-mail: S.C.Mukhopadhyay@massey.ac.nz

More information about this series at <http://www.springer.com/series/10617>

Octavian Adrian Postolache
Subhas Chandra Mukhopadhyay
Krishanthi P. Jayasundera
Akshya K. Swain
Editors

Sensors for Everyday Life

Healthcare Settings

Editors

Octavian Adrian Postolache
Instituto de Telecomunicações
Lisbon
Portugal

Krishanthi P. Jayasundera
Institute of Fundamental Sciences
Massey University
Palmerston North
New Zealand

and

ISCTE-IUL
Lisbon
Portugal

Akshya K. Swain
Department of Electrical and Computer
Engineering
University of Auckland
Auckland
New Zealand

Subhas Chandra Mukhopadhyay
Department of Engineering,
Faculty of Science and Engineering
Macquarie University
Sydney, NSW
Australia

ISSN 2194-8402 ISSN 2194-8410 (electronic)
Smart Sensors, Measurement and Instrumentation
ISBN 978-3-319-47318-5 ISBN 978-3-319-47319-2 (eBook)
DOI 10.1007/978-3-319-47319-2

Library of Congress Control Number: 2016953322

© Springer International Publishing AG 2017

This work is subject to copyright. All rights are reserved by the Publisher, whether the whole or part of the material is concerned, specifically the rights of translation, reprinting, reuse of illustrations, recitation, broadcasting, reproduction on microfilms or in any other physical way, and transmission or information storage and retrieval, electronic adaptation, computer software, or by similar or dissimilar methodology now known or hereafter developed.

The use of general descriptive names, registered names, trademarks, service marks, etc. in this publication does not imply, even in the absence of a specific statement, that such names are exempt from the relevant protective laws and regulations and therefore free for general use.

The publisher, the authors and the editors are safe to assume that the advice and information in this book are believed to be true and accurate at the date of publication. Neither the publisher nor the authors or the editors give a warranty, express or implied, with respect to the material contained herein or for any errors or omissions that may have been made.

Printed on acid-free paper

This Springer imprint is published by Springer Nature
The registered company is Springer International Publishing AG
The registered company address is: Gewerbestrasse 11, 6330 Cham, Switzerland

Preface

Sensors play a pivotal role in our everyday life. They gather data on environment, and information on weather, traffic congestion, air pollution, water pollution etc. is obtained; they gather data on human body, and information on health, treatment or therapy outcomes is obtained; they gather data on objects, and information for monitoring and control of these objects is obtained; they gather data on subjects or objects functions, and information for better decisions, control and action is obtained. For instance, the weather information is used to choose adequate clothes, the battery level sensor permits smartphone power management optimization, and the level of blood glucose allows better healthcare management. Data collected through sensors enhance our lives and our connections to each other and with our environment, allow real-time monitoring of many phenomenon around us, provide information about quality of products and services, improve the equipment control based on sensorized interfaces and contribute to increase knowledge on physical and chemical world.

The advances in electronics, embedded controller, technology for communication as well as the progress towards a better informed, knowledge-based society increase the demand for small size, affordable sensors that allow accurate and reliable data recording, processing, storing and communication. The work contains invited chapters from renowned experts, working in sensors' field, and it is split into two books that present several technologies and applications of sensors in *Environmental and Food Engineering* (ISBN 978-3-319-47322-2) and for *Healthcare Settings* (ISBN 978-3-319-47319-2).

In book *Sensors for Everyday Life—Healthcare Settings*, several sensors and their applications for healthcare setting are described.

It is approximately four centuries since human beings are developing sensors for healthcare purposes. The first instrument for sensing human health evolved from the thermoscope constructed by Galileo Galilei in 1593, to the clinical mercury thermometer developed by the Dutch Christiaan Huygens in 1665, with centigrade scale defined by the Swedish Anders Celsius in 1742 and the French Jean-Pierre Christin in 1743. In the last decades with rapid advances in materials, design, modelling and engineering, many sensors were developed for clinical diagnosis or

health monitoring as well as for improving treatments or therapy interventions. Sensors were developed to detect and quantify structures and functions of human body as well as to gather information from environment in order to optimize the efficiency, cost-effectiveness and quality of healthcare services as well as to improve people health and quality of life. This book aims promoting the exchange of ideas and the discussion on current trends in technologies and concepts that help developing and integration in health monitoring or healthcare services of new sensors with one or more of these characteristics: contribute to relevant, reliable and accurate measurements; have low cost; small size; are affordable; support large-scale implementation of devices based on these sensors. Utilization of these sensors may improve public health, healthcare services and reduce medical expenditure. These sensors will expand personal data collected to include blood, saliva and bone composition, heart and respiratory functions, body temperature and activity monitoring as well as may contribute for real-time and/or remotely diagnosis of human health changes and more efficient therapies or devices for assisted living.

How this Book is Organized

In Chapter “[FPGA Based Smart System for Non Invasive Blood Glucose Sensing Using Photoplethysmography and Online Correction of Motion Artifact](#)” a low cost, portable system for continuous blood glucose sensing is described. Photoplethysmography and artificial neural network are the main characteristics of the proposed system for non-invasive estimation of blood glucose concentration. Neural network-based adaptive noise cancellation (adaline) is used to reduce the errors related to motion artefacts. Also, a predictive model based on artificial neural network, which estimates the glucose levels using the information gathered by photoplethysmography sensors is presented. This predictive model was implemented on field-programmable gate array (FPGA).

A system for osteoporosis diagnosis based on planar interdigital sensors is proposed in Chapter “[Sensing System for Bone Health Monitoring](#)”. Planar interdigital sensors are made of comb-like or finger-like periodic pattern of parallel electrodes on a solid phase substrate. By applying an electric field through the test sample via excitation electrode, the signal received by the sensing electrode might carry useful information about the properties of skeletal bones such as impedance, density and chemical material. This system has several advantages comparing traditional osteoporosis diagnosis devices: low cost; no technical expertise is required; may be used in home healthcare setting.

In Chapter “[Cavitas Sensors \(Soft Contact Lens Type Biosensor, Mouth-Guard Type Sensor, etc.\) for Daily Medicine](#)”, an update of various *cavitas* sensors—their techniques, advantages, challenges and future trends—is provided. *Cavitas* is defined as a new category of detachable medical sensors, different than implantable or wearable. While the implantable devices are applied and detached via the

medical surgery, the wearable are applied and easily detached by subjects. The *cavitas* devices are those applied by health professionals or subject under investigations into body cavities (i.e. mouth) and are easily detachable. The chapter describes several *cavitas* devices that gather biophysical information on tear, saliva, body gas, etc. The main focus of the chapter is on *cavitas* sensors developed by the authors for saliva characterization (i.e. pH, salivary uric acid and non-invasive monitoring of saliva glucose).

In Chapter “[Development of Novel Image Sensor for Root Canal Observation](#)” a low-cost sensor for dental root canal observation, mainly fractures near the apex collateral of the root canal, is proposed. The system includes an ‘external-irradiation system’ and an ‘internal-irradiation system’. The external-irradiation probe is composed of an image fibre with a diameter of micrometres and a gradient index lens (GRIN lens) with the same diameter as the image fibre. The internal-irradiation probe is composed of an image fibre, GRIN lens and five optical fibres for illumination.

Continuing with mouth theme, a low-cost speech recognition system is presented in Chapter “[Frame-by-Frame Speech Signal Processing and Recognition for FPGA Devices](#)” based on the developed algorithms by the authors of the chapter for speech recognition decoder (voice activity detection) and for field-programmable gate array as a hardware processor. The system was tested on a FPGA emulator.

Low cost, small size sensors for vital signs detection and monitoring are described in Chapters “[Elderly Infrared Body Temperature Telemonitoring System with XBEE Wireless Protocol](#)” and “[Heart Sound Sensing Through MEMS Microphone](#)”. A real-time non-contact infrared body temperature telemonitoring system with XBee wireless protocol is described in Chapter “[Elderly Infrared Body Temperature Telemonitoring System with XBEE Wireless Protocol](#)”. The authors describe this low-cost system as an instrument for early detection of the elderly patients illness outside the hospital. In Chapter “[Heart Sound Sensing Through MEMS Microphone](#)”, a heart sound is detected by new MEMS microphone. The digital MEMS have been interfaced with microcontroller using I2S protocol. The authors proposed the characterization of heart pathologies as mitral regurgitation, mitral stenosis, aortic regurgitation and aortic stenosis by the spectral analysis of the heart sounds signal (i.e. analysis using fast Fourier Transform).

Contributions to the development of flexible sensors for activity monitoring and as human-machine interface are described in Chapters “[Flexible Printed Sensors for Ubiquitous Human Monitoring](#)”, “[Smart Textiles for Smart Home Control and Enriching Future Wireless Sensor Network Data](#)” and “[Smart Clothes for Rehabilitation Context: Technical and Technological Issues](#)”. A flexible sensors for limbs motion monitoring is described in Chapter “[Flexible Printed Sensors for Ubiquitous Human Monitoring](#)”. Multi-walled carbon nanotubes (MWCNT) were chosen as the conducting material for the electrodes included in a planar interdigital sensor. MWCNT are mixed with organic polymer polydimethylsiloxane (PDMS) to form a nanocomposite layer. The organic polymer was cast over a poly (methyl methacrylate) (PMMA) template to form the substrate. The nanocomposite layer

was patterned with CO₂ laser ablation to form interdigitated electrodes. Tensile and compressive stresses were tested on the sensor patches.

Smart textiles as human–computer interface are presented in Chapter “[Smart Textiles for Smart Home Control and Enriching Future Wireless Sensor Network Data](#)”. Examples of smart textile for smart home, commercial spaces, automobile vehicles, personal or business-owned clothing, and toys are provided. A description of a system developed by the authors of the chapter that used electronic textile as human–computer interface is provided. The proposed system for smart home aims to control a lighting home system by a voice control of a wireless sensor network. Technical and technological issues, related to safety and privacy of data in this system, are discussed in this chapter. The machine learning algorithms are proposed to protect data and maintain the wireless sensors network efficiency in communicating data with minimal energy losses.

A review on technical and technological issues-related smart clothing for rehabilitation context is presented in Chapter “[Smart Clothes for Rehabilitation Context: Technical and Technological Issues](#)”. Information on conductive textile, type of textile/fabric manufacturing, sensors based on textile, textile as antenna, textile as actuator, textile as computer interface, circuit board into textile are presented and described in this chapter. As an important challenge described by engineers on smart clothing is related to management of power supply, the authors described the relevant progress in this domain, particularly on energy harvesting by using electronic textile. Connectivity, integration of things in smart clothing, wearability, maintainability as well as issues related to design for durability and affordability of smart clothes were also discussed.

Chapter “[Wireless Sensing Systems for Body Area Networks](#)” reviews the sensing mechanisms, data detection and interpretation methods and several body area networks (BAN) applications for health monitoring, human–machine interaction and motion capturing. Two data detection and interpretation techniques for radio frequency (RF)-based sensing structures are also introduced. RF structures operating at high frequencies fabricated with flexible or textile materials have gained increasing attention in recent years. Due to the flexibility of these RF structures to conform to human body for comfortable fit, they are well-suited for BAN applications. In addition, the characteristics of these RF structures can naturally or technically be made to react to bodily phenomena such as temperature and humidity and function as sensors.

Concept and implementation of an indoor *passive* tracking system that use an array of Wi-fi transceivers and without any electronic device or tag attached to the object being tracked are presented in Chapter “[Radio Frequency Sensing for Assistive Monitoring](#)”. The sensing of an object or a person described in this chapter is made possible by exploiting the fundamental characteristic of signal attenuation due to blocking, shadowing, etc. that is prevalent in a typical wireless communication system. The feasibility in exploiting Wi-fi signal as a proximity sensor was tested. This affordable system may be a solution to the concerns-related privacy when camera is used for monitoring activity of patients in healthcare settings.

A FPGA-based implementations of a Advanced Encryption Standard (AES) and Secure Hash Algorithm-3 (SHA-3) security algorithms that allow both data integrity and data confidentiality to be provided for high-speed Internet of Things (IoT) applications are presented in Chapter “[Efficient and High-Speed FPGA Bump in the Wire Implementation for Data Integrity and Confidentiality Services in the IoT](#)”. The system enables low-cost Bump In the Wire (BITW) technology to be provided for Internet Protocol Security (IPSec) provision for all IoT applications. Using BITW technology, security mechanisms can be implemented outboard in a physically separate device so that the system that receives the protection does not need to be modified at all.

Summarizing, affordable, small size, reliable and accurate sensors, body area sensors networks, internet of things, internet of clothes have contributing to the implementation of user-centred and preventive overall lifestyle health management, high-quality preventive, predictive, personalized and participative healthcare.

Who Is It For?

This book is written for researchers and graduate students that work in the field of healthcare technologies, university professors and also for industry professionals involved in development of systems for human body structures, functions and activities monitoring, health monitoring, and healthcare services.

We would like to express our appreciation to our distinguished authors of the chapters whose expertise and professionalism have certainly contributed significantly to this book.

We are very happy to be able to offer the readers such diverse sensors technologies and applications. We hope that this book can shed light on various technological aspects-related sensors for healthcare context and stimulate further research in this field.

Lisbon, Portugal
Sydney, NSW, Australia
Palmerston North, New Zealand
Auckland, New Zealand

Octavian Adrian Postolache
Subhas Chandra Mukhopadhyay
Krishanthi P. Jayasundera
Akshya K. Swain

About the Editors



Dr. Octavian Adrian Postolache (M'99, SM'2006)

graduated in Electrical Engineering at the Gh. Asachi Technical University of Iași, Romania, in 1992, and he received the Ph.D. degree in 1999 from the same university, and university habilitation in 2016 from Instituto Superior Tecnico, Universidade de Lisboa, Portugal. In 2000, he became principal researcher of Instituto de Telecomunicações where he is now senior researcher. Since 2012, he joined Instituto Universitario de Lisboa/ISCTE-IUL Lisbon where he is currently Aux. Professor.

His fields of interests are smart sensors for biomedical and environmental applications, pervasive sensing and computing, wireless sensor networks, signal processing with application in biomedical and telecommunications, non-destructive testing and diagnosis based on eddy currents smart sensors, computational intelligence with application in automated measurement systems.

He is active member of national and international research teams involved in Portuguese and EU and International projects. He was principal researcher of different projects including EHR-Physio regarding the implementation of Electronic Health Records for Physiotherapy, and he is currently principal researcher of TailorPhy project Smart Sensors and Tailored Environments for Physiotherapy.

Dr. Postolache is author and co-author of 9 patents, 4 books, 16 book chapters, 66 papers in international journals with peer review and more than 220 papers in proceedings of international conferences.

He is IEEE senior member I&M Society, distinguished lecturer of IEEE IMS, chair of IEEE I&MSTC-13 Wireless and Telecommunications in Measurements, member of IEEE I&MSTC-17, IEEE I&MSTC-18, IEEE I&MSTC-25, IEEE EMBS Portugal Chapter and chair of IEEE IMS Portugal Chapter. He is associate editor of IEEE Sensors Journal and IEEE Transaction on Instrumentation and Measurements, and he was general chair of IEEE MeMeA 2014 and TPC chair of ICST 2014, Liverpool and ICST 2015 in Auckland. He received IEEE best

reviewer and the best associate editor in 2011 and 2013 and other awards related to his research activity in the field of smart sensing.



Dr. Subhas Chandra Mukhopadhyay (M'97, SM'02, F'11) graduated from the Department of Electrical Engineering, Jadavpur University, Kolkata, India with a **Gold medal** and received the master of Electrical Engineering degree from Indian Institute of Science, Bangalore, India. He has Ph.D. (Eng.) degree from Jadavpur University, India and doctor of Engineering degree from Kanazawa University, Japan.

Currently, he is working as a professor of Mechanical/Electronics Engineering and discipline leader of the Mechatronics Degree Programme of the Department of Engineering, Macquarie University, Sydney, Australia. He has over 26 years of teaching and research experiences.

His fields of interest include smart sensors and sensing technology, wireless sensor networks, Internet of Things, electromagnetics, control engineering, magnetic bearing, fault current limiter, electrical machines and numerical field calculation.

He has authored/co-authored over **400** papers in different international journals, conferences and book chapter. He has edited **thirteen** conference proceedings. He has also edited **fifteen** special issues of international journals as lead guest editor and **twenty-five** books with Springer-Verlag.

He was awarded numerous awards throughout his career and attracted over NZ \$4.2 M on different research projects.

He has delivered **272** seminars including keynote, tutorial, invited and special seminars.

He is a **Fellow** of IEEE (USA), a **Fellow** of IET (UK) and a Fellow of IETE (India). He is a topical editor of IEEE Sensors Journal and an associate editor IEEE Transactions on Instrumentation. He has organized many international conferences either as general chair or technical programme chair. He is the ex-**chair** of the IEEE Instrumentation and Measurement Society New Zealand Chapter. He chairs the IEEE IMS Technical Committee 18 on Environmental Measurements.



Dr. Krishanthi P. Jayasundera graduated from University of Peradeniya, Sri Lanka with honours degree in chemistry. She obtained her both master and Ph.D. in organic chemistry from Kanazawa University, Japan. She worked as postdoctoral researcher at Massey University nearly 14 years in New Zealand involving various projects focused on the chemical synthesis of architecturally interesting molecules which have biological, environmental and/or medicinal significance. Currently, she is an independent research consultant. She specializes in organic chemistry, bio-sciences, sensitivity analysis using NMR, HPLC,

SPR and so on. She has published over 30 papers in different international journals and conference proceedings.



Akshya K. Swain received the B.Sc. degree in electrical engineering and the M.Sc. degree in electronic systems and communication from Sambalpur University, Sambalpur, India, in 1985 and 1988, respectively, and the Ph.D. degree from the Department of Automatic Control and Systems Engineering, University of Sheffield, Sheffield, UK, in 1997. From 1994 to 1996, he was a Commonwealth Scholar in UK. Since September 2002, he has been with the Department of Electrical and Computer Engineering, The University of Auckland, Auckland, New Zealand. He has published over 150 papers in International Journals and

conferences. His current research interests include non-linear system identification and control, fault tolerant control, biomedical signal processing, sensor networks and control applications to power system and wireless power transfer system. Dr. Swain is an associate editor of IEEE Sensors Journal and member of the Editorial Board of International Journal of Automation and Control and International Journal of Sensors, Wireless Communications and Control.

Contents

FPGA Based Smart System for Non Invasive Blood Glucose Sensing Using Photoplethysmography and Online Correction of Motion Artifact	1
Swathi Ramasahayam, Lavanya Arora and Shubhajit Roy Chowdhury	
Sensing System for Bone Health Monitoring	23
N. Afsarimanesh, Subhas Chandra Mukhopadhyay, M. Kruger and P. Yu	
Cavitas Sensors (Soft Contact Lens Type Biosensor, Mouth-Guard Type Sensor, etc.) for Daily Medicine	45
Takahiro Arakawa and Kohji Mitsubayashi	
Development of Novel Image Sensor for Root Canal Observation	67
Masataka Fujimoto, Shinji Yoshii, Satoshi Ikezawa, Toshitsugu Ueda and Chiaki Kitamura	
Frame-by-Frame Speech Signal Processing and Recognition for FPGA Devices	87
Masashi Nakayama, Naoki Shigekawa, Takashi Yokouchi and Shunsuke Ishimitsu	
Elderly Infrared Body Temperature Telemonitoring System with XBee Wireless Protocol	103
Tonny Heng Yew Ling and Lim Jin Wong	
Heart Sound Sensing Through MEMS Microphone	121
Madhubabu Anumukonda and Shubhajit Roy Chowdhury	
Flexible Printed Sensors for Ubiquitous Human Monitoring	135
Anindya Nag, Subhas Chandra Mukhopadhyay and Júrgen Kosel	
Smart Textiles for Smart Home Control and Enriching Future Wireless Sensor Network Data	159
Olivia Ojuroye, Russel Torah, Steve Beeby and Adriana Wilde	

Smart Clothes for Rehabilitation Context: Technical and Technological Issues 185
Gabriela Postolache, Hélder Carvalho, André Catarino and Octavian Adrian Postolache

Wireless Sensing Systems for Body Area Networks 221
Xiaoyou Lin, Boon-Chong Seet and Frances Joseph

Radio Frequency Sensing for Assistive Monitoring 241
Yau Hee Kho

Efficient and High Speed FPGA Bump in the Wire Implementation for Data Integrity and Confidentiality Services in the IoT 259
Thomas Newe, Muzaffar Rao, Daniel Toal, Gerard Dooly, Edin Omerdic and Avijit Mathur

Author Index. 287

FPGA Based Smart System for Non Invasive Blood Glucose Sensing Using Photoplethysmography and Online Correction of Motion Artifact

Swathi Ramasahayam, Lavanya Arora
and Shubhajit Roy Chowdhury

Abstract Near infrared spectroscopy has become a promising technology among others for noninvasive monitoring of blood glucose. Low cost hand held easy to use devices are becoming more and more popular for monitoring blood glucose and they are likely to become noninvasive in forthcoming years. The reliability and the calibration of these instruments could still be improved, and there is a need for carrying out more studies for improving the sensitivity of the device under different physiological conditions of metabolism, bodily fluid circulation, and blood components. This chapter deals with the design of noninvasive blood glucose sensing system using photoplethysmography (PPG) based on artificial neural networks. Neural network based adaptive noise cancellation (adaline) is employed to reduce the errors introduced due to motion artifacts. Also artificial neural network is used to create the predictive model which estimates the glucose levels based on PPG signals. Error in estimating glucose levels came out to be 5.48 mg/dl using ANN on MATLAB. This predictive model created by ANN has been implemented on field programmable gate array (FPGA). Error in estimating glucose levels by the ANN model implemented on FPGA, came out to be 7.23 mg/dl. The results have been validated by performing Clarke's error grid analysis.

S. Ramasahayam (✉) · L. Arora
Centre for VLSI and Embedded System Technology, International
Institute of Information Technology Hyderabad, Hyderabad, India
e-mail: swathi.ramasahayam@research.iiit.ac.in

S.R. Chowdhury
School of Computing and Electrical Engineering, Indian Institute
of Technology Mandi, Mandi, India
e-mail: src@iitmandi.ac.in

1 Introduction

Diabetes Mellitus is a metabolic disorder and has become a major health challenge. It is characterized by the high blood glucose levels which depend on the secretion of insulin from the pancreas [1, 2]. Complications due to diabetes can be prevented by regular monitoring of glucose levels in blood plasma. Continuous blood glucose monitoring devices help in tracking the glucose levels of the patient as frequently as every minute [3, 4]. These devices are invasive in nature as they involve pricking the finger for blood sample, which is painful and has risk of spreading infectious diseases.

Several methods have been proposed for measuring the blood glucose levels non-invasively. In [5] the authors attempted to estimate the blood glucose levels based on the variations induced in the shape of the PPG due to changes in blood viscosity and vessel compliance which depends on the glucose levels. In [6] the authors proposed a method which is based on the blood volume changes identified through PPG and estimating the auto regressive model. One of the major techniques being employed for non-invasive measurement of the glucose is based on transmission photoplethysmography (PPG) in the mid infrared (2–2.5 μm) and first overtone regions (1.53–1.82 μm) [5–8] as the fundamental frequencies and first overtones fall under these regions. The absorbance of the glucose bonds(C–H, O–H) is strong in this region but because of the disadvantages like high cost of the components, strong absorption due to water and scattering due to fatty tissue we have used second overtone region (0.8–1.6 μm) for measuring the blood glucose concentration using PPG. The analog front end sensing circuit is implemented on the general purpose printed circuit board whose output is a PPG signal at the near infra-red wavelengths of 1070, 950, 935 nm of sensor (LED) where the glucose has good absorption compared to the other parameters of the blood. In this chapter we have proposed a method to estimate the blood glucose levels non-invasively from PPG along with the neural network prediction model in the processing part to carry out the regression analysis on the sensor data for accurate prediction of the glucose levels.

As the PPG is more susceptible for the motion artefact induced errors, it is necessary that this noise has to be filtered before giving it to the neural network prediction model for estimating glucose levels. Conventional filtering cannot be applied to eliminate these type of noise which has the same bandwidth as the signal. For continuous monitoring adaptive filtering of PPG is necessary [11, 12]. Here we have compared the conventional FIR based adaptive filter and the neural network based adaptive filter at the system level before giving it to neural network prediction model. A neural network model approach is well suited for characterizing the complex system where the glycaemic excursions depend on many factors like sleep pattern, anxiety, and age [9, 10], which makes the modelling of the physiological parameter difficult. A neural network can be trained to identify the complex relationship between the PPG data and the invasive measurements. The Field-Programmable Gate Arrays (FPGA) provides a potential substitute to speed

up hardware implementation [13, 14]. FPGA realization of neural network with large number of neurons is still a challenging task [15, 16].

This chapter focuses on the estimation of blood glucose concentration based on the implementation of neural network prediction model on FPGA using two different methods, FIR and adaline based adaptive filtering

2 Background

The proposed blood glucose sensing system is based on transmission photoplethysmography. Photoplethysmography (PPG) is a simple and low-cost optical technique that can be used to detect blood volume changes in the micro vascular bed of tissue. It is often used non-invasively to make measurements at the skin surface. It uses a clip which contains a light transmitter and a detector on the opposite sides to detect the cardio vascular pulse wave that propagates through the body. The PPG waveform comprises a pulsatile ('AC') physiological waveform attributed to cardiac synchronous changes in the blood volume with each heartbeat, and is superimposed on a slowly varying ('DC') baseline with various lower frequency components attributed to respiration, sympathetic nervous system activity and thermoregulation.

According to Beer-lambert's law the absorbance of light by a liquid is related to the concentration of the material by

$$A = \epsilon C l \quad (1)$$

where ϵ the molar absorptivity of solute at a particular wavelength, C is the concentration of the solute and l is the path length. Hence for a specific wavelength i , Eq. (1) may be written as

$$A_i = \epsilon_i C_i l_i \quad (2)$$

In our particular case, $i = 1$ corresponds to a wavelength of 935 nm, $i = 2$ corresponds to a wavelength of 950 nm and $i = 3$ corresponds to a wavelength of 1070 nm.

3 Methods and Procedures

The block diagram of the glucose sensing system is shown in the Fig. 1. It consists of the finger clip with LED acting as a light sensor and the photodiode as the detector to detect the small changes in the incident light as it passes through the finger.

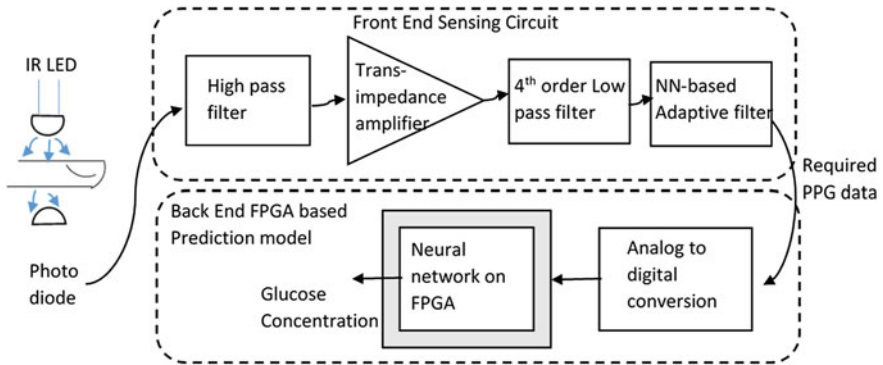


Fig. 1 Block diagram of the FPGA based glucose sensing system

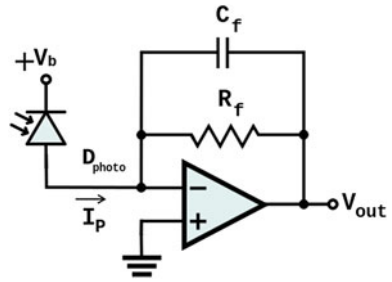
This light is converted into an equivalent current by the detector and is high pass filtered with a cut off frequency of 0.8 Hz as the frequency spectrum (FFT) of PPG signal shows a cardiac peak centered around 1 Hz. Then it is given to the trans-impedance amplifier for amplification of the signal. For this a low noise amplifier LMV796 with an amplification factor of 10 has been used. The input referred noise of the amplifier is less than $17\text{nv}/\sqrt{\text{Hz}}$. After necessary amplification it has to be low pass filtered in order to get PPG wave. Low pass filter with Sallen key topology is used with cut off frequency of 10 Hz. The order of the filter is chosen to be 4th, so that the effect of 50 Hz noise is eliminated from circuit.

3.1 Trans Impedance Amplifier

The first stage of each channel consists of an operational amplifier configured as a transimpedance amplifier to convert the photodiode output current to a voltage. The operational amplifier chosen based on circuit parameters low input bias current, input offset voltage, and noise. Although the signal is later ac-coupled, it is still important to minimize dc errors in this stage to avoid losing dynamic range. The op amp input bias current multiplied by the feedback resistor value appears at the output as an offset voltage. The op amp input offset voltage appears at the output with a gain dependent on the feedback resistor and the photodiode shunt resistance. In addition, any op amp input voltage offset appears across the photodiode, causing the photodiode dark current to increase.

Trans-impedance amplifiers are generally operated at a very high gain. This produces a strong tendency for the amplifier to go into oscillation at high frequencies above the gain bandwidth product. This problem can be eliminated by adding a capacitor in the feedback loop, which lowers the gain at very high frequencies. Figure 2 shows a typical transimpedance amplifier with a single feedback resistor.

Fig. 2 Transimpedance amplifier with photodetector



3.2 High Pass Filter

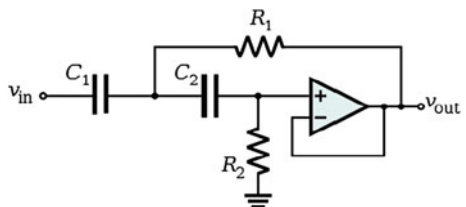
The high pass filter in the circuit diagram is used to remove the DC component in the PPG obtained. Because of the DC component, the PPG is at a value higher than the ground. Our signal of interest is only the AC component which is obtained by passing through high pass filter. In this case, we have assumed that the cutoff frequency should be 0.8 Hz.

We used a passive high pass filter which is constructed by using resistor and capacitor and the output is given to the input of 4th order active low pass filter which is constructed using operational amplifier (LM741).

3.3 Low Pass Filter

The low pass filter is constructed using two operational amplifier and resistors and capacitors. The 4th order low pass filter is constructed by cascading two 2nd order low pass filters. Since we are constructing real time filters, the filter would be having a pass band and a stop band. The stop band would be steeper if the order of the filter is high. The Q factor also decides the smoothness of the filter. We used this low pass filter to basically remove the power line signal (50 Hz) which would otherwise interfere with the PPG and would give us wrong results. We decided that the cut-off frequency for this low pass filter would be 10 Hz. The circuit of the low pass filter is as shown in Fig. 3.

Fig. 3 High pass filter



The formula for cut-off frequency is:

$$f_c = \frac{1}{2\pi RC} \tag{3}$$

After calculations by plugging in $f_c = 10$ Hz and $\pi = 3.14$, I chose $C = 100$ nF and obtained $R = 165$ k.

The Q factor was chosen to be 1 since the response was straighter.

$$Q = \frac{1}{(3 - A)} \tag{4}$$

By plugging in $Q = 1$, we obtain $A = 2$ where A is the gain of the amplifier. The gain of a non-inverting amplifier is:

$$A = 1 + \frac{R_2}{R_3} \tag{5}$$

Since $A = 2$, we obtain $R_2/R_3 = 1$, therefore I chose $R_2 = R_3 = 1$ k (Fig. 4).

The output of the low pass filter is given to an oscilloscope to view a PPG signal which is shown in Fig. 5

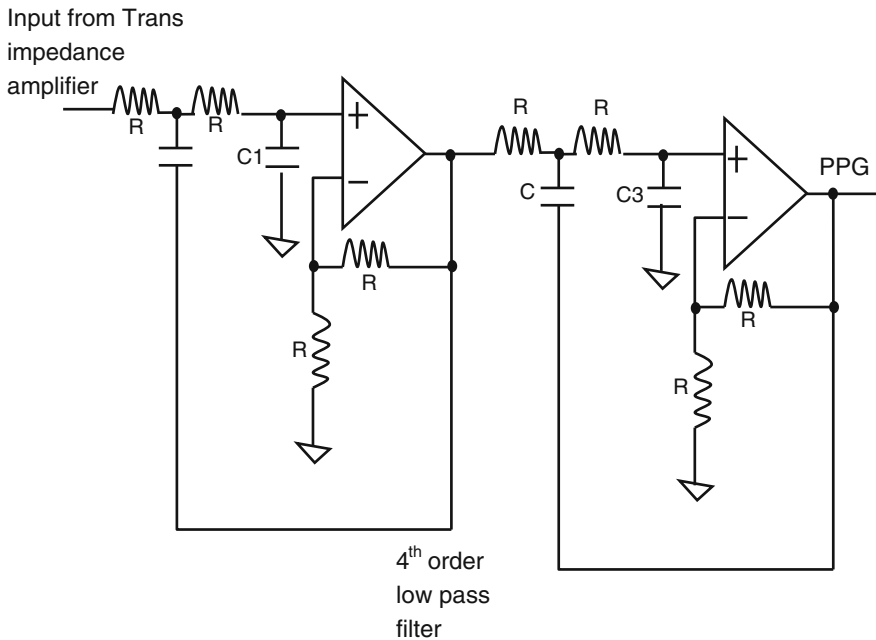


Fig. 4 Sallen key fourth order low pass filter

$$\Delta OD_{\lambda} = \log \left[1 + \left(\frac{\Delta I_{\lambda}(t_i)}{I_{\lambda}(t_{i+1})} \right) \right] \tag{6}$$

where ΔOD_{λ} is difference between optical densities at time t_i and $t_i + 1$, $\Delta I_{\lambda}(t_i)$ is the pulsatile component at time t_i and $I_{\lambda}(t_{i+1})$ is the intensity of light at time $t_i + 1$.

This difference has the effect of removing the venous and the tissue contributions to yield only the change in intensity due to the pulsating arterial blood compartment [17].

The optical densities have been calculated at three wavelengths for 50 subjects. The actual glucose values have also been determined using standard invasive glucometer. Regression analysis has been done on these values using neural network toolbox in MATLAB.

4 Adaptive Filtering

Figure shows a block diagram in which a sample from a digital input signal $X(n)$ is fed into a device, called an adaptive filter that computes a corresponding output signal sample $Y(n)$ at time n . For now, the structure of the adaptive filter is not important, except for the fact that it contains adjustable parameters whose values effect how $Y(n)$ is computed. The output signal is compared to a desired signal, by subtracting the two samples at time n . This difference signal, given by

$$E(n) = p(n) - y(n) \tag{7}$$



Fig. 5 PPG waveform for 950 nm

Is known as the error signal. The error signal is fed into a procedure which adapts the parameters of the filter from time n to $(n + 1)$ in a well-defined manner. As the time index n is incremented, it is hoped that the output of the adaptive filter becomes a closer match to the desired signal, such that the magnitude of the error signal reduces over time.

In adaptive filtering, adaptation refers to the method by which the parameters of the system are changed from time index n to time index $(n + 1)$. The number and types of parameters within the system depend on the computational structure chosen for the system.

5 Conventional Fir Based Adaptive Filtering of PPG

An adaptive filter attempts to model the relationship between two signals in an iterative manner. The Fig. 6 shows the structure of the conventional adaptive filter based on the FIR using least means squares algorithms for updating the weights of the filter based on the error signal so that the error is minimized (Fig. 7).

The primary input being the PPG signal with motion artifact. We use a triaxial accelerometer attached to the finger clip to detect the patient hand movement in x , y and z directions. These signals are used as the noise reference signals for the adaptive filter to cancel out the motion artifact.

The output of the system can be represented as

$$y(n) = \sum_{i=1}^N a_i(n)y(n-i) + \sum_{j=0}^N b_j(n)x(n-j) \quad (8)$$

Using vector notation we can write as

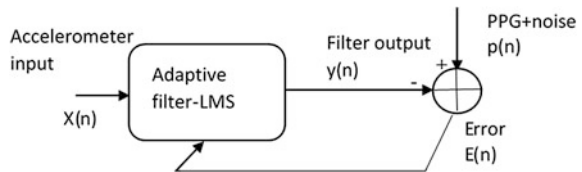
$$y(n) = W^T(n)U(n) \quad (9)$$

where $X(n) = [x(n) \ x(n-1) \ \dots \ x(n-L+1)]^T$ denotes vector transpose.

Note that this system requires L multiplies and $L - 1$ adds to implement, and these computations are easily performed by a processor or circuit so long as L is not too large and the sampling period for the signals is not too short.

The LMS algorithm is defined by below set of equations

Fig. 6 Block diagram of FIR based adaptive filter



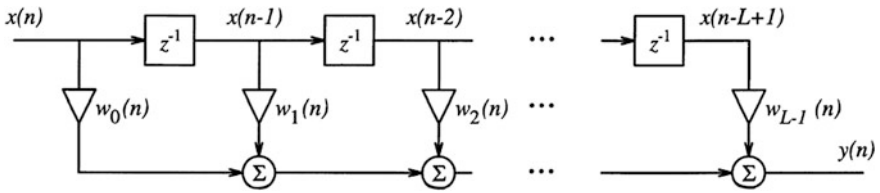


Fig. 7 Structure of the FIR filter

$$W = [W_0, W_1, W_3 \dots] \tag{10}$$

$$Y(n) = W(n) * X(n) \tag{11}$$

$$E(n) = p(n) - Y(n) \tag{12}$$

$$W(n + 1) = W(n) + 2\mu * X(n) \tag{13}$$

where $W(n)$ are filter coefficients, $x(n)$ and $y(n)$ are input and output of the filter and $p(n)$ is the desired signal.

The updating of the filter coefficients is done based on Eq. (9). Figure 8 shows the output of the conventional filter, which is the filtered PPG obtained after filtering the corrupted PPG. The output of the filter is compared to the ECG for validating the results. The output of the filter is compared with the uncorrupted ECG for validating the results. The order of the FIR filter used is 15 with an LMS adaptive step size of 0.008. The MSE is found to be about $3.4959e+03$ which is very high.

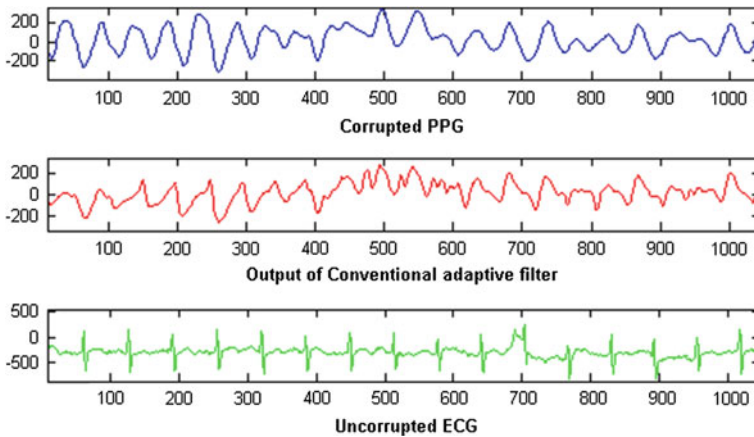


Fig. 8 Results showing the output of FIR based adaptive filter

6 Adaptive Filter Based on Adaline Neural Network

6.1 Adaptive Linear Network Architecture

The block diagram of the adaptive filter using neural network is shown in Fig. 5. It comprises of a tapped delay line with adaptive linear neuron forming a filter.

The ADALINE network shown below has one layer of S neurons connected to R inputs through a matrix of weights W . The adaptive filter is based on the adaline neural network which is basically a linear neuron similar to the perceptron but the activation function used is linear instead of the hard limit or sigmoid.

The adaline performs a sum of products calculation using the input and weight vectors and output activation function to get the final single output value. The adaline network along with the tapped delay line at the input forms the adaptive filter. The Fig. 9 shows the structure of the filter.

The input signal enters from the left and passes through $N-1$ delays. The output of the tapped delay line (TDL) is an N -dimensional vector, made up of the input signal at the current time, the previous input signal, etc.

The output of the filter is given by

$$\alpha(k) = \text{purelin}(Wp + b) = \sum_{i=1}^R W_{1,i}\alpha(k - i + 1) + b \quad (14)$$

Here the linear neural network is adaptively trained to predict the uncorrupted PPG from an accelerometer output. Here the accelerometer signal gives the network information it can use to predict the motion artifact contribution to the corrupted PPG. The filtered PPG signal is shown in the Fig. 10.

It can be seen that the filtered PPG signal from neural network is in correlation with the uncorrupted ECG (Fig. 11).

Network is trained using Widrow-Hoff learning algorithm and the mean square error is found to be 0.0878. The error is very less when compared to the conventional adaptive filter.

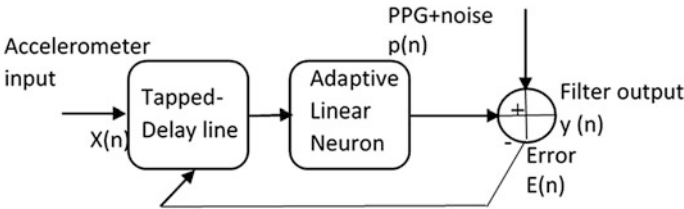


Fig. 9 Block diagram of adaptive filter based on neural network

Fig. 10 Structure of the adaptive linear neural network

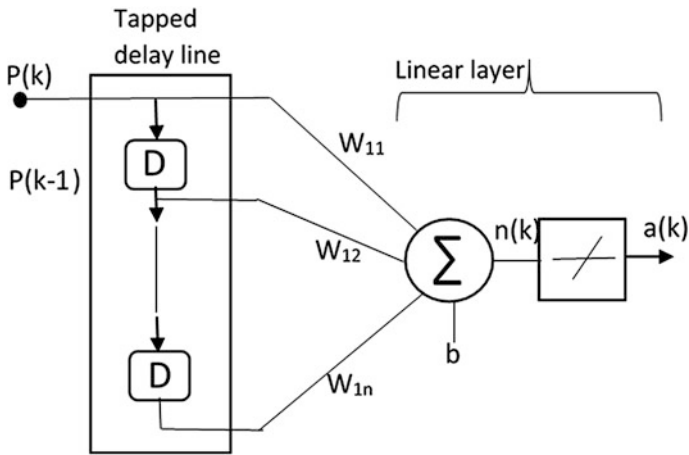
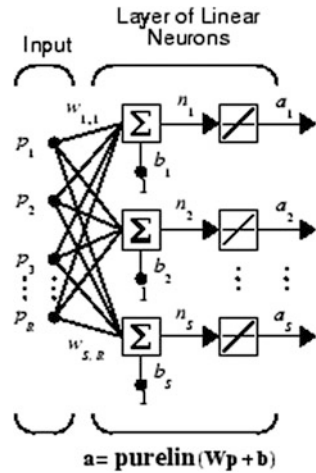


Fig. 11 Structure of neural network based adaptive filter based on adaline

7 FPGA Implementation of Multi-Layered Perceptron Neural Network Prediction Model

The dynamics of the blood glucose can be described as a nonlinear black box model. Since the output from the PPG sensor is highly sensitive to the motion artifacts and has errors due to scattering of the fatty tissue, difference in the path length because of the difference in the thickness of the finger from person to person. Due to this there is a nonlinear relationship between the input data coming from PPG and the target data which is actual glucose concentration measured from

invasive methods. Neural network model approach, is well suited to characterize such a complex system in which several factors affect future values of glucose.

We have implemented neural network prediction model on FPGA which predicts the blood glucose with a simple 2 layer feed forward, Levenberg-Marquardt back propagation network, trained with PPG output and invasive glucose measurements.

Initially MATLAB neural network toolbox has been used for training and testing the predictive model which uses a two layer feed forward network with sigmoid hidden neurons and linear output neurons. The architecture is tested with different number of neurons in hidden layer and it is chosen to be 10 based on the lowest validation error. The design environment is shown in Fig. 12.

7.1 Structure of the Feed Forward Network

Here we have used a network comprising of two layers viz., hidden layer and the output layer as shown in Fig. 13a. The hidden layer has 10 hidden neurons and the output has only one neuron. If the number of neurons is increased beyond 10 neurons, the results would be more accurate, but this would involve more computational time and moreover the resulting network could not fit within the CLB capacity of the FPGA. In the hidden layer the weighted sum of inputs with the sigmoid activation function (fs) are processed. The output layer has single neuron with linear activation function of (fl) where the weighted sum of outputs of the hidden layer with linear activation function are processed to give the final output of the network. The optical densities for various subjects has been calculated based on the Eq. (3) from the PPG output of front end analog circuit. These optical densities

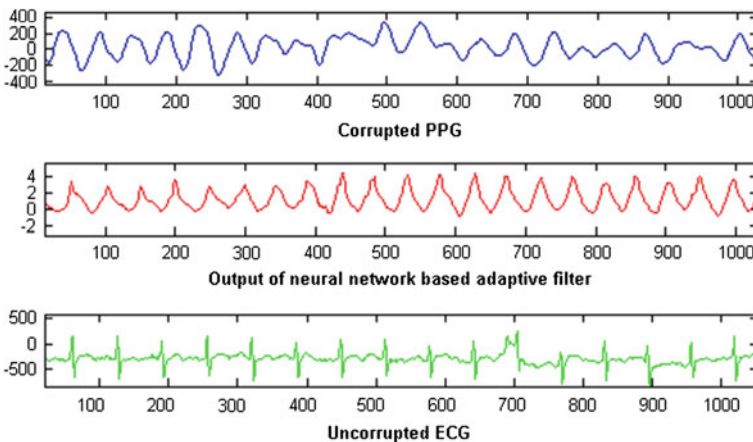


Fig. 12 Results showing the filtered PPG output of NN based adaptive filter

are given as inputs to the network and the invasive glucose values as targets to train the network and predict the near future values of glucose.

During first stage which is the initialization of weights, some small random values are assigned. During feed forward stage each input unit receives an input signal and transmits this signal with a weightage to each of the hidden neurons. Each hidden unit summarizes the inputs and its bias (b), then calculates the activation function (fs) and sends its signal to each output unit. The output unit calculates the activation function (fL) with bias to form the response of the net for the given input pattern [18, 19].

7.2 Implementing the Sigmoid Activation Function

Sigmoid functions are often used in artificial neural networks to introduce non-linearity in the model. It is used as an activation function to transform the level of neuron (weighted sum of inputs) to an output signal. The sigmoid function forms the most computationally expensive part of the neural calculation. In many applications look up tables are used to overcome this problem, but here, the design of this activation function will be illustrated without using a lookup table.

The activation function is used to limit the value of the neuron output. The sigmoid activation function is given by the equation:

$$sig(x) = \frac{1}{(1 + e^{-x})} \tag{15}$$

This equation has an exponential function which is difficult to implement on hardware with better accuracy. Implementing a sigmoid function as a lookup table is straightforward, as the approximated values can be calculated in advance. However, the lookup-table implementation is a limiting factor, as the memory

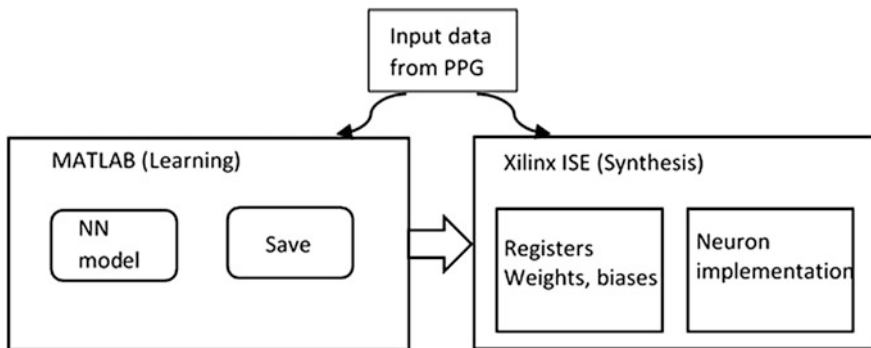


Fig. 13 Design environment of network

requirements of a pipelined neural network implementation grows. Since internal memory is limited in FPGAs, it has other purposes than serving only as a storage for values of a lookup-table approximation. There are several functions listed by Nordstrom and Svensson [19], which may be used as an approximation to the function used by McClelland and Rumelhart. These functions all have the same general characteristics. They are continuously increasing, approach 0 at $-\infty$ and 1 at $+\infty$, and have a continuous first derivative. We have implemented a close approximation of the sigmoid function. The approximation that we used in this neural network is given by the function:

$$\text{sig}(x) = \frac{1}{2} \left[\frac{x}{1 + |x|} \right] + 1 \quad (16)$$

As discussed earlier initially MATLAB was used to train the network for creating the predictive model. From this we obtain separately the input weights and biases, layer weights and biases. For each neuron we have calculated the real sigmoid value and the approximated sigmoid value and we have found that by using piece wise linear approximation we can bring the approximated sigmoid value closer to the real sigmoid value which is obtained from matlab, so that the effect of approximation can be reduced for better accuracy when implemented in hardware. Table 1 shows the weights and biases of input and hidden layers.

7.3 System Level Design

For a neuron with N inputs, N multipliers, N-1 adders and the hardware to implement the limiting function $\text{sig}(x)$ is required [20, 21]. As discussed earlier, the sigmoid approximation function can be implemented in hardware as it does not require any exponential function. A VHDL code is written for the neuron where the weighted sum of inputs along with the bias is given as input to the activation function which is shown in Fig. 13b. The output x is given by equation

Table 1 Weights and biases of input and hidden layers

W1	W2	W3	Bias
-0.7200	-1.8341	2.0734	3.2548
-2.1339	1.6408	1.4818	2.1903
-2.6487	-1.0157	1.0253	1.6855
-1.6305	-2.2957	1.0672	0.9870
-2.4648	0.3102	-1.6974	0.2725
-2.3817	-1.8592	0.2694	-0.4620
0.9911	2.0438	1.8781	1.1163
-2.4450	0.3549	-2.4238	-1.1534
1.0575	2.9467	0.0682	2.2939
-1.2526	2.7371	-1.0634	-2.6764

$$x = (a * w_{11} + b * w_{21} + c * w_{31}) + b1 \tag{17}$$

$$y = sig(x) \tag{18}$$

The functional units used by the circuit are: two adders, a divider, an absolute value and a divide-by-two circuit. Some simple optimizations have been performed on this circuit. Once the circuit for this function has been extracted, it may be used as a macro cell, much like the other macro cells in the circuit.

The training of the neural network is done offline to FPGA in order to minimize the design circuitry. Once the weights and biases of each layer have been obtained these weights will be hard implied on the FPGA. Figure 14 shows the hardware implementation of single neuron as a configuration logic blocks.

8 Results

The front end circuit for obtaining the PPG at the fingertip has been designed and implemented. The optical densities obtained from the PPG are given to the artificial neural network based prediction model. This perceptron based prediction model is first modelled at the system level using MATLAB and further has been realised on FPGA. The simulation and synthesis has been carried out using Xilinx ISE design suite 13.3. The model has been successfully uploaded on to Spartan 3E xc3s1200e-4ft256 FPGA board.

MATLAB has been used for training and testing a neural network and develop a predictive model based on the PPG data and invasive glucose measurements. The number of samples used for training are 45 and for testing are 10. The mean square

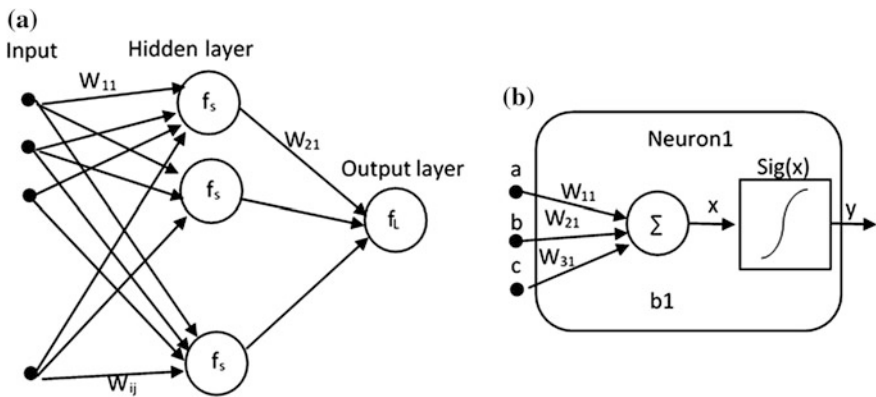


Fig. 14 Structure of a the neural network, b the single neuron

error (MSE) achieved with MATLAB is 5.84 mg/dL. The regression analysis showing the training and validation of the network are depicted in Fig. 10. The ‘R’ found to be 0.9 signifies the high correlation between the outputs and targets of the network. Figure 11 shows the technology schematic of the ANN.

Initial testing has been carried out on 15 patients, out of which 10 patients had diabetes and the system provided a positive test result, 1 patient did not have diabetes and the system provided a positive result, 1 patient having diabetes and the system yielded negative test result. Also, there was 1 patient with no diabetes and the system yielded positive test result, and three patients with no disease and the system yielded negative test result. The results of diagnosis shown in Table 2 brings out the level of accuracy of diagnosis (Figs. 16, 17 and 18).

Clinical trials have been carried out on 100 subjects, based on the invasive and the measured glucose values the Clarke error grid analysis is carried out for validating the results obtained. The grid is divided into five regions, each of which defines the extent of the prediction error [22]. Figure 19 shows the results of Clarke error grid analysis. The diagonal represents the correlation between the predicted and the reference glucose value. The regions below and above the line indicate overestimation and under estimation of actual values respectively. Table 2 details about the percentage of points in each region. Our results show that 95.38 % of points were in region A, which covers predictions within 20 % of the reference sensor. Only 4.6 % of points went to region B, which contains predictions more than 20 % away from the reference sensor but would not lead to inappropriate treatment, and no points fell in regions C, D and E.

Zone	A	B	C	D	E
Percentage (%)	95.38	4.6	0	0	0

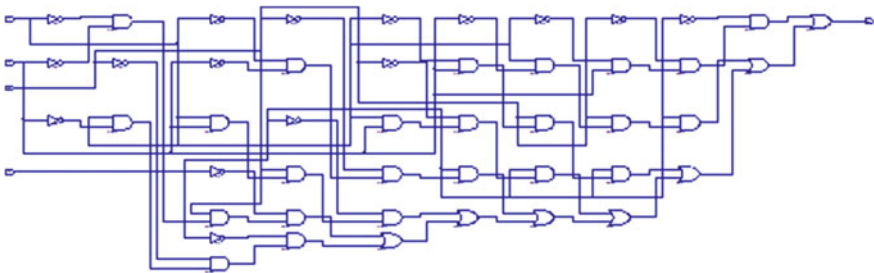


Fig. 15 Hardware implementation of the neuron

Table 2 Table showing the sensitivity specificity and accuracy

Sensitivity of diagnosis	91 %
Specificity of diagnosis	75 %
Prevalence of disease	80 %
Accuracy of diagnosis	87 %

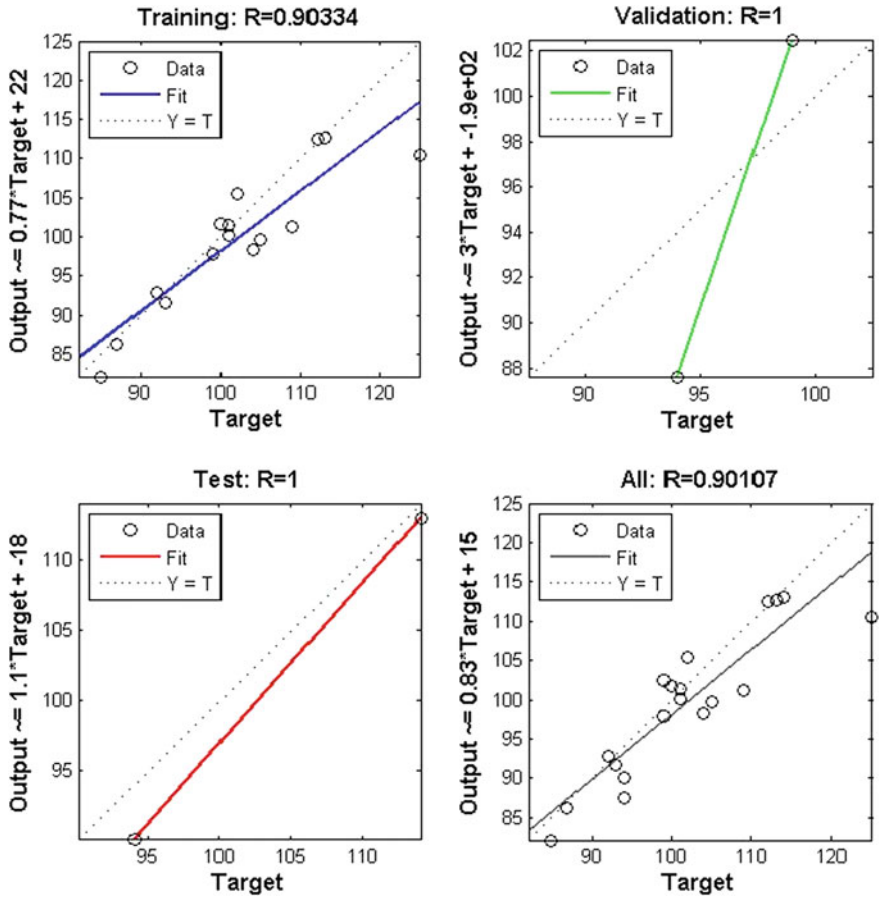


Fig. 16 Neural network regression analysis using MATLAB

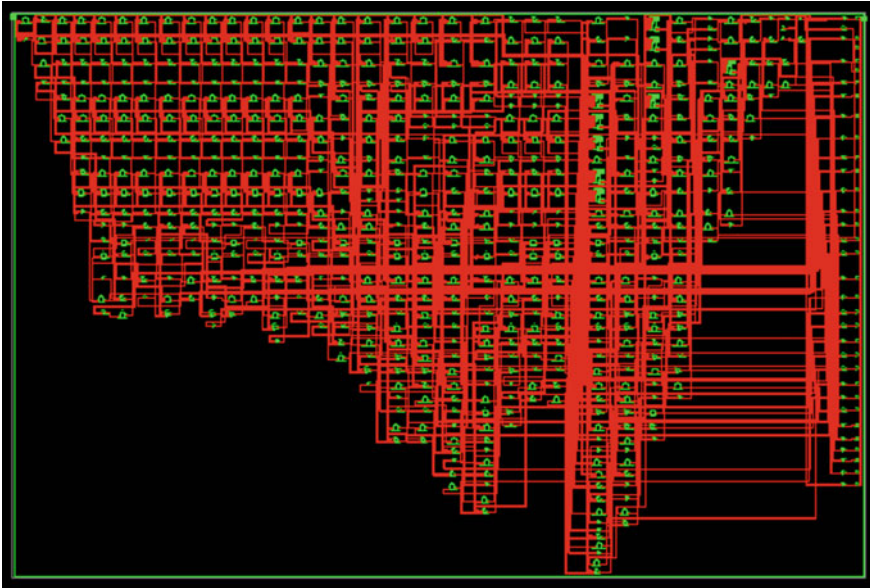


Fig. 17 Technology schematic of neural network model

Device Utilization Summary				
Logic Utilization	Used	Available	Utilization	Note(s)
Number of 4 input LUTs	244	17,344	1%	
Number of occupied Slices	169	8,672	1%	
Number of Slices containing only related logic	169	169	100%	
Number of Slices containing unrelated logic	0	169	0%	
Total Number of 4 input LUTs	272	17,344	1%	
Number used as logic	244			
Number used as a route-thru	28			
Number of bonded I/Os	32	190	16%	
Number of MULT 18X 18SIOs	9	28	32%	
Average Fanout of Non-Clock Nets	1.64			

Performance Summary			
Final Timing Score:	0 (Setup: 0, Hold: 0)	Pinout Data:	Pinout Report
Routing Results:	All Signals Completely Routed	Clock Data:	Clock Report
Timing Constraints:			

Fig. 18 Device utilization summary

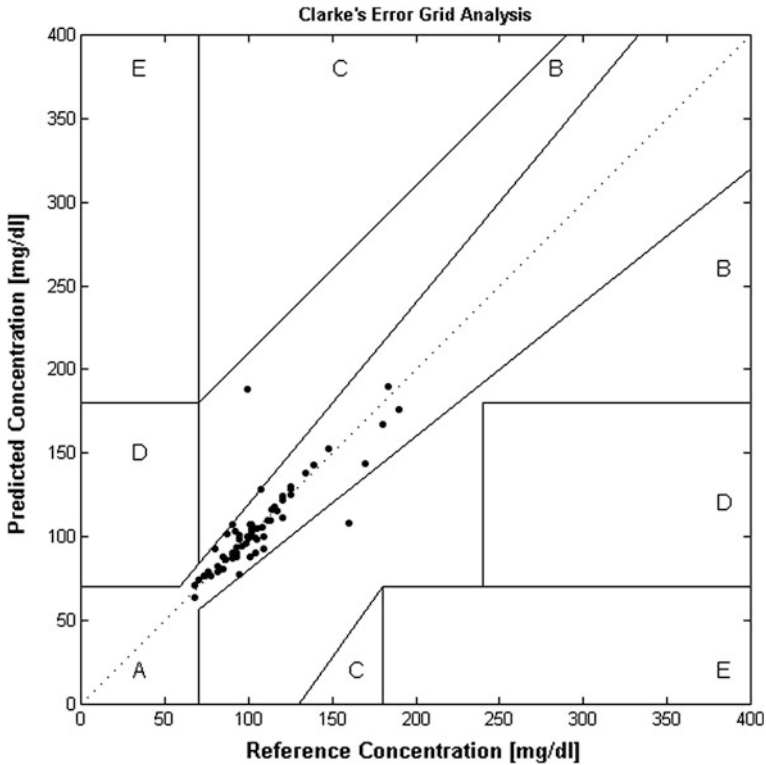


Fig. 19 Plot showing the Clarke error grid analysis

9 Conclusion

In today's world, there is necessity of a portable device which can continuously measure blood glucose level. It is observed that for the noninvasive estimation of blood glucose concentration PPG is one of the promising technique, which gives the advantages like low cost, less time delay and portability. In order to obtain the required sensitivity for the device the proper calibration of the data obtained from PPG sensing circuit is required. The choice of the proper regression technique will effect the parameters like sensitivity, specificity and accuracy of the diagnosis.

This chapter deals with the usage of neural networks in non invasive diagnostic systems. The artificial neural networks has been used to create a prediction model. The training and testing of neural networks has been carried out in MATLAB with real patient data. The trained prediction model has been implemented on FPGA. This is to find out the correspondence between the predicted value by the neural network and the actual blood glucose concentration of the patient.

A reasonable high accuracy of about 95.38 % has been obtained based on the Clarke error grid analysis which is clinically acceptable. The proposed system is well suited for continuous measurement of blood glucose levels in diabetic patients.

References

1. H.M. Heise, in *Encyclopedia of Analytical Chemistry*, vol. 1, ed. by R.A. Meyers (John Wiley Press, New York, 2000), pp. 1–27
2. DCCT Group. Intensive diabetes treatment and cardiovascular disease in patients with type1 diabetes. *N. Eng. J. Med.* **353**(25), 2643–2653 (2005)
3. J. S. Skyler. Continuous glucose monitoring: an overview of its development. *Diab. Technol. Ther.* **11**, sup. 1 (2009)
4. A. Rabiee, et al. Numerical and clinical accuracy of a continuous glucose monitoring system during intravenous insulin therapy in the surgical and burn intensive care units. *J. Diab. Sci. Technol.* **3**(4), 951–959 (2009)
5. E. Monte-Moreno. Non-invasive estimate of blood glucose and blood pressure from a photoplethysmograph by means of machine learning techniques. *Artif. Intel. Med.* **53**(2), 127–138. ISSN 0933-3657 (2011)
6. H. Karimipour, H. T. Shandiz, E. Zahedi. Diabetic diagnose test based on PPG signal and identification system. *JBiSE.* **2**(6), 465–469. doi:10.4236/jbise.2009.26067 (2009)
7. S. F.Malin, T. L. Ruchiti, T. B. Blank, S. U. Thennadil, and S. L. Monfre. Noninvasive prediction of glucose by near-infrared diffuse reflectance spectroscopy. *Clin. Chem.* **45**, 1651–1658 (1999)
8. O.S. Khalil, Spectroscopic and clinical aspects of noninvasive glucose measurements. *Clin. Chem.* **45**(2), 165–177 (1999)
9. K. J. Jeon, I. D. Hwang, S. Hahn, G. Yoon. Comparison between transmittance and reflectance measurements in glucose determination using near infrared spectroscopy. *J. Biomed. Opt.* **11**, 014022 (2006)
10. A.K. Amerov, J. Chen, G.W. Small, M.A. Arnold, Scattering and absorption effects in the determination of glucose in whole blood by near-infrared spectroscopy. *Anal. Chem.* **77**, 4587–4594 (2005)
11. C. P. Gandia, A. Facchinetti, G. Sparacino, C. Cobelli, E. J. Gomez, M. Rigla, A. deLeiva, M. E. Hernando. Artificial neural network algorithm for on-line glucose prediction from continuous glucose monitoring. *Diab. Technol. Ther.* **12**, 81–88 (2010)
12. G. Robertson, D. Lehman, W. Sandham, D. Hamilton. Blood glucose prediction using artificial neural networks trained with the aida diabetes simulator: a proof-of-concept pilot study. *J. Elect. Comput. Eng.* Article ID 681786, 11 (2011)
13. R. Yousefi, M. Nourani, I. Panahi. Adaptive cancellation of motion artifact in wearable biosensors. *34th Annual International Conference of the IEEE EMBS San Diego, California USA*
14. S. Abbaspour, A. Fallah, A. Malek. A comparison of adaptive filter and artificial neural network results in removing electrocardiogram contamination from surface EMGs. *20th Iranian Conference on Electrical Engineering* (Tehran, Iran, 2012), (ICEE20 12), May 15–17
15. Medhat Moussa, Shawki Areibi, Kristian Nichols, *On the arithmetic precision for implementing back-propagation networks on FPGA* (University of Guelph, School of Engineering, Ontario, Canada, 2003)
16. S. Ramasahayam, S. H. Koppuravuri, L. Arora, S. R. Chowdhury. Noninvasive blood glucose sensing using near infra-red spectroscopy and artificial neural networks based on inverse delayed function model of neuron. *J. Med. Syst.* **39**(1) (12/2014). doi:10.1007/s10916-014-0166-2

17. Y. Yamakoshi. Pulse glucometry: a new approach for non-invasive blood glucose measurement using instantaneous differential near infrared spectrophotometry
18. R. Raeesil, A. Kabir. Implementation of artificial neural network on FPGA. Am. Soc. Eng. Edu. (2006)
19. S. R. Chowdhury, H. Saha. Development of a FPGA based fuzzy neural network system for early diagnosis of critical health condition of a patient. Comput. bio. med. (2010)
20. T. Nordstrom, B. Svensson, Using and Designing Massively Parallel Computers for Artificial Neural Networks. J. Parallel Distrib. Process. **3**, 260–285 (1998)
21. S. A. Guccione. M. J. Gonzalez. A neural network implementation using reconfigurable architectures. *Department of Electrical and Computer Engineering* (The University of Texas at Austin, Austin, USA, 2006)
22. W.L. Clarke, D. Cox, L.A. Gonder-Frederick, W. Carter, S.L. Pohl, Evaluating clinical accuracy of systems for self-monitoring of blood glucose. Diab. Care **10**(5), 622–628 (1987)

Sensing System for Bone Health Monitoring

N. Afsarimanesh, Subhas Chandra Mukhopadhyay,
M. Kruger and P. Yu

Abstract Osteoporosis is a disease identified by low bone mass and progressive structural deterioration of bone tissue. Osteoporosis is a serious problem in postmenopausal women and aged populations. There is usually no symptom of osteoporosis until the first bone fracture occurs. Dual-energy X-ray absorptiometry (DEXA) is a gold standard to measure bone mineral density (BMD). The test can diagnose osteoporosis and can conclude if medical treatments are improving bone density. Since changes in bone density are slow, BMD studies are required to be of longer duration, up to 2 years at least, whereas changes in biochemical markers may be evident after only a few weeks. Therefore, detection and quantification of biochemical markers (especially CTX-I) together with the measurement of bone density before deciding whether treatment is required, can help identify bone loss and subsequent response to the treatment. Currently, most of the available techniques to detect and measure bone turnover markers are based on the enzyme-linked immunosorbent assay (ELISA). Although this method is a standard immunoassay technique and has been commercialized, there are serious limitations in using ELISA because it is time-consuming, expensive, requires tedious procedural steps, technical expertise, and a laboratory environment. Therefore, it is very desirable to have an electrochemical biosensing system that is rapid, low-cost, does not require technical expertise and could be applied as a point-of-care tool to establish a realistic measurement profile for osteoporotic patients. It can also be used as a prognostic device at a domestic level that may indicate the early stages of osteoporosis so that the treatment can be started at early stages of the disease before that it could induce irrecoverable loss to the skeletal bones.

N. Afsarimanesh · M. Kruger · P. Yu
Massey University, Palmerston North, New Zealand

S.C. Mukhopadhyay (✉)
Department of Engineering, Faculty of Science and Engineering,
Macquarie University, Sydney, NSW, Australia
e-mail: S.C.Mukhopadhyay@massey.ac.nz

1 Introduction

1.1 Osteoporosis and Bone Health

Osteoporosis, in which the bones become porous and fragile, is one of the world's most common diseases [1]. Figure 1 depicts healthy and osteoporotic bone. Osteoporosis can affect women and men, but women are more at risk of developing it. One in three women and one in five men over 50 years old will experience osteoporotic fractures [2, 3]. This disease is a serious problem for postmenopausal women and aged people [4].

Bone is a living tissue that is subjected to continuous remodeling, the process of replacing old bone tissue with new tissue. The activity of osteoclasts (bone resorption) and osteoblasts (bone formation) can highly affect this process [6]. During childhood and the early adulthood years, bone formation occurs faster than bone resorption, so bones become denser, heavier and larger. This condition will continue until the age of 30 when bones reach their maximum density and strength (peak bone mass). The bone condition will be relatively stable during the age of 30-45 and after that bone resorption begins to exceed bone formation. In women, bone loss is fastest in the first years after menopause [7] and this is one of the main causes of developing low bone mass or osteoporosis in later life. The hormone changes that occur in menopause directly affect the bone density. The female hormone, estrogen is essential for healthy bones. After menopause, the level of circulating estrogen falls and this can lead to a rapid decrease in bone density.

Under normal conditions, bone resorption and bone formation are coupled with each other to provide a balance in skeletal metabolism and turnover [6]. Osteoporosis usually develops when bone resorption occurs quicker than bone formation. Type I Collagen is the principle structural protein of bones which forms

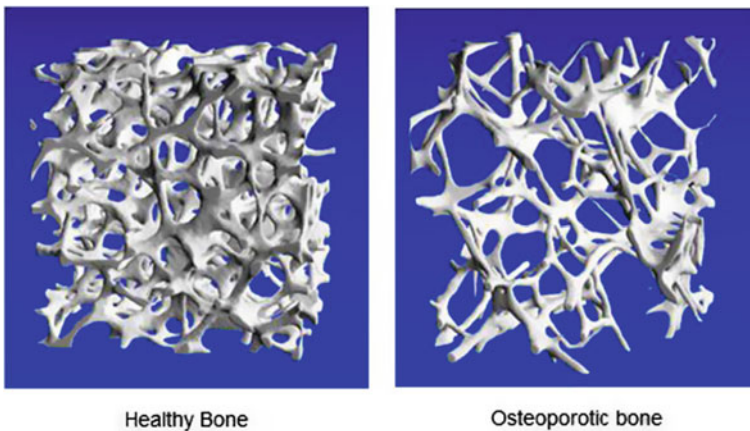


Fig. 1 Depicting healthy bone and osteoporotic bone [5]

approximately 90 % of the organic bone matrix [6]. During the process of bone resorption, type I collagen is broken down and CTx-I is released into the blood stream [8]. Hence, it can be used as a useful biomarker to measure the rate of bone resorption [9].

1.2 Contemporary Methods Available for Osteoporosis Detection and Their Limitations

Dual-energy X-ray absorptiometry (DXA) is the most accurate way and the gold standard to measure bone mineral density (BMD). DEXA scans can be used to diagnose osteoporosis and monitor the effect of therapy. This method uses dual X-ray beams at high- and low- photon energies [10]. A certain amount of X-ray is blocked by bone. Dense bones allow less of X-rays to pass through them and get to the detector. This data is sent to a computer which calculates T-score of the average density of the bones. The T-score is a comparison of a person's bone density with that of a healthy 30-year-old of the same sex. A low T-score shows that the bone is less dense than it should be [11] (Fig. 2).

As changes in bone density are very slow, BMD studies are required to be done for a longer interval, at least, two years, while changes in biochemical markers may be identified after only a few weeks [12]. Thus, measurement of BMD along with the detection and measurement of biochemical markers such as CTx-I can aid in detecting bone loss, monitoring the disease, the need for medical treatment and the response to it.

ELISA is an analytical tool which is widely used in biomedical research for the detection and measurement of a specific antigen in a liquid sample. ELISA uses enzyme-linked antigens and antibodies to detect the target molecule. Tiny quantities of antigens such as hormones, proteins, peptides, or antibodies in a liquid sample can be detected using ELISA [13]. The antigen in the liquid phase is coated into the

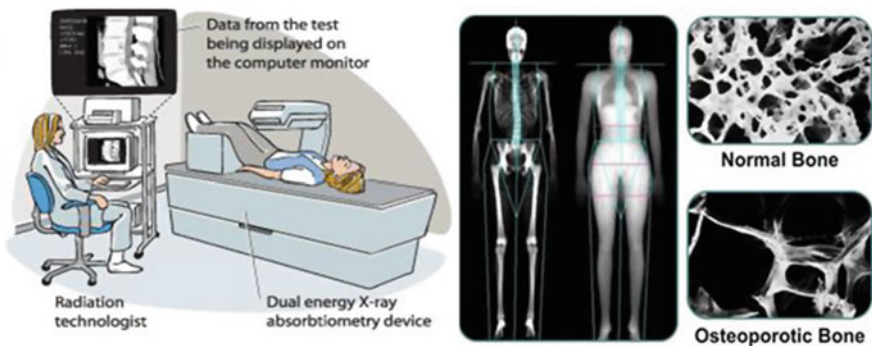


Fig. 2 Dual-energy X-ray absorptiometry (DXA)

wells of a 96-well microtiter plate which binds to a primary antibody. The antigen is then detected by a secondary, enzyme-linked antibody. A chromogenic substrate is used to change the color in the presence of the antigen. Finally, the measurement is done using spectrophotometry [14].

Figure 3 illustrates the general procedure of ELISA. However, there are some limitations on using the ELISA, it is expensive, time-consuming and requires several steps of preparation process by a trained professional. It is time consuming, expensive, calls for several steps, technical expertise and a laboratory environment to carry out the testing.

2 Motivation

It has been explained in the previous section there are some problems and limitations regarding the available methods for early detection of bone loss. The main reasons that motivated me towards the development of a novel sensing system to detect bone loss at early stages of the disease can be summarized as follow; the limitations of the available methods for early detection of osteoporosis; Lack of a domestic device which can be used by any person for a regular check-up; and to save a huge amount of costs related to Osteoporosis and individuals suffering from it.

3 Behaviour of Interdigital Sensors

3.1 Operating Principle of Interdigital Sensors

Planar interdigital sensors are made of comb-like or finger-like periodic pattern of parallel electrodes on a solid phase substrate. These electrodes are used to build up the capacitance related to the electric fields that penetrate into the Material Under Test (MUT) and carries useful information about the properties of the material sample [15]. One of the most important benefits of the planar interdigital sensors is the single-side access to the MUT. This property helps to penetrate the sample with

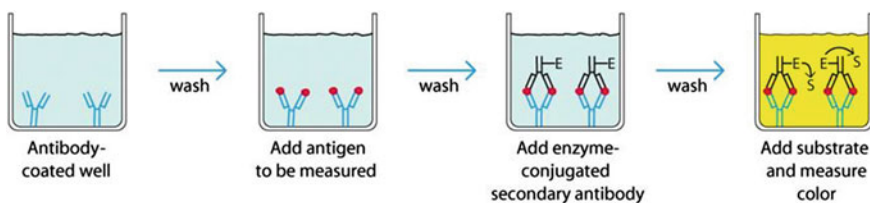


Fig. 3 ELISA technique used to detect an antigen in a given sample [14]

magnetic, electric, or acoustic fields from only one side. The strength of the output signal can be controlled by changing the number of fingers, the area of the sensor, and the spacing between them. The capability of being used for non-destructive testing is another advantage of these sensors, which makes them more useful for inline testing and process control applications [16].

Basically, planar interdigital sensors follow the operating principle of parallel plate capacitors. Figure 4 shows a gradual transition from the parallel-plate capacitor to a planar, fringing field capacitor, where electrodes open up to provide a single-side access to the MUT. The electrode pattern of the interdigital sensor can be repeated several times, in order to get a stronger signal and keep the signal to noise ratio in an acceptable range [17]. The configuration of the conventional interdigital sensor is shown in Fig. 5.

When an AC signal is applied as an excitation voltage to the terminals, an electric field is formed from positive to negative terminal. This electric field bulges through the test sample via excitation electrode and is received by the sensing

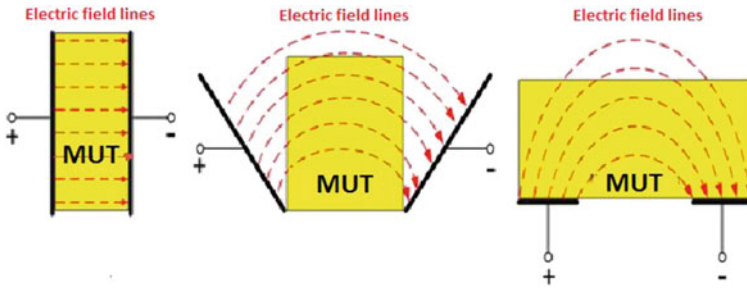
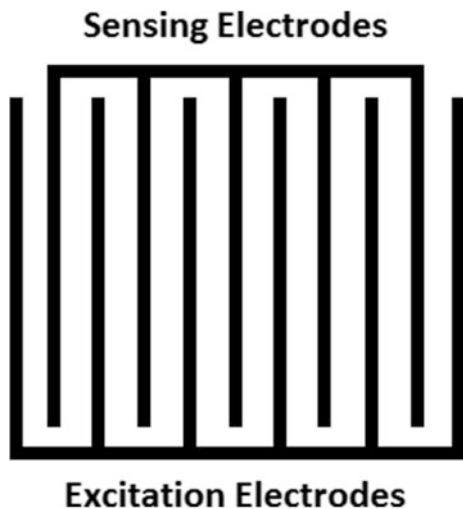


Fig. 4 Gradual transition from the parallel-plate capacitor to a planar capacitor

Fig. 5 Geometric structure of conventional planar interdigital sensor



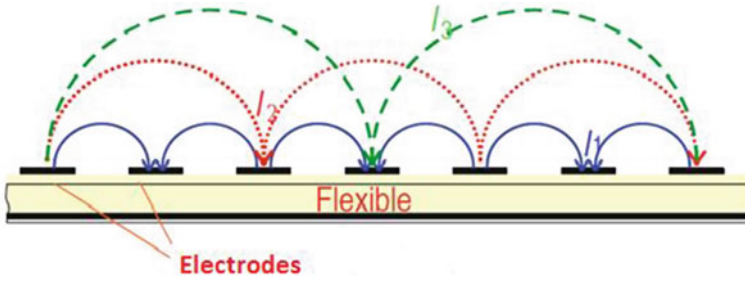


Fig. 6 Electric field formed for different pitch lengths [18]

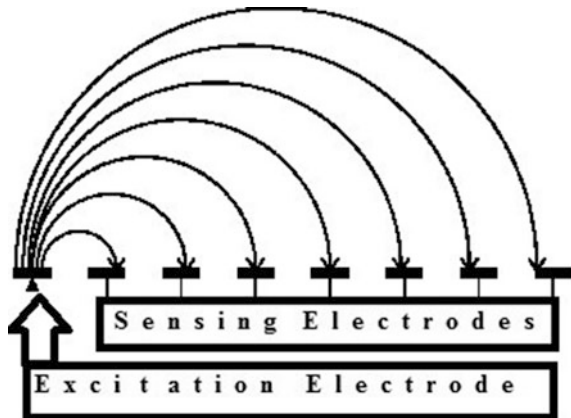
electrode which carries useful information about the properties of MUT such as impedance, density, chemical material and so on.

Figure 6 shows the electric field formed between positive and negative electrodes for different pitch lengths- the distance between two consecutive electrodes of the same polarity. As it is illustrated in the figure, different pitch length (l_1 , l_2 and l_3) shows different penetration depth. The penetration depth rises by raising the pitch length, but the electric field will get weak.

3.2 High Penetration Depth Planar Interdigital Sensors

Novel interdigital sensors are designed with more number of sensing electrodes as compared to the excitation electrodes, in order to increase the penetration depth of the fringing electric field. Different geometries have been studied in research literature [19–21]. Figure 7 shows the excitation pattern for a multi-sensing electrode in interdigital sensor geometry.

Fig. 7 Schematic excitation patterns for multi-sensing electrode interdigital sensors



The novel interdigital sensors have been fabricated based on different geometric parameters. Table 1 shows geometric parameters of four different interdigital sensors and Fig. 8 shows the schematic of a 1-5-25 and 1-11-25 configuration of newly designed planar interdigital sensors [22].

A time-dependent sinusoidal electrical perturbation is applied to the excitation electrodes of the interdigital sensor. The alternating electric field penetrates through the test sample via excitation electrode and is received by the sensing electrode which carries useful information about the properties of the material under test in close proximity of the sensor [15, 16].

The sensors were fabricated at King Abdullah University of Science and Technology (KAUST), Saudi Arabia as academic collaboration between School of Engineering and Advanced Technology, New Zealand and KAUST. The fabrication of the sensors was done by etching and photolithography techniques on a single crystal Silicon/Silicon Dioxide (Si/SiO₂) 4 inch (diameter) wafer, 525 μm thick. 36 workable sensors were patterned on one wafer (Fig. 9) with each sensor having a dimension of 10 mm × 10 mm and sensing area of 6.25 mm² (2.5 mm × 2.5 mm).

The sensors were fabricated using MEMS technology including the steps of photoresist coating, UV exposed ID pattern transfer, plasma etching metal deposition by DC magnetron sputtering and lift-off. Gold was used as electrode material due to flexibility in the methods available for its deposition as thin film electrodes. 500 nm of Gold (Au) were sputtered on top of 20 nm Chromium (Cr) to provide proper adhesion of the interdigital structures on the substrate. Then the wafer was coated with a 1 μm layer of Parylene C to protect the sensing area from corrosion by the solutions used during experimentation. Moreover, it prevents moisture diffusion into the Si/SiO₂ substrate that could affect its dielectric properties which would change sensor response. After that, the bonding pads were opened using plasma etching process.

These sensors have several applications in manufacturing process [23], environmental monitoring [21, 24–27], humidity and moisture sensing system [28, 29], photosensitive detection [30] and gas sensor [31]. A sensing system was developed based on the interdigital sensor to detect dangerous contaminated chemicals in seafood [19, 27]. Another one was developed based on the electrochemical impedance spectroscopy technique to monitor the presence of phthalates in aqueous solution [24–26].

Table 1 Geometric design parameters for four types of interdigital sensors

Sensor type	Pitch length (μm)	Number of sensing electrodes	Number of excitation electrodes	Sensing area (mm ²)
1-5-25	25	40	9	6.25
1-5-50	50	30	7	6.25
1-11-25	25	44	5	6.25
1-11-50	50	33	4	6.25

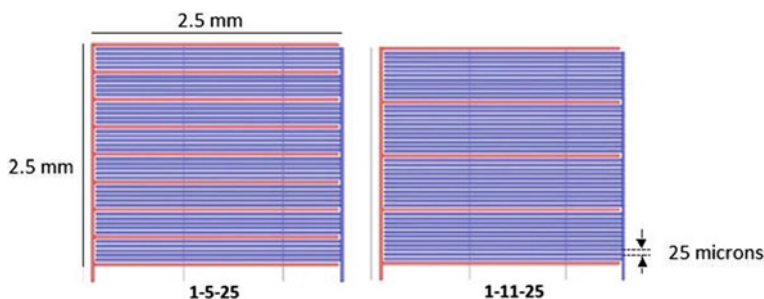


Fig. 8 1-5-25 and 1-11-25 configuration of Novel interdigital sensors

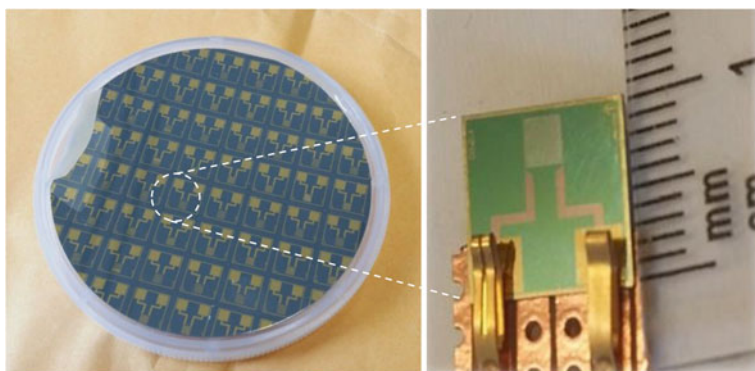


Fig. 9 Silicon wafer sensors fabricated using MEMS technology

4 Electrochemical Impedance Spectroscopy

Electrochemical Impedance Spectroscopy (EIS) is a popular and powerful technique to measure the resistive and capacitive properties of materials by applying a small AC signal. EIS method can be applied in non-destructive testing, label-free detection and single-sided access for different biological and chemical analysis. Different application of EIS had been reported such as the detection of fat content in meat [32], biotoxins in shell fish [19], bacterial endotoxin in food [33], phthalates in water and juices [25], determination of the corrosive behavior of materials [34, 35] and analysis of electrical properties for soymilk coagulation process [36]. EIS has several applications in different research areas such as, corrosion mechanisms [37], coating evaluation [38, 39], optimization of batteries [40] and biosensing [41].

Among some methods available for impedance measurements, Frequency Response Analysis (FRA) has become a de facto standard for EIS measurement. FRA is a rapid approach to evaluating the impedance variation at real-time. This technique measures the impedance of the system over a wide frequency range and compares the results with reference data. The advantage of the correlation process is

the minimization of noise, but this may cause the attenuation of the output signal. FRA is a single sinusoidal wave input method in which a small amplitude alternative current(AC) sine wave of a given frequency is overlaid on a dc bias potential, applied to the electrode and then measurement of resulting AC current is done. At low-amplitude AC potential, the system remains pseudo-linear. The process is repeated for the desired frequency range, and impedance is computed for five to ten measurements per decade change in frequency. In order to ensure the system repeatability, stability, and linearity, this method is rendered viable only for a stable and reversible system in equilibrium. For this reason, instantaneous impedance measurements are required for non-stationary systems [42–44].

Impedance analysis of linear systems is much easier than non-linear systems. In EIS measurement experiments, a small AC signal is applied to the cell. With such a low voltage, the system can be considered as a pseudo-linear system. If the system is non-linear, the current response of the system will contain harmonics of the excitation frequency and may be damaged by the harmonics. Figure 10 illustrates that pseudo-linearity of systems can be achieved by considering a small enough portion of the curve [43].

Electrochemical impedance can be measured by applying a small AC signal and then measuring the phase shift in current signal with respect to the applied potential. Electrochemical impedance is measured using a low excitation signal so that the cell's response is pseudo-linear. In a linear system, this current response to a sinusoidal excitation potential will result in a sinusoidal current at the same frequency but shifted in phase as shown in Fig. 11.

Impedance is defined as the measurement of the ability of a circuit to oppose the flow of electrical current when a voltage is applied. In an AC circuit, impedance

Fig. 10 Current versus voltage curve showing pseudo-linearity

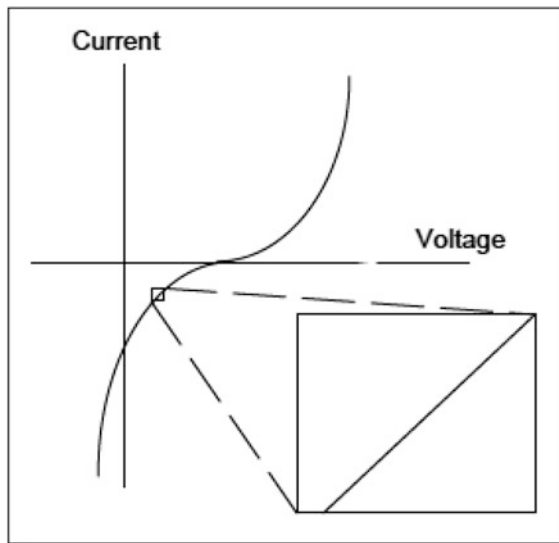
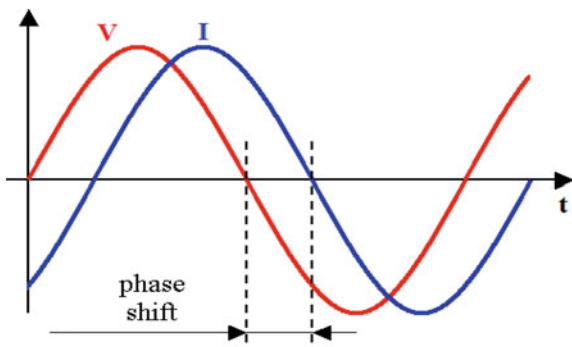


Fig. 11 Phase shift in current signal with reference to the applied voltage



is represented as a complex value which involves real part (resistance) and imaginary part (reactance).

The Nyquist plot is a popular format for evaluating electrochemical impedance data such as double layer capacitance (C_{dl}), electrolytic solution resistance (R_s), and electrode polarization resistance (R_p). These parameters will be discussed in the following sections. Nyquist plot represents imaginary impedance component against real impedance component at each excitation frequency. The Nyquist plot offers several advantages. The effects of solution resistance can be observed easily using this format. The electrochemical parameters can be calculated from the Nyquist plot, for example, solution resistance can be obtained by extrapolating the curve to the x-axis. Moreover, it is possible to compare the results of two or more separate experiments. One major drawback of the Nyquist plot is that there is no information about the frequency in the Nyquist plot which makes it difficult to calculate the double layer capacitance [43]. The Bode plot represents the absolute impedance and the phase shift vs. frequency. Unlike the Nyquist plot, the Bode plot shows frequency information at one of its axes, that is why the relationship between frequency and impedance can be easily observed from the plot.

Randle's equivalent circuit is the most frequently discussed equivalent circuit [45] used to interpret and analysis EIS experimental results in electrical form as shown in Fig. 12. It includes of solution resistance R_s in series connected to a

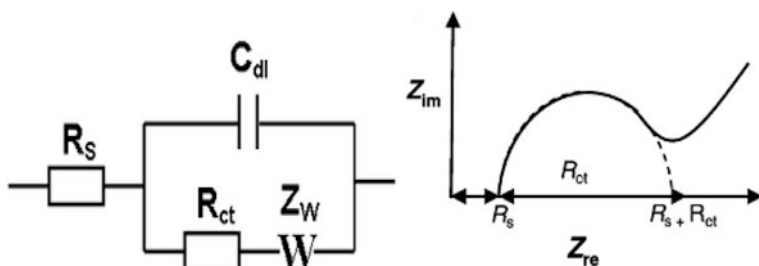


Fig. 12 Randle's equivalent circuit model and the Nyquist plot for the Randle's equivalent circuit

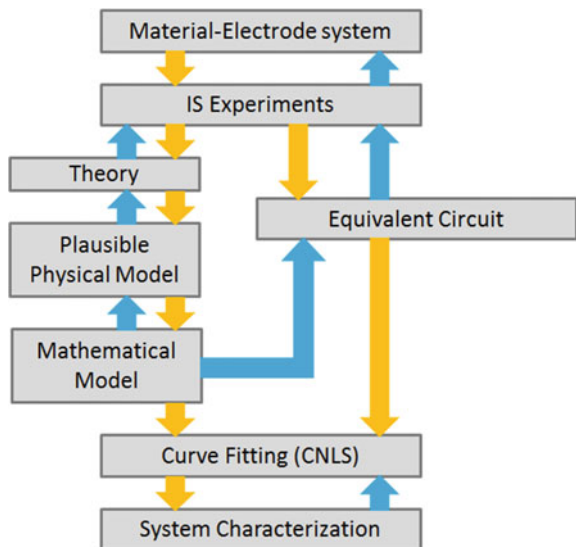
parallel combination of double layer capacitance C_{dl} to the charge transfer resistance R_{ct} in series with Warburg impedance Z_w [41].

This model was introduced by Randle in 1947 [46]. The model can be used to describe both kinetics and diffusion processes taking place at the electrode-electrolyte interface.

The Nyquist plot from the equivalent circuit consists of a semi-circular region followed by a 45° straight line, as shown in Fig. 12. In this model, the impedance of a faradaic reaction consists of an active charge transfer resistance R_{ct} and an electrochemical element of diffusion which is called Warburg element. The semi-circular region shows a slower charge transfer at higher frequencies whereas the straight line describes a faster mass-transfer at lower frequencies. R_{ct} can be calculated by extrapolating the semicircle to Z_{real} axis. Solution resistance R_s can be calculated by reading the real axis value at the high-frequency intercept which is the intercept near the origin of the Nyquist plot. R_{ct} can be calculated by extrapolating the semicircle to Z_{real} axis as illustrated in Fig. 12. C_{dl} can be calculated from the frequency at the maximum of semicircle portion in the Nyquist plot using $\omega = 1/R_{ct} C_{dl}$ [45].

In order to obtain the Randle’s circuit parameters, the fitting of the model to the experimental data should be performed using the complex nonlinear least-squares (CNLS) curve fitting techniques. Figure 13 shows the flow chart for the measurement and characterization of an electrode- electrolyte system [45].

Fig. 13 Flow diagram for the measurement and characterization of an electrode–electrolyte system



5 Experiments Using the Elisa Kit

The Serum CrossLaps[®] ELISA kit from IDS Company was procured locally from Abacus ALS, New Zealand. This kit contains streptavidin coated microtitre plate, a biotinylated antibody, peroxidase conjugated antibody, known concentration antigen solutions, incubation Buffer, washing buffer and stopping solution. This is a special test to measure the concentration of CTx-I in blood plasma. I started the experiments with the Serum CrossLaps[®] ELISA to obtain the standard curve, measure unknown samples and get some idea about the antigen- antibody techniques.

5.1 Assay Procedure

The antibody solution was prepared 30 min before starting the assay by mixing biotinylated antibody, peroxidase conjugated antibody and incubation buffer in the volumetric ratio of 1 + 1 + 100.

After that, standards and control were pipetted into the wells followed by adding the prepared antibody solution to them. At this stage, a complex between the antigens and antibodies was formed and this complex binds to the streptavidin surface via a biotinylated antibody. After one step incubation (120 ± 5 min), the wells were emptied and washed 5 times manually with diluted washing buffer. Then a chromogenic substrate was pipetted into the wells and incubated for 15 ± 2 min in the dark mixing apparatus (300 rpm). Then, the colour reaction was stopped with sulphuric acid. Finally, the measurement was done using the spectrophotometer. ELISA procedure has been summarized in the form of a flow chart given in Fig. 14.

5.2 Experimental Results from ELISA

The Serum CrossLaps[®] ELISA kit was used to obtain the standard curve by testing six standards. The concentration of known samples is 0, 0.147, 0.437, 0.798, 1.693 and 2.669 ppb. The standard curve obtained from ELISA is given in Fig. 15. All samples were tested in duplicate and the assay was performed at room temperature. Once the standard curve was obtained the experiments were performed for two unknown samples, obtained from sheep blood. The concentration of CTx-I in the first sample was 0.6514 ppb and in the second sample, it was 0.5049 ppb.

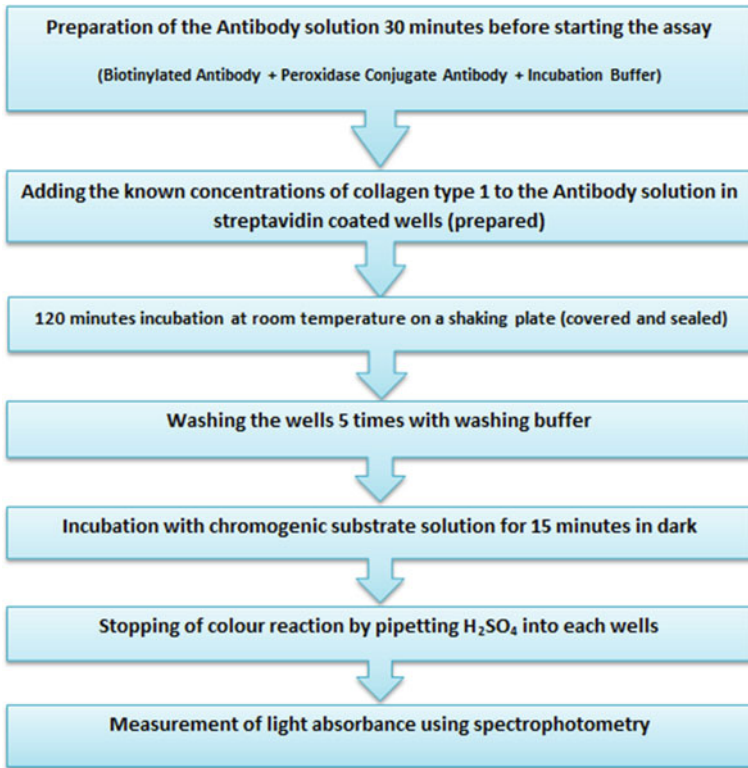
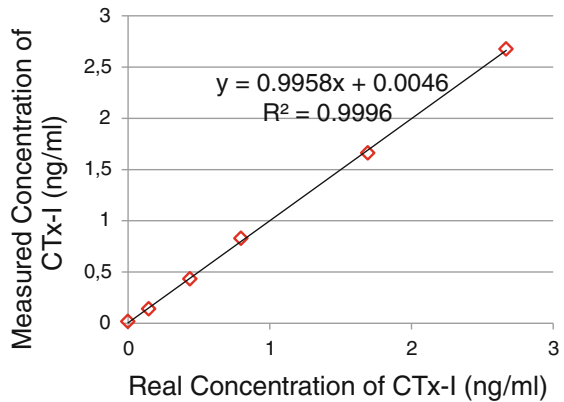


Fig. 14 ELISA procedure

Fig. 15 The standard curve of ELISA



6 Experiments Using the Developed Sensing System

In order to develop a successful smart sensing system the sensor is required to be selective to CTx-I and should be able to attract and attach the CTx-I for detection and quantification purpose. Antigen-antibody based technique was used to make the sensor selective for a particular analyte (CTx-I). Biotinylated antibody, peroxidase conjugated antibody and standard antigens from an ELISA kit were also used for the developed sensing system and Streptavidin-agarose was purchased from Sigma-Aldrich, USA. The same procedure as ELISA was followed to prepare the antigen-antibody solution.

6.1 Experimental Set up

The experimental setup consisted of a high precision LCR meter (Hioki 3532-50 LCR Hi Tester) which was connected to the computer through RS232 port, a digital thermometer and humidity meter, the sensor and material under test (MUT). The sensor was connected to the excitation and sensing probes via gold contact clamp pin connector. The block diagram and the experimental setup are shown in Fig. 16.

EIS experiments were performed using Hioki 3532-50 LCR Hi Tester. All experiments were carried out using slow mode of the testing equipment. EIS experiments were performed using Hioki 3532-50 LCR Hi Tester. All experiments were performed using slow mode of the testing equipment. A Vrms of a unit magnitude of the sinusoidal signal with a frequency sweep between 42 and 100 kHz was applied to the sensor via gold plated pins developed to avoid soldering the electrodes. Each experiment was repeated three times, and the average of them used to ensure the reliability and reproducibility of the results.

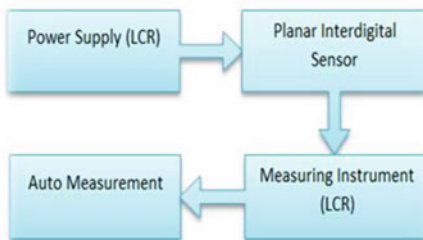


Fig. 16 The block diagram of measurement system and the experimental setup

6.2 Sensor Functionalization and EIS Testing

The initial step began with profiling the bare interdigital sensor in air in order to characterize the sensor and determine the optimal frequency range. After that, the sensor was functionalized by coating the sensing area of the sensor with 4 μL of streptavidin agarose and then the sensor was characterized using EIS technique to see the changes with respect to the uncoated sensor. Actually, streptavidin agarose behaves as a cross-linker between the electrodes and antibodies. In the next stage, the antibody-antigen solution was prepared the same as ELISA. The prepared solution was then incubated for an hour before pipetting 8 μL of that on the sensing surface which was coated with streptavidin. Then, another gap of one hour was given before the sensor was washed five times with a washing buffer solution. Finally, the profiling of the sensor was done using EIS technique and the LCR meter.

Figure 17 shows the schematic of the steps required to prepare the biosensing surface for the selective binding of CTx-I molecules on the electrode surface.

6.2.1 Results and Discussions

Five known concentration samples (0, 0.147, 0.437, 0.798 and 1.693 ppb) were tested with the developed sensing system. The standard solution with zero concentration of CTx-I was considered as the control. Experiments were performed at room temperature with a humidity level of 31 %. Sample testing by developed sensing system was performed immediately after preparing the solutions. Figure 18 shows the imaginary part of the impedance in the frequency domain for all five CTx-I concentrations. As illustrated in the figure, the capacitive reactance (Z_{imag}) shows a drastic variation—especially in at lower frequencies—with a change in CTx-I concentration which is attributed to the dielectric properties of the MUT.

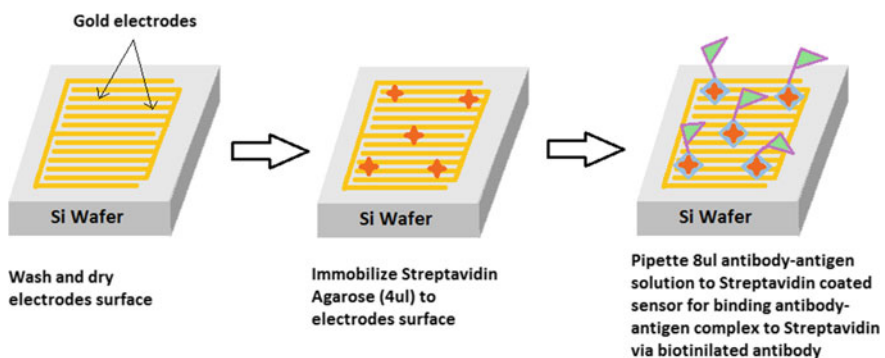


Fig. 17 Graphical illustration of the steps required to prepare the sensing surface for CTx-I sensing

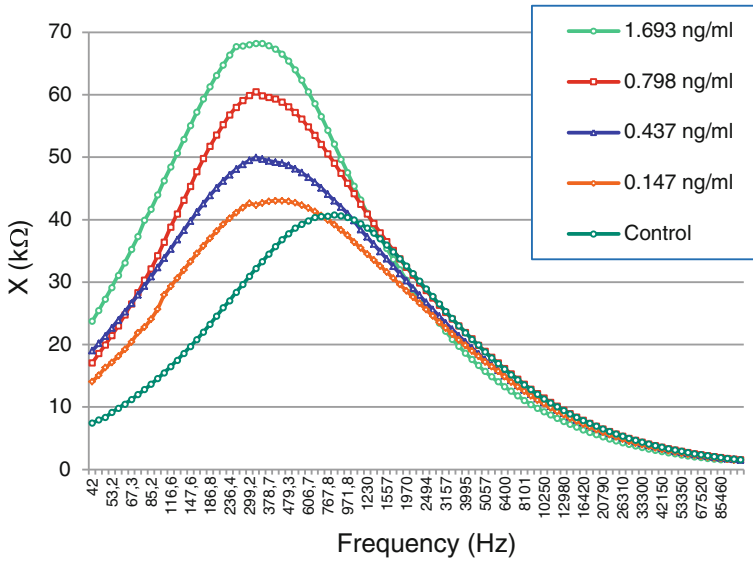


Fig. 18 Imaginary part of impedance versus frequency

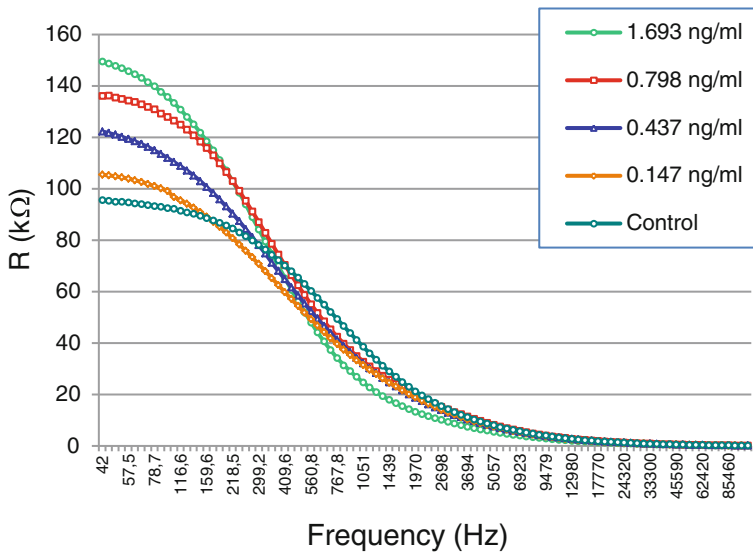


Fig. 19 Real part of impedance versus frequency

The real part of impedance vs. frequency for different concentration of CTx-I is plotted in Fig. 19. Not much variation can be observed in the real part of the impedance (Z_{real}) which is related to the Faradic current and the ionic properties of

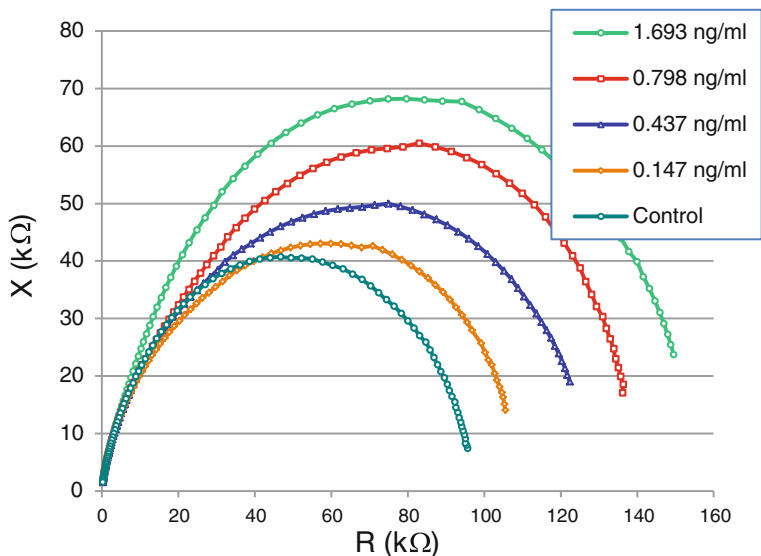


Fig. 20 Nyquist plot for different CTx-I concentrations

the sample. Figure 20 shows the Nyquist plot for the impedance spectrum obtained for all five concentration of CTx-I in a frequency range of 42–100 kHz. It is observed that the diameter of the semicircle increases by increasing the concentration of CTx-I.

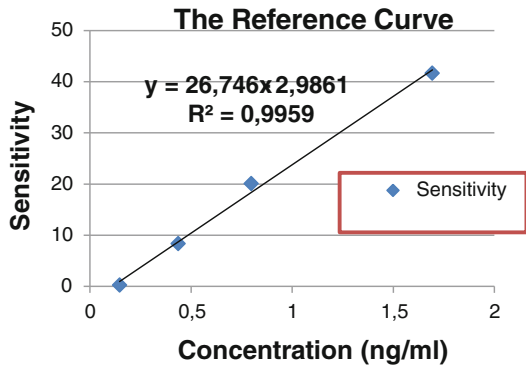
The sensitivity of sensor was calculated by using the reactance data using the following equation:

$$Sensitivity(\%) = \frac{Z_{imag}(Control) - Z_{imag}(Sample)}{Z_{imag}(Control)} \times 100$$

A reference curve was obtained by plotting the sensitivity against the concentration at a particular frequency (700 kHz) that was selected from the sensitive area of frequency, which is shown in Fig. 21. This curve can be used to determine the concentration of CTx-I in any unknown concentration sample.

Two samples from sheep blood plasma were measured using the developed sensing system; the concentration of CTx-I was determined as 0.6229 ppb for the first sample and 0.5280 ppb for the second one. The results were compared with the results obtained from the ELISA technique with the error of 4.3 % for the first sample and 4.6 % for the second sample.

Fig. 21 Reference curve for the sensitivity of the sensor versus concentration



6.2.2 Complex Nonlinear Least Squares Curve Fitting

Complex non-linear least square method (CNLS) has been used to estimate the equivalent circuit and component parameters by fitting the experimental data to its theoretically estimated response based on Randle’s model. It interprets the processes executing inside a chemical cell into its equivalent circuit. The fitted Nyquist plot is given in Fig. 22 where the points on the graph represent the experimentally observed data and the line shows the theoretically fitted response for the equivalent circuit. The proposed equivalent circuit for the electrochemical processes is shown in Fig. 23.

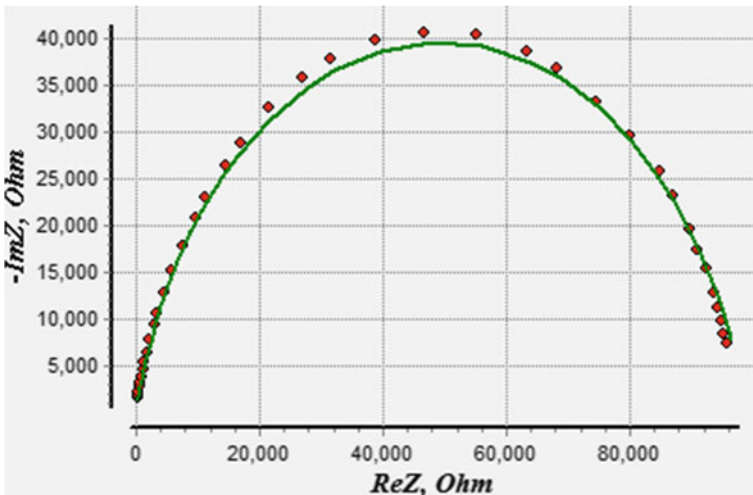
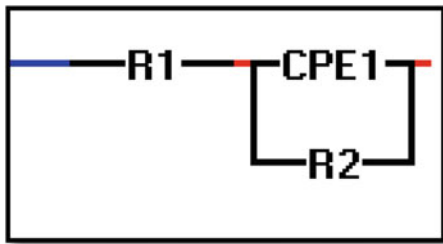


Fig. 22 CNLS fitted curve of Nyquist plot

Fig. 23 Proposed equivalent circuit by CNLS



The algorithm uses statistical analysis to calculate the residual mean square $r_{amplitude}^2$ for experimentally observed values in measured spectra by complex nonlinear least square using following relation [47, 48].

$$r_{amplitude}^2 = \sum_{i=1}^N \frac{(Z'_{iobs} - Z'_{icalc})^2 + (Z''_{iobs} - Z''_{icalc})^2}{Z'_{iobs}{}^2 + Z''_{iobs}{}^2} \quad (1)$$

where

Z'_{iobs} The observed real impedance

Z'_{icalc} The calculated real impedance

Z''_{iobs} The observed imaginary impedance

Z''_{icalc} The calculated imaginary impedance

$r_{amplitude}^2$ shows the deviation of the experimentally observed value from the optimal solution

Table 2 shows estimated component parameters of the equivalent circuit. CPE1 is constant phase element, P and n are parameters of constant phase element, representing pre-exponential factor and exponent, respectively. Since n is near to one, CPE1 behaves as a capacitor [49]. The error was <2.8 % for the equivalent circuit parameters.

Table 2 Equivalent circuit parameters

Component parameters	0.147 ng/ml	0.437 ng/ml	0.798 ng/ml	1.693 ng/ml
R1(Ω)	1.790E-14	1.686E-14	1.657E-14	1.660E-12
R2(Ω)	1.153E05	1.347E05	1.480E05	1.596E05
P1	1.535E-08	1.588E-08	1.036E-08	6.464E-09
n1	0.7944	0.7944	0.8345	0.8823
$r_{amplitude}^2$	0.0133	0.0100	0.0161	0.0246

7 Conclusion

Five known standard solutions were tested using the proposed sensing system, using them a reference curve was plotted which could be used to measure the concentration of CTx-I of any unknown sample. After that, the concentration of CTx-I of two unknown samples was measured using the developed system and the results were compared with the results of ELISA where the error was $< 5\%$ for the proposed sensing system.

References

1. I.O. Foundation. Available: <http://www.iofbonehealth.org/>. Last accessed on 16 May 2016
2. L.J. Melton, E.A. Chrischilles, C. Cooper, A.W. Lane, B. L. Riggs, How many women have osteoporosis? *J. Bone Min. Res.* **20**, 886–892 (2005)
3. J. Kanis, O. Johnell, A. Oden, I. Sernbo, I. Redlund-Johnell, A. Dawson et al., Long-term risk of osteoporotic fracture in Malmö. *Osteoporos. Int.* **11**, 669–674 (2000)
4. A. Khan, M. Fortier, Osteoporosis in menopause. Review date: 2014-Sept, 2014
5. R. Müller, Bone microarchitecture assessment: current and future trends. *Osteoporos. Int.* **14**, 89–99 (2003)
6. M.J. Seibel, S.P. Robins, J.P. Bilezikian, *Dynamics of Bone and Cartilage Metabolism: Principles and Clinical Applications* (Academic Press, 2006)
7. K.I. Mac Pherson, Osteoporosis and menopause: a feminist analysis of the social construction of a syndrome. *Adv. Nurs. Sci.* **7**, 11–22 (1985)
8. A. Srivastava, G. MacFarlane, V. Srivastava, S. Mohan, D. Baylink, A new monoclonal antibody ELISA for detection and characterization of C-telopeptide fragments of type I collagen in urine. *Calcif. Tissue Int.* **69**, 327–336 (2001)
9. A. Papaioannou, S. Morin, A.M. Cheung, S. Atkinson, J.P. Brown, S. Feldman et al., 2010 clinical practice guidelines for the diagnosis and management of osteoporosis in Canada: summary. *Can. Med. Assoc. J.* **182**, 1864–1873 (2010)
10. R.I. Gafni, J. Baron, Overdiagnosis of osteoporosis in children due to misinterpretation of dual-energy x-ray absorptiometry (DEXA). *J. Pediatr.* **144**, 253–257 (2004)
11. DXA. Available: <http://www.medbroadcast.com/Procedure/GetProcedure/Bone-Mineral-Density-Scan#detailedimage1>. Last accessed on 20 September 2016.
12. R.H. Christenson, Biochemical markers of bone metabolism: an overview. *Clin. Biochem.* **30**, 573–593 (1997)
13. S. Paulie, H. Perlmann, and P. Perlmann, Enzyme-linked Immunosorbent assay. eLS (2003)
14. S.D. Gan, K.R. Patel, Enzyme immunoassay and enzyme-linked immunosorbent assay. *J. Invest. Dermatol.* **133**, e12 (2013)
15. A.S. Abu-Abed, R.G. Lindquist, Capacitive interdigital sensor with inhomogeneous nematic liquid crystal film. *Prog. Electromagnet. Res. B* **7**, 75–87 (2008)
16. A.V. Mamishev, K. Sundara-Rajan, F. Yang, Y. Du, M. Zahn, Interdigital sensors and transducers. *Proc. IEEE* **92**, 808–845 (2004)
17. Y. Chen, C. Zhu, M. Cao, T. Wang, Photoresponse of SnO₂ nanobelts grown in situ on interdigital electrodes. *Nanotechnology* **18**, 285502 (2007)
18. M.S.A. Rahman, S.C. Mukhopadhyay, P.-L. Yu, Novel planar interdigital sensors, in *Novel Sensors for Food Inspection: Modelling, Fabrication and Experimentation* (Springer, 2014), pp. 11–35

19. A.M. Syaifudin, K. Jayasundera, S. Mukhopadhyay, A low cost novel sensing system for detection of dangerous marine biotoxins in seafood. *Sens. ActuatorsB Chem.* **137**, 67–75 (2009)
20. A.M. Syaifudin, S. Mukhopadhyay, P. Yu, Electromagnetic field computation using COMSOL multiphysics to evaluate the performance of novel interdigital sensors. *Appl. Electromagnet. Conf. (AEMC)* **2009**, 1–4 (2009)
21. A.M. Syaifudin, M. Yunus, S. Mukhopadhyay, K. Jayasundera, A novel planar interdigital sensor for environmental monitoring, in *Sensors*, (IEEE, 2009), pp. 105–110
22. H. Arwin, Application of ellipsometry techniques to biological materials. *Thin Solid Films* **519**, 2589–2592 (2011)
23. Y. Yang, G. Chiesura, G. Luyckx, T. Vervust, F. Bossuyt, J. Vanfleteren, et al., In situ on-line cure monitoring of composites by embedded interdigital sensor, in *16th European Conference on Composite Materials (ECCM-16)* (2014)
24. A.I. Zia, A.M. Syaifudin, S. Mukhopadhyay, P. Yu, I. Al-Bahadly, C.P. Gooneratne, et al., Electrochemical impedance spectroscopy based MEMS sensors for phthalates detection in water and juices, in *Journal of Physics: Conference Series* (2013), p. 012026
25. A.I. Zia, S.C. Mukhopadhyay, P.-L. Yu, I. Al-Bahadly, C.P. Gooneratne, J. Kosel, Rapid and molecular selective electrochemical sensing of phthalates in aqueous solution. *Biosens. Bioelectron.* **67**, 342–349 (2015)
26. A. Zia, S. Mukhopadhyay, I. Al-Bahadly, P. Yu, C. P. Gooneratne, and J. Kosel, Introducing molecular selectivity in rapid impedimetric sensing of phthalates, in *Instrumentation and Measurement Technology Conference (I2MTC) Proceedings*, 2014 IEEE International (2014), pp. 838–843
27. A. Syaifudin, K. Jayasundera, S. Mukhopadhyay, A novel planar interdigital sensor based sensing and instrumentation for detection of dangerous contaminated chemical in seafood,” in *Instrumentation and Measurement Technology Conference, I2MTC’09* (IEEE, 2009), pp. 701–706
28. J. Fischer, H. Dejmekova, J. Barek, Electrochemistry of pesticides and its analytical applications. *Curr. Org. Chem.* **15**, 2923–2935 (2011)
29. M. Khafaji, S. Shahrokhian, M. Ghalkhani, Electrochemistry of levo-thyroxin on edge-plane pyrolytic graphite electrode: application to sensitive analytical determinations. *Electroanalysis* **23**, 1875–1880 (2011)
30. L. Li, F. Yang, J. Yu, X. Wang, L. Zhang, Y. Chen et al., In situ growth of ZnO nanowires on Zn comb-shaped interdigitating electrodes and their photosensitive and gas-sensing characteristics. *Mater. Res. Bull.* **47**, 3971–3975 (2012)
31. M. Dhull, A. Arora, Design of MEMS Based Microheater for Enhanced Efficiency of Gas Sensors. *J. Therm. Eng. Appl.* **2**, 16–21 (2015)
32. S.C. Mukhopadhyay, C.P. Gooneratne, A novel planar-type biosensor for noninvasive meat inspection. *Sens. J. IEEE* **7**, 1340–1346 (2007)
33. M.S.A. Rahman, S.C. Mukhopadhyay, P.-L. Yu, J. Goicoechea, I.R. Matias, C.P. Gooneratne et al., Detection of bacterial endotoxin in food: New planar interdigital sensors based approach. *J. Food Eng.* **114**, 346–360 (2013)
34. C. Xhoffer, K. Van den Bergh, H. Dillen, Electrochemistry: a powerful analytical tool in steel research. *Electrochim. Acta* **49**, 2825–2831 (2004)
35. C.V. Vidal, A.I. Muñoz, Effect of physico-chemical properties of simulated body fluids on the electrochemical behaviour of CoCrMo alloy. *Electrochim. Acta* **56**, 8239–8248 (2011)
36. X. Li, K. Toyoda, I. Ihara, Coagulation process of soymilk characterized by electrical impedance spectroscopy. *J. Food Eng.* **105**, 563–568 (2011)
37. C. Liu, Q. Bi, A. Leyland, A. Matthews, An electrochemical impedance spectroscopy study of the corrosion behaviour of PVD coated steels in 0.5 N NaCl aqueous solution: Part II.: EIS interpretation of corrosion behaviour. *Corros. Sci.* **45**, 1257–1273 (2003)
38. A. Ghasemi, V. Raja, C. Blawert, W. Dietzel, K. Kainer, Study of the structure and corrosion behavior of PEO coatings on AM50 magnesium alloy by electrochemical impedance spectroscopy. *Surf. Coat. Technol.* **202**, 3513–3518 (2008)

39. R. M. Souto, M. a. M. Laz, and R.L. Reis, Degradation characteristics of hydroxyapatite coatings on orthopaedic TiAlV in simulated physiological media investigated by electrochemical impedance spectroscopy. *Biomaterials*, **24**, 4213–4221 (2003)
40. D. Andre, M. Meiler, K. Steiner, C. Wimmer, T. Soczka-Guth, D. Sauer, Characterization of high-power lithium-ion batteries by electrochemical impedance spectroscopy. I. Experimental investigation. *J. Power Sources* **196**, 5334–5341 (2011)
41. F. Lisdat, D. Schäfer, The use of electrochemical impedance spectroscopy for biosensing. *Anal. Bioanal. Chem.* **391**, 1555–1567 (2008)
42. B.-Y. Chang, S.-M. Park, Electrochemical impedance spectroscopy. *Ann Rev Anal Chem* **3**, 207–229 (2010)
43. G. Instruments, Basics of electrochemical impedance spectroscopy, in *G. Instruments, Complex impedance in Corrosion* (2007), pp. 1–30
44. I.I. Suni, Impedance methods for electrochemical sensors using nanomaterials. *TrAC Trends Anal. Chem.* **27**, 604–611 (2008)
45. J.R. Macdonald, E. Barsoukov, Impedance spectroscopy: theory, experiment, and applications. *History* **1**, 8 (2005)
46. J.E.B. Randles, Kinetics of rapid electrode reactions. *Discuss. Faraday Soc.* **1**, 11–19 (1947)
47. A. Zia, A. Syaifudin, S. Mukhopadhyay, I. AlBahadly, P. Yu, C.P. Gooneratne, et al., MEMS based impedimetric sensing of phthalates, in *Instrumentation and Measurement Technology Conference (I2MTC)*, 2013 IEEE International (2013), pp. 855–860
48. M.S. Abdul Rahman, S. C. Mukhopadhyay, P.-L. Yu, J. Goicoechea, I.R. Matias, C.P. Gooneratne, et al., Detection of bacterial endotoxin in food: New planar interdigital sensors based approach. *J. Food Eng.* **114**, 346–360 (2013)
49. C. Hsu, F. Mansfeld, Technical note: concerning the conversion of the constant phase element parameter Y_0 into a capacitance. *Corrosion*, **57** (2001)

Cavitas Sensors (Soft Contact Lens Type Biosensor, Mouth-Guard Type Sensor, etc.) for Daily Medicine

Takahiro Arakawa and Kohji Mitsubayashi

Abstract We introduce “Cavitas sensors” attached to body cavities such as the contact lens and mouthguard. “No implantable” and “no wearable” sensors have many advantages for non-invasive daily medicine. *Cavitas* is the etymological origin of the word “cavity” in Latin. Hence collectively, *cavitas* sensors provide biological information from within a body cavity. Many types of contact lens (CL) sensors using electrical and optical methods have been developed for monitoring chemicals of glucose, lactate, electrical conductivity in tear fluid, and transcutaneous gases at eyelid mucosa. In addition, some mouthguard sensors have been investigated for a real-time measurement of chemicals in saliva. Here, we review the challenges regarding the integration of biosensors into monitoring for biological information and daily medicine of body cavities. The self-detachable cavitas sensors allow us to improve the quality of life and living standards in the near future.

1 Introduction

A measurement of biophysical quantities of human body has been investigated for the medical and health care fields. In particularly, many wearable sensors have been developed and commercialized in the world because of their perspectives for human monitoring of relevant parameters in health care, sports and medical applications [1, 2]. The majority of existing wearable devices focus on measurement and assessment of physical parameters. Utilization of biophysical information with the systems are expected to provide proactive management of health that can improve public health and reduce medical expenditure. However, the investigation of non-invasive measurement of chemical substances has been delayed and is required for collecting the biological information. The non-invasive chemical technique would also affect the

T. Arakawa · K. Mitsubayashi (✉)

Department of Biomedical Devices and Instrumentation, Institute of Biomaterials and Bioengineering, Tokyo Medical and Dental University, 2-3-10, Kanda-Surugadai, Chiyoda-ku, Tokyo 101-0062, Japan
e-mail: m.bdi@tmd.ac.jp

control of the physical condition in patients suffering from life-style related diseases. For example, self-monitoring of blood glucose (SMBG) is traditionally invasive, and is most commonly performed with finger-prick testing using a blood glucose meter for diabetic patients. However, the compliance often impaired due to the unpleasant, painful, carries a risk of infection and may induce anxiety or fear. Additionally, finger-prick testing only provides a single measurement. Continuous glucose monitoring can overcome these limitation, enable short-term fluctuations to be monitored, demonstrate immediate effects of dietary and therapeutic interventions [3]. Minimally invasive approaches to glucose monitoring might therefore offer a reasonable compromise, provides the required sensitivity and precision whilst minimize impact on quality of life. Though such approaches are sometimes critiqued for discomfort, the need for frequent calibration, and susceptibility to biofouling, effective biosensor design can overcome these limitations.

The bio/chemical samples excreted from human body are not only urine and feces, but include also sweat, expiratory air (breath), saliva, nasal secretion (rhinorrhoea), body odor and tears. Though urine and feces have been applied widely by clinicians, these samples do not provide sufficient biochemical information for daily health care. Human secretions provide information about the health and well-being of an individual. Extracting this information is the goal of developing non-invasive techniques for diagnosis and health care monitoring. From these point of views, the wearable sensors also have tremendous potential for evaluating chemical markers relevant to health or fitness [4, 5].

Recently, volatile chemicals in body gas from skin-surface and breath are focused as non-invasive and conventional approaches. The expiratory gas is the air which enters and leaves the lungs during respiration. The main function of breath is the gaseous exchange carried out between the blood and alveolar air during in- and ex-halation of air. Human expiratory components are considered to provide information about the health and reproductive status of an individual. If possible to develop the novel gas sensor with high sensitivity and selectivity for volatile substances, the expiratory air may be applied for diagnosing and monitoring disease states in human subjects. Various volatile organic compounds (VOCs) exist, such as those the transpired by humans, breath, body odor, smell of the living environment and aroma of food [6, 7]. Certain compounds, which are indicators of disease may also be metabolized by body, skin and breath [8]. The human body emits various non-volatile and volatile molecules, depending on a person's genetics, stress and immune status [9]. Human odor caused by the combined action of the skin gland and volatile organic compounds, which are regulated by human hormonal control and the bacterial population localized at skin surface [10]. Many sensor technologies employing enzymatic reactions have been developed, such as bio-sniffers (biochemical gas sensors) for gaseous chemicals involving ethanol, acetaldehyde (alcohol metabolism), trimethylamine (fish-odor syndrome), methylmercaptan (halitosis), actone (diabetes, lipid metabolism) [11–14]. Authors also developed an imaging system of gaseous ethanol based on bio-chemiluminescence and bio-fluorescence measurement employing an EM-CCD camera for imaging of body gaseous chemicals in breath air and transdermal human gas [15–19].

From 1990s, authors have paid attention to human body cavity [20, 21]. Our body has many body cavities such as cavitas oris (oral cavity), cavitas pharyngis, saccus lacrimalis, cavitas nasi, cavitas abdominalis, cavitas infraglotticum, cavitas larynges, cavitas oris propria, cavitas peritonealis, cavitas thoracis, cavitas tympanica, etc. Cavitas is the etymological origin of the word “cavity” in Latin.

Authors have developed many sensor devices to apply to the human cavities (cavitas oris, cavitas pharyngis, conjunctival sac) for non-invasive monitoring of biomedical information in the permanent body fluid in the human cavities. Then authors named and have called them “Cavitas sensors”. “Cavitas” is a new category of detachable medical sensors between “Implantable” and “Wearable” (Fig. 1) [22]. While the implantable one is the medical devices applied via the medical surgery (no detachable one by human subjects), the wearable one is detachable device applied by subjects themselves but no enough to collect the fruitful medical information. Recently, many cavitas sensors have been developed and commercialized in the world. Author’s belief that new consciousness of daily medicine (health care, Pre-symptomatic and Preventive Medicine) with cavitas and wearable sensors is necessary to improve the quality of life in view of the aging of society and the rapid changes in living environments. As the one of the examples, Parviz’s team developed contact lens amperometric glucose sensors with in-built wireless electronics for continuous data transmission [23, 24]. The device is now being currently developed by Google.

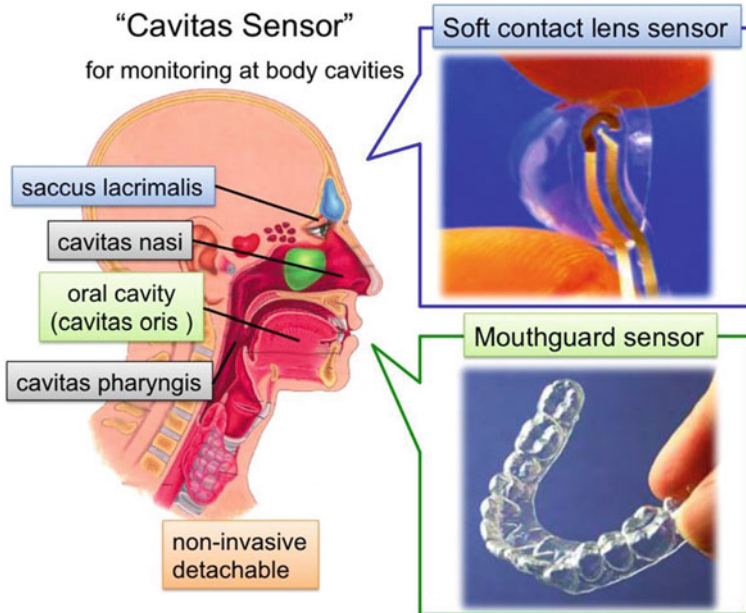


Fig. 1 Concept image of “Cavitas sensors” for detachable and non-invasive monitoring at body cavities

This chapter provides an update of various potential cavitas sensors and techniques and devices along with their advantages, challenges and future trends. Especially, authors focused oral cavitas sensors such as teeth sensor, mouthguard sensor for saliva analysis, and eye cavitas sensor such as contact lens type sensor for tear chemicals and eyelid transcutaneous gas at conjunctiva sac.

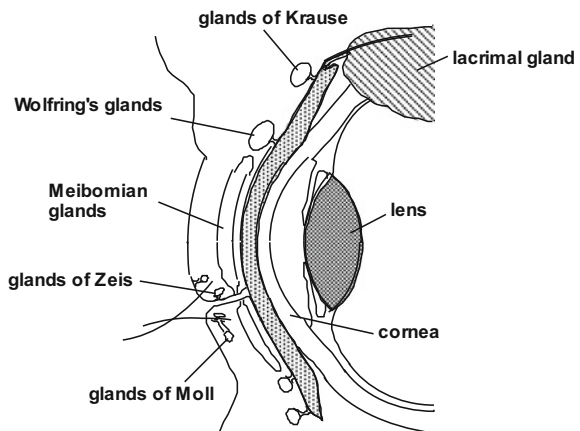
2 Contact Lens Sensors in Conjunctiva Sac

2.1 Tear Fluid

The pre-corneal and conjunctival tear film forms an interface between the air and ocular tissues (Fig. 2) [25]. The lacrimal secretory system has two components: (1) the large orbital and smaller palpebral portions of the lacrimal gland, which together account for about 95 % of the aqueous component of tears, and (2) the accessory lacrimal glands of Krause and Wolfring located in the conjunctival stroma [26]. Some important functions of tears are (a) lubrication of the eyelids, (b) formation of a smooth and even layer over an otherwise irregular corneal surface, and (c) provision of anti-bacterial systems for the ocular surface and nutrients for the corneal epithelium [26].

The lacrimal glands are innervated by parasympathetic fibers which are carried in the lacrimal nerve, a branch of the ophthalmic nerve. Excessive lacrimation is caused by abnormal stimuli to the cornea or conjunctiva, and also by sneezing, coughing, and psychic stimuli. Average specific gravity of 1.01 for tears has been reported, and the pH generally is around 7.4, but values from 5.2 to 8.3 have been observed because alkaline tears are shed after corneal injuries [27]. The quantity of electrolyte in tears is composed chiefly of Na^+ and Cl^- , though considerable K^+ also may be present (Na^+ 120–165 mmol/L, K^+ 20–42 mmol/L, and Cl^- 118–135 mmol/L) [28].

Fig. 2 Glands that produce tears sheathe the eye when the lids close [37]



The three principal tear proteins are lysozyme, lactoferrin, and tear-specific pre-albumin (TSP). Comparison with serum levels shows similar concentrations for Na^+ , Cl^- , HCO_3^- (20–42 mmol/L), Mg^{2+} (0.5–0.9 mmol/L), and urea. However, other electrolytes are present at markedly different levels: K^+ and lactate (2–5 mmol/L) are higher, and Ca^{2+} (0.4–1.1 mmol/L), glucose (0.1–0.60 mmol/L) and protein (5–9 mg/mL) are lower in tears than in serum [29].

Tear fluid to be used for chemical analysis is commonly collected by either filter paper or glass capillary pipettes. The samples are usually pooled and then analyzed by a variety of techniques. It is, however, recognized that precise estimations of the chemical composition, or the physical properties, of tear fluid are subject to large error owing to a number of factors. These include (1) the small sample size (approximately 7 μL) [30]; (2) evaporation during collection; (3) wide variability between individuals; (4) diurnal variations [31]; and, the most importantly, (5) the method of collection [28]. Despite many attempts to “standardize” tear collection, there are inherent flaws that make the collection of perfectly reliable and reproducible samples for analysis very difficult.

As mentioned above, the eye site with tear and conjunctiva sac are important for monitoring physiological chemicals and blood gases related the health condition and disease situation. The eye-cavity sensor at conjunctiva sac may be useful for being applied directly on the surface of the cornea (most sensitive organ) for monitoring the tear analyte without the several noted problems.

2.2 Tear Conductivity Sensor

Electrical conductivity is considered to be an indirect function of electrolyte activity, or osmolality [32]. The fluid-specific conductivity is the sum of the contributions from all charged species. At very low concentrations, the specific conductivity will vary nearly linearly with concentration [33]. The conductivity measurement would not distinguish among the types of ions present. But comparison between the conductivity values for several physical conditions and monitoring of fluctuations in fluid conductivity are possible [32], because the relative proportions of each ion are known for biologic fluids such as sweat, tears, saliva and airway fluid [34, 35]. Microfabrication technology for the manufacture of integrated circuits can produce planar integrated electrode arrays with areas on the order of a few square millimeters [36], decreasing the sample volume required to evaluate the conductivity of body fluid. Polyimide has been used as a substrate to achieve flexibility, but toxicity problems remain because of the use of substances such as chromium and nitric acid in the pre-position and etching stages of the microfabrication techniques used to obtain the desired integrated electrode patterns [32].

A safety and flexible sensor constructed in a sandwich configuration with a hydrophilic polytetrafluoroethylene membrane placed between two gold deposited layers was evaluated for use as a conductimetric sensor in biologic fluids [20].

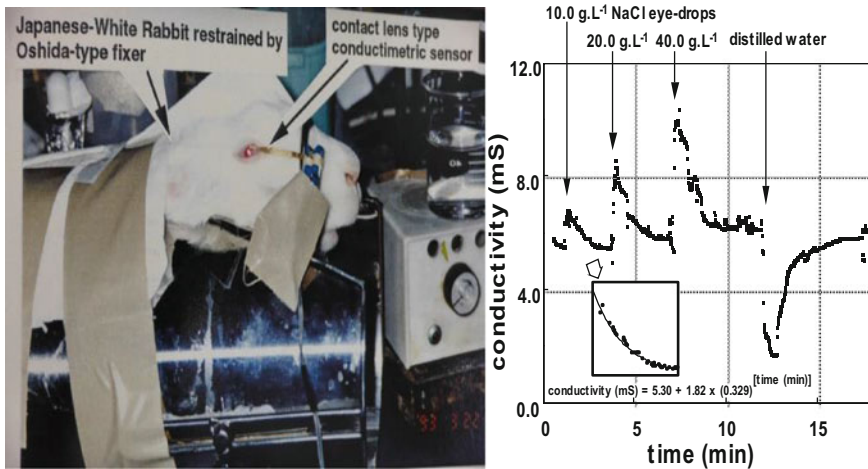


Fig. 3 *Left* photograph of flexible conductimetric sensor attached to rabbit eye. *Right* effect of 20.0 μL eye-drops (arrows; 10.0, 20.0, 40.0 g/L NaCl and distilled water) on tear conductivity. *Inset* figure enlargement of the response curve to eye-drops of 10.0 g/L NaCl and regression curve [20]

The conductivity was measured using the device at frequencies ranging from 100 Hz to 100 kHz, and the device was calibrated at 100 kHz against sodium chloride solutions over the range of 0.1–50.0 g/L, which include physiologic ion concentrations. Attached to a contact lens, the flexible conductimetric sensor can be placed directly onto the surface of the rabbit eye like contact lens to monitor the electrical conductivity of tear fluids. Tear flow with a mean turnover rate of 64.9 % per minute was elicited by eye-drops of high concentration sodium chloride and distilled water (Fig. 3).

As the physiological application, the flexible 3 mm-wide conductimetric sensor was placed inside the human subjects temporal lower cul-de-sac (similar to Schirmer test strip), and was used to evaluate electrolyte concentration and turnover rate in tear for normal, healthy volunteers (aged between 20 and 85 years) and patients suffering from Keratoconjunctivitis sicca (KCS) (aged between 50 and 69 years) in a normal, light indoor environment [21, 37] (Fig. 4).

The tear electrolyte concentration for normal eyes was calculated from tear conductivity to give a mean value of 297 mEq/L (S.D. 30 mEq/L; $n = 33$) which was consistently with previously reported values. The mean concentration of tear electrolyte for KCS eyes 325 mEq/L (S.D. 41 mEq/L; $n = 29$) was higher than that for normal eyes. Tear turnover rate was calculated by a single exponential equation of tear conductivity change, following the application to the eye-drops of 40.0 g/L sodium chloride solution.

The mean turnover rate was 40.4 % per minute (S.D. = 14.8 % per minute; $n = 86$), being in agreement with previously reported values. The mean tear turnover rate for KCS eyes (22.1 %/min, S.D. 7.4 %/min; $n = 19$) is extremely lower

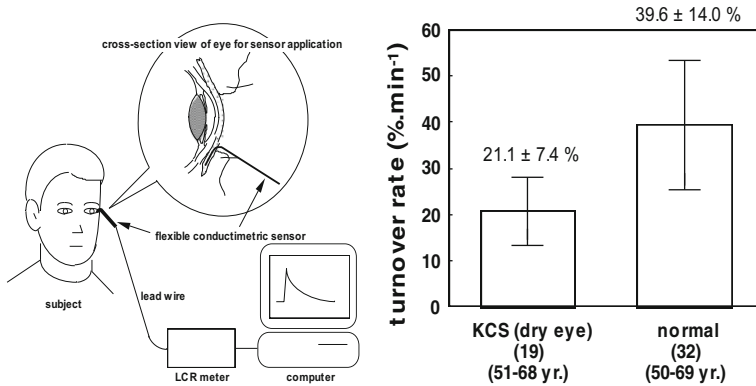


Fig. 4 Left schematic diagram of tear conductivity measurement at human conjunctiva. Right comparison of tear turnover rates between in KCS patient and normal eyes [21]

than that for control normal eyes (39.6 %/min, S.D. 14.0 %/min; n = 32, 50–69 years). The high electrolyte concentration and low turnover rates of tears for KCS eyes is considered to be related to the lower rate of tear secretion from lacrimal gland. The flexible sensor could be used for estimating the dynamics of tear flow with static and dynamic techniques.

2.3 Eyelid Transcutaneous Gas Sensor

A transcutaneous oxygen sensor has been in use for monitoring arterial oxygen pressure in premature infants to prevent Retinopathy of Prematurity at neonatal intensive care unit (NICU) [38, 39]. Commercially available sensors with a rigid cylindrical cell are fixed to the infant skin with adhesive plaster, thus resulting in common skin rashes and general discomforts on the infants. A new oxygen sensor with good flexibility and wearability, such as a clinical wet-pack, has been required for transcutaneous monitoring in comfort.

The conjunctiva has high gas penetration and supplies the cornea with oxygen [40, 41]. A conjunctival oxygen monitoring [42–44] was considered as a possible application for the new oxygen sensor, which would obviate the need of heating. Isenberg et al. evaluated a conjunctival oxygen monitor using 10 newborn subjects and published a pilot report in 2002 [45]. The correlation coefficient between conjunctival oxygen tension and pulse oximetry was significant ($p < 0.001$). Although the sensor unit they used was placed on the eye, the size of the sensor was too large for general application.

A thinner and flexible oxygen sensor as one of the Soft-MEMS (micro electrical mechanical system) devices was developed in order to monitor transcutaneous oxygen tension from conjunctiva [46–49]. The wearable oxygen sensor with

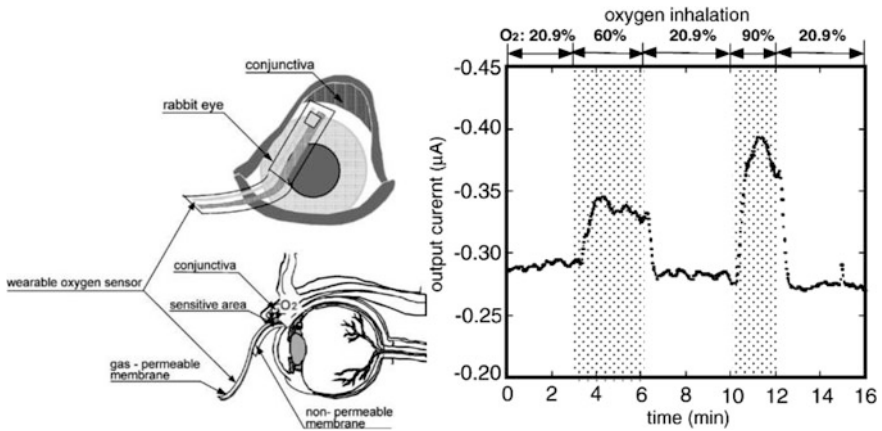


Fig. 5 Left illustration of affixing the wearable oxygen sensor at eyelid conjunctiva (upper figure) and cross section of attached sensor (lower figure). Right typical response of flexible sensor for transcutaneous oxygen monitoring (inhaled O_2 conc.: 20.9, 60, 90 %) at the rabbit conjunctiva [48]

membrane structure was constructed by pouching KCl electrolyte solution by non-permeable membrane and gas-permeable membrane with Pt- and Ag/AgCl electrode patterned by using photolithography and sputtering methods. The wearable oxygen sensor (width: 3 mm, thickness: 84 μm) was applied to the electrochemical measurement with a fixed potential of -550 mV versus Ag/AgCl, thus obtaining the calibration range to dissolved oxygen from 0.01 to 8.0 mg/L. The sensor was also evaluated in gas phase by purging with 10 % oxygen gas and the response time to reach 90 % of the steady current after purging was approximately 45 s, sensor outputs and responses were stable during repeated measurements at 3.66 % of the coefficient of variance. As the physiological application, the wearable sensor was placed onto a conjunctiva of a Japanese white rabbit without any thermoregulation. As an experiment, the rabbit inhaled standard air (20.9 %) and high concentration oxygen (60 and 90 %) (Fig. 5). As the result, sensor output increased and decreased synchronously with high concentration oxygen and standard air inhaling, respectively. This suggests that the sensor could be a new transcutaneous oxygen sensor.

3 Soft Contact Lens Type Biosensors for Tear Chemicals

Continuous glucose monitoring does not measure blood glucose directly, but rely instead on measurement of the glucose levels in other biological fluids [50]. With reference to continuous monitoring, relationships between general physical conditions and constituents of biological fluids such as tears, mucus, sweat and saliva

were reported [51–55]. For example, correlation between the glucose concentration in tears and blood glucose was reported [56]. Tear glucose level changes with a delay of approximately 5 min in comparison with blood sugar level [57]. On the other hand, authors reported a flexible electrochemical conductimetric sensor and oxygen sensors for bioinstrumentation on eye site [48, 58] in previous works.

In 1995, authors developed a flexible glucose sensor by immobilized glucose oxidase within a gold-coated, hydrophilic polytetrafluoroethylene membrane without the use of harmful substances in a simple fabrication process [59]. The sensor was calibrated against glucose solutions from 6.7 to 662 mg/L including tear sugar level. Non-uniform deposition of the gold layer using a mesh mask was more effective for immobilizing enzyme within the PVA-SbQ matrix, giving a device with high current output and excellent calibration characteristics. Ethanol sterilization had a negligible effect on output current and is therefore a suitable method for use in tear glucose sensing application.

If accompanying with optical transparency, the visible device would be placed to an eye-surface directly like contact lens. Authors previously developed a transparent and flexible oxygen electrode, constructed using microfabrication techniques with gas-permeable membrane and indium-tin oxide (ITO) electrode [58]. Then, a transparent and flexible glucose sensor was constructed using the visible oxygen electrode. The sensor device has flexible structure and good optical transparency (less than 0.6 abs) at the visible wavelength from 400 to 700 nm. The sensor was possible to be used for measuring glucose from 0.06 to 1.24 mmol/L (correlation coefficient: 0.999), including the reported concentration of tear glucose in normal (0.14 mmol/L), with good reproducibility.

As the physiological study, authors have constructed the tear glucose sensor for on-site tear sugar monitoring at eye site. The sensor was constructed by immobilizing GOD onto a flexible oxygen electrode (Pt working electrode and Ag/AgCl counter/reference electrode), which was fabricated using “Soft-MEMS” techniques onto a functional polymer membrane [60]. In purpose of bio-instrumentation, adhesive agents were not used for constructing the flexible biosensor. Linear relationship between glucose concentration and output current was obtained in a range of 0.025–1.475 mmol/L, with a correlation coefficient of 0.998. Based on the basic characteristics investigation, the glucose sensor was applied to measure glucose in tear fluids on an eye site of a Japan white rabbit. The change of tear glucose level induced by oral-administration of glucose was monitored as a current change of the sensor attached on the eye site. In this investigation, the tear glucose level varied from 0.16 to 0.46 mmol/L. Although there was a delay of several tens of minutes towards blood sugar level, it is considered to be possible that non-invasive continuous glucose monitoring can be realized using the flexible biosensor.

The most significant feature of the sensor is that flexible and biocompatible polymers were used for all structural members. In particular, phospholipid polymer, which is so-called MPC polymer, was used for the sensing region. MPC polymer has molecular configuration, which is similar to a cell membrane. Such a configuration was carried out by the techniques of polymer chemistry [61, 62]. Utilizing

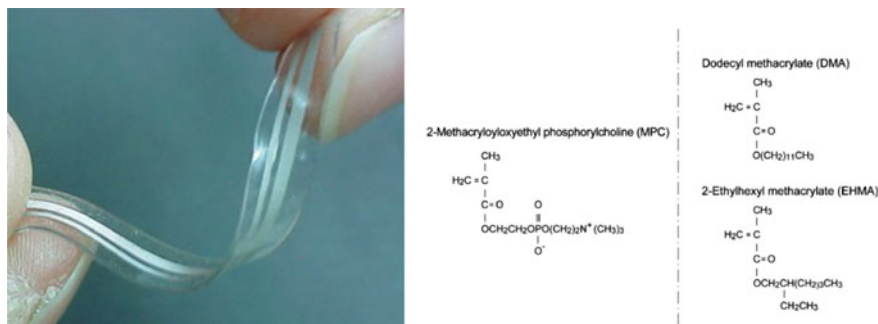


Fig. 6 Left photograph of flexible glucose sensor using functional polymers and electrodes (Pt and Ag/AgCl). Right chemical structures of monomers. 2-Methacryloyloxyethyl phosphorylcholine (MPC), dodecyl methacrylate (DMA) and 2-ethylhexylmethacrylate (EHMA) for biocompatible sensors [63, 64]

this sort of a polymer as a contacting part to measuring site, biocompatible sensor can be achieved. A novel biocompatible biosensor utilizes the physical and chemical functions of hydrophobic polydimethyl siloxane (PDMS) and hydrophilic 2-methacryloyloxyethyl phosphorylcholine (MPC) copolymerized with dodecyl methacrylate (DMA). The glucose sensor was constructed by immobilizing glucose oxidase (GOD) onto a flexible hydrogen peroxide electrode (Pt working electrode and Ag/AgCl counter/reference electrode) [63]. The electrodes were fabricated using ion beam sputtering technique onto those functional polymers. The sensor showed novel functions of flexibility and it was stretchable so that the sensor could normally work when it was released after expanding to 120 % longer than that of normal length. GOD was then immobilized onto the surface of the sensor using MPC polymer (Fig. 6).

Different type of biocompatible polymers, 2-methacryloyloxyethyl phosphorylcholine (MPC) copolymerized with 2-ethylhexylmethacrylate (EHMA): PMEHE was also evaluated as a sensitive membrane of biosensor (Fig. 6). The enzyme membrane was formed by immobilizing GOD onto a porous polytetrafluoroethylene (PTFE) membrane using the phospholipid polymer (PMEHE) [64]. The flexible glucose sensor using biocompatible polymer PMEHE also showed a linear relationship between output currents and glucose concentration in 0.05–1.00 mmol/L, with a correlation coefficient of 0.999, covering the normal tear glucose level of 0.14–0.23 mmol/L.

As the physiological approach, an ultra-soft contact lens (CL) biosensor for in situ monitoring of tear glucose was fabricated using Biocompatible PMEHE polymer and PDMS [65]. The CL biosensor was designed for in situ monitoring of tear glucose level. PDMS was used as the body material of the sensor. The soft PDMS contact lens (base curve radius: 8.6) was tentatively read using a wired line in the preclinical experiment (Fig. 7). The ultra-soft CL sensor showed a good flexibility and soft characteristics as a commercial available one. This device kept the electrical performance without electrical breaking after mechanical bending.

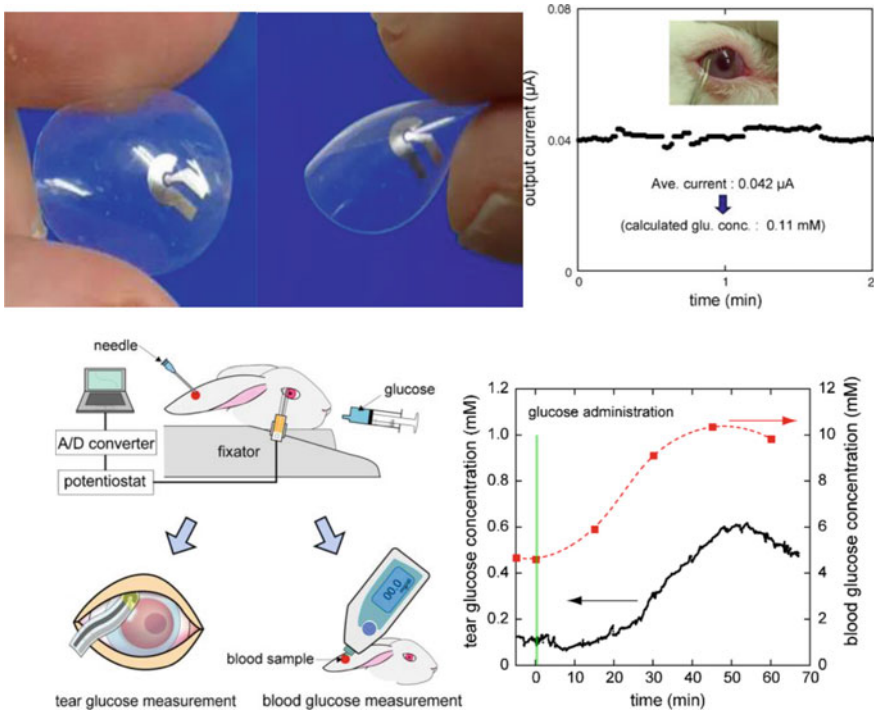


Fig. 7 Left-upper photographs of SCL biosensor showing the flexibility not only lens but also coated electrodes. Left-lower OGTT Comparison experiments between tear glucose by SCL biosensor and blood one by a commercially available test-kit. Right-upper stable tear glucose monitoring using CL biosensor on eye site (estimated to 0.11 mmol/L). Right-lower temporal changes both in tear and blood glucose [66]

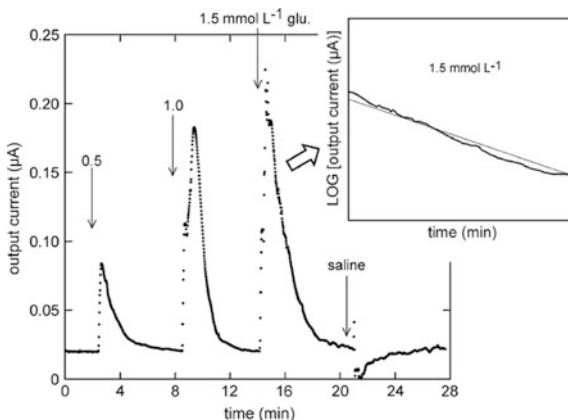
The SCL biosensor showed a good relationship between the output current and glucose concentration in a range of 0.03–5.0 mmol/L, with a correlation coefficient of 0.999. Also, the SCL biosensor was applied to a rabbit for the purpose of tear glucose monitoring. The SCL sensor succeeded to a real time measurement of tear glucose concentration which is approximately one-tenth of blood glucose one. The basal tear glucose was estimated to 0.11 mmol/L. Also, the change of tear glucose induced by the change of blood sugar level was assessed by the oral glucose tolerance test (OGTT). As a result, tear glucose level increased with a delay of 10 min from blood sugar level (Fig. 7). This result demonstrated the meaningful relationship between the tear sugar level and blood glucose one with the time delay. The result showed that the SCL biosensor is expected to provide further detailed information about the relationship between dynamics of blood glucose and tear glucose.

Novel ocular biomonitoring with the SCL-biosensor was also carried out. The SCL biosensor worn on the eye of the rabbit and the glucose levels in tear fluids were monitored in situ. The SCL biosensor was confirmed to be useful both in the static state and the dynamic state. According to the result of animal test, the tear glucose level of rabbit was estimated to 0.12 mmol/L. The tear turnover was evaluated using SCL-biosensor by an instillation of different glucose solutions 0.5, 1.0 and 1.5 mmol/L glucose, respectively. The peak current indicates instillation of glucose (Fig. 8). The inverse peak indicates dilution of tear glucose by instillation of physiological sodium chloride solution [67].

The tear turnover was calculated using semi-log regression curve. The rabbit's tear turnover rate due to secretion of fresh tears was $29.6 \pm 8.42 \%$ /min, which is slightly slower than the human quoted rate of 40 %/min. The result indicated that SCL-biosensor is useful for advanced biomonitoring on eye. Since PDMS is a flexible and workable polymer, the SCL-biosensor can be optimized to any surface of the human body. It is expected to realize 'ubiquitous biomonitoring' by further studies such as communication techniques.

There are a number of methods available to thwart the attacks mentioned here. These primarily involve the use of cryptographic protocols to ensure the confidentiality and authenticity of sensor data and network participants. Although these are the primary defences against attack, there exist other mechanisms that are useful for hindering some of the attacks, such as: Tuning of sensors to defend against overwhelming sensor stimuli and anti-replay and redundancy mechanisms to ensure defence against replay attacks through the use of a freshness counter. These mechanisms are outside the scope of the work presented here which concentrates on the use of basic cryptographic/security primitives for node and network protection.

Fig. 8 Temporal change of tear glucose level due to instillation of standard glucose (three higher peaks indicates instillation of 0.5, 1.0 and 1.5 mmol/L glucose, respectively). The inverse peak indicates dilution of tear glucose by instillation of physiological sodium chloride solution [67]



4 Mouthguard Sensors in an Oral Cavity

4.1 Salivary Fluids in a Human

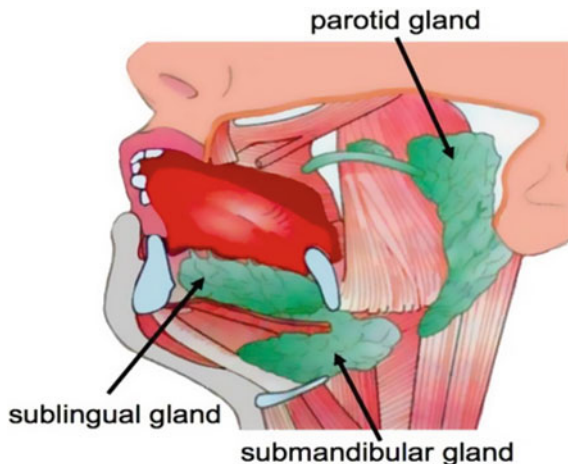
Although there are numerous small glands distributed over the buccal mucosa, saliva is secreted mainly by the parotid, the sub maxillary and sub lingual glands (Fig. 9). Parotid saliva is nonviscous; sublingual and sub maxillary saliva are viscous because of their mucoprotein content [68].

In general, saliva fluid includes many kinds of composition such as amino acids, ions, proteins, sugar, nucleotides, microorganism, etc. Saliva is also a complex biofluid comprising numerous constituents permeating from blood via transcellular or paracellular paths. Saliva have attracted the attention of several researchers to develop portable in vitro salivary diagnostic tools [69]. Saliva is a great diagnostic fluid providing an alternative to direct blood analysis via the permeation of blood constituents without any skin piercing for blood sampling.

4.2 pH Sensing

Continuous monitoring of pH in saliva would be extremely beneficial for maintaining healthy mouth conditions, e.g., degradation of tooth enamel [70] and detection of Gastroesophageal Reflux Disease (GERD) [71], as well as drug activity, as in some cases this can depend on saliva pH [72]. Zuliani, et al. reported on the preparation of a potentiometric strip based on a planar screen printed substrate for the direct measurement of pH in saliva samples [73]. The potentiometric strip consists of a solid contact pH-selective and of a solid-contact ionogel reference electrode prepared on a dual screen printed substrate. The screen printing protocols

Fig. 9 Schematic diagram of salivary glands [22]



were adjusted to relatively improve the batch reproducibility and the stability of the pH sensor. The pH of real saliva samples were monitored using the optimized potentiometric strip.

4.3 Salivary Uric Acid Sensor in Oral Cavity

Kim et al. has demonstrated a wearable salivary uric acid (UA) sensor using a mouthguard platform [74]. Salivary UA is a bio-indicator for some diseases, including hyperuricemia, gout, Lesch–Nyhan syndrome and renal syndrome [75]. Especially, high concentration of UA relate a future risk of type 2 diabetes and its severity and complications [76]. UA can also be an indicator of physical stress induced reactive oxygen species (ROS), acting as a free radical scavenger [77]. While blood UA (BUA) measurements require invasive blood collection, salivary uric acid (SUA) measurements could be carried out non-invasively and in a continuous real-time manner. Shibasaki et al. [78] and Soukup et al. [79] have found a good correlation of UA blood and saliva levels, demonstrating that this metabolite can be monitored in saliva in a non-invasive way without need for blood sampling. Kim et al. demonstrates the instrumented mouthguard capable of non-invasively monitoring salivary uric acid (SUA) levels (Fig. 10). The enzyme (uricase)-modified screen-printed electrode system has been integrated onto a mouthguard platform along with anatomically miniaturized instrumentation electronics featuring a potentiostat, microcontroller, and a Bluetooth Low Energy (BLE) transceiver. The BLE chipset has been adopted to enable wireless connectivity to a smart watch, smartphone, tablet, portable media player, laptop or any other BLE-enabled device.

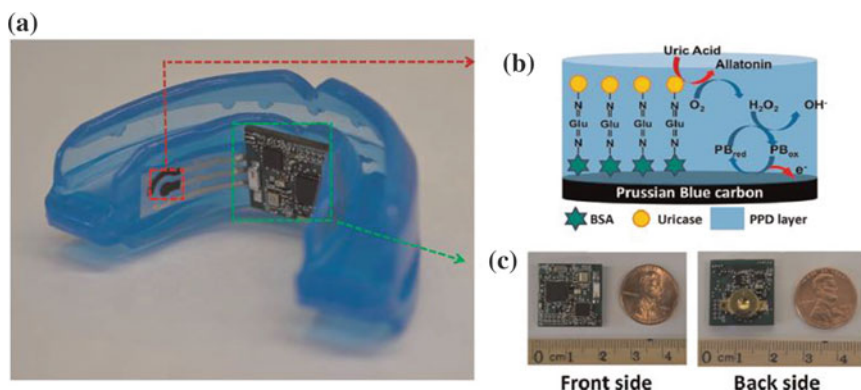


Fig. 10 **a** Photograph of mouthguard biosensor integrated with wireless amperometric circuit board. **b** Reagent layer of Prussian-Blue carbon working electrode containing uricase for SUA biosensor. **c** Photograph of the wireless amperometric circuit board: front (*left*) and back (*right*) [74]

Two watch batteries (2×1.55 V, 33 mAh each) in series were utilized as a power source on the mouthguard. The mouthguard biosensor system shows high sensitivity, selectivity, and stability towards uric acid detection in human saliva, covering the concentration ranges for both healthy people and hyperuricemia patients. The wireless mouthguard biosensor system has been reported to monitor SUA level in real-time.

4.4 *Glucose Sensor in Oral Cavity*

We have developed detachable “Cavitas sensors” to apply to the human oral cavity for non-invasive monitoring of saliva glucose [22]. Saliva glucose concentrations range approximately from 20 to 200 $\mu\text{mol/L}$ in normal and diabetic individuals, closely follow circadian blood glucose fluctuations [80], and offer promising opportunities for non-invasive monitoring [81]. Saliva and blood glucose levels correlate reasonably in a sample of individuals [82–85]. However, a much stronger correlation is observed within the same individual, enabling blood glucose concentrations to be estimated from saliva glucose measurements [86].

A salivary biosensor incorporating Pt and Ag/AgCl electrodes on a mouthguard support as dental material with an enzyme membrane was developed and tested. Electrodes are formed on the polyethylene terephthalate glycol surface of the mouthguard. The Pt working electrode is coated with a glucose oxidase (GOD) membrane. Figure 11 is a schematic image of the glucose biosensor on the polyethylene terephthalate glycol (PETG) mouthguard support. Pt and Ag electrodes were formed on the PETG through a sputtering process. Each electrode sensor consisted of a 0.20 mm^2 Pt working electrode and a 4.0 mm^2 Ag/AgCl reference/counter electrode, both insulated with PDMS on a 0.5 mm thick PETG layer. 30 units of GOD were applied to the sensing region of the working electrode. In order to optimize enzyme entrapment, 2.0 mL of 1.0 wt% PME solution was spread over the sensing region to form the PME overcoat. The biosensor seamlessly is integrated with a glucose sensor and a wireless measurement system. One watch battery (1.5 V button battery (SR716SW)) was utilized as a power source between the mouthguard materials inside of the cheek (Fig. 12). When investigating in vitro performance, the biosensor exhibits a robust relationship between output current and glucose concentration. In artificial saliva (Table 1) composed of salts and proteins, the glucose sensor is capable of highly sensitive detection over a range of 5–1000 $\mu\text{mol/L}$ of glucose, which encompasses the range of glucose concentrations found in human saliva (Fig. 13). Artificial saliva containing various proteins, was prepared from disodium hydrogen phosphate, anhydrous calcium chloride, potassium chloride, sodium chloride, urea and type II mucin from porcine stomachs according to a protocol reported by Fusayama et al. [87]. Authors demonstrated the ability of the sensor and wireless communication module to monitor saliva glucose in a phantom jaw imitating the structure of the human oral cavity. Stable and long-term real-time monitoring (exceeding 5 h) with the

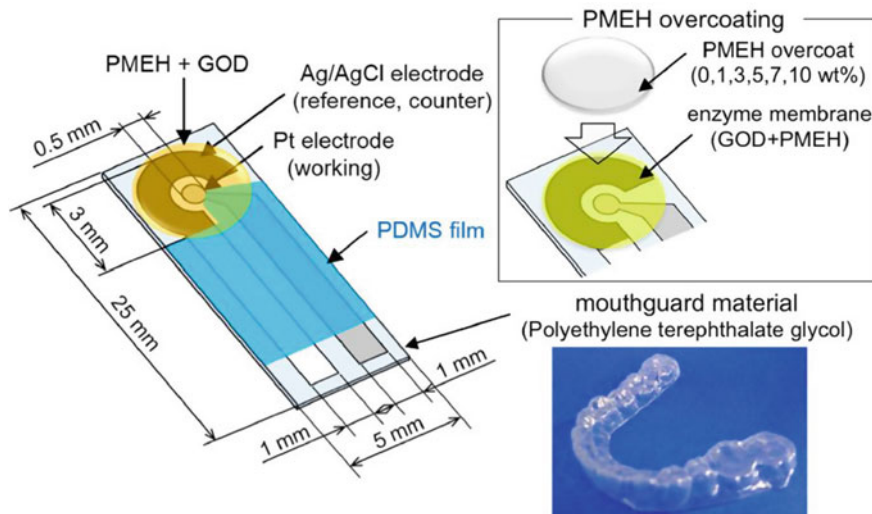


Fig. 11 Schematic image of the glucose biosensor on the polyethylene terephthalate glycol mouthguard support. Pt and Ag electrodes were formed on the PETG through a sputtering process. Each electrode sensor consisted of a 0.20 mm^2 Pt working electrode and a 4.0 mm^2 Ag/AgCl reference/counter electrode, both insulated with PDMS on a 0.500 mm thick PETG layer. 30 units of GOD were applied to the sensing region of the working electrode. In order to optimize enzyme entrapment, $2.0 \mu\text{L}$ of $1.0 \text{ wt}\%$ PMEH solution was spread over the sensing region to form the PMEH overcoat [22]

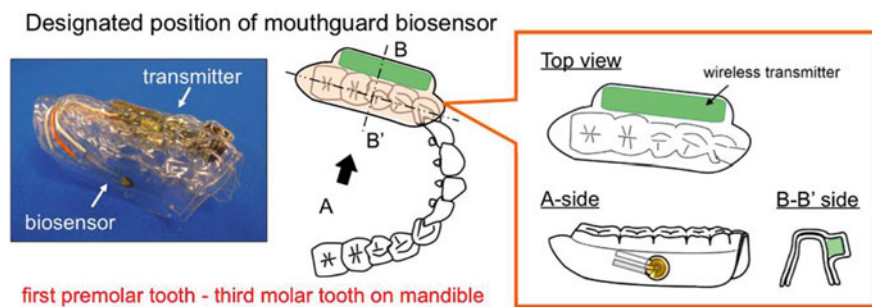


Fig. 12 Schematic image of the mouthguard biosensor to custom-fit the patient's dentition. The device consisted of a glucose sensor and wireless transmitter incorporating a potentiostat for stable glucose measurement. The wireless transmitter was neatly encased in PETG [22]

telemetry system is achieved. The mouthguard biosensor will be useful as a novel method for real-time non-invasive saliva glucose monitoring for better management of dental patients. In addition, selectivity of the mouthguard sensor was evaluated by comparing output current in response to $100 \mu\text{mol/L}$ glucose, galactose, fructose, mannitol, sorbitol and xylitol solutions after 180 s. The glucose sensor was

Table 1 Artificial saliva composition for evaluation of glucose sensor

Reagent	Composition (pH 7.4)	
	g/L	mmol/L
Disodium hydrogen phosphate	0.60	4.23
Calcium chloride (anhydrous)	0.60	5.41
Potassium chloride	0.40	5.37
Sodium chloride	0.40	6.84
Porcine mucin	4.00	—
Urea	4.00	66.6

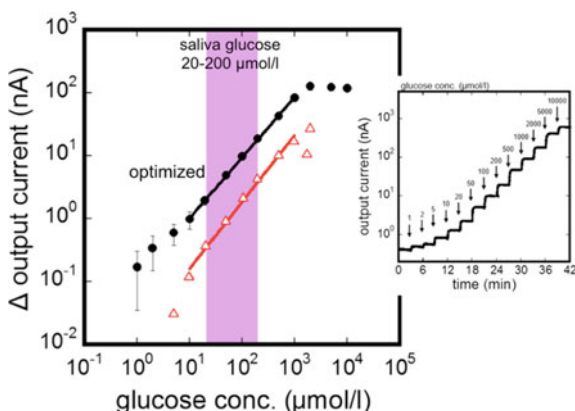


Fig. 13 Calibration curves of the optimized glucose sensor on PETG. An electrode area of 16.8 mm² and a 1.0 wt% PMEHL overcoat was identified as the optimum. The calibration range was 10–1000 μmol/L which encompassed the physiological saliva glucose range in humans (20–200 μmol/L). Output current of the glucose sensor without a PMEHL overcoat was substantially decreased, because of proteins in artificial saliva adhering to the electrode surface [22]

Fig. 14 Selectivity of the glucose sensors was evaluated by comparing mean relative output current in response to 100 μmol/l glucose, galactose, fructose, mannitol, sorbitol and xylitol solutions [22]

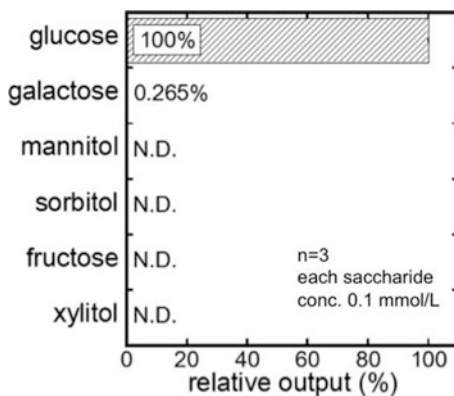




Fig. 15 Photographs (*front- and side-views*) of invisible “Smart mouth gear” for monitoring salivary glucose. The mouthguard biosensor to custom-fit the patient’s dentition. The device consisted of a glucose sensor and wireless BLE transmitter incorporating a potentiostat for stable glucose measurement. The wireless transmitter was neatly encased in PETG mouth guard material

shown to be highly selective for glucose based on the substrate specificity of GOD (Fig. 14). Fructose, mannitol, sorbitol and xylitol including some foods were not detected, producing a negligible output current less than 0.05 % of the magnitude of the output current produced by glucose. Galactose was detected to a minimal extent, producing an output current at 0.265 % of the magnitude of the output current produced by glucose.

In our laboratory, an invisible mouthguard biosensor using thinner and transparent dental materials integrated with small Bluetooth low energy (BLE) wireless module for real-time monitoring of saliva glucose has also been developed. This mouthguard type biosensor was integrated with a glucose sensor and BLE wireless measurement system. The electrodes were formed on the mouthguard surface which made of a transparent PETG.

Stable and long-term monitoring (more than 10 h) using telemetry system has been established. The thinner mouthguard biosensor would be useful for real-time, non-invasive and unconsciousness method for subject person as a novel health care management in dental field. And also this “Smart mouth gear” (Fig. 15) would be invisible from anyone and natural for future daily medicine.

5 Conclusion

The human secretions such as tear, saliva, sweat, body gas, etc. will provide important information about the health and well-being of an individual. Extracting this information is the goal of developing non-invasive techniques for diagnosis. Especially, the body cavities will be suitable site to monitoring the body chemicals related human diseases and conditions. “Cavitas sensor” such as the contact lens type and mouthguard sensor is a novel category of subject detachable devices for daily medicine, “no implantable” and “no wearable”. In the near future, many types of cavitas sensor would be developed and commercialized for managing the aging society in the world. The fabrication of the cavitas sensor is required to use safe, non-toxic, un-harmful chemicals and materials and techniques and to apply the right materials in human body sites (not only soft and flexible to skin and mucosa, but

also rigid and hard to tooth and bone). It is the author's belief that the daily medicine (Health care, Pre-symptomatic and Preventive Medicine) with cavitas and wearable sensors is necessary to improve the quality of life in view of the aging of society and the rapid changes in living environments.

References

1. E. Ghafar-Zadeh, *Sensors* **15**, 3236–3261 (2015)
2. S.R. Corrie, J.W. Coffey, J. Islam, K.A. Markey, M.A.F. Kendall, *Analyst* **140**, 4350–4364 (2015)
3. B.W. Bode, T. Battelino, *Int. J. Clin. Pract.* **64**(166), 11–15 (2010)
4. G. Matzeu, L. Florea, D. Diamond, *Sens. Actuators B: Chem.* **211**, 403–418 (2015)
5. A.J. Bandodkar, W. Jia, C. Yardımcı, X. Wang, J. Ramirez, J. Wang, *Anal. Chem.* **87**, 394–398 (2015)
6. A. Hierlemann, R. Gutierrez-Osuna, *Chem. Rev.* **108**, 563–613 (2008)
7. M. Shirasu, K. Touhara, *J. Biochem.* **150**(3), 257–266 (2011)
8. W. Miekisch, J.K. Schubert, F.E. Gabriele, G.F. Noeldge-Schomburg, *Clin. Chim. Acta* **347**, 25–39 (2004)
9. S.K. Pandey, K.H. Kim, *Trends Anal. Chem.* **30**(5), 784–796 (2011)
10. C.D. Natale, A. Macagnano, R. Paolesse, E. Tarizzo, A. Mantini, A. D'Amico, *Sens. Actuators, B* **65**, 216–219 (2000)
11. K. Mitsubayashi, K. Yokoyama, T. Takeuchi, I. Karube, *Anal. Chem.* **66**(20), 3297–3302 (1994)
12. K. Mitsubayashia, H. Matsunaga, G. Nishio, S. Toda, Y. Nakanishi, *Biosens. Bioelectronics* **20**, 1573–1579 (2005)
13. H. Kudo, X. Wang, Y. Suzuki, M. Ye, T. Yamashita, T. Gessei, K. Miyajima, T. Arakawa, K. Mitsubayashi, *Sens. Actuators B: Chem.* **161**(1), 486–492 (2012)
14. M. Ye, P.J. Chien, K. Toma, T. Arakawa, K. Mitsubayashi, *Biosens. Bioelectron.* **73**, 208–213 (2015)
15. X. Wang, E. Ando, D. Takahashi, T. Arakawa, H. Kudo, H. Saito, K. Mitsubayashia, *Talanta* **82**, 892–898 (2010)
16. X. Wang, E. Ando, D. Takahashi, T. Arakawa, H. Kudo, H. Saito, K. Mitsubayashi, *Analyst* **136**, 3680 (2011)
17. T. Arakawa, E. Ando, X. Wang, M. Kumiko, H. Kudo, H. Saito, T. Mitani, M. Takahashi, K. Mitsubayashi, *Luminescence* **27**, 328–333 (2012)
18. T. Arakawa, X. Wang, K. Kajiro, K. Miyajima, S. Takeuchi, H. Kudo, K. Yano, K. Mitsubayashi, *Sens. Actuators B Chem.* **186**, 27–33 (2013)
19. T. Arakawa, K. Kita, X. Wang, K. Miyajima, K. Toma, K. Mitsubayashi, *Biosens. Bioelectron.* **67**, 570–575 (2015)
20. K. Mitsubayashi, K. Yokoyama, T. Takeuchi, E. Tamiya, I. Karube, *Anal. Chem.* **65**, 3586 (1993)
21. K. Mitsubayashi, K. Ogasawara, K. Yokoyama, T. Takeuchi, T. Tsuru, I. Karube, *Technol. Health Care* **3**, 117–121 (1995)
22. T. Arakawa, Y. Kuroki, H. Nitta, P. Chouhan, K. Toma, S. Sawada, S. Takeuchi, T. Sekita, K. Akiyoshi, S. Minakuchi, K. Mitsubayashi, *Biosens. Bioelectron.* **84**, 106–111 (2016)
23. H. Yao, A.J. Shum, M. Cowan, I. Lähdesmäki, B.A. Parviz, *Biosens. Bioelectron.* **26**, 3290–3296 (2011)
24. Y.T. Liao, H. Yao, A. Lingley, B. Parviz, B. Otis, *IEEE J. Solid State Circ.* **47**, 335–344 (2012)
25. S.Y. Borelho, *Sci. Am.* **211**, 78–84 (1964)

26. E.R. Berman, *Biochemistry of the Eye* (Plenum Press, New York and London, 1991), pp. 63–88
27. A. White, *Principles of Biochemistry* (Mcgraw-Hill Kogakusha, Ltd., Tokyo, Japan, 1973), pp. 905–927
28. N.J. Haeringen, *Surv. Ophthalmol.* **26**, 84–96 (1981)
29. R.M. Stanifer, *Tear film, in Biochemistry of the Eye*, ed. by R.E. Anderson, Manuals Program (American Academy of Ophthalmology, San Francisco, 1983), pp. 7–22
30. S. Mishima, A. Gasset, S.D. Klyce Jr., *Invest. Ophthalmol. Vis. Sci.* **5**, 264–276 (1966)
31. R.J. Fullard, L.G. Carney, *Exp. Eye Res.* **38**, 15–26 (1984)
32. J.M. Fouke, A.D. Wolin, K.G. Saunders, M.R. Neuman, E.R. Jr, McFadden. *IEEE Trans. Biomed. Eng.* **35**, 877–881 (1988)
33. D.F. Evans, M.A. Matesich, *The measurement and interpretation of electrolytic conductance, in Techniques of Electrochemistry*, ed. by E. Yeager, A.J. Salkind (Wiley, New York, 1973), pp. 1–59
34. H. Shwachman, *Pediatrics* **32**, 85 (1963)
35. T. McKendrick, *Lancet* **1**, 183 (1962)
36. N.F. Sheppard Jr., R.C. Tucker, C. Wu, *Anal. Chem.* **65**, 1199–1202 (1993)
37. K. Ogasawara, K. Mitsubayashi, T. Tsuru, I. Karube, *Graefes Arch. Clin. Exp. Ophthalmol.* **234**, 542–546 (1996)
38. R. Huch, A. Huch, D.W. Lubbers, *J. Perinat. Med.* **1**, 183–191 (1973)
39. D.W. Lubbers, A. Huch, R. Huch, *Klin. Wschr.* **51**, 411–420 (1973)
40. W.C. Shoemaker, P.M. Lawner, *Crit. Care Med.* **11**, 946–947 (1983)
41. B.A. Weissman, I. Fatt, J. Rasson, *Invest. Ophthalmol. Vis. Sci.* **20**, 123–125 (1981)
42. S. Podolsky, J. Wertheimer, S. Harding, *Resuscitation* **18**, 31–36 (1989)
43. H. Haljamae, I. Frid, J. Holm, S. Holm, *Acta Anaesthesiol. Scand.* **33**, 610–616 (1989)
44. M. Brown, J.S. Vender, *Crit. Care Clin.* **4**, 493–509 (1988)
45. S.J. Isenberg, D. Neumann, S. Fink, R. Rich, *J. Perinat.* **22**, 46–49 (2002)
46. K. Mitsubayashi, T. Endo, S. Sasaki, I. Karube, *Anal. Sci.* **17**(Suppl.), i773/i775 (2000)
47. K. Mitsubayashi, Y. Wakabayashi, D. Murotomi, T. Yamada, T. Kawase, S. Iwagaki, I. Karube, *Sens. Actuators B Chem.* **95**, 373–377 (2003)
48. S. Iguchi, K. Mitsubayashi, T. Uehara, M. Ogawa, *Sens. Actuators B* **108**, 733–737 (2005)
49. H. Kudo, S. Iguchi, T. Yamada, T. Kawase, H. Saito, K. Otsuka, K. Mitsubayashi, *Biomed. Microdevices* **9**, 1–6 (2007)
50. G.S. Wilson, R. Gifford, *Biosens. Bioelectron.* **20**, 2388–2403 (2005)
51. K.M. Daum, R.M. Hill, *Invest. Ophthalmol. Vis. Sci.* **22**, 509–515 (1982)
52. S.F.P. Man, G.K. Adams, D.F. Proctor, *J. Appl. Physiol.: Respir. Environ. Exerc. Physiol.* **46**, 205–211 (1979)
53. K. Mitsubayashi, M. Suzuki, E. Tamiya, I. Karube, *Anal. Chim. Acta* **289**, 27–34 (1994)
54. A. Romano, F. Rolant, *Metab. Pediatr. Syst. Ophthalmol.* **11**, 78–85 (1988)
55. T.R. Stolwijk, J.A. van Best, H.H.P.J. Lemkes, R.J.W. de Keizer, J.A. Oosterhuis, *Int. Ophthalmol.* **15**, 377–381 (1991)
56. D.K. Sen, G.S. Sarin, *Br. J. Ophthalmol.* **64**, 693–699 (1980)
57. W.F. March, F.E. Smith, P. Herbrechtsmeier, A. Domschke, C. Morris, *Diabetes* **50**(Suppl.), A125 (2001)
58. K. Mitsubayashi, Y. Wakabayashi, S. Tanimoto, D. Murotomi, *Biosens. Bioelectron.* **19**, 67–71 (2003)
59. K. Mitsubayashi, J.M. Dicks, K. Yokoyama, T. Tamiya, I. Karube, *Electroanalysis* **7**(1), 83–87 (1995)
60. S. Iguchi, H. Kudo, T. Saito, M. Ogawa, H. Saito, K. Otsuka, A. Funakubo, K. Mitsubayashi, *Biomed. Microdevices* **9**, 603–609 (2007)
61. K. Ishihara, T. Ueda, N. Nakabayashi, *Polym. J.* **22**, 355–360 (1990)
62. K. Ishihara, H. Nomura, T. Mihara, K. Kurita, Y. Iwasaki, N. Nakabayashi, *J. Biomed. Mater. Res.* **39**(2), 323–330 (1998)

63. H. Kudo, T. Sawada, E. Kazawa, H. Yoshida, Y. Iwasaki, K. Mitsubayashi, *Biosens. Bioelectron.* **22**, 558–562 (2006)
64. H. Kudo, T. Yagi, M.X. Chu, H. Saito, N. Morimoto, Y. Iwasaki, K. Akiyoshi, K. Mitsubayashi, *Anal. Bioanal. Chem.* **391**, 1269–1274 (2008)
65. M.X. Chu, H. Kudo, T. Shirai, K. Miyajima, H. Saito, N. Morimoto, K. Yano, Y. Iwasaki, K. Akiyoshi, K. Mitsubayashi, *Biomed. Microdevices* **11**, 837–842 (2009)
66. M.X. Chu, K. Miyajima, D. Takahashi, T.o. Arakawa, K. Sano, S. Sawada, H. Kudo, Y. Iwasaki, K. Akiyoshi, M. Mochizuki, K. Mitsubayashia, *Talanta* **83**, 960–965 (2011)
67. M.X. Chu, T. Shirai, D. Takahashi, T. Arakawa, H. Kudo, K. Sano, S. Sawada, K. Yano, Y. Iwasaki, K. Akiyoshi, M. Mochizuki, K. Mitsubayashi, *Biomed. Microdevices* **13**, 603–611 (2011)
68. A. White, P. Handler, E.L. Smith, *Principles of Biochemistry* (Mcgraw-Hill Kogakusha, Ltd., Tokyo, Japan, 1973), pp. 905–927
69. A. Vasudeva, A. Kaushik, Y. Tomizawa, N. Norena, S. Bhansali, *Sens. Actuators B* **182**, 139–146 (2013)
70. A. Millward, L. Shaw, E. Harrington, A. Smith, *Caries Res.* **31**, 44–49 (1997)
71. D. Lazarchik, S. Filler, *Am. J. Med.* **103**, 107S–113S (1997)
72. S. Ghimenti, T. Lomonaco, M. Onor, L. Murgia, A. Paolicchi, R. Fuoco, L. Ruocco, G. Pellegrini, M.G. Trivella, F. Di Francesco, *PLoS ONE* **6**, e28182 (2011)
73. C. Zuliani, G. Matzeu, D. Diamond, *Electrochim. Acta* **132**, 292–296 (2014)
74. J. Kim, S. Imani, W.R. deAraujo, J. Warchall, G. Valdés-Ramírez, T.R.L.C. Paixão, P. Mercier, J. Wang, *Biosens. Bioelectron.* **74**, 1061–1068 (2015)
75. W.L. Nyhan, *J. Inherit. Metab. Dis.* **20**, 171–178 (1997)
76. A.I.J.L.I. Costa, I. Igual, J. Bedini, L. Quint, I. Conget, *Metabolism* **51**, 372–375 (2002)
77. Y. Hellsten, P.C. Tullson, E.A. Richter, J. Bangsbo, *Free Radic. Biol. Med.* **22**, 169–174 (1997)
78. K. Shibasaki, M. Kimura, R. Ikarashi, A. Yamaguchi, T. Watanabe, *Metabolomics* **8**, 484–491 (2012)
79. M. Soukup, I. Biesiada, A. Henderson, B. Idowu, D. Rodeback, L. Ridpath, K.G. Bridges, *Diab. Metab. Syndr.* **4**, 14 (2012)
80. M. Yamaguchi, M. Mitsumori, Y. Kano, *I.E.E.E. Eng. Med. Biol. Mag.* **17**(3), 59–63 (1998)
81. P. Mascarenhas, B. Fatela, I. Barahona, *PlosOne* **9**(7), e101706 (2014)
82. A. Sener, C. Jurysta, N. Bulur, B. Oguzhan, I. Satman, T.M. Yilmaz, W.J. Malaisse, A. Sener, *J. Biomed. Biotechnol.* 430426 (2009)
83. P. Abikshyeet, V. Ramesh, N. Oza, *TargetsTher.* **5**, 149–154 (2012)
84. C. Liu, Y. Sheng, Y. Sun, J. Feng, S. Wang, J. Zhang, J. Xu, D. Jiang, *Biosens. Bioelectron.* **70**(15), 455–461 (2015)
85. A. Soni, S.K. Jha, *Biosens. Bioelectron.* **67**, 763–768 (2015)
86. W. Zhang, Y. Du, M.L. Wang, *Sens. Bio-Sens. Res.* **4**, 96–102 (2015)
87. T. Fusayama, T. Katayori, S. Nomoto, *J. Dent. Res.* **42**, 1183–1197 (1963)

Development of Novel Image Sensor for Root Canal Observation

Masataka Fujimoto, Shinji Yoshii, Satoshi Ikezawa, Toshitsugu Ueda and Chiaki Kitamura

Abstract The development of dental instruments such as dental microscope and cone-beam computed tomography has greatly improved the precision of current dental treatments. However, observation of fractures near the apex collateral of the root canal remains difficult when using these instruments. In this study, we developed two types of probes: an ‘external-irradiation system’ and an ‘internal-irradiation system’. The external-irradiation probe is composed of an image fibre with a diameter of 500 μm and a gradient-index lens (GRIN lens) with the same diameter as the image fibre. The internal-irradiation probe is composed of an image fibre, GRIN lens, and five optical fibres for illumination, with diameters of 300, 250, and 65 μm , respectively. In an observation experiment of the resolution chart using these probes, both probes could observe lines and spaces of 10–100 μm using an external light source. To evaluate resolution, visibility was measured for each image, and higher visibility was observed as the lines and spaces were increased. We attempted to illuminate the observation area with optical fibres inside the probe; however, it was difficult because of the low intensity of the light. Furthermore, we observed the actual root canal of an extracted tooth. In future, we would like to redesign the GRIN lens and a suitable offset of the optical fibres.

1 Introduction

Dental caries without proper dental treatment reaches to the soft tissue, called dental pulp, which contains nerves and blood vessels. When a bacterial infection by dental caries reaches to dental pulp and the periodontal tissue at the apex of the tooth,

M. Fujimoto (✉) · S. Yoshii · C. Kitamura
Division of Endodontics and Restorative Dentistry, Kyushu Dental University,
Kitakyushu, Japan
e-mail: r12fujimoto@fa.kyu-dent.ac.jp

S. Ikezawa · T. Ueda
Graduate School of Information, Production and Systems, Waseda University,
Shinjuku, Japan

endodontic treatment is necessary [1]. During endodontic treatment, dentists remove all the caries and unnecessary parts to access the entrance of root canal. After the removal of the dental pulp inside the tooth, the root canals are washed with a cleaning solution. The entrance of the root canal is very small hole by the naked eye. However, a large part of the treatment relies on the hands of the dentist; therefore, the treatment is often performed blindly. In recent years, the development of a dental microscope enabled the observation of tooth fractures and narrowed root canals, which were previously difficult to observe [2–4]. Moreover, the three-dimensional diagnosis of teeth, along with the diagnosis of a range of peri-apical lesions that are difficult to observe in dental X-ray photographs, was enabled by the development of cone-beam computed tomography (CBCT) [5–10]. The development of these dental instruments has greatly improved the precision of dental treatment. However, despite these instruments, the observation of collaterals of the root canals and the fractures near the apex remains difficult. With the dental microscope, the entrance of the root canal is clearly visible, but not the apical part of the root canal. Also, CBCT lacks sufficient resolution to observe fine structures of the root canal.

Currently, small-diameter endoscopes are commercially available. However, they were applied for industrial use instead of dentistry. In addition, the irradiation intensity of the illumination light in these instruments is not uniform. Furthermore, the endoscopes have 3000 pixels, which is not sufficient for use in dental treatment.

Therefore, in previous studies [11–13] we presented the development of a novel dental endoscope for the observation of the fine structures of the root canals. The fabricated endoscope probe was constructed with only an image fibre, which has 15,000 pixels, and its diameter at the end was 600 μm . The images were captured using two methods. The first method is external irradiation, which illuminates the observation area using outside light. The other is internal irradiation, which uses illumination from the lights inside the image fibre. To evaluate the resolution, lines and spaces of 10, 20, 50, and 100 μm width were observed using both methods. However, observation was impossible unless the tip of the endoscope was in contact with the samples.

In this study, to solve the aforementioned problems of our previous endoscopes, we fabricated two new prototypes. We included a gradient index lens (GRIN lens), which is employed in various medical and research devices [14–17]. The first prototype—an external-irradiation system—had a high-resolution probe constructed using only an image fibre and a GRIN lens. The second prototype—an internal-irradiation system—was capable of illuminating the observation area and capturing the images with a single endoscope probe. By fabricating two probes, we attempt to observe a resolution chart and teeth that were already prepared for root canal treatment.

2 System Requirements

Figure 1 shows the final image of our endoscope. The objective image is transmitted to the opposite side of the image fibre and reaches a CMOS sensor. This CMOS sensor has full-color capability, a 2-megapixel lens, and video capture capability. The captured image is displayed on the monitor of a personal computer (PC) in real time. The optical fibre illuminates the observation area. In previous studies, we developed a dental endoscope to observe the fine structures of the root canals. However, because the probe was constructed using only an image fibre, observation was impossible unless the tip of the endoscope was in contact with the samples. In this study, we develop two types of probes to solve the aforementioned problems. The specification of the two types of probes are described in the following sections.

Considering the requirements of the endoscope, the diameter and resolution of the probe are the key points. Figure 6 is an illustration of the root canal model. Dentists perform root canal preparation at approximately 500–600 μm at the apical of the root canals. The entrance of the root canals is approximately 1 mm, and to insert the probe into the root canals, the entire diameter was chosen to be smaller than 600 μm . Next, we consider the resolution requirements. The diameter of collaterals and the width of the fractures is regarded as 50–100 μm . For the naked eye, we require four pixels for observation, and the diameter of the core of the image fibre is 4 μm . Therefore, a desirable resolution higher than 12–25 μm is chosen (Fig. 2).

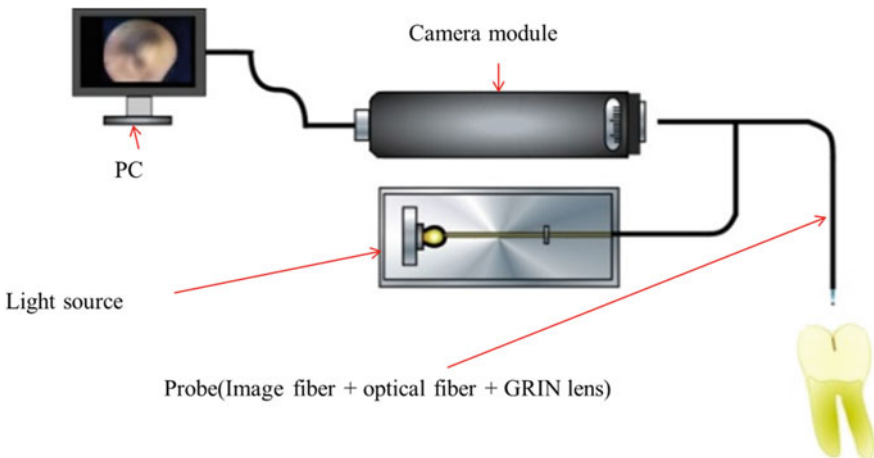
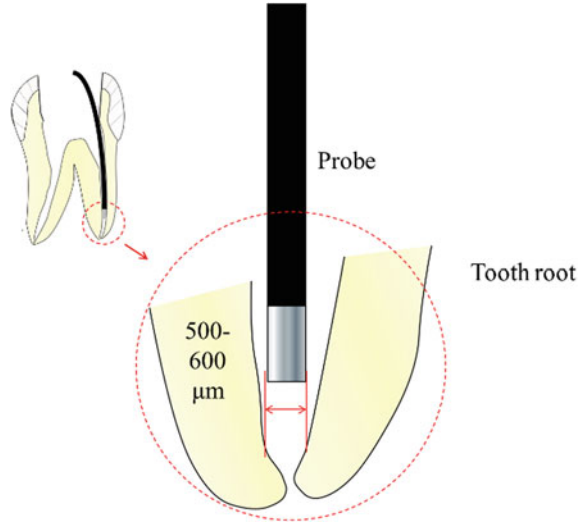


Fig. 1 Final image of our endoscope

Fig. 2 Model of the root canal



3 Experimental Setup of the External-Irradiation System

3.1 Gradient-Index Lens (GRIN Lens)

The GRIN lens is cylindrical and is used in several microscopes. A GRIN lens has a simple shape and low fabrication cost, which makes it easy to set up an optical system (Fig. 3).

This lens has been applied to various medical devices around the endoscopes and microscopes. The principle of the GRIN lens is similar to that of a mirage. The GRIN lens has a gradient of a certain refractive index, and the highest refractive index is placed on the centre axis of the lens. The light rays inside the GRIN lens draw a curve according to the gradient of the refractive index.

The imaging of the GRIN lens is shown using the following equations [18–20].

$$N(r) = n_0 \left(1 - \frac{\sqrt{A}}{2} r^2 \right)$$

Here, n_0 is the refractive index of the medium on the cylindrical axis, \sqrt{A} is the refractive-index-distribution constant, and r is the radius of the cylinder of the GRIN lens. The emitted light into the GRIN lens draws a curve and exits from the other end face. When the light travels through the lens, the ray propagates on a sine wave according to the meandering path. The length of the wave in one period is defined as one pitch of the GRIN lens. The working distance of the GRIN lens can be altered by the pitch of the GRIN lens, and the pitch of the GRIN lens depends on the lens length. The relationship between the pitch and lens length can be expressed by the following equation.

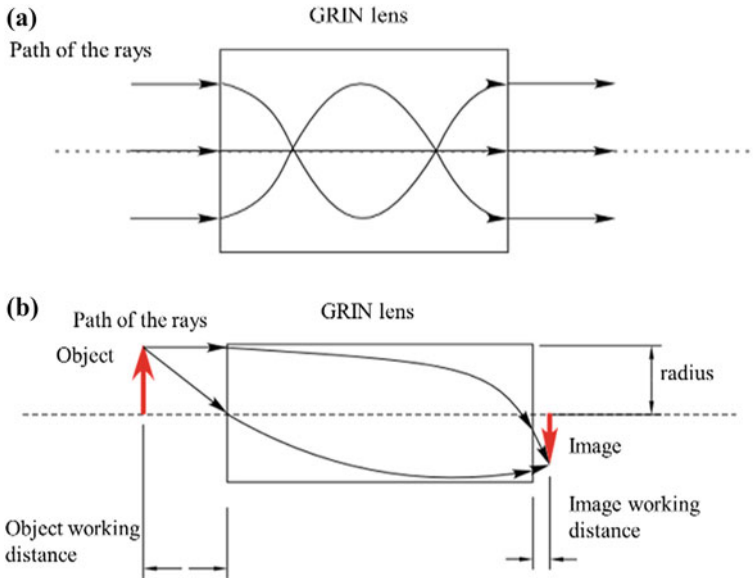


Fig. 3 a Path of rays inside the GRIN lens, and b imaging of the GRIN lens

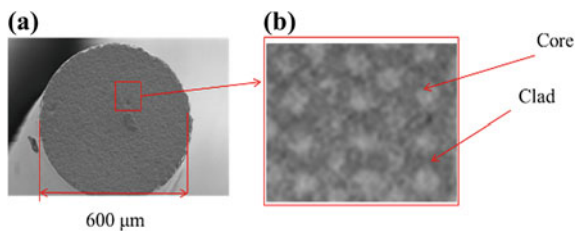
$$Z = \frac{2\pi P}{\sqrt{A}}$$

where Z is the length and P is the pitch of the GRIN lens.

3.2 Image Fibre

The image fibre is a bundle of fibres with a large number of small-diameter (4 μm) cores. The image fibre can transmit an image to the end surface of the fibre from the opposite side surface. A photograph of the cross section of the image fibre is shown in Fig. 4. The outermost layer is a silicone resin, and the image acquisition area is coated with acrylate resin in a quartz jacket.

Fig. 4 Photographs of the image fibre



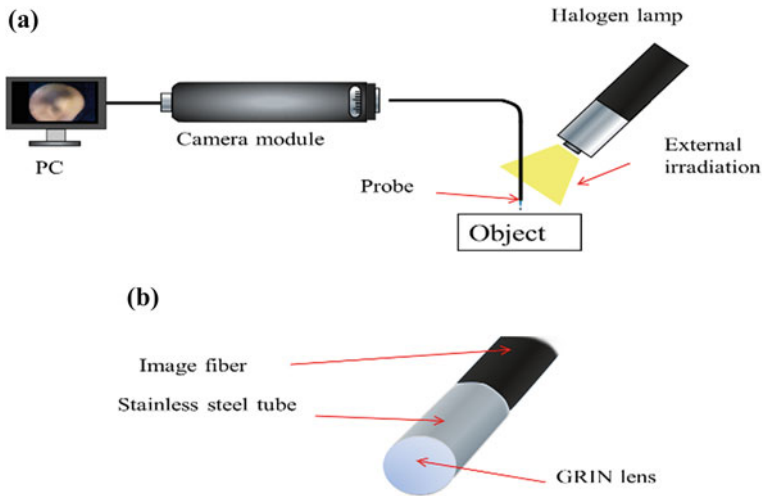


Fig. 5 **a** Endoscope with the external-irradiation system, and **b** illustration of the probe in the external-irradiation system

3.3 System Construction

The external-irradiation probe is constructed using the image fibre and GRIN lens. The used image fibre has 15,000 cores and a diameter of 600 μm . The GRIN lens has a 500 μm diameter, an image working distance of 0.0 mm, and a lens length of 0.75 mm. The pitch of the GRIN lens is 0.25λ . They were adhered inside of a stainless steel tube with an ultraviolet curable adhesive. These figures show the construction of the fabricated probe and a schematic diagram of the external-irradiation system. In this system, a halogen lamp from outside the system was used as the illuminating light for observation (Fig. 5).

3.4 Observation Method

Using the fabricated endoscope probe, an observation sample was observed. The endoscope probe was mounted on a stage capable of fine position adjustments shown in Fig. 6. The following figure shows the resolution chart used as an observation sample. This resolution chart has a grid-pattern with a line and space drawn at every 10, 20, 50, and 100 μm . In this experiment, the surface of the endoscope probe could capture the images by coming in contact with the sample surface. Therefore, we performed the observation experiments by filling 97 %-pure glycerol between the end of the probe and sample surface to increase the numerical aperture (NA) (Figs. 7 and 8).

Fig. 6 Situation of the observation experiments

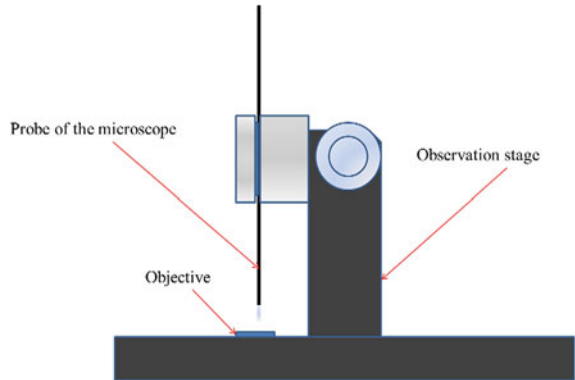
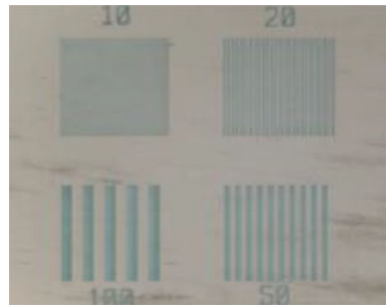


Fig. 7 Resolution chart



To compare our endoscope, we captured the images using a commercially available endoscope. The following figures show the results of the image observation.

As a result, the 50 and 100 μm lines and spaces can be observed; however, the 10 and 20 μm lines and spaces are not clearly visible.

4 Observation Results of the External-Irradiation System

Figure 9 is a photograph of the end of the probe. Using this probe, we captured images of the resolution chart, and the following figures are our observation results.

While observing the images with our endoscope, we noted that the tip of the probe was almost in contact with the surface of the resolution chart. Our endoscope system can observe all widths of the lines and spaces. The image captured by our system is clearer to the naked eye than the one captured using the commercially available endoscope (Fig. 10).

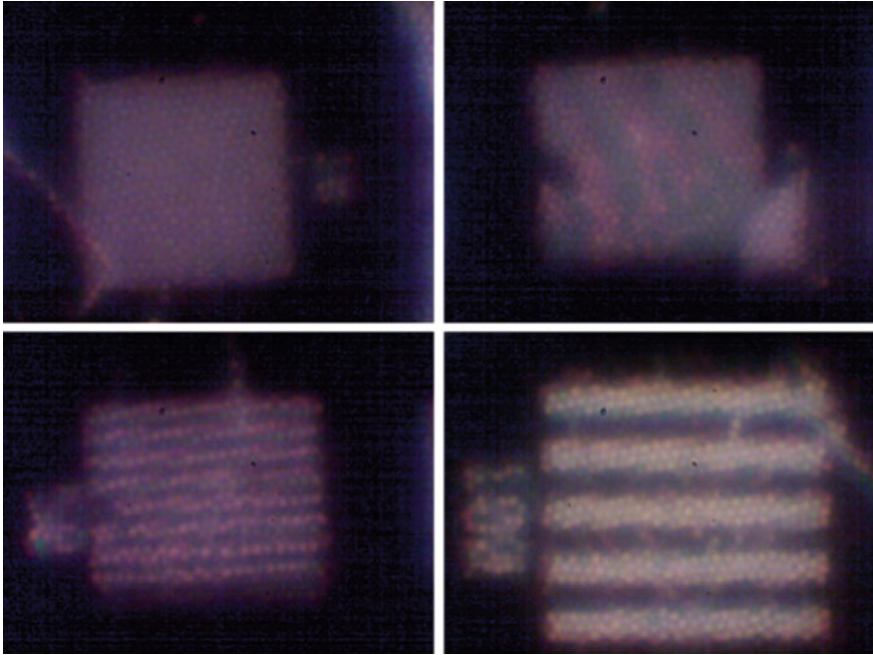


Fig. 8 Images captured using commercially available endoscope

Fig. 9 Photograph of our fabricated probe



5 Evaluation of the External-Irradiation System

For quantitative evaluation, the visibility for each image was measured. After trimming the acquired images, we converted them to greyscale images. In addition, we cut out a line at the centre of each image and analysed the visibility by

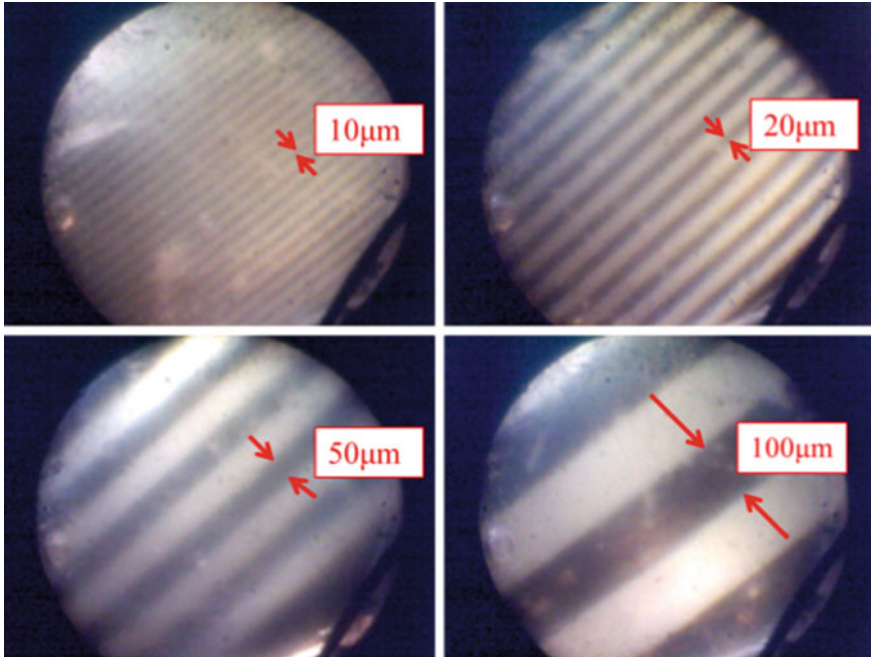


Fig. 10 Captured images using the external-irradiation system

calculating the greyscale value for each pixel on that line. The visibility is determined by the following equation.

$$Visibility = \frac{I_{max} - I_{min}}{I_{max} + I_{min}}$$

Here, I_{max} and I_{min} are the averages of the local maximum and minimum values of the visibility on the completed graph. Following are the evaluation methods for analysing the visibility.

First, the obtained images were rotated as the lines and spaces were parallel to the horizontal axis. The images were converted to greyscale and then rotated as the lines and spaces were parallel to the horizontal axis. The 400×400 -square-pixel centre section of the image was cut out. In Fig. 9, vertical lines are shown in the centre of the image, and the greyscale value of each pixel on the line was measured. Then, the greyscale value was plotted on the graph.

A slope correction was applied to the graph, and the result was approximated using a low-pass filter. The average maximum and minimum values of the final graph were substituted, and these values were applied to Eq. 1. For these calculations, we defined the average visibility. The following Figs. 11 and 12 are the final graphs of each image.

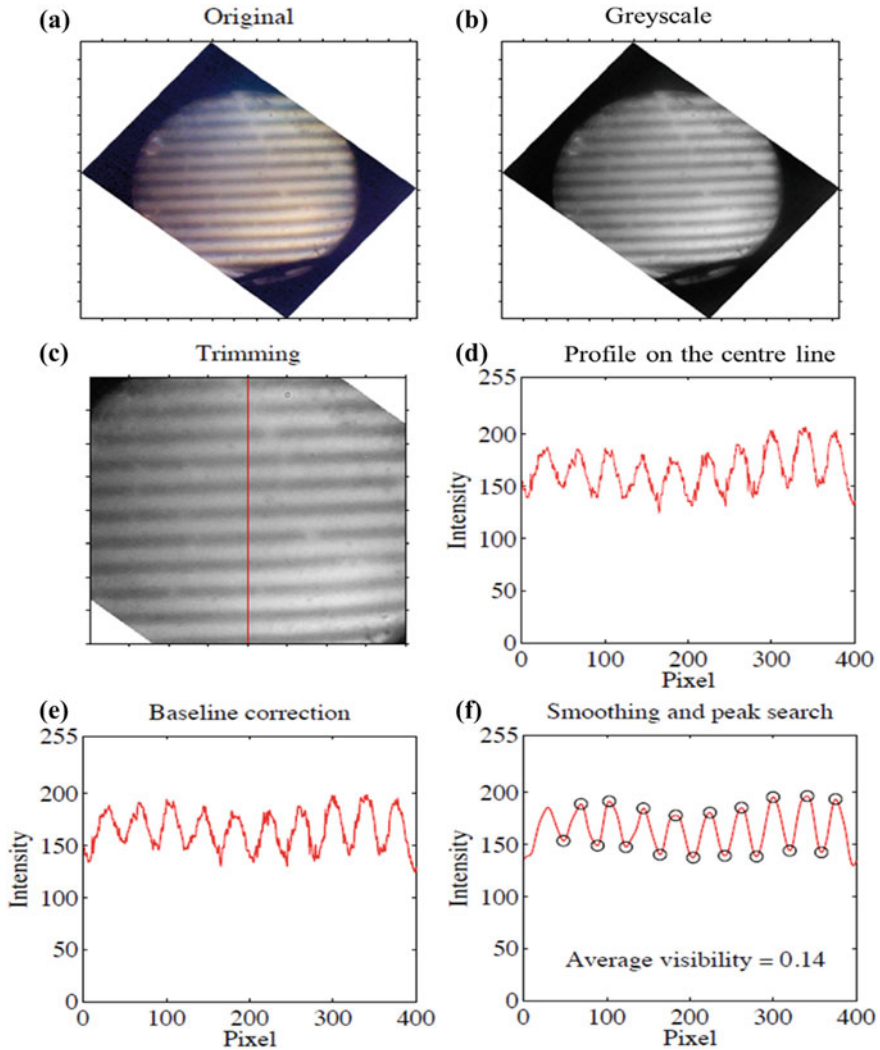


Fig. 11 **a** Rotated original image, **b** greyscaling image, **c** trimming and drawing a centre line, **d** profiling on the centre line, **e** baseline correction, **f** smoothing and peak search

6 Experimental Setup of the Internal-Irradiation System

The external-irradiation probe can observe the images of the lines and spaces; however, the probe end must be in contact with the surface of the objectives. When observing inside the root canal, touching the probe end to the surface of the root canal wall is difficult. The root canals have a curve, which makes it difficult for the instruments to reach. Moreover, as dentists can only see the area where the probe is

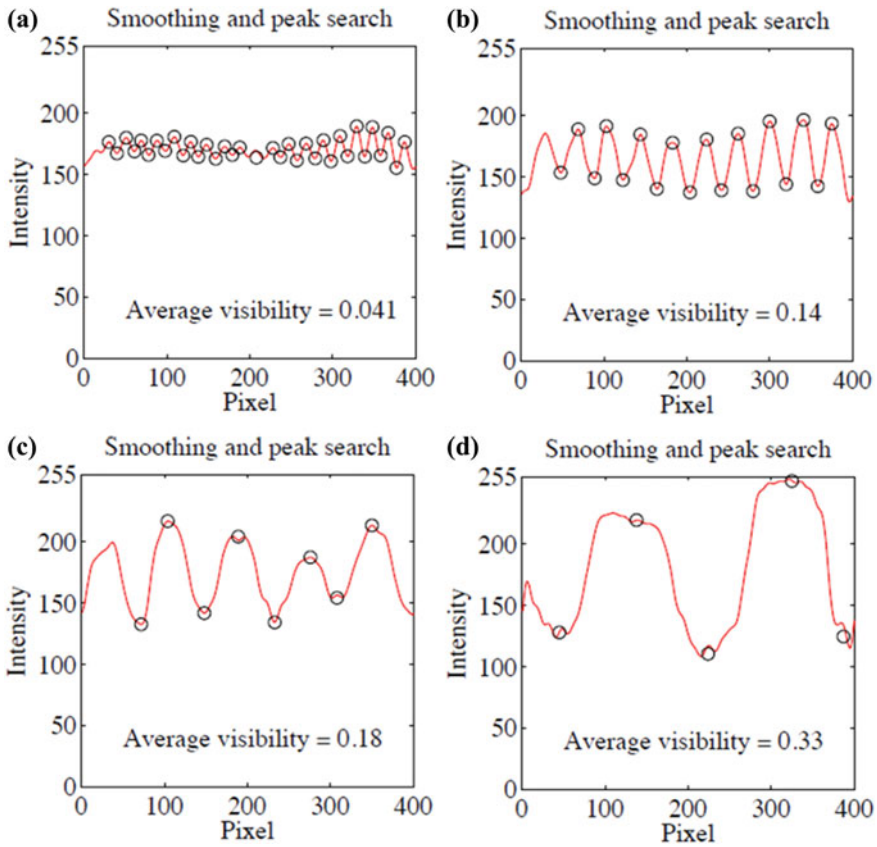


Fig. 12 Final graph of each image, **a** 10 μm , **b** 20 μm , **c** 50 μm , **d** 100 μm

touching, it difficult for them to understand what they are observing. Therefore, to solve this problem, we considered extending the working distance of our probe. Furthermore, the external-irradiation probe has to illuminate the observed area from outside the probe. It is difficult for the outside illumination light to reach the apex of the root canal. Thus, our probe must also solve the illumination problem.

6.1 Improvement of the System Construction

We fabricated an external-irradiation system; however, the GRIN lens used for this system has a 0.0 mm object working distance similar to the system that uses only an image fibre. Therefore, we considered optimizing the object working distance by changing the pitch of the GRIN lens. In addition, the illumination light is secured

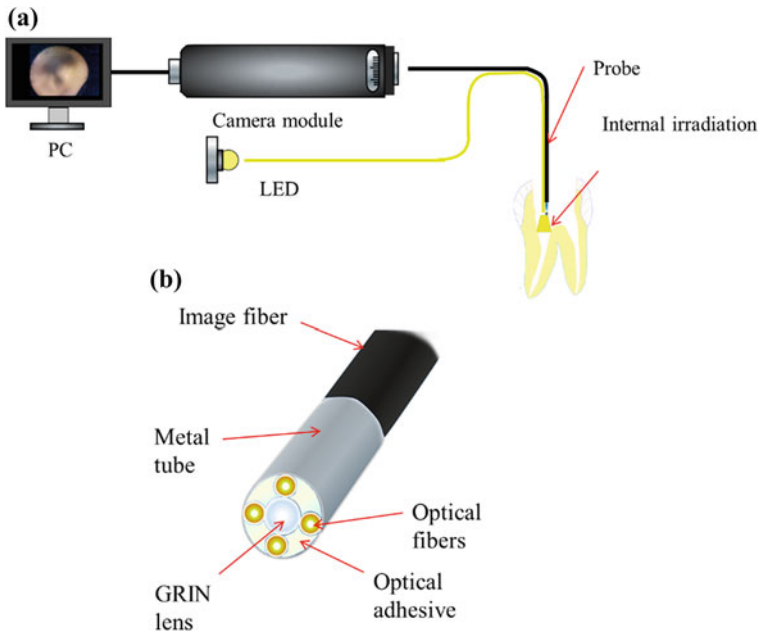


Fig. 13 **a** Endoscope with the internal-irradiation system, and **b** illustration of the probe in the internal-irradiation system

by the probe. The following figure is an illustration of the idea for improving our endoscope (Fig. 13).

This probe not only has a GRIN lens and image fibre but also has optical fibres to illuminate the observation area. The illumination light travels inside the optical fibres, and an LED light was used as the light source because it does not harm the human body [21–23].

6.2 Specification of the Image Fibre and GRIN Lens for Internal-Irradiation System

Considering the construction of the probe, the internal-irradiation probe consists of optical fibres. For this reason, the diameter of the image fibre must be smaller than that of the external-irradiation probe. Therefore, the image fibre used in this system is 300 μm in diameter and has 6000 pixels. The distance between the cores is 3.38 μm . On the PC monitor, a minimum of two pixels are necessary for observation. We require four pixels to observe with the naked eye, and for ideal observation, 10 pixels are required. For these reasons, it is necessary for the objective image to have a size of 12–16 μm on the surface of the image fibre to

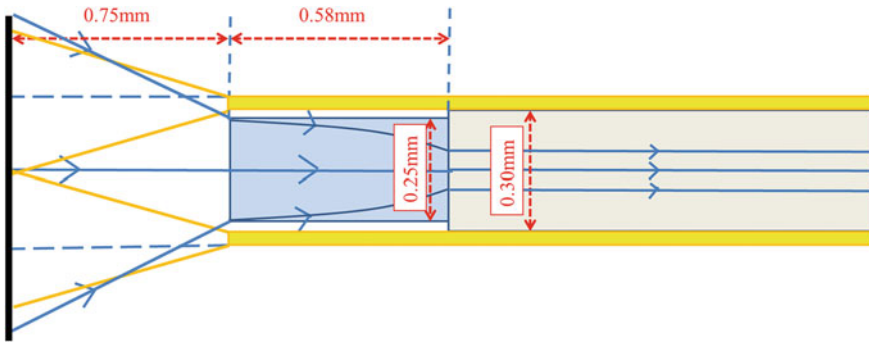


Fig. 14 Calculated relationship of the image working distance and pitch of the GRIN lens

observe by the naked eye. Our fine observation target, such as collaterals of the root canals and fractures, is regarded as $50\ \mu\text{m}$. From the above specifications, magnification of the GRIN lens is decided (Fig. 14).

The pathway of the ray in the internal-irradiation probe is shown in this Fig. 12. The GRIN lens used had a diameter, length, and pitch of $250\ \mu\text{m}$, $0.58\ \text{mm}$, and $0.29\ \lambda$, respectively. The working distance was $0.75\ \text{mm}$. The GRIN lens was adhered to the observation side of the distal end of the image fibre, and the optical fibres for the light source were placed around the GRIN lens and image fibre. The materials, adhered by a UV curing adhesive, were covered with a stainless steel tube. We adhered the materials under an enhanced view using a microscope and irradiated UV from the lens side for 2 h. The optical fibres used for the light source were $65\ \mu\text{m}$ in diameter, and the NA was 0.37. The end of the optical fibre was directly contacted with the LED light source, and the illumination light was transmitted to the observation area.

7 Results of the Internal-Irradiation System

This figure shows a cross-sectional view of the internal-irradiation probe. This photograph was captured using a digital microscope. The surface of the optical fibres and the GRIN lens can be observed. In this image, the position of the GRIN lens and image fibre has a deviation. We attempted to observe the images by using the illuminating light only from the optical fibres; however, the intensity of the light is not sufficiently high to observe the objectives. To evaluate the resolution of the probe, we observed the resolution chart. The following figure shows the observation results for the resolution chart (Fig. 15).

In this figure, we can observe the deviation of the centre axis of the GRIN lens and image fibre. We assume that the difference in the diameter between the image fibre and GRIN lens caused the deviation of the centre axis (Fig. 16).

Fig. 15 Cross section of our internal-irradiation probe

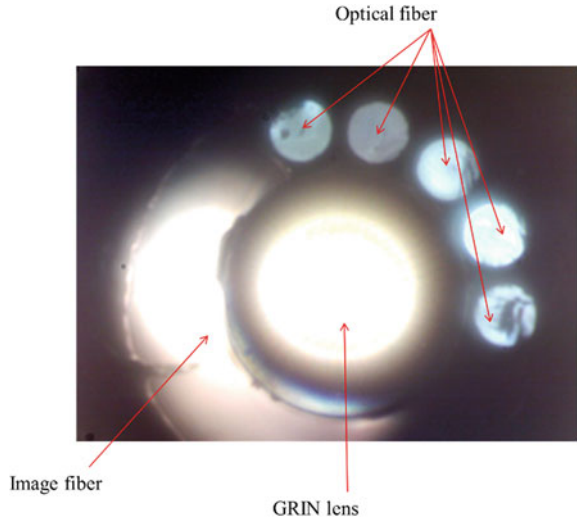
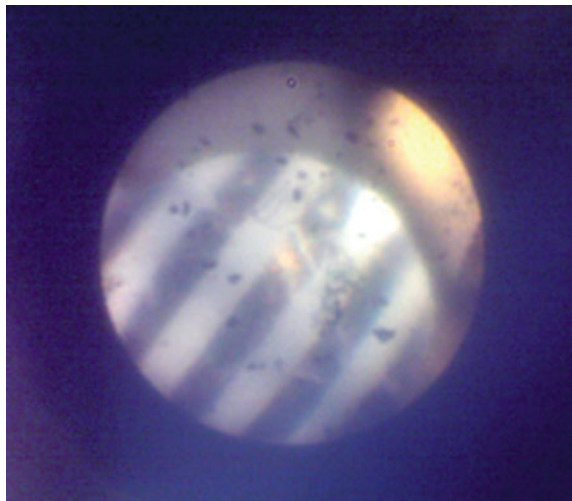


Fig. 16 Image obtained using our internal-irradiation probe



8 Latest Research Progress

In this section, we present our latest research progress. First, we attempt to observe an actual human tooth using our external-irradiation probe. The following figure shows a schematic diagram of the observation experiment and captured images (Fig. 17).

The probe end was positioned near the entrance of the root canal, and we could observe the root canal and isthmus.

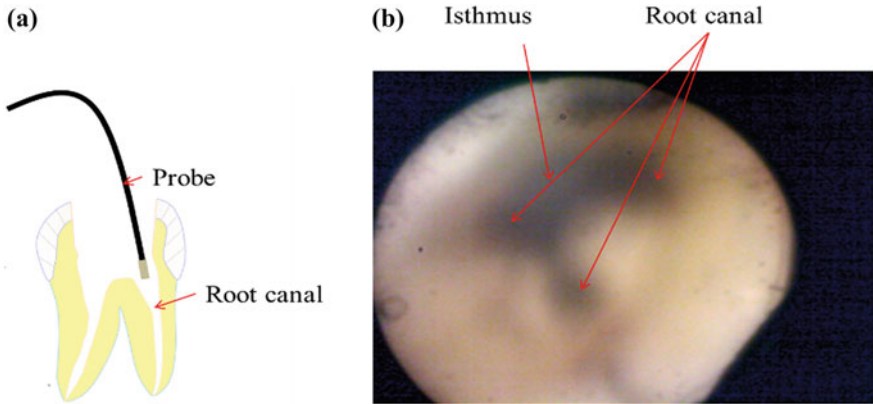


Fig. 17 **a** Illustration of our observation, and **b** image of a human tooth obtained using our endoscope

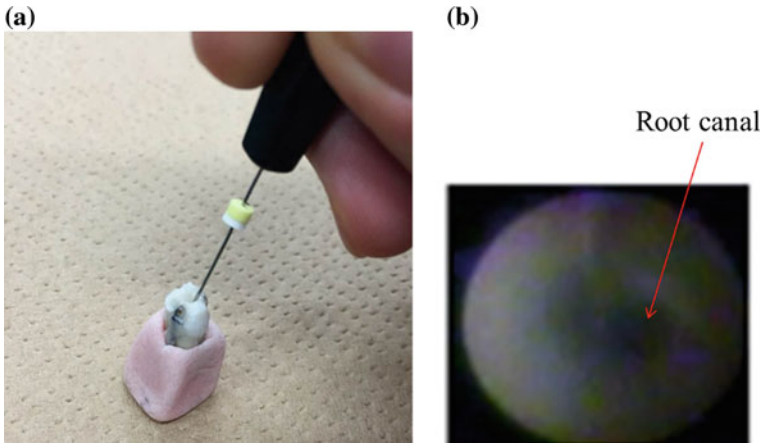
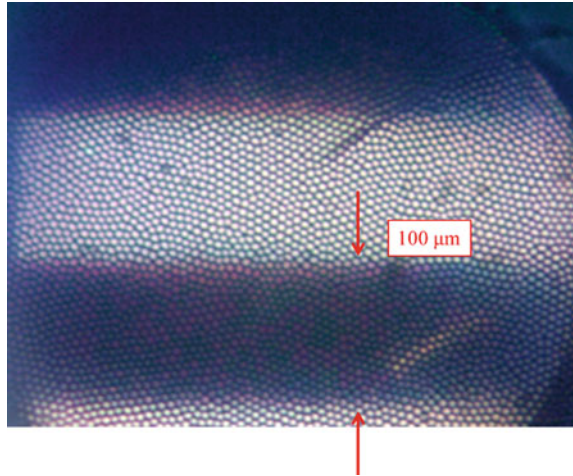


Fig. 18 **a** Situation of the observation experiments with the jointly developed endoscope, and **b** image of a human tooth obtained using this endoscope

In another experiment, we used an endoscope that was jointly developed with a company. This endoscope has a 3000-pixel resolution and is 600 μm in diameter. We observed the samples made with a fractured tooth. The observation situation and captured image are shown in the following figures (Fig. 18).

In this image, we can confirm the surface of the root canal wall and the fractures, and the image resolution is low. However, this probe can illuminate inside the root canal by itself and is capable of fine focusing. Therefore, our endoscope can observe high-resolution images. On the other hand, this endoscope has a better operability than ours.

Fig. 19 Image obtained using novel internal-irradiation probe



Finally, we present the improvement of our internal-irradiation probe. To solve the deviation of the centre axis between the GRIN lens and image fibre, we change the GRIN lens diameter such that it is the same as the image fibre. In addition, a higher-NA objective lens was used in the new endoscope. The following figure was captured using our new endoscope (Fig. 19).

In this image, the 100 μm line and space is observed. Furthermore, the cores could be observed in this image because we changed the objective lens between the CMOS and the end of the image fibre. This clear image is observed at a working distance of approximately 0.3 mm.

9 Discussions

When fabricating the two probes, we observed the tooth, which had finished being prepared for a root canal. In this experiment, we prototyped the internal-irradiation and external-irradiation type probes. We observed the observation samples unless using illumination light from outside with both the probes. The external-irradiation probe has a high resolution and is constructed using only a 15,000-pixel image fibre and a GRIN lens. In contrast, the external-irradiation probe is capable of illuminating the observation area and capturing the images using a single endoscope probe. We fabricated a probe consisting of five optical fibres with diameters of 65 μm . Then, to facilitate the insertion of the probe into the root canal, a 300 μm diameter image fibre was used to miniaturize the entire probe diameter. The GRIN lens was mounted at the tip of the image fibre in order to extend the working distance. The two types of probes were used to observe both a resolution chart and an actual root canal. The fabricated probes were low cost (approximately one-hundredth the cost of a conventional device).

First, we describe the external-irradiation probe. The GRIN lens used in this probe extends out from the tip. When inserting this probe into the root canal, the probe can break easily. Therefore, it is necessary to fit the end surface of the GRIN lens and probe end. During observation, this probe needs to be in contact with the objective surface. An actual tooth root has a curve; thus, the working distance needs to extend. This probe can observe 10, 20, 50, and 100 μm lines and spaces in the resolution chart. As the diameter of the collaterals and the width of the fractures in the root canals are approximately 100 μm , our endoscope has sufficient resolution for observation. We analysed the visibility of each image; the value of visibility increased as the width of the line and space increased. In lines and spaces of 10 μm , a very small value was obtained compared with the other images; therefore, the probe is considered to be suitable for observing structures with sizes of 20–100 μm . From the above, our endoscope probe is suitable for observing small tooth fractures and collaterals of the root canal. However, the obtained images of the actual root canals and isthmus are of low resolution. Furthermore, this probe was difficult to insert into the root canal because of its large diameter; therefore, it is necessary to fabricate a probe with a smaller diameter.

Next, we describe the internal-irradiation probe. The intensity of the illumination light transmitted in the optical fibres from the LED was observed to be low. Therefore, we consider methods to increase the efficiency of transmitting the light from the LED, such as adding more optical fibres for illumination or increasing the intensity of the LED light. Currently, we are attempting to increase the intensity of the light by contacting the fibres directly with white LEDs. In future, we plan to mount the lens for condensing the light between the LED and optical fibres to efficiently concentrate the illumination light. The illumination light from the optical fibres for a light source has to be uniformly for observation area; thus, optimizing the offset at the probe tip is necessary. In this experiment, we used five optical fibres, and their places are edge inside the stainless steel tube.

The methods of placing fibres uniformly and adding more fibres are necessary to ensure uniform and sufficient illumination light. From the actual observed image, the deviation of the central axis occurred between the GRIN lens and image fibre. It was considered that the deviation occurred owing to the different diameters of the image fibre and GRIN lens. To prevent this problem, we used the same diameter for the GRIN lens and image fibres and adjusted the central axis of the GRIN lens and image fibres using an attachment jig. In our latest research, our endoscope allows us to observe high-resolution images, which enables us to confirm the cores of the image fibre and low deviation of the centre axis. This enables us to capture the images more efficiently than with the previous probe. In future, we will evaluate our new endoscope probe and compare it with a commercially available endoscope and the external-irradiation probe.

Unnecessary mixed bubbles were observed in the images obtained from both probes. These bubbles occur in the adhering step of the GRIN lens and image fibre. Therefore, when applying the adhesive, we would like to use a special dispenser and adhesives after the degassing treatment. Moreover, cure conditions such as the irradiation time of UV and the amount of UV irradiation must be considered.

We also tried to build a three-dimensional image using the images obtained from the endoscope and X-ray photographs. In current dentistry, building a three-dimensional image is a great help to dentists in clinical and research fields, and various studies are in progress [24–27]. A three-dimensional image was built using an image obtained from the endoscope. However, an accurate three-dimensional image was difficult to build, and high resolution is important to build a three-dimensional image. Thus, improved image resolution of endoscopes is necessary not only for diagnosis but also for constructing 3D images.

10 Conclusions

We fabricated two types of endoscope probes. The results of our study indicate that it is possible to develop an endoscope capable of observing the collaterals of the root canals. We will redesign the GRIN lens to extend the working distance and obtain sufficient light for observations to improve our endoscope.

References

1. F.J. Vertucci, Root canal morphology and its relationship to endodontic procedures. *Endod. Topics* **10**, 3–29 (2005)
2. F.J. Vertucci, Root canal anatomy of the human permanent teeth. *Oral. Surg. Oral. Med. Oral. Pathol. Oral. Radiol.* **58**, 589–599 (1984)
3. T. Von Arx, Frequency and type of canal isthmuses in first molars detected by endoscopic inspection during periradicular surgery. *Int. Endod. J.* **38**, 160–168 (2005)
4. M. Del Fabbro, S. Taschieri, Endodontic therapy using magnification devices: a systematic review. *J. Endodont.* **38**, 269–275 (2010)
5. A. Dawood, S. Patel, J. Brown, Cone beam CT in dental practice. *Br. Dent. J.* **207**, 23–28 (2009)
6. T.P. Cotton, T.M. Geisler, D.T. Holden, S.A. Schwartz, W.G. Schindler, Endodontic applications of cone-beam volumetric tomography. *J. Endodont.* **33**, 1121–1132 (2007)
7. C. Estrela, M.R. Bueno, C.R. Leles, B. Azevedo, J.R. Azevedo, Accuracy of cone beam computed tomography and panoramic and periapical radiography for detection of apical periodontitis. *J. Endodont.* **34**, 273–279 (2008)
8. A.K. Suomalainen, A. Salo, Peltola J.S. Robinson, The 3DX multi image micro-CT device in clinical dental practice. *Dentomaxillofac. Rad.* **36**, 80–85 (2007)
9. K. Nakato, M. Naitoh, M. Izumi, K. Inamoto, E. Arijii, H. Nakamura, Effectiveness of dental computed tomography in diagnostic imaging of periradicular lesion of each root of a multirrooted tooth: A case report. *J. Endodont.* **32**, 583–587 (2006)
10. B. Hassan, M.E. Metska, A.R. Ozok, P. van der Stelt, P.R. Wesselink, Detection of vertical root fractures in endodontically treated teeth by a cone beam computed tomography scan. *J. Endodont.* **35**, 719–722 (2009)
11. S. Yoshii, T. Nishino, T. Nishihara, C. Kitamura, Y. Zhang, H. Zhang, S. Ikezawa, L. Zimin, T. Ueda (2015) Development of a low cost diagnostic system for dental therapy. In: *6th International Conference on Sensing Technology*, pp. 492–496

12. S. Yoshii, Y. Zhang, S. Ikezawa, C. Kitamura, T. Nishihara, T. Ueda, Study of endoscopy for dental treatment. *Int. J. Smart Sensing Intell. Syst.* **6**, 1–17 (2013)
13. M. Fujimoto, S. Yoshii, S. Ikezawa, T. Ueda, C. Kitamura (2015) Development of dental endoscope. In: *9th International Conference on Sensing Technology*, pp. 551–556
14. M. Osanai, T. Suzuki, A. Tamura, T. Yonemura, I. Mori, Development of a micro-imaging probe for functional brain imaging. *Neurosci. Res.* **75**, 46–52 (2013)
15. J. Knittela, L. Schnieder, G. Buess, B. Messerschmidt, T. Possnerb, Endoscope-compatible confocal microscope using a gradient index-lens system. *Opt. Commun.* **188**, 267–273 (2001)
16. Y. Mao, S. Chang, S. Sherif, C. Fluerau, Graded-index fibre lens proposed for ultrasmall probes used in biomedical imaging. *Appl. Opt.* **46**, 5887–5894 (2007)
17. X. Li, W. Yu, Deep tissue microscopic imaging of the kidney with a gradient-index lens system. *Biomed. Opt. Express* **4**, 652–658 (2013)
18. L. Yulin, L. Tonghai, J. Guohua, H. Baowen, H. Junmin, W. Lili (2007) Research on micro-optical lenses fabrication technology. *Optik: Int. J. Light Elec. Optics.* **118**, 395–401
19. Y. Suematsu, K. Iga, S. Ito, A light beam waveguide using hyperbolic-type gas lenses. *IEEE Trans. Microw. Theory Techn.* **14**, 657–665 (1966)
20. K. Nishizawa, Principle and application on gradient index optical imaging. *The Rev. Laser Eng.* **8**, 748–758 (1980)
21. A.K.S. Braz, B.B.C. Kyotoku, R. Braz, A.S.L. Gomes, Evaluation of crack propagation in dental composites by optical coherence tomography. *Dent. Mater.* **25**, 74–79 (2009)
22. A.G. Mignani, F. Baldini, In-vivo biomedical monitoring by fiber-optic systems. *IEEE/OSA J. Lightwave Technol.* **13**, 1396–1406 (1995)
23. K.-C. Huang, P.R. Wesselink (2011) The pulse excitation of UV LED source for fluorescence detection. In: *2011 IEEE Instrumentation and Measurement Technology Conference (I2MTC)*, pp. 1–4
24. T. Hopp, P. Baltzer, M. Dietzel, W.A. Kaiser, N.V. Ruiter, 2D/3D image fusion of X-ray mammograms with breast MRI: Visualizing dynamic contrast enhancement in mammograms. *Int. J. Comput. Assist. Radiol. Surg.* **7**, 339–348 (2012)
25. A.S. Abdelrehim, A.A. Farag, A.M. Shalaby, M.T. El-Melegy, 2D-PCA shape models: Application to 3D reconstruction of the human teeth from a single image. *Med. Comput. Vis. Large Data Med. Imag. Lect. Notes Comput. Sci.* **8331**, 44–52 (2014)
26. A. Abdelrahim, A. Shalaby, S. Elhabian, J. Graham, A. Farag (2013) A 3D reconstruction of the human jaw from a single image. In *Image Processing (ICIP) 20th IEEE International Conference*, pp. 3622–3626
27. Y. Hirogaki, T. Sohmura, H. Satoh, J. Takahashi, K. Takada, Complete 3-D reconstruction of dental cast shape using perceptual grouping. *IEEE Trans. Med. Imag.* **20**, 1093–1101 (2001)

Frame-by-Frame Speech Signal Processing and Recognition for FPGA Devices

Masashi Nakayama, Naoki Shigekawa, Takashi Yokouchi
and Shunsuke Ishimitsu

Abstract This paper discusses and experiments on frame-by-frame speech signal processing and recognition for Field Programmable Gate Array (FPGA) devices. The system proposes applications including a voice conversion system that needs signal processing and speech recognition for each frame because it requires real-time processing at each frame. Owing to the processing speed, the authors propose algorithms for FPGA as a hardware processor for Voice Activity Detection (VAD) and speech recognition decoder. However, resources for FPGA devices as gate circuits are minimal, therefore, the algorithms need to be customized in order to implement the FPGA. The algorithms are customized for VAD using a 2nd-order autocorrelation function, and for speech recognition using Euclidian distance. These methods implement an FPGA emulator that demonstrates VAD of speech and noise sections and a speech recognition experiment for discriminating Japanese vowels.

1 Introduction

Speech interfaces that include speech recognition have been introduced in many applications such car navigation and computing. Currently, these interfaces are increasing in number. However, speech recognition requires many calculations and a large amount of processing time; hence, a significant amount of effort has been spent to address these issues [1]. Furthermore, the speech interface requirements of

M. Nakayama (✉) · S. Ishimitsu
Graduate School of Information Sciences, Hiroshima City University,
3-4-1 Ozuka-higashi, Asaminami-ku, Hiroshima 731-3194, Japan
e-mail: masashi@hiroshima-cu.ac.jp

N. Shigekawa
Graduate School of Engineering, University of Fukui, 3-9-1 Bunkyo,
Fukui 910-8507, Japan

T. Yokouchi
National Institute of Technology, Kagawa College, 551 Khoda, Takuma,
Mitoyo, Kagawa 769-1192, Japan

cell phones and smartphones must also be addressed, as they have the most popular speech interface applications [2]. Hence, many researchers and engineers have attempted to implement speech recognition as software using state-of-the-art decoding algorithms. Conventional decoding algorithms use statistical approaches including Hidden Markov Models (HMMs) and Deep Neural Network (DNNs) [3]; however, these approaches require acoustic feature parameters to be modeled statistically, which requires high calculation costs and a large number of samples. Owing to the advanced developments in PC hardware, such systems respond to users rapidly enough for practical use.

On the other hand, speech recognition cannot achieve the instantaneous processing of data that consists only of a few frames. Currently, discrimination and recognition processing can be achieved using a Gaussian Mixture Model (GMM); however, this approach needs resources and time for calculation. Whether GMM is a similar model to HMM, it has only one state transition. GMM also requires the model parameters to be estimated as in HMM. Hence it is too difficult to use without a laptop, PC, or workstation. For these reasons, light weight, low energy, and fast methods are needed in the speech interfaces of wearable and portable devices. With respect to processing speed, hardware decoding is faster than software decoding. Hence there have been efforts to use Digital Signal Processors (DSPs) and Field Programmable Gate Arrays (FPGAs) to achieve faster processing. Several studies have attempted to develop a speaker discrimination decoder from a narrow vocabulary using microcomputers and DSPs [4–6]. Other research has implemented these decoders using conventional statistical decoding on hardware including FPGA devices [7, 8]. One group transplanted HMM speech recognition to a microcomputer, which has completely semi-contentious distributions [9]. In the above research, the implementation and transplanting of speech recognition decoders has been roughly realized.

For these proposed methods, the fastest processing they can achieve is by hardware processing with logical gates and/or other innovative processing methods in the future. On the other hand, the authors proposed an algorithm for sound quality improvement using frame-by-frame processed signal estimation that requires faster processing than that of microcomputers and DSPs [10–12]. The method recognizes vowels and consonants, including the unvoiced section at each frame during the processing. However, this is too slow when implemented using conventional methods on microcomputers and DSPs. Because conventional algorithms contain processing that is too complex for FPGAs, which consist of logic circuits of AND, OR, and NOT gates, the procedures that can be considered for an FPGA device must take a simple approach. For these reasons, a new hardware decoding method for speech recognition and VAD are proposed in this study.

This paper investigates speech processing and recognition using an FPGA system. Thus the paper describes the fundamentals of speech signal processing and recognition for FPGA to implement them on an FPGA emulator. First, Sect. 2 discusses the fundamentals of speech analysis and its algorithms for FPGA implementation. Section 3 shows the concept and overview of the proposed system, with frame-by-frame speech signal processing and recognition system on an FPGA

device. Section 4 shows VAD using a 2nd-order autocorrelation function for the preprocessing of speech recognition. Section 5 shows speech recognition experiment for vowels using the Euclidian distance between referred samples and target samples, which is then implemented in an FPGA emulator. Finally, Sect. 6 discusses the conclusion and future work derived from this research.

2 Speech Analysis for FPGA Implementation

2.1 *Fundamentals of Speech*

In humans, speech is generated by the vibrations of vocal cords via articulators [13]. Speech itself is defined as combinations and/or sequences of phonemes and other sub-word units. In general, all languages are comprised of syllable units, but a few languages are composed of mora units. In various languages, speech is formed by utterances of words and sentence sounds that are combined and connected using vowels and consonants. In particular, the Japanese language, are able to count by both unit language, follows the combinations /V/, /VC/, and /CV/. On the other hand, English is able to count by only syllable unit language except mora unit, add to /CVC/ to them of mora unit. Phonemes in Japanese include 17 consonants and 5 vowels, while the phonemes of English include 22 consonants and 20 vowels. However, these numbers depend on specific researchers and the definitions they use [14].

The quality and harmonics of speech sound change, and they depend on vocal chord vibrations that are airborne via articulators that are cavities between the oral and nasal cavity. Airborne sound emits from the nostril and mouth, and then it emphasizes high-frequency components as its emitting characteristics [15]. A sound wave is composed of sequences of triangle waves, so it is similar to pulse sequences, which cause open and closure quotient at vocal chord [16]. The fundamental frequency, generally called the pitch, cycles between peaks in a sound wave. The pitch defines and contains the personal information of each person as a pitch frequency and the harmonics that contribute to its quality. The language information contains frequency responses as a spectrum envelope [13]. Formant frequencies are found in the spectrum of peaks in envelopes [17]. Thus, frequency analysis is very important in identifying the language and personal information of a speaker or singer.

2.2 *Spectrum Analysis of Speech*

The previous section described the importance of spectrum analysis for speech, which can be analyzed to determine the fundamental frequency F_0 and n formant

frequencies F_n as the personal and language information of a speaker or singer [15]. This section describe different analysis methods using spectrum analysis.

Figure 1a–e show a spectrum analysis of Japanese vowels /a/, /i/, /u/, /e/ and /o/ uttered by a 20-year-old Japanese male. The vowels are analyzed using a 44.1 kHz, 16 bit sample and 2200 point FFT. There are found the formant frequencies by peaking respectively. Figure 2a, b show comparisons of FFT and LPC analyses. Figure 2a shows the analysis using a conventional FFT method. By contrast, Fig. 2b shows an analysis using LPC. These results can be used to analyze the frequency characteristics; however, it is difficult to show the spectrum envelope when the conventional FFT is employed. To extract and show the linguistic information and sub-word information, a spectrum envelope using LPC and/or source-filter analysis are often used to determine phonemes and additional units such as sub-words.

In Fig. 1a–c, the circles indicate the peaks of formant frequencies. As can be seen from the image, it is difficult to local max points with a spectrum envelope using FFT. However, it is easy to determine a spectrum envelope and its formants using LPC. Thus, speech analysis employs LPC analysis for its robustness in locating formant peaks.

2.3 Fundamentals of the Autocorrelation Function

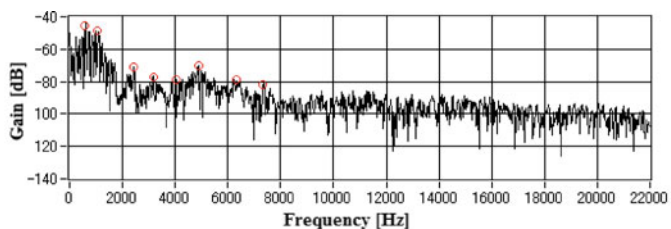
The system also uses VAD during preprocessing for robust signal extraction and recognition using FPGA decoding. To discriminate the speech into vowels and other units including consonants and noise sections, we focused on the periodicity of sounds because VAD processing does not employ complicated processing or a complex algorithm. We expected to realize VAD without a training phase for discrimination and detection.

Vowels have fundamental frequencies such as pitch, and consonants and noise have no periodic components. By focusing on these characteristics, the system can easily discriminate between sections with and without periodic sections of speech. The following Eq. (1) shows the autocorrelation function [18]:

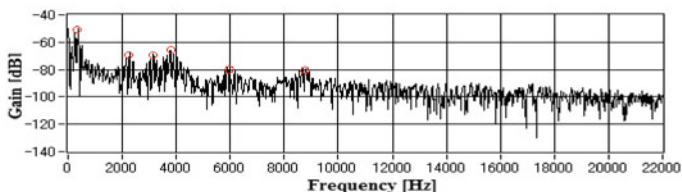
$$R(j) = \frac{1}{N} \sum_{i=1}^N x(i) \cdot x(i+j) \quad (1)$$

where $x(i)$ is the signal and i is its variable, $R(j)$ is the autocorrelation function and j is its variable, and N is the section of integration. Figure 3a, b show the speech of Japanese vowel /a/ and the noise sound in a room used in daily life. Figure 4a, b show the autocorrelation functions of vowel speech and noise sound.

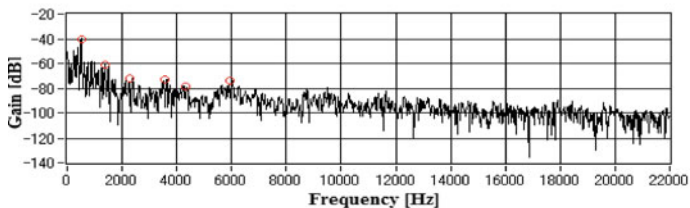
The amplitude of speech and noise in the autocorrelation function are different because periodic sounds of vowels increase, but no periodic sounds of noise decrease. Thus the autocorrelation function can be expected to discriminate



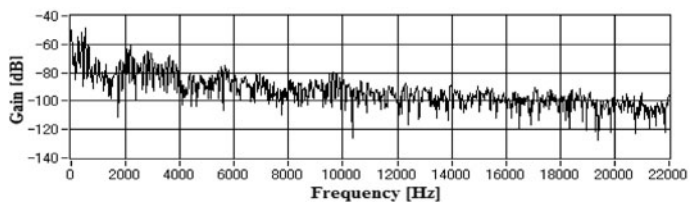
(a) Vowel /a/.



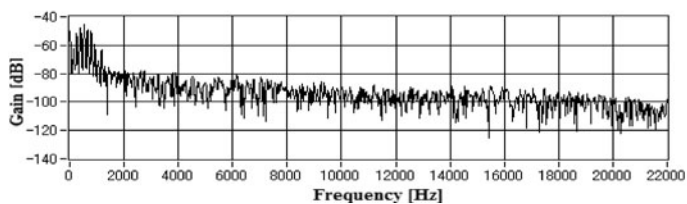
(b) Vowel /i/.



(c) Vowel /u/.

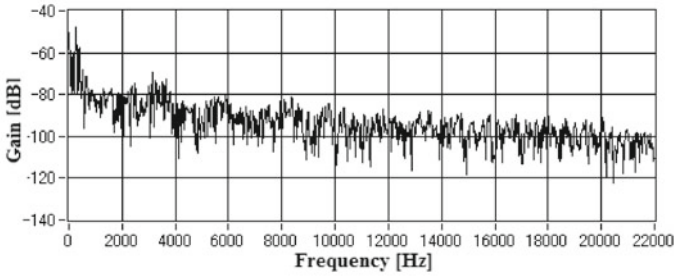


(d) Vowel /e/.

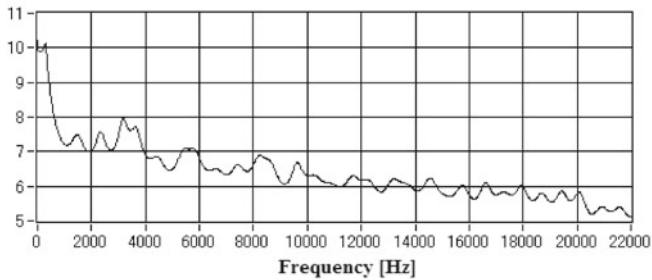


(e) Vowel /o/.

Fig. 1 Spectrum analysis of Japanese speech vowels



(a) FFT analysis.



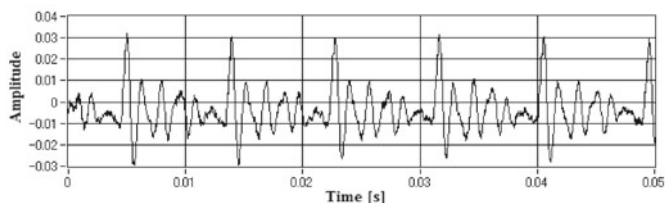
(b) LPC analysis.

Fig. 2 Comparisons of FFT analysis and LPC analysis

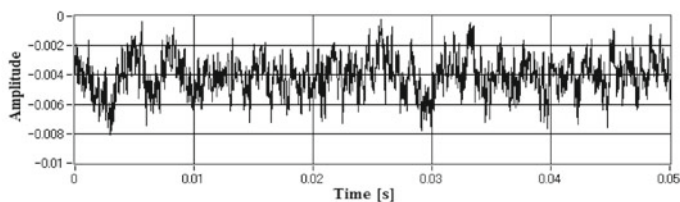
between speech and no speech sections including those with no periodic noise except periodic noises.

2.4 Euclidean Distance for Vowel Recognition

To discriminate the vowels, we calculate the Euclidean distance between formants referenced by table of formants and a target of sound. The table with index i lists the values of representative formants 1 and 2 such as $F_{i,1}$ and $F_{i,2}$ before the recognition phase. Target sound with index j , calculated using formants 1 and 2 such as $F_{j,1}$ and $F_{j,2}$ measured by the spectrum envelope of the sound, are unknown vowel sounds. During the processing of each frame, the frame extracts values of formants $F_{t,1}$ and $F_{t,2}$, which are compared with all vowel candidates in the domain space. By these processing, the vowel candidates conducts by the following equation:

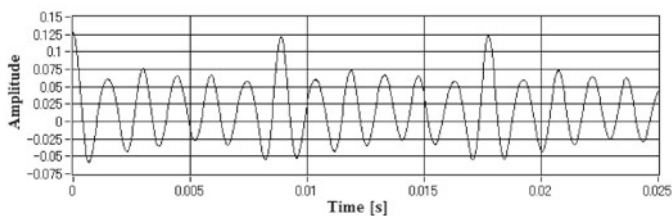


(a) Japanese speech vowel /a/.

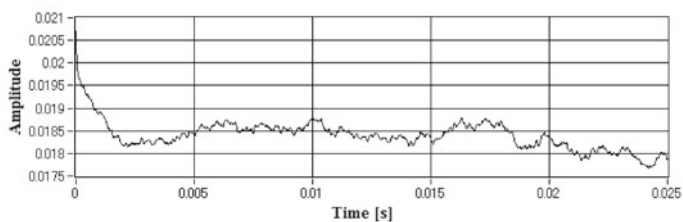


(b) Noise sound.

Fig. 3 Speech and noise sound



(a) Autocorrelation of speech.



(b) Autocorrelation of noise sound.

Fig. 4 Performance evaluations for autocorrelation functions

$$V = \arg \min_{Vowel \in i} \sqrt{(F_{i,1} - F_{t,1})^2 - (F_{i,2} - F_{t,2})^2} \quad (2)$$

where V is the estimated vowel, i is a candidate vowel of domain $Vowel$, t is an unknown target, and each $F_{\{i,t\},\{1,2\}}$ is formants F_1 and F_2 . Using this procedure, FPGA devices can estimate the recognition result V at each frame.

3 Frame-by-Frame Speech Signal Processing and Recognition on FPGA

3.1 Fundamentals of FPGA

FPGA circuits can achieve any combination of logical circuits desired by users. They are composed of logical circuit components such as AND, OR, NAND, and FF (flip-flop) components. Hence, FPGA logic is quite different from the logic of DSPs and microcomputers. This research employs the LabVIEW development environment, which is one of the most widely used development environments for FPGA devices [19]. This environment is composed of a Graphical Use Interface (GUI) and compilers for an FPGA circuit.

3.2 Frame-by-Frame Speech Signal Processing and Recognition in FPGA

Figure 5 shows the concept and overview of the proposed system on an FPGA device. There are two main processing stages: signal processing and speech recognition. First, the system detects sections that contain speech using second-order autocorrelation with sound quality improvement that is optional treatment. Next, the

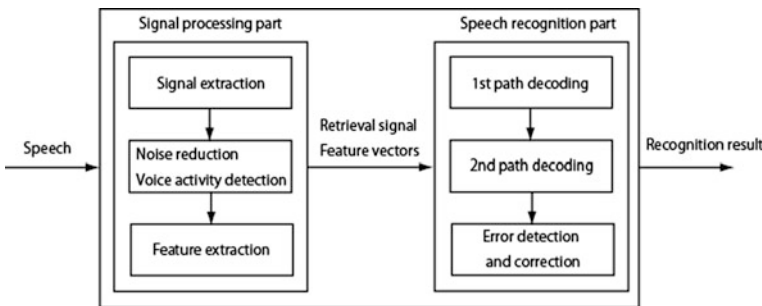


Fig. 5 Frame-by-frame speech signal processing and recognition in FPGA devices

detected frames are used to discriminate and recognize the vowel candidates using referred and target formant frequencies.

During the 1st stage (speech processing), the system extracts data from every frame of a speech signal. Then each frame is analyzed and assigned a frame status as a speech frame or no-speech frame, including consonants and noise. This research determines the status of the speech section or no-speech section using 2nd-order autocorrelation functions. In general, an autocorrelation function analyzes the periodicity of sound. However, in the research, a 2nd-order autocorrelation is employed because one of the authors determined that processing at least two times can emphasize and improve the robustness of periodicity detection. The effective duration of τ_c is used because its parameters are expected to represent one-dimensional parameters by slope angle and/or decreasing gain level [20]. However, the parameters for this research are changed in order to implement them for an FPGA device. In addition, noise reduction processing can apply to the frame if the user hope and add to this processing stage with the discrimination result of speech nor no-speech status.

During the 2nd stage (speech recognition), the system discriminates between vowels and/or consonants. This speech recognition is often called the fundamental method using Euclidean distance. The recognition algorithm can implement two-stage decoding, which often introduces a state-of-the-art speech recognition decoder for rough and precise calculations. However, this research into decoding is used only for one-stage decoding because it highly simplifies speech recognition.

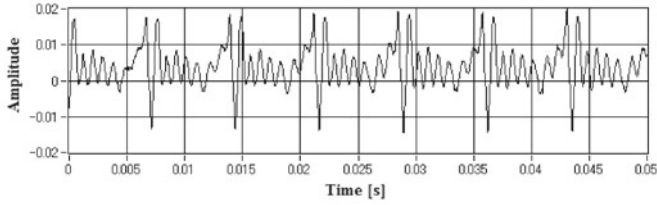
4 Voice Activity Detection Using Second-Order Autocorrelation

4.1 Robustness of Second-Order Autocorrelation

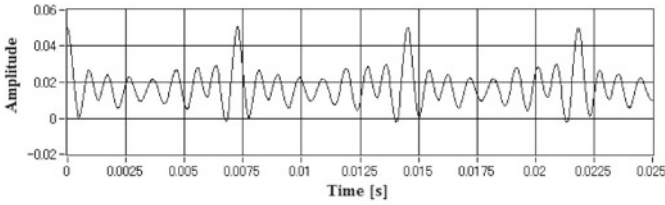
The FPGA's calculation resources are limited. Hence VAD and recognition methods must require few calculations. In this section, VAD with a 2nd-order autocorrelation is proposed. Autocorrelation is one of most well-known analysis methods for evaluating the periodicity of a signal [18]. Conventional autocorrelation $R(j)$ can be calculated using the following equation:

$$R(j) = \frac{1}{N} \sum_{i=1}^N x(i) \cdot x(i+j) \quad (3)$$

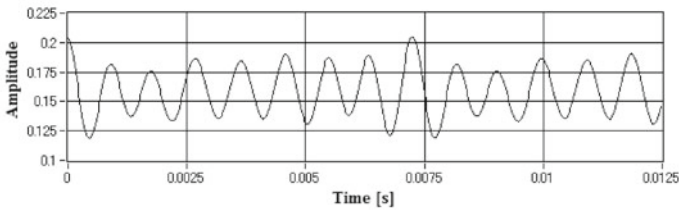
where $x(i)$ is the speech signal. The value of $R(j)$ increases if the sound has a periodic signal, and decreases when there is little periodicity. Figure 6a–c show the sounds of the vowel /a/ in its original form and as autocorrelation functions.



(a) Speech.



(b) Autocorrelation function.

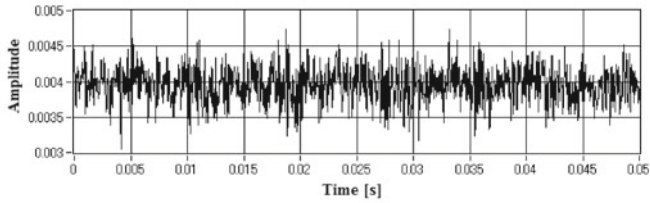


(c) 2nd-order autocorrelation function.

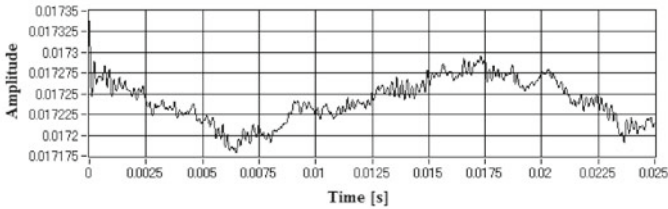
Fig. 6 Autocorrelation functions of speech

The vowel was uttered by a 20-year-old male in a calm condition. Figure 6a shows the speech, Fig. 6b shows the autocorrelation of the speech, and Fig. 6c shows the 2nd-order autocorrelation of the speech. Both Fig. 6b, c confirm the periodicities of the speech, but the waveform in Fig. 6c has a stronger periodicity. This periodicity detection is more robust than when the conventional method as autocorrelation is employed.

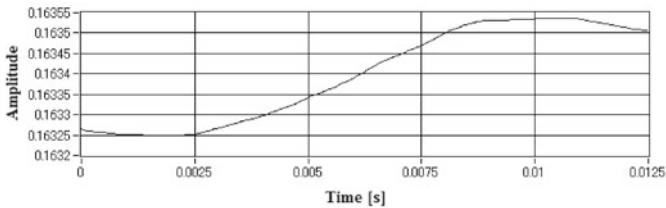
By contrast, Fig. 7a–c show the original sound and autocorrelation functions when one of the samples is an aperiodic sound such as noise. Figure 7a shows the noise, Fig. 7b shows the autocorrelation of this noise, and Fig. 7c shows its second-order autocorrelation. Neither signal in Fig. 7b, c contains the periodicities of those in Fig. 7b, c. From these results, second-order autocorrelation is clearly suitable for speech detection.



(a) Noise.



(b) Autocorrelation function.



(c) 2nd order autocorrelation function.

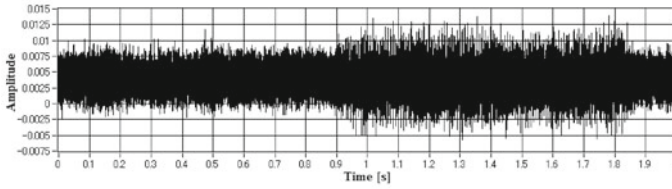
Fig. 7 Autocorrelation functions of noise

4.2 VAD for Isolated Vowels

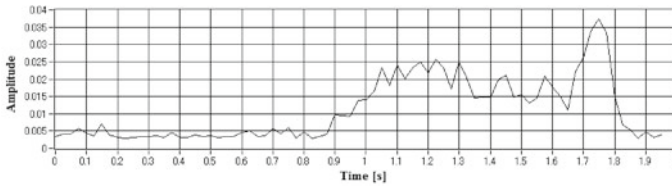
Section 4.1 describes the robustness of 2nd-order autocorrelation. However, the autocorrelation cannot be used directly for utterance detection. For detection it is necessary to calculate the estimated value of the voiced section $A(l)$ from the second-order autocorrelation, as in the following equation:

$$A(l) = \sum_{k=0}^{K-1} |R'(k+1) - R'(k)| \tag{4}$$

Generally, speech sounds are composed of combinations of consonants and vowels, and the vowels have a periodicity from the pitch generated by the vocal chords. Equation (4) has a high value except during the utterance of consonants; hence the voiced sections are easy to detect in this way. By contrast, the value is



(a) Speech sound.



(b) VAD result.

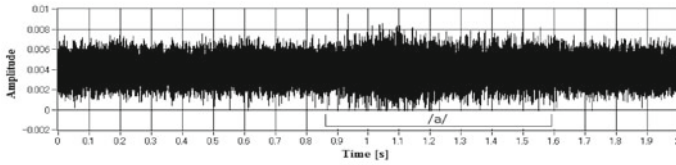
Fig. 8 VAD of Japanese vowel /a/ with high SNR

low when the speech is unvoiced or there is stationary noise. This approach has one weak point: the value is high when the background noise has periodicity. However, this algorithm does not require any initial settings such as those of parameter estimations. Hence it is a strong detection method for the most part. The most aggressive design approach is to use no initial setting, wherein VAD works correctly without any implementation for settings.

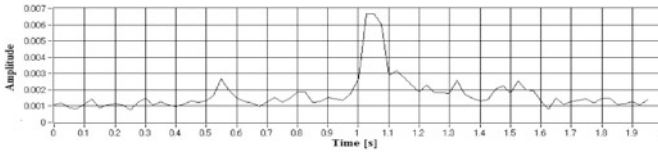
Detection performance depends on the Signal-to-Noise Ratio (SNR). If the amplitude of the signal is larger than that of the noise, the SNR is high, and if it is smaller, the SNR is low. In this evaluation, environments with noise and high and low SNRs were tested. Figure 8a shows the vowel /a/ with a high SNR, and Fig. 8b shows its VAD. From Fig. 8b, it is clear that VAD performs correctly because the utterance was detected between approximately 0.9 and 1.8 s. In addition, Fig. 9a shows a vowel /a/ with a low SNR, and Fig. 9b shows its VAD. Similar to the high-SNR case, the VAD result for a low-SNR signal determines the utterance to be between 0.9 and 1.8 s.

4.3 VAD for Sentence Units

To evaluate the overall performance of VAD, a sentence unit was evaluated. ATR 503 sentences, which are example sentences for speech research in Japanese, were used. A01 sentences of ATR sentences were uttered once by a 20-year-old male [21].

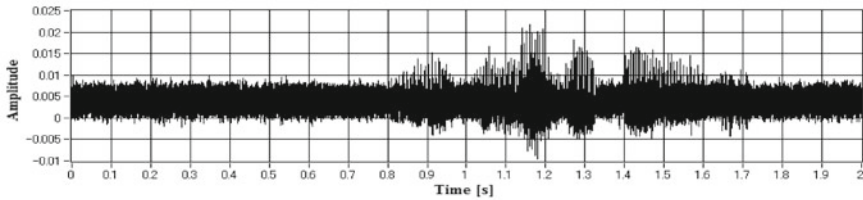


(a) Speech sound.

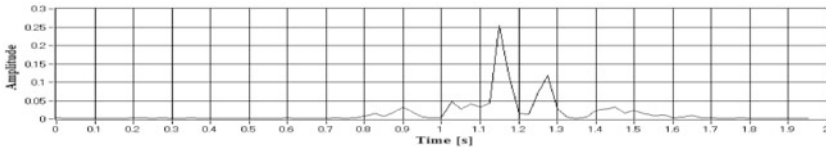


(b) VAD result.

Fig. 9 VAD of Japanese vowel /a/ with low SNR



(a) Speech sound.



(b) VAD result.

Fig. 10 VAD of Japanese sentence

Figure 10a shows the sentence utterance in a high-SNR environment, and Fig. 10b shows the VAD result. From Fig. 10b, it is clear that the vowel sections generated high VAD values and the consonants generated low values. However, the noise sections are much lower compared with the voiced sections. Hence these results show the practical possibility of using VAD for sentence utterances.

5 Speech Recognition Experiment

As a final experiment, vowel recognition using formant distances was evaluated. Generally, speech is generated by the sound of vocal chords and air passing through the oral and nasal cavities. Hence, in the research fields of phonetics and speech signal processing, a source-filtered model is generally accepted for the analysis of speech. In this theory, it is assumed that vocal chords are a source generator and the articulation path is a filter. In particular, vowel features depend on and are represented by the articulation path characterized as resonance frequencies. This means that vowels can be discriminated by their resonance frequencies, which are called formant frequencies in these fields. Hence the most simple speech recognition uses formant discriminations with the first and second formants. Since this approach is the simplest method, the algorithm is a good candidate for implementation in FPGA devices. Figure 11 shows a block diagram of the procedure of the FPGA emulator in LabVIEW, from National Instruments.

As a basic experiment, samples were used where several speakers uttered Japanese vowels including /a/, /i/, /u/, /e/, and /o/. Representative formants for F_1 and F_2 were calculated by averaging frames in VAD. The formants were compared with vowel templates. The recognition compares the distances between the measured formants and their templates. Table 1 shows the experimental results of this method of vowel recognition. This method achieved a recognition rate of 75 % or higher for each vowel. Hence the system is expected to work correctly at approximately this rate of vowel recognition.

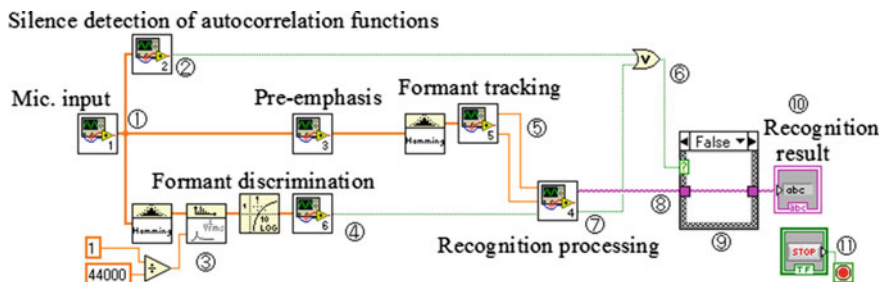


Fig. 11 Implementation of system in FPGA simulator

Table 1 Vowel recognition results

		Recognition result					Correct rate (%)
		/a/	/i/	/u/	/e/	/o/	
Utterance	/a/	122	0	23	0	15	76.3
	/i/	0	121	3	36	0	75.6
	/u/	0	1	119	0	40	74.4
	/e/	0	25	0	128	7	80.0
	/o/	0	0	0	0	160	100.0

6 Conclusion and Future Work

This paper proposed and evaluated a frame-by-frame speech recognition method for implementation in FPGAs. Algorithms implemented in FPGAs are expected to be calculated quickly compared with calculations by conventional microcomputers and DSPs. However, there are few resources in FPGAs. Hence a speech recognition method using only a few frames of speech sound was proposed. The system was demonstrated on an FPGA emulator. The experiments showed the effectiveness and robustness of VAD and speech recognition from just a few frames of speech. The proposed system is expected to demonstrate a rate of recognition of 75 % or higher. Along with this proposed method, a sound quality improvement algorithm could be implemented on an actual system for clear sound estimation [10]. As a direction for future work, the authors plan to implement such an algorithm in an FPGA.

References

1. J. Benesty, M. Sondhi, Y. Huang, *Springer Handbook of Speech Processing* (Springer, 2008)
2. T.Z. Hua, L. Boerge, *Automatic Speech Recognition on Mobile Devices and Over Communication Networks* (Springer, 2008)
3. D. Yu, L. Deng, *Automatic Speech Recognition: A Deep Learning Approach* (Springer, 2015)
4. K. Kokubo, N. Hataoka, T. Lee, T. Kawahara, K. Shikano, Computational reduction of contentious speech recognition software “Julius” on super microprocessor. *J. Inf. Process.* **50**, 2597–2606 (2009) (in Japanese)
5. C.G. Concejero, V. Rodellar, A.A. Marquina, E. Martinez, P. Gomez, Designing an independent speaker isolated speech recognition system on an FPGA. *Res. Microelectron. Electron.* 81–84 (2006)
6. S.P. Nedevischi, R.K. Patra, E.A. Brewer, Hardware speech recognition for user interfaces in low cost, low power devices. *Proc. Des. Autom. Conf.* 684–689 (2005)
7. K. Okamoto, H. Tamukoh, M. Sekine, Sound preprocessing circuit by consonant and vowel recognition system. *IEICE Technical Report VLD2011-93 (CPSY2011-56, RECONF2011-52)*, 13–18 (2012) (in Japanese)
8. S.J. Melnikoff, S.F. Quigley, M.J. Russell, Implementing a simple continuous speech recognition system on an FPGA, in *Proceedings of the 10th Annual IEEE Symposium on Field-Programmable Custom Computing Machines*, 275–276 (2002)
9. S.J. Melnikoff, S.F. Quigley, M.J. Russell, Speech recognition on an FPGA using continuous hidden Markov models, in *Proceedings of 12th International Conference on Field-Programmable Logic and Applications*, 201–211 (2002)
10. M. Nakayama, Japan Patent JP2011-84323 (JP2012-220607A) (2011)
11. M. Nakayama, N. Shigekawa, T. Yokouchi, Hardware speech recognition system for processing and recognition at moment. *IEICE Technical Report, EA2010-99* (2010–12) (2010) (in Japanese)
12. M. Nakayama, N. Shigekawa, T. Yokouchi, S. Ishimitsu, Frame-by-frame speech recognition as hardware decoding on FPGA devices, in *The 9th International Conference on Sensing Technology, ICST 2015*, Auckland, New Zealand, 860–863 (2015)
13. T. Chiba, M. Kajiyama, *The Vowel: Its Nature and Structure* (Tokyo-Kaiseikan Pub. Co., Ltd., Tokyo, 1941)

14. B. Kavanagh, The phonemes of Japanese and English: a contrastive analysis study. *J. Aomori Univ. Health Welfare* **8**, 283–292 (2007)
15. J. Sundberg, *The Science of the Singing Voice* (Northern Illinois University Press, 1989)
16. C.T. Herbst, S. Ternström, A comparison of different methods to measure the EGG contact quotient. *Logoped. Phoniatr. Vocol.* **31**, 126–138 (2006)
17. G. Fant, *Acoustic Theory of Speech Production* (Mouton & Co., The Hague, Netherlands, 1960)
18. L.R. Rabiner, On the use of autocorrelation analysis for pitch detection. *IEEE Trans. Sig. Process.* **25**, 24–33 (1977)
19. LabVIEW, National Instruments Corporation. <http://www.ni.com/labview/>
20. K. Kato, K. Fujii, K. Kawai, Y. Ando, T. Yano, Blending vocal music with a given sound field due to the characteristics of the running autocorrelation function of singing voices. *J. Acoust. Soc. Am.* **115**, 2437 (2004)
21. ATR 503 sentences, Speech Resources Consortium (in Japanese). <http://research.nii.ac.jp/src/ATR503.html>

Elderly Infrared Body Temperature Telemonitoring System with XBee Wireless Protocol

Tonny Heng Yew Ling and Lim Jin Wong

Abstract Real time non-contact elderly infrared body temperature telemonitoring system with XBee wireless protocol is an emerging technology in both electronic and computer worlds. The technology plays an important role in elderly healthcare services. Non-contact elderly infrared body temperature telemonitoring system with XBee wireless protocol helps in monitoring body temperature of the elderly based on the elderly healthcare's history to provide the necessary treatment. Doctor or nurse can check the complete details of the elderly's profile from remote location and can recommend a suitable medication. The main purpose of this technology is to provide efficient healthcare facility remotely and to monitor the elderly in their natural environment such as homes where the non-contact infrared thermometer devices are attached. Real time non-contact elderly infrared body temperature telemonitoring system with XBee wireless protocol can greatly assist in disease management to maximize health, prevent complications, and conserve healthcare resources. With the aid of assistive technologies, elderly are allowed to live independently and to enjoy a better quality of life. Furthermore, this technology allows for extending healthcare resources to more people who currently have little or no access to healthcare services. This chapter identifies and discusses a real time non-contact elderly infrared body temperature telemonitoring system with XBee wireless protocol that links to computer and records the body temperature readings automatically.

T.H.Y. Ling (✉)

School of Engineering and Technology, University College of Technology
Sarawak, 96000 Sibul, Sarawak, Malaysia
e-mail: tonnyling@ucts.edu.my

L.J. Wong

Department of Electrical and Electronic Engineering, Laila Taib College,
96000 Sibul, Sarawak, Malaysia
e-mail: wlimjin@yahoo.com

1 Introduction

Recent developments in sensors, data recorders, and communication networks allow the unprecedented measurements of physiological and sociological data for use in geriatrics care. Monitoring physiological markers and elderly behaviours could lead to a better understanding of aging process and disease in the elderly [1].

As the worldwide population gets older, there is an increasing need for technologies capable of monitoring and assisting elderly anytime and anywhere so as to give them a more independent lifestyle.

With the upcoming reform of the healthcare system as well as the greater emphasis on care in the home and other living environments, geriatric providers will need alternate ways of monitoring disease, activity, response to therapy, and elderly safety.

Most of the present day technologies are not able to collect and match different types of data easily, or send the data over the Internet or another broad network to be stored in a system as well as to present, notify and assist healthcare professionals to make important decisions.

XBee network or more accurately known as the IEEE 802.15.4/XBee on the other hand, is known to be a low power consumption device with good and stable data transmission range, higher network flexibility and large number of nodes [2].

This chapter identifies and discusses the important issues regarding the use of real time non-contact elderly infrared body temperature telemonitoring system with XBee wireless protocol technologies in the elderly.

An infrared thermometer will be used in this study, and XBee is chosen to be connected to the infrared thermometer device. A pair of XBee will be used, one is to transmit and another one is to receive the data. XBee Receiver will be connected to a microcontroller to process the readings obtained from the infrared thermometer device. The received infrared thermometer readings will be recorded.

An interfacing system created by using Visual Studio will record the readings into a database and show the results to users. The first systematic measurement of human body temperature was performed by the German physician named Carl Wunderlich. In 1861, he measured the temperatures of one million healthy individuals. The average temperature value was reported as 37 °C [3].

The normal core body temperature of a healthy, resting adult human being is stated to be 37 °C. Though the body temperature measured on an individual can vary, healthy human body can maintain a fairly consistent body temperature that is around the mark of 37 °C.

Real time non-contact elderly infrared body temperature telemonitoring system with XBee wireless protocol is an emerging technology enabling the gathering of real-time data contributing towards decision making by healthcare professionals in the case of remote monitoring of body temperature of the elderly. Recent research, however, does not describe in details regarding how hardware, software and wireless communication perform together as a system to fully support a remote based healthcare application.

The data obtained in this study will be recorded in a computer equipped with graphical user interface to allow for easy access to the elderly’s daily body temperature readings and precise measurement time of the body temperature.

2 Human Body Temperature

Human body temperature varies due to metabolism rate. The higher (faster) the metabolism rate, the higher the human body temperature. The slower the metabolic rate, the lower the human body temperature.

Core body temperature is found in the blood supplying organs such as the brain and those in the abdominal and thoracic cavities. Apart from that, other factors that might affect the body temperature are the time of day and the part of body that the temperature is measured at.

Body temperature is lower in the morning due to the rest the body received, and higher at night after a day of activity and also after food intake. Oral temperature, the most convenient type of temperature measurement, is at 37 °C and is the accepted standard temperature for the normal core body temperature.

Body temperature is a vital sign and it is important to measure it accurately. A healthy body maintains its temperature within a narrow range using homeostatic thermoregulation mechanisms. The normal range for core body temperature in the literature varies, although 36–37.5 °C is acceptable in clinical practice [4].

Table 1 shows the normal range for the core body temperature in Fahrenheit and Celsius and the normal range are within 97.8–98.6 °F and 36.6–37.0 °C.

Table 1 Range of core body temperature in Fahrenheit and Celsius

Body temperature in degrees	
Fahrenheit	Celsius
99	37.2
98.6	37.0
97.8	36.6
105.5	40.8
105	40.6
104.5	40.3
104	40
103.5	39.7
103	39.4
102.5	39.2
102	38.9
101.5	38.6
101	38.3
100.5	38.1
100	37.8
99.5	37.5

It is important to acquire an accurate body temperature reading, allowing physician to make efficient treatment to patients especially elderly. A real time body temperature reading enables the doctor to give efficient advice to the elderly.

Measuring body temperature is important in the study of human body temperature regulation in daily life [5]. Normal body temperature does not change much with aging. But as we get older, it becomes harder for the body to control its temperature. This is because aging decreases elderly ability to sweat.

Elderly may not be alert enough to inform others when their bodies are becoming overheated. Fever is an important sign of illness in elderly persons. Fever is often the only symptom of a certain illness for several days.

Any fever that is not explained by a known illness should be checked by a healthcare provider. Body temperature is a vital sign and it is important to measure the body temperature accurately. Body temperature represents the balance between heat production and heat loss. If the rate of heat generated equates to the rate of heat lost, the core body temperature will be stable [4].

3 Normal Human Body Temperature Range

Every person has own body temperature and there are many factors that can affect the body temperature. When measuring body temperature, some basic aspects have to be considered. These basic aspects are influence of normal thermoregulation, gender, ageing and site of measurement [6].

The temperature of a body is an expression of its molecular excitation. The temperature difference between two points indicates a potential for heat to move from the warmer to the colder point. The human body's core temperature varies from day to day, and from time to time, but these fluctuations are small, usually no more than 1.0 °C. Humans are homoeothermic and body temperature is regulated at about 37 ± 1 °C.

The thermoregulatory center in the hypothalamus plays a very active role in keeping body temperature in the normal range. External and internal heat sources influence body temperature. The normal body temperature range of a human adult is 36.1–37.2 °C [7]. Table 2 shows the human body temperature range.

Table 2 Human body temperature range

Body temperature range	Hypothermia (low temperature) (°C)	Normal	Hyperthermia (high temperature)
Baby (birth to 2 years)	36	36–37	37–38
Children (3–12 years)	36	36–36.77	38
Adult (13–40 years)	36.1	36.1–37.2	37.5
Elder (above 40)	35	35.77–36.94	37.44–37.94

Temperature is read to establish a baseline of normal body temperature for the location and measuring conditions. The main reason for examining body temperature is to hunt for any signs of systemic infection or inflammation in the presence of a fever or high significantly above the individual's normal temperature. Temperature depression needs to be evaluated. It is also important to review the trend of the patient's temperature.

4 Types of Body Temperature Measuring

Thermometers are widely used to measure the body temperature in various applications. There are two standard units used for measuring temperature—Celsius and Fahrenheit. There are different kinds of thermometers that are more accurate in terms of temperature measurement and are very easy to use. The Celsius thermometers use the Celsius ($^{\circ}\text{C}$) as the measurement unit while the Fahrenheit thermometers use Fahrenheit ($^{\circ}\text{F}$) as the temperature measurement unit.

The clinical thermometers are used to measure the body temperature of the patient. The traditional thermometer measures temperature through the utilization of mercury or colored alcohol in a glass tube. It can be used under the tongue, in the rectum or under the arm. This type of thermometer is being used less and less nowadays because of the risks associated with its use. Users can be exposed to the toxic mercury or alcohol if the glass tube were to break.

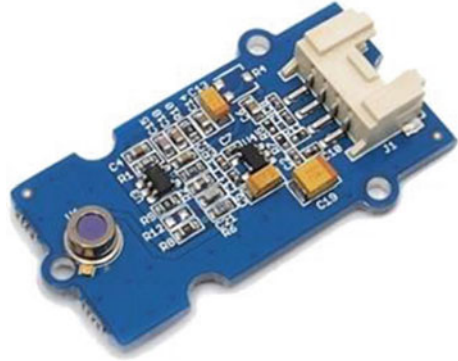
Human ear is located near to the brain. This makes human ear an accurate point to measure the body temperature. The temperature of the eardrum is measured by the ear (Tympanic) thermometers. However, the eardrum is the most fragile and delicate body part. Therefore, the body temperature cannot be measured by touching the eardrum. For temperature measurement at human ear, infrared sensors are used to remotely sense the temperature of the eardrum. Thermopile, an infrared sensor, is commonly used in ear thermometers.

A thermopile is a thermoelectric device that consists of an array of thermocouples connected in series. Thermopiles do not respond to absolute temperature, but generate an output voltage proportional to a local temperature's difference or temperature gradient. It is widely used in non-contact temperature measurement applications and temperature monitoring systems.

Infrared body temperature measuring device is chosen to measure body temperature in this study because it is non-intrusive to the elderly. Infrared temperature measurement technology is more and more receptive by businesses and manufacturers in recent years. Emissivity is a term used to quantify the energy-emitting characteristics of different materials and surfaces. IR sensors have adjustable emissivity settings, usually from 0.1 to 1.0, that allow accurate temperature measurements of several surface types [8].

The emitted energy from an object reaches the IR sensor through its optical system, which focuses the energy onto one or more photosensitive detectors. The detector then converts the IR energy into an electrical signal, which in turn is

Fig. 1 Non-contact IR sensor module



converted into a temperature value based on the sensor's calibration equation and the target's emissivity [9]. Figure 1 shows the non-contact IR sensor module.

5 Telemonitoring of the Elderly

Scanail et al. [10] presented a review of approaches to mobility telemonitoring of the elderly in their living environment. Telemonitoring has become increasingly popular in recent years due to rapid advances in both sensor and telecommunication technology.

Low-cost, unobtrusive, telemonitoring systems have been made possible by a reduction in the size and cost of monitoring sensors and recording or transmitting hardware. These hardware developments coupled with the many wired (PSTN, LAN, and ISDN) and wireless (RF, WLAN, and GSM) telecommunications options now available, has led to the development of a variety of telemonitoring applications.

Sirisha et al. proposed an independent system that automatically logs vital parameters of patients for easy access. The data is accessible to doctors through mobile devices for convenience. Data of all patients is stored in a common database. The patient monitoring system is first interfaced with a Zigbee co-ordinator. After power up, the patient monitoring system uses a timer program that runs on an ATMEL based microcontroller along with the attached interface sensors [11].

Zhou et al. proposed a real-time system for in-home activity monitoring of elders. The development of the whole system can assist the independent living of elders and improve the efficiency of eldercare practices. Their system allows for data to be collected, silhouettes extracted, features further analyzed and visualized into graphs from which eldercare professionals are able to understand massive video monitoring data within a short period of time [12].

Petcu et al. proposed an advanced telemedicine system for remote monitoring of patients and elderly people. This study develops solutions to improve the access,

efficiency, effectiveness, and quality of clinical and business processes utilized by healthcare and social care organizations, practitioners, patients, and consumers in an effort to improve the health status of patients [13]. The platform serves as a technological enabler to help elderly people to stay independent in their own houses and to help those suffering from chronic diseases and those living in isolated sites.

Suh et al. have presented a study titled “A Remote Patient Monitoring System for Congestive Heart Failure”. Their study aims to develop weight and activity with Blood Pressure Monitoring System (WANDA). WANDA is built on a three-tier architecture. The first tier consists of sensors that measure patients’ health related measurements and transmits data to the second tier. WANDA utilizes a Bluetooth weight scale, blood pressure monitor, activity monitor, and questionnaire systems to collect health related measurements and transmit data [14].

The second tier consists of web servers that receive data from the first tier and maintains data integrity. An abstraction of file formats and a shared ID table is used to merge WANDA data that is stored across several databases. In addition, when the obtained values are out of the acceptable range, the second tier sends alert messages to healthcare providers via text message or e-mail. The third tier is a back-end database server in WHI SOPHI that performs backup and recovery jobs by applying an offline backup.

6 Wireless Technology

Bluetooth is one of the common technologies used in a lot of electronic gadgets such as laptop, mobile phone, mouse and keyboard. Bluetooth is a wireless technology with global standard for expanding range of devices and services. It was invented by telecom vendor Ericsson in 1994. Bluetooth also uses unlicensed radio transmission to transmit and receive data in the speed of 2.4–2.485 GHz. Bluetooth is mainly developed to be used in personal area network (PAN). PAN is defined as a network of devices in the range of a person which can communicate with each other [15].

The Bluetooth is wireless, inexpensive and automatic. There are other ways to get around using wires, including infrared communication. Infrared refers to light waves of a lower frequency than human eyes that can receive and interpret data. Bluetooth networking transmits data via low-power radio waves. Bluetooth uses spread-spectrum to transmit data automatically. It is unlikely that two transmitters will be on the same frequency at the same time [16].

Bluetooth has a high data rate over short distance. For medical applications where data packets may be quiet large (overhead is large to ensure reliability), this is an important feature. However, the power consumption of Bluetooth devices can be quite high.

In addition to Bluetooth, WiFi has become a dominant standard for WLAN (wireless LAN). It is mainly developed to operate as a wireless Ethernet. WiFi is an open-standard technology that allows the wireless connectivity between equipment and local area networks [17]. It runs in unlicensed radio spectrums. WiFi can be set as open access to allow public to connect to it.

The range of the WiFi is about 50–150 m. The encryptions of the WiFi are WEP based on IEEE 802.11 and WPA based on IEEE 802.11i. Nowadays, those two encryptions can be hacked easily so it is not recommended to be used in personal area network. WiFi is designed for a longer connection and supports devices with a substantial power supply.

A newly emerging technology called XBee, sometimes referred to as Bluetooth Low Energy technology, is a lower power version of Bluetooth. XBee has been designed to provide enhanced power performance over Bluetooth. XBee may potentially be very important in future medical sensor applications [18].

Amaranadha reddy and Damodhar proposed a real time monitoring system for physiological signals using wireless sensor network. The wireless sensor network (WSN) used to observe the human physiological signals in their study is XBee, equipped with lower power consumption, small volume, high expansion, stylization and two-way transmission [19].

XBee is generally used for home care, digital home control, industrial and security control. They developed a suite of home care sensor network system by XBee's characteristic that is embedded sensors, such as the biosensor to observe heart rate and blood pressure. The biosensor transmits measured signals via XBee, and then sends to the remote wireless monitor to acquire the observed human physiological signals. XBee wireless module S1 series is shown in Fig. 2.

Fig. 2 XBee wireless module



The technology defined by the XBee specification is intended to be simpler and less expensive than other wireless protocols, such as Bluetooth or WiFi. Typical application areas are home entertainment control, wireless sensor networks, industrial control, embedded sensing, medical data collection, smoke and intruder warning and building automation [18].

7 Comparison of Wireless Protocols

Bluetooth and XBee are intended for portable products, short ranges, and limited battery power. Obviously, the Bluetooth and XBee protocols consume less power as compared with WiFi. Consequently, these two protocols offer very low power consumption and, in some cases, will not measurably affect battery life [20].

In summary, Bluetooth and XBee are suitable for low data rate applications with limited battery power (such as mobile devices and battery-operated sensor networks), due to their low power consumption leading to a long lifetime.

The short-range wireless scene is currently held by four protocols: the Bluetooth, UWB (Ultra-wideband), ZigBee, and WiFi. ZigBee provides self-organized, multi-hop, and reliable mesh networking with long battery lifetime.

Pothuganti and Chitneni conducted a comparative study of wireless protocols: Bluetooth, UWB (Ultra-wideband), ZigBee, and WiFi. The study presented a broad overview of the four most popular wireless standards: Bluetooth, UWB (Ultra-wideband), ZigBee, and WiFi with a quantitative evaluation in terms of the transmission time, data coding efficiency, protocol complexity, and power consumption [20].

The demand for wireless solutions continues to grow with its new standards have come forward and other existing standards have strengthened their position in the marketplace. Table 3 compares three popular wireless standards being used today and lists some of the design considerations that differentiate them.

Table 3 Comparisons between wireless protocols

Wireless parameter	XBee	Bluetooth	WiFi
Frequency band	2.4 GHz	2.4 GHz	2.4 GHz
Range	Indoors: up to 30 m outdoors: up to 100 m	9 m	75–90 m
Current consumption	25–35 mA (Tx mode) 3 μ A (standby mode)	60 mA (Tx mode)	400 mA (Tx mode) 20 mA (standby mode)
Maximum number of nodes per network	64 K	7	32 per access point
Number of channels	16	19	13
Maximum quiet bandwidth required	3 MHz (static)	15 MHz (dynamic)	22 MHz (static)
Typical network join time	30 ms typically	>3 s	Variable, 1 s typically

8 Arduino Uno Microcontroller

The Arduino Uno is a microcontroller board based on the ATmega328 chip. It has 14 digital input/output pins (of which 6 can be used as PWM outputs), 6 analog inputs, a 16 MHz crystal oscillator, a USB connection, a power jack, an ICSP header, and a reset button. It contains everything needed to support the microcontroller.

Arduino UNO can be connected to a computer with a USB cable or to an AC-to-DC adapter or battery to get started. The UNO differs from all preceding boards in that it does not use the FTDI USB-to-serial driver chip. Instead, it features the ATmega8U2 programmed as a USB-to-serial converter. Arduino Uno contains the processor (which all computers have) and memory, and some input/output pins that user can control [21].

Figure 3 shows the Arduino Uno microcontroller board, means hardware is reasonably priced and development software is free. The Arduino programming language is a simplified version of C or C++ [22].

9 Visual Studio

Microsoft Visual Studio is an Integrated Development Environment (IDE) developed by Microsoft. It is used to develop computer programs for Microsoft Windows, as well as web sites, web applications and web services. Visual Studio uses Microsoft software development platforms such as Windows API, Windows Forms, Windows Presentation Foundation, Windows Store and Microsoft Silverlight. It can produce both native code and managed code [23].

Figure 4 shows the concept of the form for the Real time non-contact elderly infrared body temperature telemonitoring system with XBee wireless protocol. It consists of three main sections: elderly profile, current reading of body temperature and previous record of body temperature.

Fig. 3 Arduino Uno microcontroller board



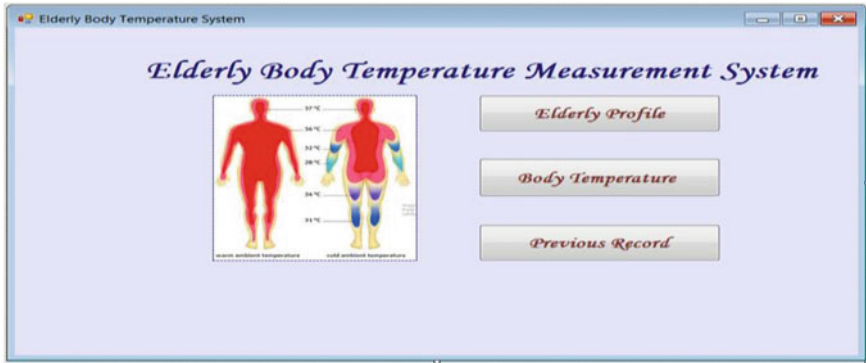


Fig. 4 Form of the elderly body temperature measurement system



Fig. 5 Form of the elderly profile

Figure 5 shows the form for the elderly profile. The form enables user to save and update personal data such as user ID, name, age, NRIC, gender, contact no and home address.

Figure 6 shows the form of real time elderly body temperature reading in chart form.

Visual Studio supports different programming languages and allows the code editor and debugger to support (to varying degrees) nearly any programming language, provided a language-specific service exists. Built-in languages include C, C++ and C++/CLI (via Visual C++), VB.NET (via Visual Basic.NET), C# (via Visual C#), and F# (as of Visual Studio 2010) [24].

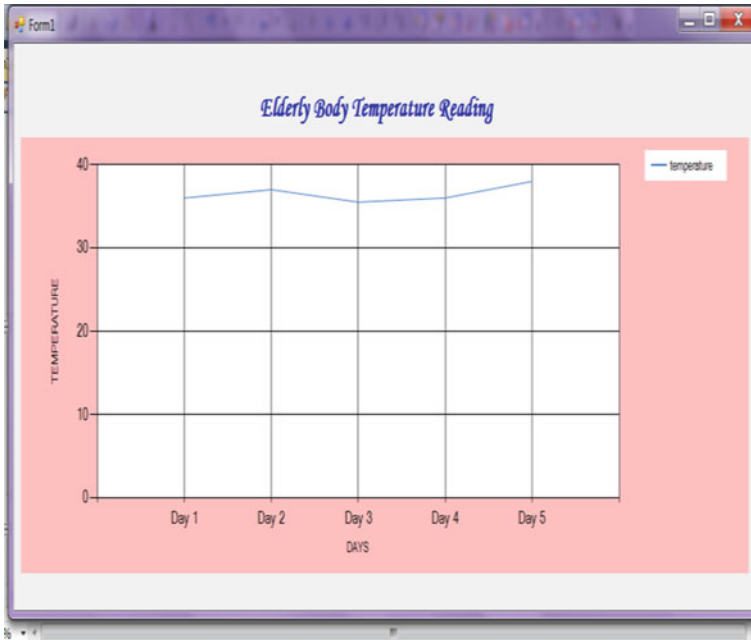


Fig. 6 Form of the elderly body temperature reading

10 System Architecture

The reading from non-contact elderly infrared body temperature telemonitoring system will be sent to the computer via XBee wireless protocol. Figure 7 shows how the Elderly Infrared Body Temperature Telemonitoring System with XBee Wireless Protocol works. Arduino Uno microcontroller will be the main part to get the body temperature reading from the receiver XBee.

The infrared body temperature sensor module will be connected to the transmitter XBee. The microcontroller will be programmed to read the input data from analog port via receiver XBee. The 16×2 LCD display will be used to display the temperature reading obtained from the microcontroller. A program written by the Visual Studio will be used to record the data received from the microcontroller.

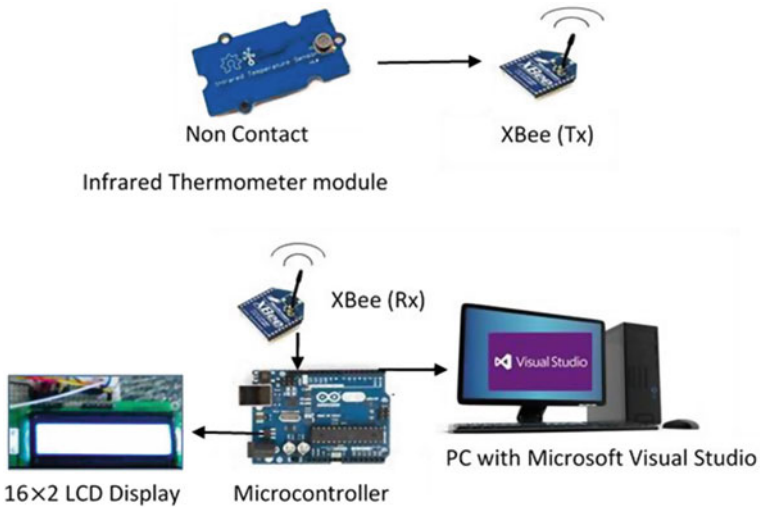


Fig. 7 Block diagram of the system

Ordinary body temperature thermometer only stores limited readings due to the memory limitation of the device. With the use of the computer, large memory is available when compared to the ordinary body temperature thermometer. Visual Studio 2014 will be used to create a computer interface that can record the data and create a table of elderly body temperature readings.

XBee needs to be configured by using the X-CTU program before it can be used. X-CTU is used to update or change the firmware on the radios. X-CTU can switch XBee radio from router to coordinator or switch between API and AT modes. One limitation of X-CTU is that it only works on Windows. One can download the latest X-CTU from Digi's X-CTU page.

XCTU includes all of the tools a developer needs to quickly get up and running with XBee. Unique features like graphical network view that graphically represents the XBee network along with the signal strength of each connection, and the XBee API frame builder that intuitively helps to build and interpret API frames for XBees being used in API mode, combine to make development on the XBee platform easier than ever [25].

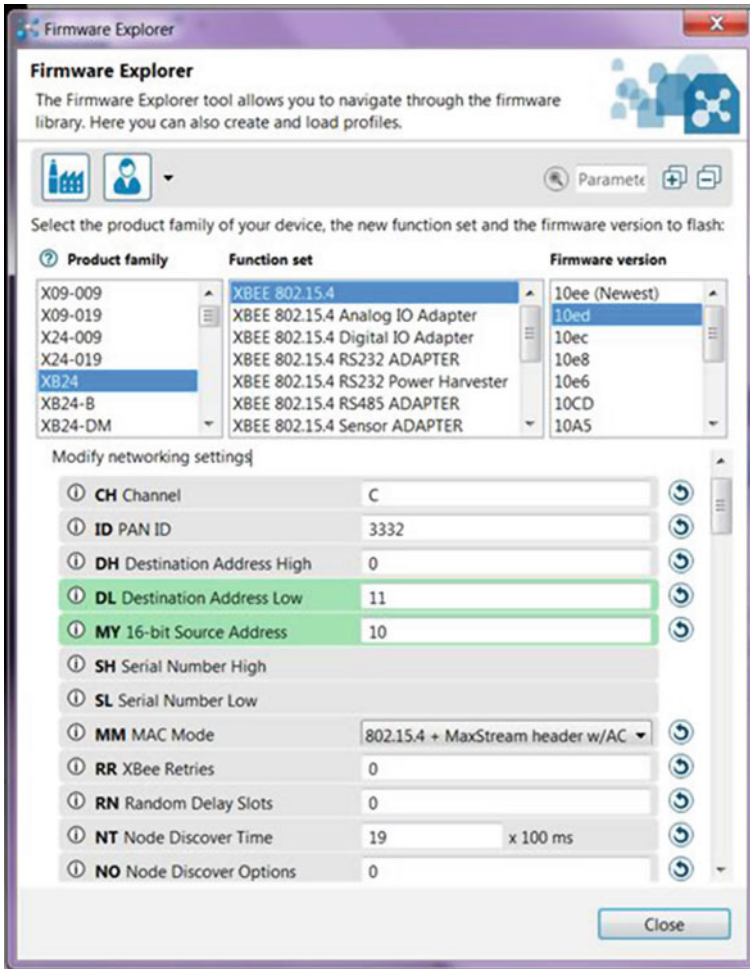


Fig. 8 XBee setup as transmitter

Two XBees are needed in this study as the wireless protocol to send the body temperature reading obtained by Arduino to the computer. In order to use those two XBees, it is required to program one of the XBees into a coordinator device and another as the end device. In Fig. 8, the first XBee is configured as transmitter and

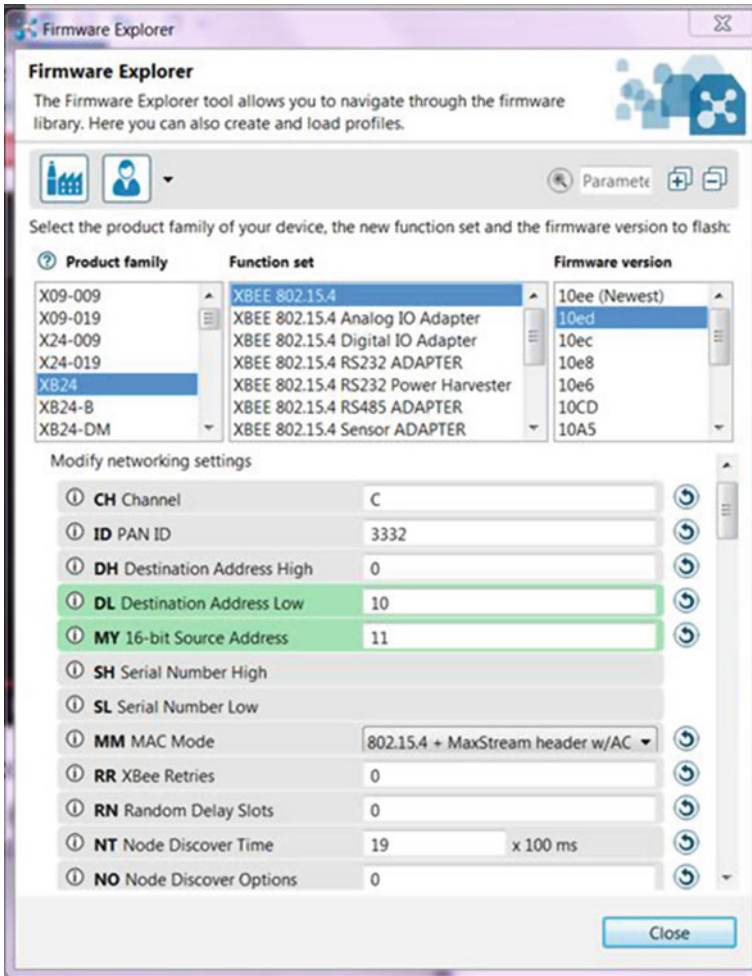


Fig. 9 XBee setup as receiver

XBee in Fig. 8 is configured as receiving device. Those two XBees need to have the same PAN ID in order to send and receive data in the same ID.

DL and MY are Destination Address Low and 16-bit Source Address respectively. Those DL of the first modem is set to source MY for the transmitter XBee and DL is set to MY of the modem for the receiver XBee. As shown in Figs. 8 and 9, the two XBees were configured with the destination address of each other.

Fig. 10 XBee Tx and XBee Rx of the system

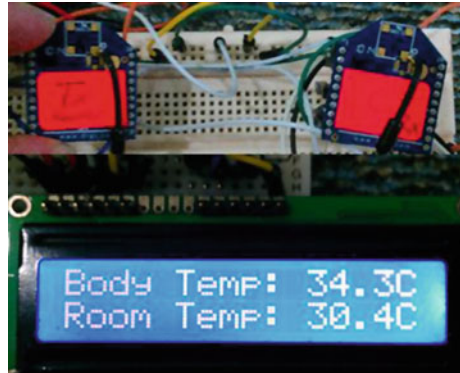
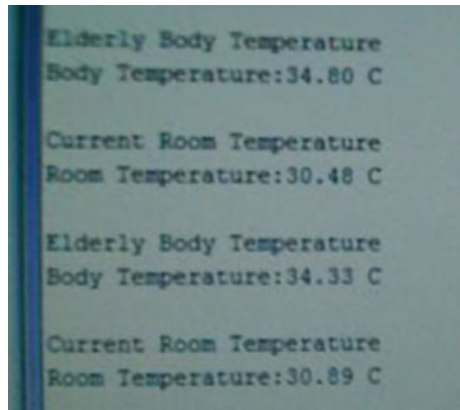


Fig. 11 Serial data from the microcontroller system



The transmitter XBee is set to analog input and the sample rate is set at 20 ms (hex value 14). The receiver XBee is set to PWM output in which physical pin 6 and the I/O input address are set as MY source address of the transmitter XBee.

Figure 10 shows the XBee transmitter sending the data wirelessly to XBee receiver. The body temperature reading obtained by XBee receiver will then read by the Arduino microcontroller. The result of the sensor reading will then be displayed on the 16×2 LCD and computer via Visual Basic software.

The Arduino Uno can display the serial data through com port as shown in Fig. 11.

11 Conclusion

Real time non-contact elderly infrared body temperature telemonitoring system with XBee wireless protocol is useful and able to give earlier symptoms of illness in the elderly. It allows care givers to rest at ease because their loved ones are in safe condition. It will bring advantages to hospitals and physicians. Hospitals and physicians need reliable wireless monitoring system to observe real time physiological data from elderly's patients outside the hospital with high and reliable accuracy.

This system incorporated with the advanced wireless transceiver and non-intrusive body biomedical sensor is able to record and document the elderly body temperature reading, hence healthcare can maintain at its optimum standard.

Real time non-contact elderly infrared body temperature telemonitoring system with XBee wireless protocol can provide continuous physiological data, as well as better information regarding the general health of the elderly. Thus, such monitoring system will reduce healthcare costs by disease prevention and enhance the quality of elderly's life with disease management.

To avoid unexpected health problems and to obtain higher accuracy in diagnosis of the health conditions of an elderly's patient, efficient and comprehensive data collecting, monitoring and controlling play an important role to improve the healthcare system. As such, elderly infrared body temperature telemonitoring system with XBee wireless protocol is proposed and recommended for use by physicians in hospitals.

References

1. H.G. Kang, D.F. Mahoney, H. Hoeing, V.A. Hirth, P. Bonato, I. Hajjar, L.A. Lipsitz, In situ monitoring of health in older adults: technologies and issues. *J. Am. Geriatr. Soc.* **58**(8), 1579–1586 (2010)
2. H. Daud, N.F.I. Gulcharan, M.A.M. Azhar, M.Z. Samsudin, N. Mohd Nor, T. Ibrahim, Monitoring heart rate and body temperature using wireless technology (Zigbee). *Appl. Mech. Mater.* **490–491**, 1565–1574 (2014)
3. <http://hypertextbook.com/facts/LenaWong.shtml>
4. L. McCallum, D. Higgins, Measuring Body Temperature. *Nursing Times*, pp. 20–22 (2013)
5. K. Yamasue, H. Hagiwara, O. Tochikubo, C. Sugimoto, R. Kohno, Measurement of core body temperature by an ingestible capsule sensor and evaluation of its wireless communication performance. *Adv. Biomed. Eng.* **1**, 9–15 (2012)
6. M. Sund-Levander, E. Grodzinsky, Time for a change to assess and evaluate body temperature in clinical practice. *Int. J. Nurs. Pract.* **15**(4), 241–249 (2009)
7. T.H.Y. Ling, L.J. Wong, J.E.H. Tan, K.Y. Kiu, Non-intrusive human body temperature acquisition and monitoring system. in *6th International Conference on ISMS, IEEE Computer Society Conference Publishing Services (CPS)*, ISSN: 2166-0670, IEEE (2015)
8. D. Peng, S. Wan, *Industrial Temperature Monitoring System Design Based on Zigbee and Infrared Temperature Sensing* (Nanchang Hangkong University, 2013)
9. R. Wotiz, Infrared thermal detectors (2012)

10. C.N. Scanail, S. Carew, P. Barralon, N. Noury, D. Lyons, G.M. Lyons, A review of approaches to mobility telemonitoring of the elderly in their living environment. *Ann. Biomed. Eng.* **34**(4), 547–563 (2006)
11. B. Sirisha, T. Sraddha, K. Vijayanand, Real-time multi-patient monitoring system using arm and wireless sensor network. *Int. J. Commun. Netw. Secur.* **2**(2), 41–47 (2013). ISSN: 2231-1882
12. Z. Zhou, W. Dai, J. Eggert, J.T. Giger, J. Keller, M. Rantz, Z. He, A real-time system for in-home activity monitoring of elders. in *31st Annual International Conference of the IEEE EMBS* Minneapolis, Minnesota, USA, IEEE (2009)
13. V. Petcu, A. Petrescu, I. Nastase, Advanced Telemedicine system of systems for remote monitoring of patients and elderly people, *Med E Tel Luxembourg* (2010)
14. M. Suh, C-A. Chen, J. Woodbridge, M.K. Tu, J.I. Kim, A. Nahapetian, L.S. Evangelista, M. Sarrafzadeh, *A Remote Patient Monitoring System for Congestive Heart Failure* (Springer Science and Business Media, LLC, 2011)
15. R. Sharma, N. Thakur, S. Kumar, Review paper on wireless sensor networks. in *Proceedings of the International Conference on Recent Trends In Computing and Communication Engineering* (2013)
16. G. Fleishman, Inside Bluetooth 2.0. Macworld.com (2005)
17. T. Gao, D. Greenspan, M. Welsh, R.R. Juang, A. Alm, Vital signs monitoring and patient tracking over a wireless network. in *Proceedings of the 27th Annual International Conference of the IEEE EMBS*, Shanghai, September 2005
18. <https://docs.zigbee.org/zigbee-docs/dcn/09-4962.pdf>
19. P. Amaranadha reddy, J. Damodhar, A real time monitoring system for physiological signals using wireless sensor network. *Int. Eng. Trends Technol.* **3**(4) (2012)
20. K. Pothuganti, A. Chitnenni, A comparative study of wireless protocols: Bluetooth, UWB, ZigBee and Wifi, Vol. **4**(6), 655–662 (2014) (ISSN 2231-1297)
21. A.G. Smith, *Introduction to Arduino* (2011)
22. W. Durfe, *Arduino Microcontroller Guide* (University of Minnesota, 2011)
23. D.D. Sarkar, Visual studio professional: a benchmark in bioinformatics. *Int. J. Comput. Sci. Technol.* **6**(2) (2015)
24. A. Kennedy, D. Syme, K. Takeda, *F# at Microsoft Research* (Microsoft Research, Cambridge, 2012)
25. Digi International Inc., *An Introduction to ZigBee. Part Number 019-0162–C* (2008)

Heart Sound Sensing Through MEMS Microphone

Madhubabu Anumukonda and Shubhajit Roy Chowdhury

Abstract MEMS are becoming the most popular and playing a vital role in development of the non-invasive diagnostic instruments. The MEMS microphones are very useful in development cardio auscultation systems due to its size and free ambient noises. The heart sound signals can be detected at cardiac auscultation points using different microphones. This chapter covers the detection of heart sound signals (S1 and S2) using the inexpensive MEMS microphone. The MEMS microphone has been suitably interfaced with a microcontroller. Using an algorithm that has been developed, the non-stationary phonocardiograph (PCG) signal has been transformed into stationary systole and diastole signals for further analysis. Further the systole and diastole signals have been analysed using Fast Fourier transform to detect the high intensity peaks of S1 and S2 in the frequency range of 50–200 Hz.

1 Introduction

In modern medicine various sensors are available for monitoring the day to day events of human health by means of physical parameters like sound, pressure, temperature, electromagnetic radiation and electric potentials [1]. These sensors are playing a vital role in the development of non-invasive diagnostic instruments [2]. Also all these sensors are available in Micro-Electro-Mechanical Systems (MEMS) based chip and addressing the most of the medical applications like surgical tools, medical imaging, capsules for cancer detection and cardiac diagnosis etc. [3, 4].

M. Anumukonda (✉)
Centre for VLSI and Embedded System Technology, International Institute
of Information Technology Hyderabad, Hyderabad, India
e-mail: madhubabu.a@research.iiit.ac.in

S.R. Chowdhury
School of Computing and Electrical Engineering, Indian Institute
of Technology Mandi, Mandi, India
e-mail: src@iitmandi.ac.in

The MEMS microphone has the acoustic sensor that is mainly used for the detecting the phonocardiography signals to measure the acoustics of the heart sound [5]. The present work focuses on implementation of low cost heart sensing system using MEMS microphone for detection of heart sounds and analyses using Fast Fourier Transform (FFT) to detect the high intensity peaks of heart sound signals.

The chapter is organized as follows: Sect. 2 presents the Motivation. Section 3 presents the background about the auscultation areas, heart sounds and MEMS microphones used for present work. Section 4 explains the system design details about the proposed system for heart sound sensing, data acquisition, pre-processing and analysis. Section 5 shows the results and discussion.

2 Motivation

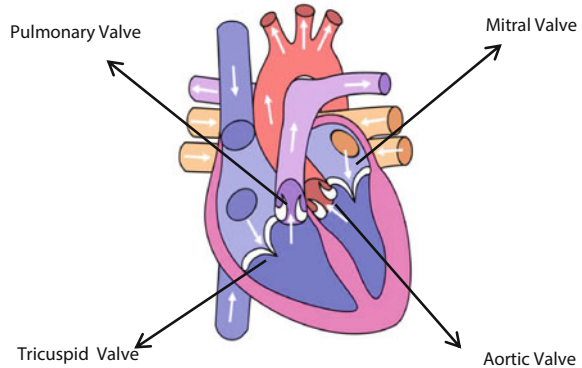
From ancient days to modern digital era, stethoscope is the primary instrument in PCG for heart sound detection to diagnose the humans for illnesses [6]. The heart sounds detected are very low and falls in lowest band of human hearing. The medical practitioner needs a lot of clinical expertise for listening and analyse the heart sounds by comparing normal versus abnormal hear sounds for diagnosis [7]. This manual analysis leads to complication in analysis of heart sounds. These complexities can be overcome with the new advancements in VLSI and signal processing techniques leading to improvement of measurement accuracy and reproducibility of PCG signal and analysis using computer aided methods giving the best diagnosis compared to the manual analysis [8].

3 Heart Sounds and Auscultation Areas

The heart sounds are generated due to the contraction and expansion of the heart valves as the blood flows into the heart and rest of body [9]. During heart examination, the medical practitioner listen the heart sound with the help of stethoscope and evaluates the heart sound components separately over the cardiac cycle. Each cardiac cycle consists of systolic and diastolic stages. The heart sounds are measured at four major valves of the heart and these are called as areas of auscultation. Investigation of heart sound at each auscultation area provides the functionality of the heart and thereby detects abnormalities of the heart to diagnosis the illness [8]. The four heart sound areas (Fig. 1) are Aortic area (right second intercostal space), pulmonic area (left second intercostal space), Tricuspid area (mid left sternal border), and Mitral area (fifth intercostal space, mid clavicular line). All these areas correspond to the one of the heart valve and these are as follows:

Mitral valve: The mitral valve controls the flow of blood from the upper-left chamber (the left atrium) to the lower-left chamber (the left ventricle).

Fig. 1 Heart valves



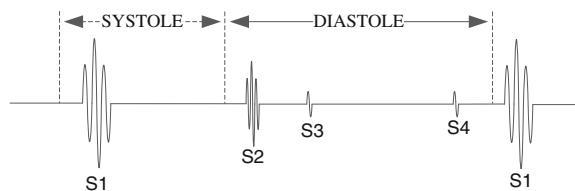
Aortic valve: The Aortic valve controls the blood flow from the heart’s lower-left chamber (the left ventricle) into the aorta. The aorta is the main vessel that supplies blood to the rest of the body.

Tricuspid valve: The tricuspid valve controls the blood flow from the heart’s upper-right chamber (the right atrium) to the lower-right chamber (the right ventricle).

Pulmonary valve: The pulmonary valve controls the blood flow between the heart’s lower-right chamber (the right ventricle) and the pulmonary artery, controlling the blood flow between the heart and lungs.

These four heart valves pumps the blood through the heart. During pumping of the blood, the four major heart sounds are generated due to opening and closing of the heart valves. The closing of mitral and tricuspid valves and opening of the aortic and pulmonary valves generates the first heart sound, S1 during the systole cycle. S1 is best listens as “dub” at the apex of the heart. The closing of the aortic and pulmonary valves and opening of the mitral and tricuspid valves generates the second heart sound, S2 during the diastole cycle. S2 is best listens as “lub” at the base of the heart. When the blood flow hits the ventricular wall during the rapid filling phase generates the third heart sound, S3 in the pre-diastole cycle. S3 is best listened at the apex as “lub-dub-sum” and it is a low pitched audible sound. When the blood flow hits the ventricular wall during the atrial systole generates the fourth heart sound, S4 in the pre-systolic cycle. S4 is best listened at the apex as “da-lub-dub” and it is a low pitched audible sound. Figure 2 shows the pictorial representation of S1, S2, S3 and S4 heart sounds during cardiac systole-diastole

Fig. 2 Cardiac systole-diastole cycle



cycle. The present work concentrated on detection and analysis of primary heart sounds S1 & S2 signals.

4 Heart Valve Pathology

There are two major pathological conditions; stenosis and regurgitation caused during the blood flow through the heart valves. Regurgitation is the blood flowing backwards due to improper close of heart valve. The heart Stenosis is the blood flow through the narrowed heart valves. The heart valve stenosis and regurgitation causes the small amount of blood pumps from the heart to the body organs. This makes the heart to work harder to pump the blood and thereby leads to heart failure.

Mitral regurgitation (MR) is the backflow of blood into the left atrium. Aortic regurgitation (AR) is the backflow of blood from an enlarged aortic valve into the left ventricle. Tricuspid regurgitation (TR) is the backflow of blood from the right ventricle to the right atrium. Pulmonary regurgitation (PR) is the backflow of blood from the pulmonary arteries to the right ventricle.

Mitral stenosis (MS) is due to narrowing of the mitral valve and causes blood to back up in the left atrium instead of flowing into the left ventricle. Aortic stenosis (AS) is due to narrowing of the aortic valve. This regulates the blood flow from left ventricle into the aorta. Tricuspid stenosis (TS) is due to narrowing of the tricuspid valve. This regulates the blood flow from right atrium into the right ventricle. Pulmonary stenosis (PS) is due to narrowing of the pulmonary valve and regulates the blood flow from the right ventricle into the pulmonary arteries.

Tricuspid and Pulmonary valve problem occurs rarely compared to the Mitral and Aortic valves. The present work concentrated on detection and analysis of Mitral and Aortic pathology.

5 Mems Microphones

The present available heart sound detection systems built using the piezoelectric and electret condenser microphones. These systems have complex electronics for heart sound detection, amplification, Analog to digital circuitry and increase the cost of the system. Also these types of systems suffer from the ambient problems like mechanical vibrations, temperature variations, and electromagnetic interference. These shortcomings can be overcome by MEMS microphones based heart sound detection system, which are smaller in size and has inbuilt digital interface easily integrated with any system without much overhead of electronic components.

MEMS microphone is single chip with built-in sound transducer and combination of different interface components using CMOS technology [5]. Mainly two types of MEMS microphones are available and they are Analog MEMS and Digital MEMS [10]. The Analog MEMS have transducer with output amplification.

Fig. 3 Digital MEMS microphone block diagram [10]

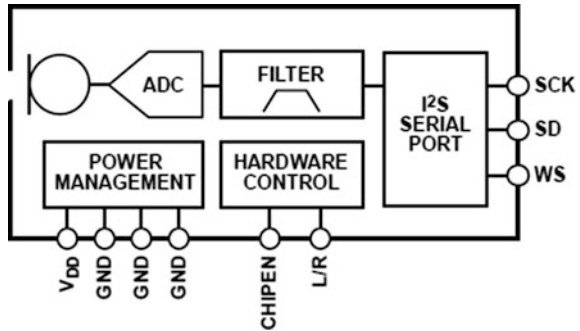


Table 1 Microphone parameters used for heartsound measurement

Parameter	Value
Directionality	Omni
Sensitivity	-26 dBFS
Frequency response	60 Hz to 15 kHz
SNR	61 dBA
Dynamic range	87 dB

The digital MEMS have additional Analog to digital converters to get direct digital output. The digital output available in two types either Pulse Density Modulation (PDM) format or Integrated Interchip-Sound (I2S) format. In the present research we used the digital MEMS microphone with digital output type I2S format. Figure 3 shows the digital MEMS microphone block used to measure the heart sounds. This microphone has high sensitivity of -26 dBFS and flat frequency response between 60 and 15 kHz. Due to high sensitivity and flat frequency response major heart sounds can be measured with good quality.

Table 1 shows the parameters of the MEMS microphone used for heart sound measurement.

6 Spectral Analysis of Heart Sound

In 1965 Cooley and Tukey provided the Fast Fourier Transform algorithm [11] to calculate DFT of signal. Fast-Fourier transform is the one of the well-known method in signal processing for the analysing frequency components and their amplitudes. Equation 1 shows the FFT implementation of N-point DFT by computing two N/2 points. Where $x(2n)$ are even number of samples, $x(2n + 1)$ are odd number of samples and $W_{N/2}^{nm}$ W_N^m are twiddle factors.

$$X(m) = \sum_{n=0}^{(N/2)-1} x(2n)W_{N/2}^{nm} + W_N^m \sum_{n=0}^{(N/2)-1} x(2n+1)W_{N/2}^{nm} \quad (1)$$

The PCG signal is a non-stationary signal and its frequency varies over the cardiac cycle [12]. But the frequency of variation is minimal in systole and diastole cycles. So the Short-Time Fourier Transform (STFT) is more suitable to analysis the heart signal. The STFT is same as the Fourier Transform of the signal after passing through the sliding time window $w(t)$ as given in Eq. 2.

$$X(m, w) = \sum x(n)w(n-m)e^{-jwn} \quad (2)$$

where $w(n)$ is the discrete-time window function, $x(n)$ is discrete-time signal.

The location of sliding window gives the time information for the time-varying frequency analysis. Also the size of the window determines time-frequency resolution for the signal analysis, so the window size needs to be choosing to balance the time and frequency requirement. In the present analysis both systole and diastole samples are separated over the cardiac cycle time period. After separation of the systole and diastole cycles, passed through the window technique and applied the Fast Fourier transform individually to measure the high intensity peaks of the frequency components in systole and diastole cycles.

7 System Implementation

The proposed heart sound sensing system consists of heart sound detection, data acquisition and heart sound analysis. The heart sound sensing is carried using digital MEMS microphone,

Microcontroller is used for the heart data acquisition and MATLAB is used for the heart sound analysis on host PC. Figure 4 shows the proposed block diagram for heart sound sensing system. Each component will be described as follows.

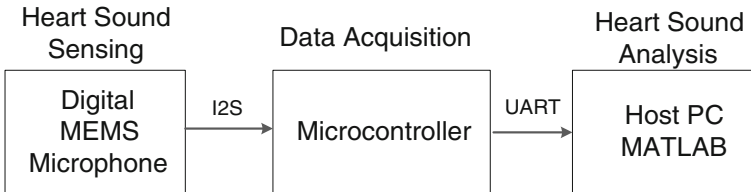


Fig. 4 Heart sound sensing block diagram

7.1 Heart Sound Sensing

The digital MEMS microphone is used for the heart sound sensing. The MEMS microphone has in built MEMS transducer, signal conditioning, an Analog-to-digital converter, antialiasing filters, power management, and a 24-bit I2S interface. In microcontroller I2S interface is developed to interface with digital microphone for collection of digital data samples. Figure 5 shows the timing diagram for the I2S format. The heart sounds frequencies are generated in the range 20 and 200 Hz. This microphone has the good sensitivity between 60 and 15 kHz frequency response. So this microphone can easily sense the major heart sounds S1 and S2 which are fall in frequency range of 60–250 Hz.

7.2 Data Acquisition

The data acquisition interface is developed on 32-bit microcontroller for heart sensing samples from MEMS microphone. The data acquisition has I2S receiver implementation for the collection of data samples from microphone I2S transmitter interface. Also the microcontroller has data buffer for storage of collected samples, UART interface for sending the data to host PC for further analysis. The data sample frequency of I2S receiver is 1.024 kHz for collection of 16,000 samples per second and stored in data buffer. The heart sound data samples are collected at the pulmonic area for heart.

7.3 Heart Sound Analyses

The heart sound sensing and data acquisition is done in a controlled environment to free from the breathing noise, artefacts and voice in fetched samples. The raw samples are processed to extract the real heart sounds. Figures 6, 7 shows the data acquisition and analysis flow chart of the heart samples collected using microphone. The extraction and analyses of heart sounds from the raw samples is implemented using MATALAB in host PC. The MATLAB code performs three functions, first collecting the samples from ARM processor data buffer using UART interface, secondly filters the all the unwanted frequencies using band pass filters and finally performs STFT on processed samples to detect the frequencies of the heart sounds.

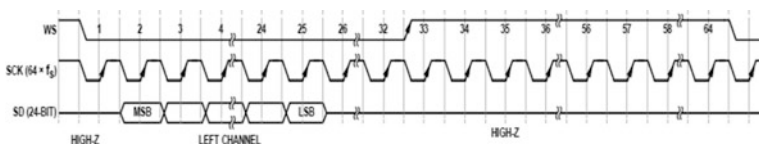
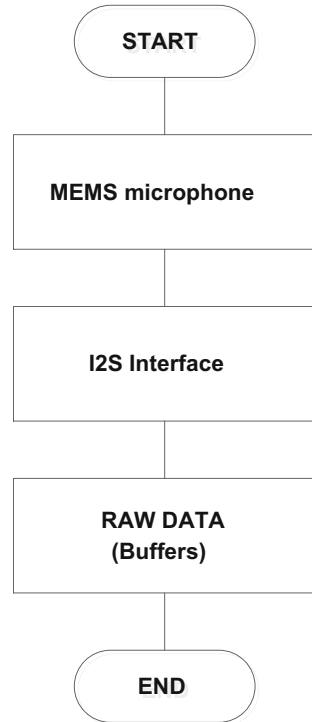


Fig. 5 Sample acquisition I2S format

Fig. 6 Data acquisition flowchart



The raw samples have unwanted frequencies and these can be removed using the band pass filter (see Fig. 8) of cut of frequencies between 50 and 200 Hz. The filtered raw samples are free from the external noises and contain the only heart sound frequency components. The heart sound signal sensing over a cardiac cycle is non-stationary and the frequency analysis on this provides in-appropriate frequency components. But dividing the systole and diastole cycle shows the stationary behaviour and frequency response gives the correct values. The filtered heart samples are manually separated by ratio of 30:70 for cardiac period to extract the systole and diastole samples. After separating the systole and diastole samples applied the window technique and 128 point FFT to identify the peak frequency components in a cardiac cycle. The peak of the frequency component on systole samples identifies the first heart sound S1 and peak of frequency component on diastole samples identifies the second heart sound S2.

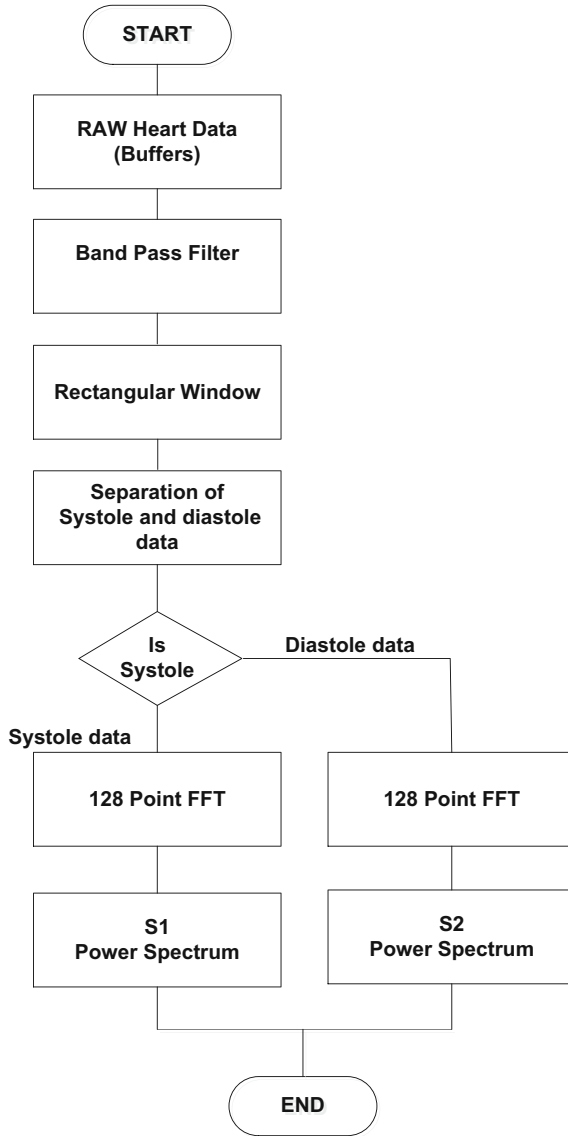


Fig. 7 Heart sound analysis flow chart

Fig. 8 Band pass filter response

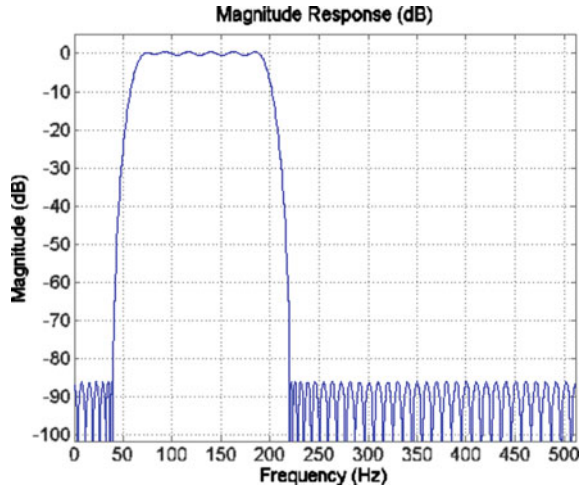


Fig. 9 Heart sounds samples (S1 and S2) before pre processing

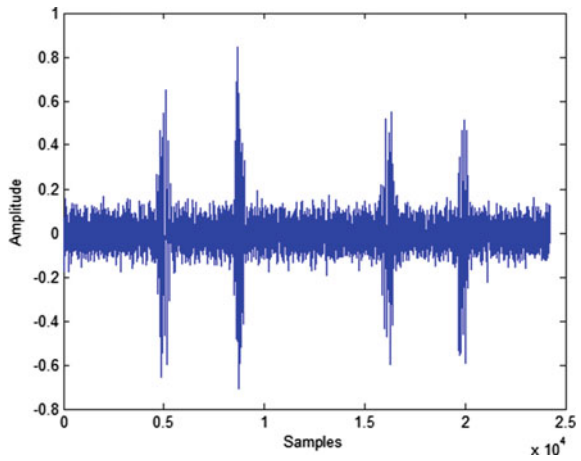


Fig. 10 Heart sound samples (S1 and S2) after pre-processing

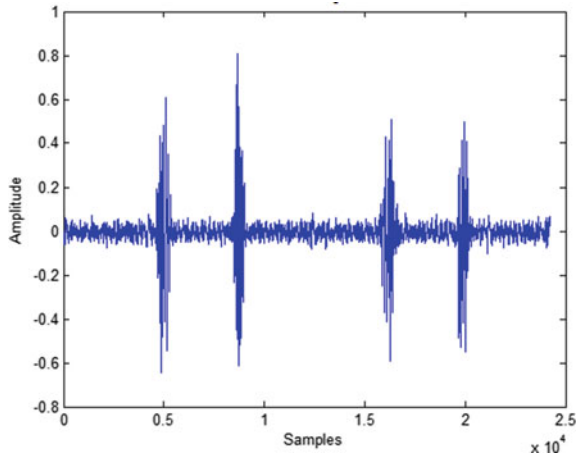


Fig. 11 Processed samples of heart sounds S1

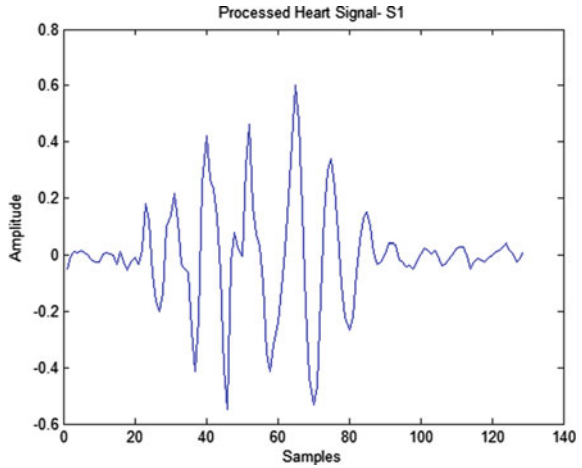
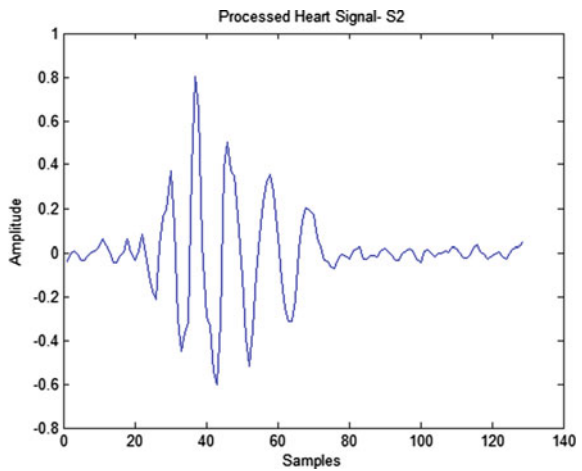


Fig. 12 Processed samples of heart sounds S2



8 Result and Discussion

As mentioned above the heart sound samples over a cardiac cycle are detected using MEMS microphone and samples are shown in Fig. 9. The input samples have resolution of 24 bits per sample and sampled at frequency 1.024 kHz. These samples are processed using band pass filter and extracted heart sound samples are as shown in Fig. 10. The processed S1 and S2 heart sounds after separating the systole and diastole cycles using algorithm depicted in Fig. 7 are shown in Figs. 11 and 12. Finally the frequency response of S1 and S2 heart sounds are shown in Figs. 13 and 14 after FFT analysis. The frequency spectrum shows the S1 and S2 high intensity/amplitude peaks. The detected S1 and S2 peaks are observed in the range of 50–200 Hz. Along with normal heart sounds pathological heart sounds are also detected using MEMS microphone and identified the Mitral and Aortic

Fig. 13 Frequency response of heart sounds S1

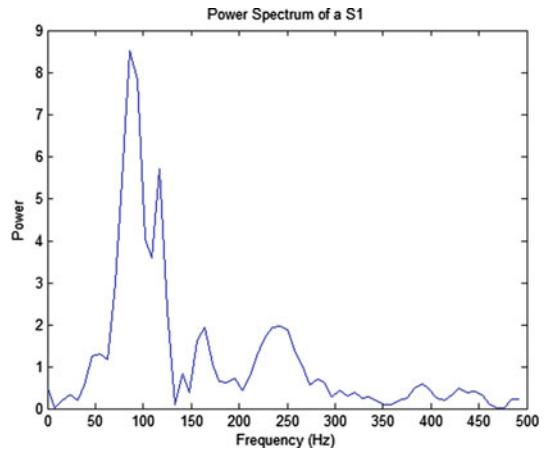


Fig. 14 Frequency response of heart sounds S2

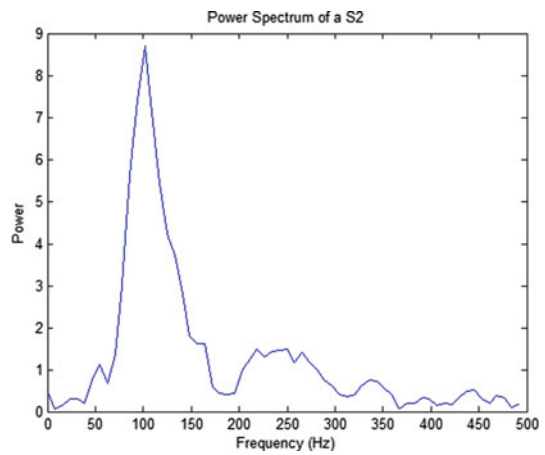


Fig. 15 Frequency response of heart sounds (MS)

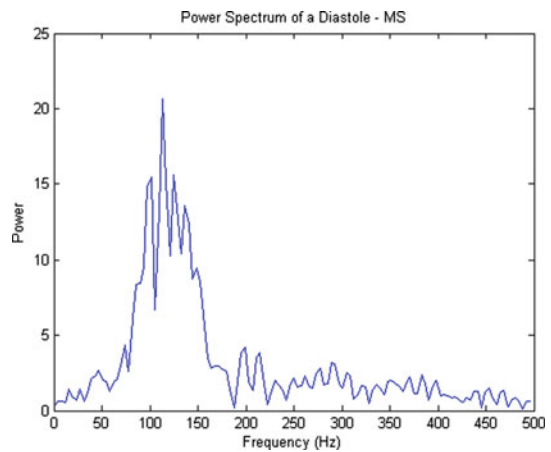


Fig. 16 Frequency response of heart sounds (AS)

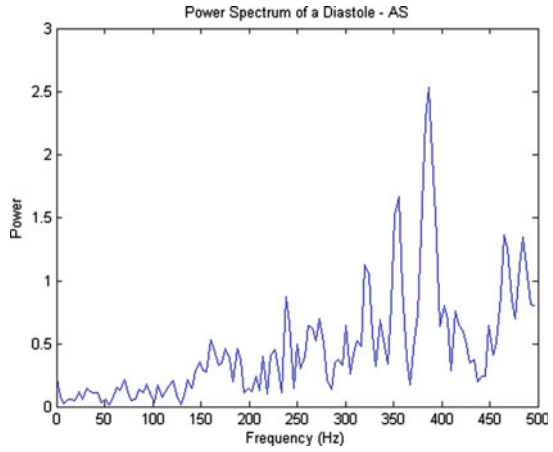


Fig. 17 Frequency response of heart sounds (MR)

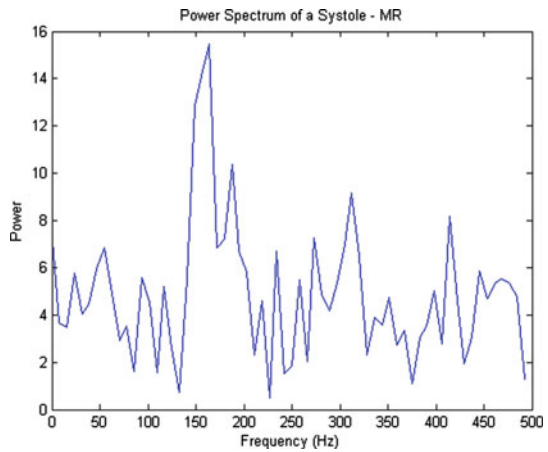
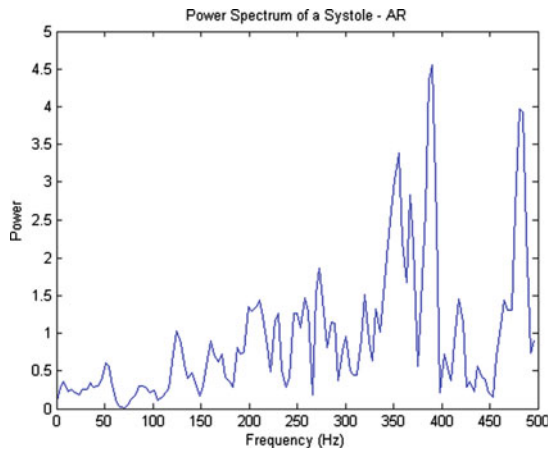


Fig. 18 Frequency response of heart sounds (A)



pathology. The frequency response of heart sound diastole cycle for the Mitral Stenosis (MS), Aortic Stenosis (AS) is shown in Figs. 15 and 16. The frequency response of heart sound systole cycle for the Mitral regurgitation (MR), Aortic regurgitation (AR) is shown in Figs. 17 and 18.

9 Conclusion

This chapter focused on the inexpensive heart sound sensing system for detection of the major heart sounds S1 and S2 using MEMS microphone. The digital MEMS have been interfaced with microcontroller using I2S protocol. Finally the non-stationary heart sound signal has been separated into stationary systole and diastole cycles and Fast Fourier Transform (FFT) has been applied for detecting high intensity peaks of S1 and S2. Along with normal heart sounds S1 and S2, also sensed the heart sound pathologies like Mitral regurgitation (MR), Mitral stenosis (MS), Aortic regurgitation (AR) and Aortic Stenosis (AS). The same experiment setup can be used for further analysis of heart sound signals and also detecting the complex heart sound signals S3 and S4 for better diagnosis.

References

1. F. Khoshnoud, C.W. de Silva Recent, Advances in MEMS sensor technology-biomedical applications, in *IEEE Instrumentation & Measurement Magazine*, Feb 2012
2. N. Maluf, D.A. Gee, K.E. Petersen, G.T.A. Kovacs, Medical Applications of MEMS (2000), pp. 300–306. ISBN: 0780326369
3. K.J. Rebello, Applications of MEMS in surgery, in *Proceedings of the IEEE*, vol. 92, no. 1, Jan 2004
4. G. Iddan, G. Meron, A. Glukhovskiy, P. Swain, Wireless capsule endoscopy. *Nature* **405**, 417 (2000)
5. K. Gilleo, MEMS in medicine. <http://www.allflexinc.com/wp-content/uploads/2013/09/Medical-Electronics-MEMS.pdf>
6. E. Delgado-Trejos, A.F. Quiceno, J.I. Godino, M. Blanco, G. Castellanos, Digital auscultation analysis for heart murmur detection. *Ann. Biomed. Eng.* **37**(2), 337–353 (2009)
7. S. Mangione, Cardiac auscultatory skills of physicians-in-training: a comparison of three english-speaking countries. *Am. J. Med.* **110**, 210–216 (2001)
8. B. Karnath, W. Thornton, Auscultation of the heart. *Hospital Physician* September (2002), pp. 39–43
9. J.A. Shaver, J.J. Leonard, D.F. Leon, Auscultation of the heart: part 4: examination of the heart. American Heart Association (1990)
10. J. Lewis, Analog and digital MEMS microphone design considerations. MS-2472-Analog devices technical article. <http://www.analog.com/media/en/technical-documentation/technical-articles/Analog-and-Digital-MEMS-Microphone-Design-Considerations-MS-2472.pdf>
11. A. Oppenheim, R. Schaffer, Digital signal processing. Englewood Cliffs, NJ, Prentice Hall (1975), p. 87
12. D. Chen, Time-frequency analysis of the first heart sound. Part2: an, appropriate time-frequency representation technique! *Med. Biol. Eng. Comput.* **35**, 311–323 (1997)

Flexible Printed Sensors for Ubiquitous Human Monitoring

Anindya Nag, Subhas Chandra Mukhopadhyay and Jürgen Kosel

Abstract The flexible printed sensors based on nanomaterials available currently have numerous challenges attached to it. The formation of nanocomposite for the electrodes is an issue mainly regarding the solubility of the conducting material. Mostly, the electrodes are not highly conductive in the flexible sensors fabricated due to the non-uniform distribution of conductive material in the polymer. The process of introducing conductive material as electrodes needs manual processing and thus becomes expensive. The sensitivity of the flexible sensor saturates with time due to the constant bending leading to deformation marks on the substrate material. This also leads to uneven surface and eventually inappropriate reading of the sensor. It is difficult to decrease the inter-electrode distance due to the spreading of the conductive ink in the printed sensors. There are many drawbacks to the current method of fabrication of flexible printed sensor. This research follows a novel approach to developing a sensor via the fabrication and characterization of a flexible, strain sensitive patch which would be used for bio-medical applications. Based on the laser-ablation technology, some prototype sensors have been designed and fabricated. It shows the experimental results obtained from the developed sensor on the detection of limb movements. The sensors would also be explored for other novel applications in future.

1 Introduction

The application of science in health monitoring has been one of the ongoing research works since last two decades. Health monitoring is a broad concept which includes a lot of categories under its domain. Human behaviour, physiological parameters are two broad areas which have consisted of a large sector of health

A. Nag · J. Kosel
Massey University, Palmerston North, New Zealand

S.C. Mukhopadhyay (✉)
Department of Engineering, Faculty of Science and Engineering,
Macquarie University, Sydney, NSW, Australia
e-mail: S.C.Mukhopadhyay@massey.ac.nz

monitoring. It has always been a challenging phenomenon to ubiquitously monitor people with different daily schedules. Sensing technology is one sector which has made substantial progress in analysing different parameters of a human being. Smart homes are being developed specialized in examining the daily activities of a human being. Sensors are being connected to devices or attached to people to determine any anomaly from the normal schedule and take actions if necessary. But the concept of smart homes has got many disadvantages related to it. Specialized automated homes have to be made extensively with sensors connected to the appliances communicating wired or wirelessly. This involves high cost, which increases proportionally with the number of activities being monitored. People living in those homes are always in a wary of being monitored by caretakers. That would hamper the private life of a person. The sensors functioning inside those homes would also have to be accurate at their highest level, especially if the sensing system is working in a router-end device system. A lot of sensors and sensing systems have been developed and worked upon to working in these homes. Even some of the sensing systems have been commercialized for specific purposes. Monitoring physiological parameters and activities are two major sections which cover almost everything a person does on a daily basis. Sensors related to biomedical purposes are the ones used to monitor defined parameters by analysing the biological signal inside the body. These sensors are substantially used for ubiquitous health monitoring. They are connected or placed at specific locations of the human body to determine specified parameters. The recent advancements with biosensors are that they are built small in size [1, 2] and consume lower power [3, 4]. Continuous research is going on apply these kinds of sensors to different applications. They work on a different phenomenon like with enzymes, analysts, nanomaterials, etc.

The design and fabrication of the sensors are one of the preliminary and critical steps of the sensing system. The designing of the sensor determines the application and characteristic of the sensor. My Ph.D. work currently focuses on the fabrication of novel sensors that would be used for different applications. The idea of my fabrication would be based low-cost, easy to fabricate sensors which could be replicated if needed in future.

2 Problem Definition

The current field of sensing technology has got an exponential leap in the health monitoring sector since last three decades [5–8]. A lot of daily activities and physiological parameters are being monitored with different kinds of sensors available in the market. Copious amount of problems still prevails with the present condition of fabrication of sensors. The flexible printed sensors used for health monitoring [9–11] are not of the optimum quality which affects the long-term sensitivity. The reason lies in the design and fabrication procedure of the sensor. The electrodes of flexible sensors are constructed with conductive inks [12] or metallic nanoparticles [13]. The fabrication of the nanoparticles itself takes several

steps [14, 15] which increase the total cost of production of sensors. To use the nanoparticles as electrodes, these nanoparticles need to be fabricated with specific dimensions and combined with hydrophilic solvent. The insolubility of the nanoparticles in water is another issue for most of the nanocomposite based polymers. So, most of the nanocomposite based sensors are a mixture of the nanoparticles with the polymer. This degrades the conductivity to a large extent. Polymers used [16, 17] for the fabrication of flexible sensors have very low solubility in water. So, the acuteness of the sensors to test at hydrous conditions will be very low. The spreading of the conductive inks is another issue for the sensors printed with different printing techniques [18, 19]. The bending of sensors is another problem for flexible substrates. The sensor bent continuously for different activities leaves a trail at the location being bent. The sensor slowly becomes uneven causing the sensitivity to saturate. These are some of the drawbacks that need to be addressed. Sensing systems that are used for monitoring are of high technical complexity which can be addressed only by professionals. So, in the case of any faulty situations, it becomes difficult for a layman to confront the situation. Secondly, the total cost of the sensing system involved in monitoring different parameters is high which is difficult to afford by most of the people other than the ones having automated developed homes. So, to check or monitor the abnormality of any parameter, a person has to visit professionals. Some of the sensors commercially available for people are very application specific. For example, glucometer available for the measurement of glucose cannot be used for any other monitoring purpose. So, there needs to be a system which can be used multi-functionally to monitoring vital signs and activities of a person. Now, the current sensors those are available for usage or testing does not have the theory to be used as a multiple parameter monitoring sensors. So, a novel sensor needs to be developed and work upon to address the situation. The third problem that persists in the current research field that many of the activities are still not addressed for monitoring purposes. For example, gesture recognition is one such area which can be looked upon to determine the present condition of a person. Some people especially have a tendency to change their moods very frequently, a ubiquitous monitoring of the gesture of those people is very important to avoid any unnecessary incidents. The testing for human gesture recognition has been previously done with the robotics which is very different from the real-time scenario. So, there needs to be a system which addresses the gestures of different people to comprehend their emotional condition. There are some other activities which could be considered for detection purposes to avoid the problems related to those activities.

3 Motivation

After getting interest in the field of sensing technology, I have always learned that sensors with silicon substrates are mostly used for monitoring purposes [20, 21]. But in the case of health monitoring, it is difficult to attach the sensor to any part of

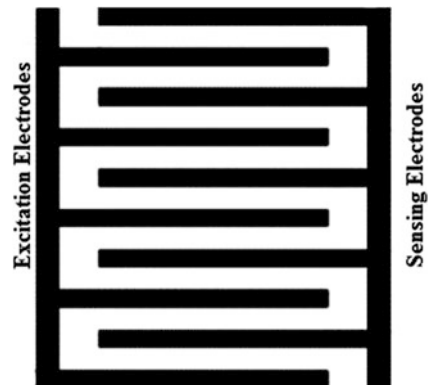
the body due to the sensor's stiffness, intransigency, complexity in fabrication procedure. For example, the electrodes in silicon sensors need a precise balance between the gold and the chromium for lift-off purposes. These limitations are neutralized by the flexible sensors. But still there are some drawbacks regarding the fabricating techniques of the existing flexible sensors as explained in the previous section. So, I have been motivated to contribute novelty in the domain of fabrication of new sensors. My work would hopefully address the problems encountered with earlier flexible sensors. Some prototypes have been manufactured and characterized to determine the changes caused on addressing the drawbacks. The sensor patches have also been tested for some applications. Finally, the outcome of my Ph.D. work is to develop a novel sensor dealing with the problems faced previously which would be used for some known and novel applications. The sensor would be used for monitoring multiple parameters. Since the sensor to be developed in my work is novel; the output of the sensor needs to be validated. This would be done by testing the sensor on different subjects and determining a characteristic curve between the input and output of the sensor for a particular application.

4 Interdigital Sensors: Principle and Operation

These sensors are designed on the idea of a parallel plate capacitor with its electrodes repeated in a finger or digitated patterns. It provides a non-invasive, single sided access of measurement to the material under test (MUT). The excitation electrode, supplied with an alternating voltage would generate an electric field towards the sensing voltage. The figure of the interdigitated pattern is shown in Fig. 1. This field generated between the electrodes, bulges from the sensing to the excitation electrodes due to its planar structure. This field passing through the material placed nearby changes its properties which are studied via the capacitive reactance of the applied field. The penetration of electric field through the material is shown in Fig. 2.

Now, if a non-homogenous material is placed on the sensing surface, the variation of the electric field along x-axis generates an exponentially decaying electric

Fig. 1 Configuration of interdigital electrodes [23]



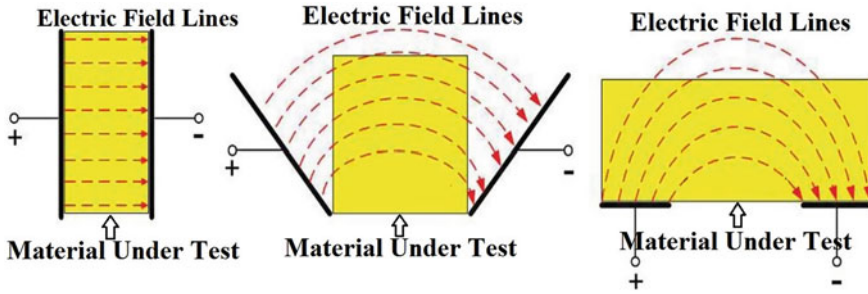


Fig. 2 Penetration of electric field in an interdigital sensor [23]

field along the z-axis which penetrates through the medium [22]. The height of the electric field is varied by varying the distance between the two electrodes of opposite polarity.

The net electric field generated is also varied by varying the ratio of excitation to sensing electrode [24]. The most common configurations are 1:1, 1:3, 1:5, 1:11. The advantages of these sensors are its non-invasive and singular measurement. The change in impedance and phase angle is studied over a range at different frequencies to analyse the ‘operative’ or ‘most sensitive frequency’. This frequency is fixed for the testing purposes. The interdigital sensors were used in a wide variety of applications [20, 21, 24, 25] for monitoring and detection purposes.

5 Carbon Nanotubes and Nanocomposites

Carbon nanotubes (CNTs) are sp^2 hybridized carbon atoms rolled into cylindrical sheets in a graphene plane. They consist of two p–n–p junctions through which the electron transport takes place via tunneling. The diameter and length are the two prime parameters of CNTs. CNTs have been synthesized over the years by various techniques like arc-discharge technique, laser vaporization and chemical vapor deposition (CVD). The arc-discharge method produces CNTs with less purity and CNTs produced with laser vaporization method are of low yield. Therefore, the most common and advantageous among them is the CVD method. The growth directions of these nanotubes are mainly governed by two factors: the applied field and the Van der Waal’s forces existing between them. They have been used for its definite advantages over other materials. High thermal range, high tensile strength, and stiffness are some of the attributes of CNTs apart from its flexibility and high electrical conductivities. CNTs exist in two different forms: Single-walled and multi-walled. The difference in the two forms is differentiated at the time of their growth by applying different catalysts during the growth period. Two-thirds of single-walled CNTs are semi-conductive or quasi-metallic in nature. But the capacitance of single-walled nanotubes is three or four times higher than that of

multi-walled. The electrical properties and conductivities of single-walled CNTs could be affected by the type of the catalytic particles, ion-doping or side-wall functionalization. Acid treatment tends to leave open-ended tubes. The ones other than metallic CNTs are sp^3 hybridized. Multi-walled CNTs are used as electrodes for their ability to disperse in the polymer matrix and a higher rate of conductivity than single-walled. Their missing into the polymer leads to an increase in elastic modulus and a decrease in tensile strength. Surface functionalization of nanotubes increases the interfacial adhesion and chemical bonding with the polymer. The peak current of multi-walled CNTs is proportional to the length of the tubes. This also leads to a difference in the electron transfer behavior.

6 Flexible Sensors

Flexible sensors [26–28] have been used for quite some time due to their distinct advantages over sensors with rigid substrates. The flexible sensors are developed with organic and inorganic polymers with nanomaterials on the top layer as electrodes. The dynamic nature of sensors with flexible substrates makes them applicable for a wider range of applications compared to rigid substrates. Among the different constituting materials, the flexible substrate is the most important parameter of these kinds of sensors. Rigid electrodes like silicon were placed on top bendable foil [29] to constitute an overall bendable sensing device. These devices were fabricated with chemical etching process thus reducing the cost of production. These sensors are capable of handling fast transistor switching processes in display drive electronic systems. Other fabrication techniques like ink-jet printing, screen printing had been used to a large extent to fabricate flexible sensors with different conductive materials like gold nanoparticles [30, 31], carbon nanotubes [32–34], etc. Electronic skins [35, 36] are another than device capable of sensing pressure and self-healing mechanically. These sensors were fabricated by screen printing Polyvinylidene fluoride and its copolymer Trifluoroethylene (TrFE) (P (VDF-TrFE)) on Polyimide (PI) and Polyethylene terephthalate (PET) compounds. P (VDF-TrFE) was used due to its mechanical flexibility and pyro, piezo and ferroelectric properties. The proposed system had been used for many purposes like soft robotics and biomedical prostheses. Among other organic polymeric compounds, PDMS had been used widely due to its mechanical flexibility and insulated properties.

7 Fabrication of Novel Sensors Patch

The idea of my Ph.D. work is to develop a novel flexible sensing system for the ubiquitous monitoring of multiple activities and physiological parameters. The term ‘flexible’ is associated with the stretchability and bendability of the sensor in both

horizontal and vertical directions. The advantages of using a flexible substrate instead of a rigid one are in its increase in applications, efficiency and durability.

There are a lot of polymers [27, 37, 38] tested as a substrate for flexible sensors. The use of a polymer mainly depends on the use of the sensor. In my work, PDMS would be used the organic polymer. There are certain advantages of using PMDS over other polymers. Some of them are:

1. It is cheaper than other polymers. So, the fabricated prototype can be replicated at a low cost.
2. It has high transparency. Thus, any change in a critical circuitry can be done easily.
3. It is hydrophobic in nature. So, the output of the sensor would not be affected by sweat or any solvent in particular.

The organic polymer was cast over a Poly (methyl methacrylate) (PMMA) template to form the substrate. The reasons PMMA was chosen as a base was because:

1. The cured PDMS can be taken off easily from the PMMA template without any prior treatment, unlike silicon.
2. The PMMA template would not react with the PDMS.
3. The PDMS with adheres perfectly to the template without any intermolecular gap.

Carbon nanotubes (CNTs) were chosen as the conducting material for the electrodes. In spite of the availability of other nanotube and nanowire materials, CNTs were chosen because of its certain advantages like:

1. They are highly flexible.
2. They are very light and as a result, make a great replacement of metallic nanowires.
3. They have a high range of electrical conductivity which varies between Single-walled and multi-walled CNTs.
4. They are high tensile strength and stiffness.
5. They are resistant towards temperature change.

CNTs are of two types: Single-walled and multi-walled. The use of each type is determined by its application. The proposed work involves the use of multi-walled carbon nanotubes (MWCNT) due to the following attributes:

1. The proportion of conductors over semi-conductors is higher in MWCNT than single-walled.
2. The conductivity of MWCNT is 100× higher than single-walled.
3. MWCNT does not require any stabilizing layer when used for industrial purposes.
4. They readily form compounds with a number of polymers compared to single-walled.

In this work, MWCNT functionalized with the carboxylic group is used as the electrodes. The advantages of using a functionalized MWCNT are:

1. They help in better dispersion with the mixed polymer.
2. Carboxylic ($-\text{COOH}$) or hydroxyl ($-\text{OH}$) group functionalization helps in increasing the interfacial bonding between the nanotubes and the polymer.
3. The amount of CNT material required to form any nanocomposite is reduced with functionalization.
4. They provide better compatibility and higher flexibility.

MWCNTs are mixed with PDMS to form a nanocomposite layer. This layer was patterned with CO_2 laser ablation to form interdigitated electrodes. There are also other techniques like 3-D printing [39], inkjet printing [18], photolithography [40] for forming the patterns. But the CO_2 laser patterning had been preferred over other techniques because of its following advantages:

1. It takes very less time for sample preparation.
2. No additional equipment is required for patterning, in contrast, to which a template and photoresist are required for photolithography.
3. The thickness of the electrodes can be adjusted by the power and speed rates of the laser which is not possible in screen printing.

The schematic for the fabrication of the sensor patch is shown in Fig. 3. The experimental steps were performed in the sequence shown below.

The PDMS was initially molded on the PMMA template. A casting knife (SHEEN, 1117/1000 mm) was used to adjust the thickness of the PDMS layer (Fig. 4). The thickness was set to 1000 μm . Then the desiccation of the PDMS substrate is done to remove any air bubbles present inside it (Fig. 5).

The desiccated PDMS substrate was then cured at 80 $^\circ\text{C}$ for 8 h (Fig. 6). Then a layer of nanocomposite formed by mixing CNTs with PDMS at 4.0 wt% is cast over the cured PDMS. The thickness of the casted layer was adjusted to 100 μm by

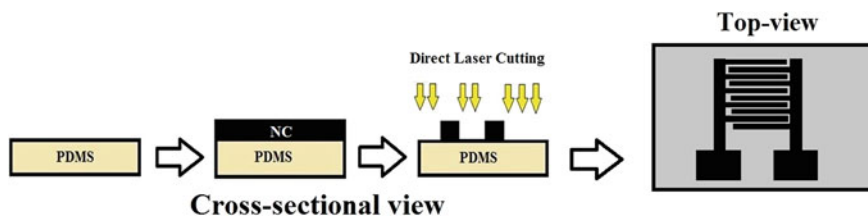


Fig. 3 Schematic diagram of the fabrication steps

Fig. 4 Casted PDMS on PMMA template

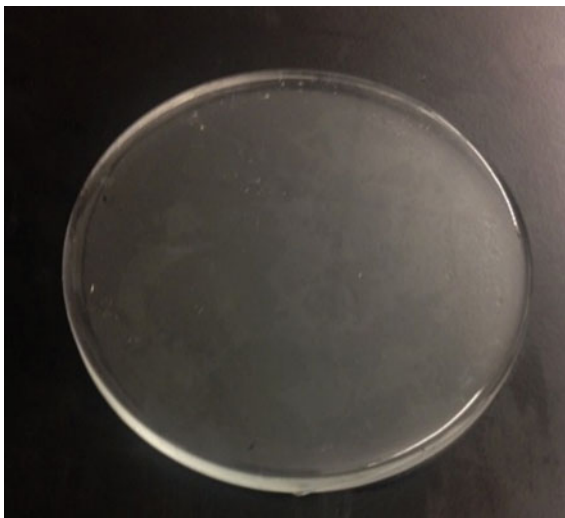
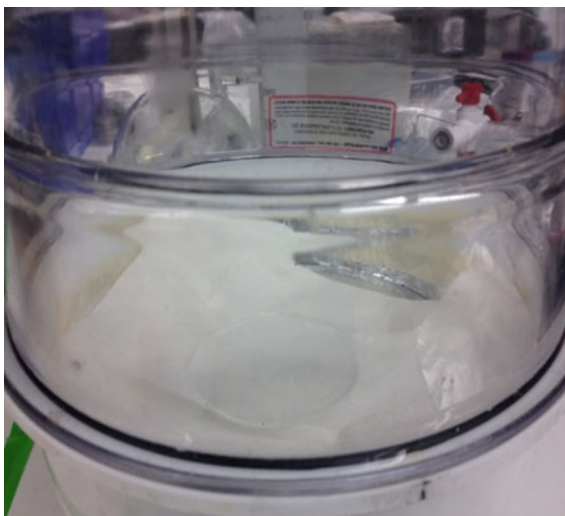


Fig. 5 Desiccation of the PDMS substrate

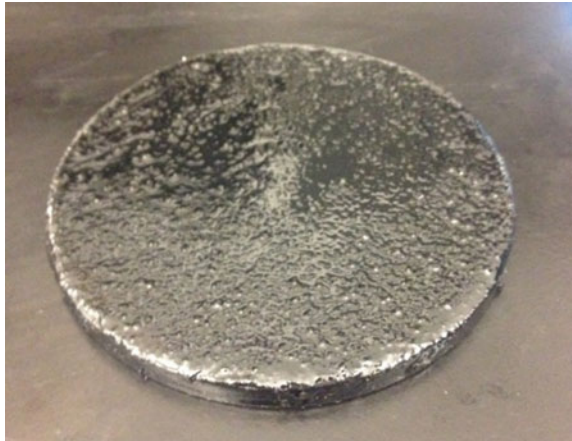


the casting knife (Fig. 7) followed by its desiccation for 2 h (Fig. 8). The sample was then again cured at 80 °C for 8 h (Fig. 9). The SEM images of the nanocomposite formed with CNT-PDMS are shown in Fig. 10. The cured sample was then laser ablated to form the electrodes in the patterns of interdigitated electrodes (Fig. 11).

Fig. 6 Curing of PDMS template



Fig. 7 Casting of nanocomposite on PDMS substrate



Different power and speed settings were tried to vary the thickness of the electrodes. The power-speed setting of 2.4 W–7 m/min was found comparatively to be the optimal one regarding flexibility and conductivity. The configuration of the electrode is given in Fig. 12.

Fig. 8 Desiccation of the PDMS nanocomposite



Fig. 9 Curing of nanocomposite



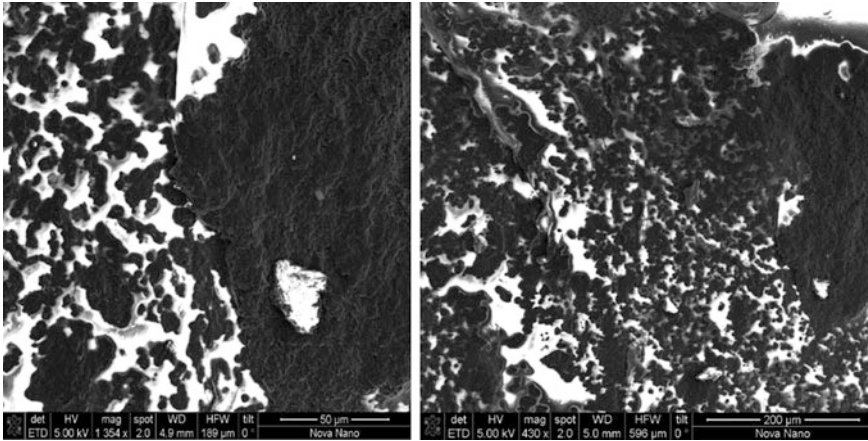
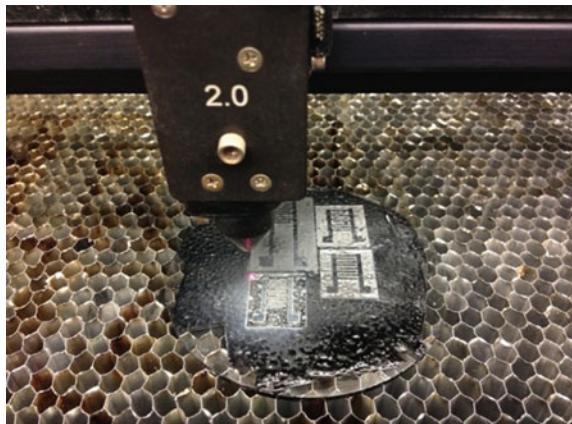


Fig. 10 SEM images of CNT/PDMS nanocomposite

Fig. 11 CO₂ laser cutting of the sample



8 Characterization of the Sensor Patch

The characterization of the sensor patch was done before its experimental application on physiological parameter monitoring. The conductivity and short circuit of the sensor patch were tested. The following characteristic results show the profiling of the sensor along with its stress–strain and capacitance–strain relationship.

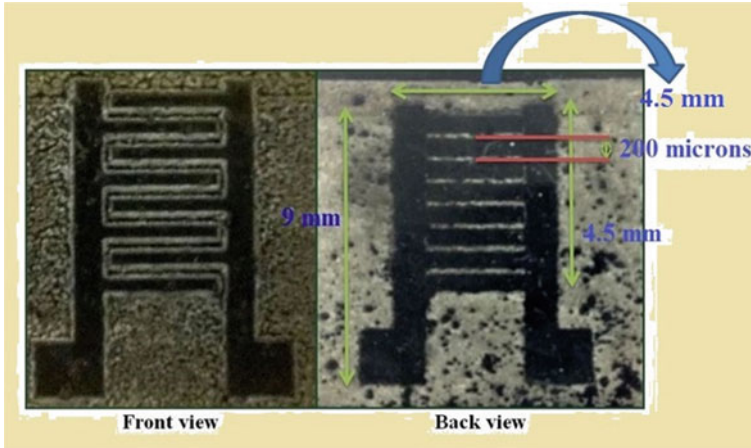


Fig. 12 Configuration of sensor patch

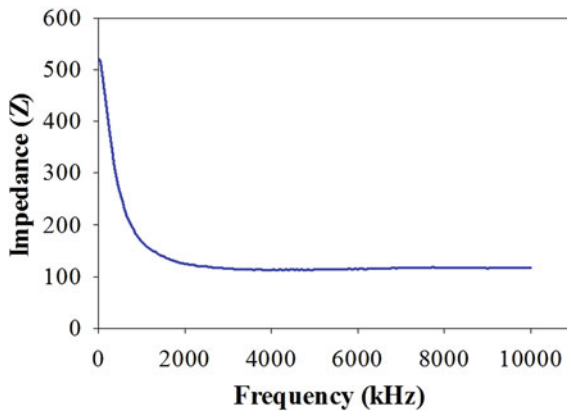
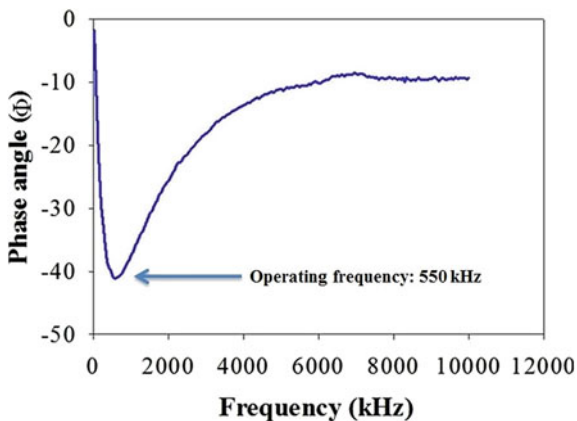


Fig. 13 Impedance-frequency relation for the sensor patch

8.1 Impedance Spectroscopy

Impedance measurements of the sensor patch were performed by a Precision Impedance Analyser (Agilent 4294A). A frequency sweep between 10 kHz and 10 MHz was done to calculate the frequency response of the system. The response of impedance and the phase angle of the first sensor patch towards the given frequency range are shown in Figs. 13 and 14. The gradual change in impedance shows an increase in the reactance part of the impedance, which is more prominent from the phase angle and frequency graph.

Fig. 14 Phase angle-frequency relation for the sensor patch



The phase angle was calculated between the input voltage and output current of the patch. It is seen from the phase angle-frequency graph that the sensor patch is capacitive in nature. The operative range of the sensor is considered between 10 Hz and 10 MHz. As evident from the graph, the most sensitive frequency is 550 kHz.

8.2 Stress–Strain Relationship

The stress–strain relation of the sensor patches was analysed to determine the strain dependency on the stresses in different directions. Two different types of stresses, tensile and compressive, were tested on the sensor patches as shown in Fig. 15. The direction of stress was also varied horizontally and vertically as shown in the same figure. Horizontal stress refers to the force applied parallel to the electrodes, whereas vertical stress refers to the force applied perpendicular to the electrodes.

The stress–strain relationship for the sensor patch was tested with INSTRON (VS02477052 R: F). The measurements were initially done at N and mm for strain and stress respectively.

The relation of strain to tensile and compressive stress is almost ideal [41] as can be seen from Fig. 16. The yield points for the tensile and compressive stress are (385, 599.4) and (388.7, 420) in the horizontal direction.

The compressive stress has a contorting effect on the patch. This could be due to the anisotropic geometry of the electrodes. The fracture points for the tensile stress were (1420 μm , 2060 mN) and (–1680 μm , –840 mN). The lower limit of negative strain was caused due to the excessive bending of the patch. Hysteresis behaviour was not noticeable for this patch.

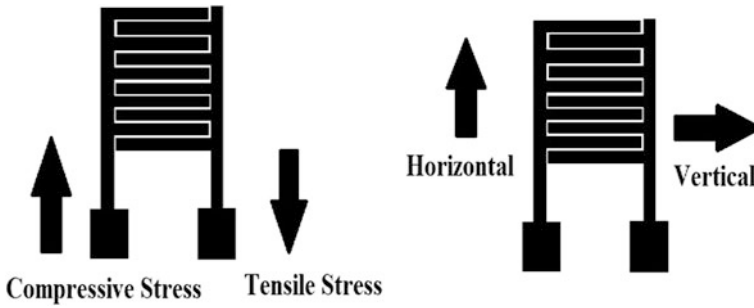
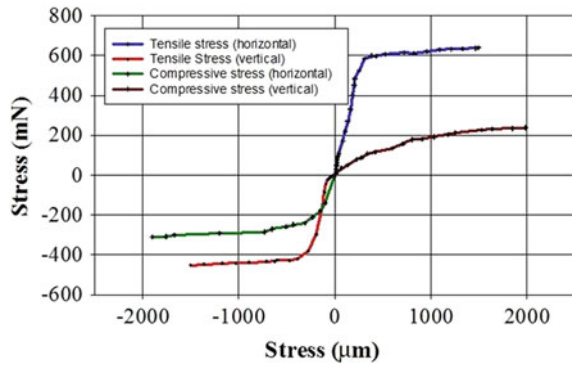


Fig. 15 Direction and types of applied stress

Fig. 16 Stress–strain relation for sensor patch

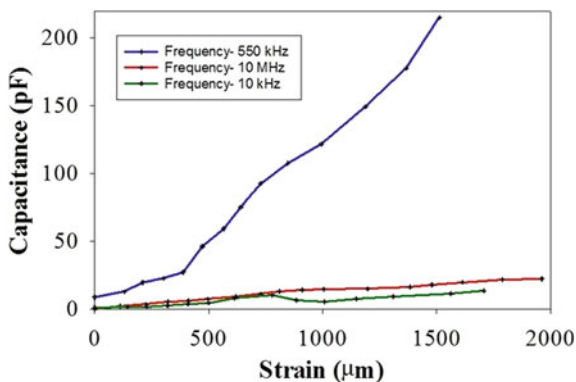


8.3 Capacitance–Strain Relationship

The relationship between capacitance and strain was analysed before experiments to verify the dependence of capacitance on the strain. The measurements were done by connecting the LCR meter to the sensor patch while applying vertical and horizontal stresses. The change in capacitance on strain is linear initially, followed by an exponential rise. The two sensor patches characterized showed similar readings with slight differences. Two frequencies, other than the operating frequency was considered for measurements. This was done to evaluate the response of capacitance towards frequency values of different ranges.

Figure 17 shows the capacitance–strain relation of sensor patch I. The patch showed a response only towards the operating frequency, 550 kHz. The change in capacitance was very low in the other two cases, especially that of 10 MHz. The change like capacitance takes place due to the continuously changing inter-electrode distance. This changes the alignment of the charges on the two oppositely charged electrodes, which as a result changes the resultant electric field.

Fig. 17 Capacitance–strain relation for sensor patch



The flexible patch was fabricated using PDMS as the substrate and CNT/PDMS as the nanocomposite layer. Interdigitated pattern was cut on the nanocomposite layer using a CO_2 laser. Different power and speed settings in the laser generated electrodes with different thicknesses. Two sensor patches were chosen for characterization and experimental work after testing the fabricated patches for conductivity and short circuits. The characterization of the patches was done which proved them to be strain sensitive capacitive sensors. The stress–strain and capacitance–strain relations were shown to analyze the flexibility of the developed samples.

9 Experiments Results

Two of the parameters that were being tested are limb movement. Movement of limbs are the two physiological activities monitored with the sensor. The sensor was connected to an LCR meter (E4980A) with a frequency range of 20 Hz–2 MHz for detecting the capacitance change on different physiological parameters. 16048D test lead (KEYSIGHT) connector with BNC-alligator leads was connected to the LCR meter and the sensor. An AC voltage of 1 V with specified operating frequencies of the sensor patches was set in the LCR meter before experiments. The data was connected from the computer via a GPIB-USB converter. The experimental results are given below. The measurements were done in pF range.

The use of the sensor to monitor a physiological event through the change in capacitance based on the deformation–reformation occurrence on the sensor patch. Figure 18 depicts the notion. The expanded state of the sensor patch is useful for measuring limb movements while both expanded and contracted states occurred during the monitoring of limb movements.

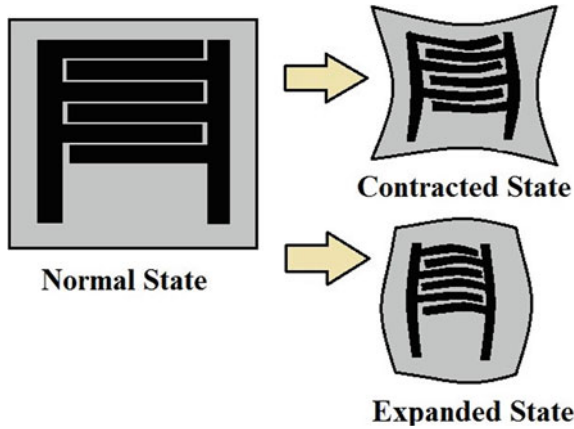


Fig. 18 Change in configuration of the sensor patch



Fig. 19 Experimental set-up of limb movements

9.1 Results with Sensor Patch

The sensor patch has been tested for monitoring of the physiological movements. The patch was attached to different subjects to test the functionality of the fabricated device. Some of the results are given below. To test the sensor for biophysical parameter monitoring, the patch was attached to the skin using biocompatible tapes (VHB 3M RP) as shown in Fig. 19. The sensor was attached only after the skin was completely dried to minimize the effect of sweat or water on the attachment of the tapes. The presence of sweat would lead to an additional capacitive layer between the sensor and skin leading to erroneous results. The measurements of the sensor

capacitance were done by a Precision LCR meter (E4980A) at 150 kHz. BNC to alligator clips was used to connect the instrument to the sensor attached to the body. The sensor was attached to the elbow and knee to detect the movement of limbs.

9.2 Limb Movements

The limb movements were monitored by attaching the sensor patch on the joints of arms and legs with biocompatible tapes. The experimental set-up is shown in Fig. 19.

People of different age groups were tested for limb movement to validate the functionality of the sensor patch. Figures 20, 21, 22, 23 showed the sensor output when the limbs were moved in an oscillatory fashion. The terms ‘movement’ and ‘rest’ shown in the figures refer to the motion and rest of the limb. The arms were moved from a fully extended position, i.e., resting on the table to a fully flexed

Fig. 20 Detection of left arm movement

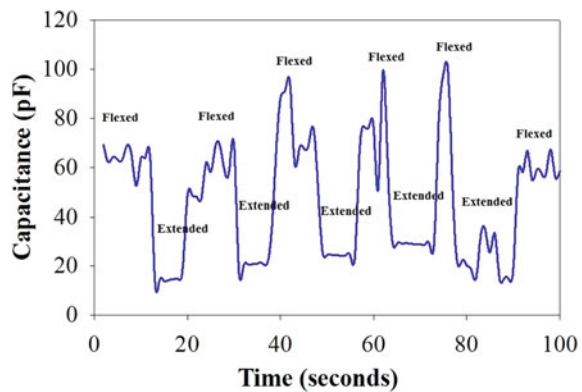


Fig. 21 Detection of right arm movement

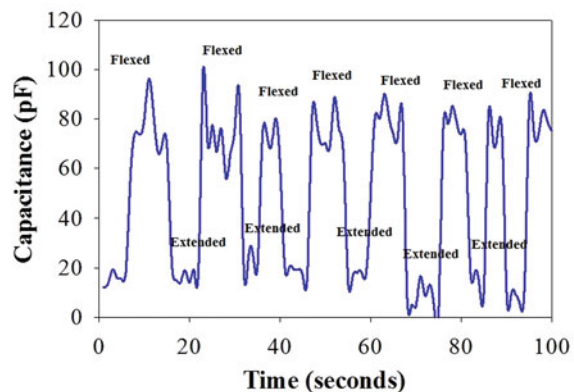


Fig. 22 Detection of left leg movement

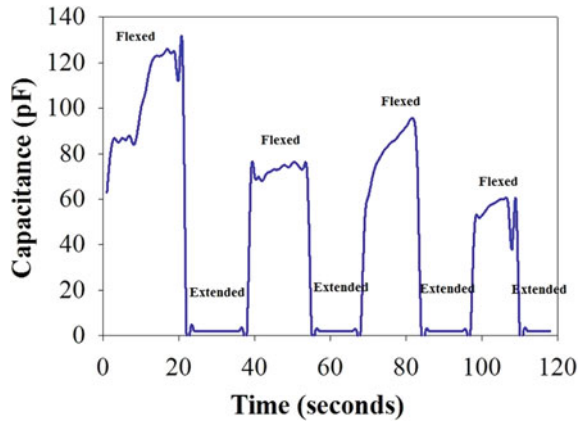
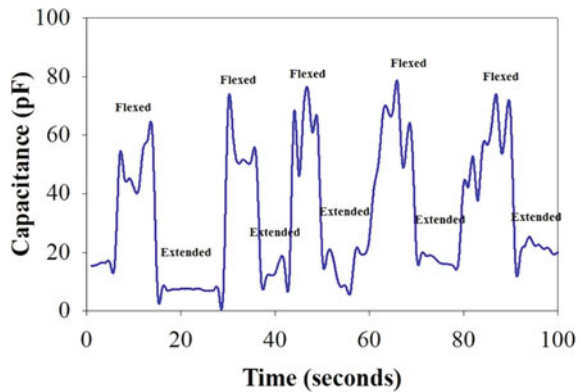


Fig. 23 Detection of right leg movement



position via bending the elbow. The leg movement was done in a similar fashion by bending the knee from an extended to a flexed position.

The results show that limb movements can be clearly detected with the sensor patch. The limbs were flexed up to the angle of 156° , considering the extended limb to be zero degrees. There are a few issues that can be addressed to optimize the performance. For example, in Figs. 21 and 23 output fluctuations are observed, especially during the extended state. This can lead to contradictory assumptions of the state of the limb. The reason for this is the attachment of the sensor to the skin, which turned out to be somewhat unreliable. Movements of the limbs loosened the sensor patch from the skin, leading to the observed artefacts.

The different angular change on a reference of a limb of a subject is shown in Fig. 24. This experiment was performed to determine a relation between the changes in capacitance on each degree movement of the limb. It is seen from

Fig. 24 Different angular measurements of the limbs of a subject

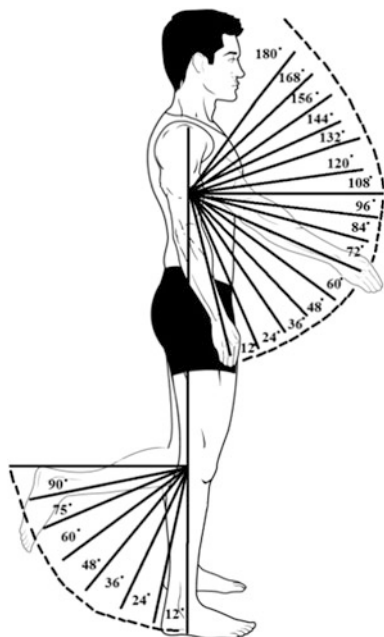


Fig. 25 Change of capacitance as a function of the limb movement

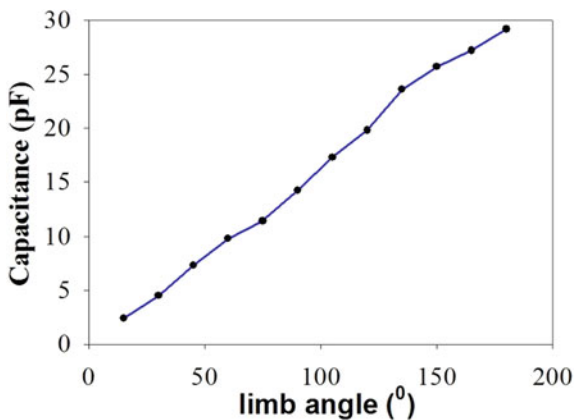


Fig. 25 that the sensor patch shows that the change of capacitance is linear with the degree movement of the limbs. The sensitivity can be calculated by:

$$\text{Sensitivity} = \frac{\Delta C}{\Delta \text{Limb angle}} = \frac{17.32 - 14.33}{102.08 - 90.48} = 0.257 \text{ pF/degree}$$

10 Conclusion

A planar interdigital sensor with an effective data acquisition system has been designed. The sensors responded distinctively to air, water, cheese and butter. Sensors have different values for different materials so they are effective in measuring dielectric properties of various materials and as both the sensors are of same interdigital structure but with varying pitch lengths, their values may differ but follow the same trend. The same set-up was used to measure the di-electric property of pelts and establish a relationship between the dielectric property and looseness of the skin. From the above results it is clear that sensor output voltage drops and raises along with the looseness values for the samples in each group. It is seen that we could co-relate looseness with the di-electric property of the skins. More experiments are being done to establish a relationship between the dielectric property of sheepskin and their looseness.

References

1. J. Wang, Nanomaterial-based electrochemical biosensors. *Analyst* **130**, 421–426 (2005)
2. F.W. Scheller, U. Wollenberger, A. Warsinke, F. Lisdat, Research and development in biosensors. *Curr. Opin. Biotechnol.* **12**, 35–40 (2001)
3. M. Zhang, M.R. Haider, M.A. Huque, M.A. Adeeb, S. Rahman, S.K. Islam, A low power sensor signal processing circuit for implantable biosensor applications. *Smart Mater. Struct.* **16**, 525 (2007)
4. A. Agah, K. Vleugels, P.B. Griffin, M. Ronaghi, J.D. Plummer, B.A. Wooley, A high-resolution low-power incremental ADC with extended range for biosensor arrays. *Solid-State Circuits, IEEE J.* **45**, 1099–1110 (2010)
5. E. Udd, J.P. Theriault, A. Markus, Y. Bar-Cohen, Microbending fiber optic sensors for smart structures, in *OE/FIBERS'89*, 478–482 (1990)
6. V. Giurgiutiu, *Structural health monitoring: with piezoelectric wafer active sensors* (Academic Press, London, 2007)
7. G. Park, H.H. Cudney, D.J. Inman, An integrated health monitoring technique using structural impedance sensors. *J. Intell. Mater. Syst. Struct.* **11**, 448–455 (2000)
8. C.D. Kidd, R. Orr, G.D. Abowd, C.G. Atkeson, I.A. Essa, B. MacIntyre et al., The aware home: a living laboratory for ubiquitous computing research. *Cooperative buildings. Integrating information, organizations, and architecture*, ed. (Springer, 1999), pp. 191–198
9. I. Kang, M.J. Schulz, J.H. Kim, V. Shanov, D. Shi, A carbon nanotube strain sensor for structural health monitoring. *Smart Mater. Struct.* **15**, 737 (2006)
10. J.A. Rice, B.F. Spencer Jr., *Flexible smart sensor framework for autonomous full-scale structural health monitoring* (Newmark Structural Engineering Laboratory. University of Illinois at Urbana-Champaign. 1940–9826, 2009)
11. J.A. Rice, K. Mechtov, S.-H. Sim, T. Nagayama, S. Jang, R. Kim et al., Flexible smart sensor framework for autonomous structural health monitoring. *Smart structures and Systems* **6**, 423–438 (2010)
12. S. Magdassi, *The chemistry of inkjet inks* (World scientific Singapore, 2010)
13. R.H. Baughman, A.A. Zakhidov, W.A. de Heer, Carbon nanotubes—the route toward applications. *Science* **297**, 787–792 (2002)

14. J. Lin, C. He, Y. Zhao, S. Zhang, One-step synthesis of silver nanoparticles/carbon nanotubes/chitosan film and its application in glucose biosensor. *Sens. Actuators B: Chem.* **137**, 768–773 (2009)
15. O. Zhou, H. Shimoda, B. Gao, S. Oh, L. Fleming, G. Yue, Materials science of carbon nanotubes: fabrication, integration, and properties of macroscopic structures of carbon nanotubes. *Acc. Chem. Res.* **35**, 1045–1053 (2002)
16. J. Lötters, W. Olthuis, P. Veltink, P. Bergveld, The mechanical properties of the rubber elastic polymer polydimethylsiloxane for sensor applications. *J. Micromech. Microeng.* **7**, 145 (1997)
17. S. Logothetidis, Flexible organic electronic devices: materials, process and applications. *Mater. Sci. Eng., B* **152**, 96–104 (2008)
18. P. Calvert, Inkjet printing for materials and devices. *Chem. Mater.* **13**, 3299–3305 (2001)
19. X. Li, J. Tian, G. Garnier, W. Shen, Fabrication of paper-based microfluidic sensors by printing. *Colloids Surf., B* **76**, 564–570 (2010)
20. S. Mukhopadhyay, A. Nag, A. Zia, X. Li, J. Kosel, Novel sensing approach for LPG leakage detection: Part I: operating mechanism and preliminary results (2015)
21. S. Mukhopadhyay, A. Nag, A. Zia, X. Li, J. Kosel, Novel sensing approach for LPG leakage detection: Part II: effects of particle size, composition and coating layer thickness (2015)
22. A.I. Zia, M.S.A. Rahman, S.C. Mukhopadhyay, P.-L. Yu, I.H. Al-Bahadly, C.P. Gooneratne et al., Technique for rapid detection of phthalates in water and beverages. *J. Food Eng.* **116**, 515–523 (2013)
23. A. Rahman, M.S. Bin, *Novel planar interdigital sensors for the detection of bacterial endotoxins: a thesis presented in partial fulfilment of the requirements for the degree of Doctor of Philosophy* (Electronics Engineering at Massey University, Palmerston North, New Zealand, 2012)
24. A. Nag, A.I. Zia, S. Mukhopadhyay, J. Kosel, Performance enhancement of electronic sensor through mask-less lithography. 2015 9th International Conference on Sensing Technology (ICST) (2015), pp. 374–379
25. A.I. Zia, N. Afsarimanesh, L. Xie, A. Nag, I. Al-Bahadly, P. Yu, et al., Improved detection limits for phthalates by selective solid-phase micro-extraction. 2015 9th International Conference on Sensing Technology (ICST) (2015), pp. 733–738
26. C. Ashruf, Thin flexible pressure sensors. *Sensor Review* **22**, 322–327 (2002)
27. C. Pang, C. Lee, K.Y. Suh, Recent advances in flexible sensors for wearable and implantable devices. *J. Appl. Polym. Sci.* **130**, 1429–1441 (2013)
28. M. Segev-Bar, H. Haick, Flexible sensors based on nanoparticles. *ACS Nano* **7**, 8366–8378 (2013)
29. R.S. Dahiya, S. Gennaro, Bendable ultra-thin chips on flexible foils. *Sens. J., IEEE* **13**, 4030–4037 (2013)
30. N. Zhao, M. Chiesa, H. Siringhaus, Y. Li, Y. Wu, B. Ong, Self-aligned inkjet printing of highly conducting gold electrodes with submicron resolution. *J. Appl. Phys.* **101**, 064513 (2007)
31. D. Huang, F. Liao, S. Molesa, D. Redinger, V. Subramanian, Plastic-compatible low resistance printable gold nanoparticle conductors for flexible electronics. *J. Electrochem. Soc.* **150**, G412–G417 (2003)
32. P. Chen, H. Chen, J. Qiu, C. Zhou, Inkjet printing of single-walled carbon nanotube/RuO₂ nanowire supercapacitors on cloth fabrics and flexible substrates. *Nano Res.* **3**, 594–603 (2010)
33. K. Kordás, T. Mustonen, G. Tóth, H. Jantunen, M. Lajunen, C. Soldano et al., Inkjet printing of electrically conductive patterns of carbon nanotubes. *Small* **2**, 1021–1025 (2006)
34. L. Yang, R. Zhang, D. Staiculescu, C. Wong, M.M. Tentzeris, A novel conformal RFID-enabled module utilizing inkjet-printed antennas and carbon nanotubes for gas-detection applications. *Antennas and Wirel. Propag. Lett., IEEE* **8**, 653–656 (2009)

35. B.C. Tee, C. Wang, R. Allen, Z. Bao, An electrically and mechanically self-healing composite with pressure-and flexion-sensitive properties for electronic skin applications. *Nat. Nanotechnol.* **7**, 825–832 (2012)
36. S. Khan, L. Lorenzelli, R.S. Dahiya, Screen printed flexible pressure sensors skin. *Advanced Semiconductor Manufacturing Conference (ASMC), 2014 25th Annual SEMI (2014)*, pp. 219–224
37. Y. Zhou, L. Hu, G. Grüner, A method of printing carbon nanotube thin films. *Appl. Phys. Lett.* **88**, 123109 (2006)
38. J.J. Boland, Flexible electronics: within touch of artificial skin. *Nat. Mater.* **9**, 790–792 (2010)
39. H. Lipson, M. Kurman, *Fabricated: the new world of 3D printing* (John Wiley & Sons, 2013)
40. E.F. Nuwaysir, W. Huang, T.J. Albert, J. Singh, K. Nuwaysir, A. Pitas et al., Gene expression analysis using oligonucleotide arrays produced by maskless photolithography. *Genome Res.* **12**, 1749–1755 (2002)
41. W. Ramberg, W.R. Osgood, Description of stress–strain curves by three parameters (1943)

Smart Textiles for Smart Home Control and Enriching Future Wireless Sensor Network Data

Olivia Ojuroye, Russel Torah, Steve Beeby and Adriana Wilde

Abstract The increasing number of objects within homes connected to the Cloud is not going to recede. Our growing acceptance of automated appliances and items connected in wireless sensor networks (WSN) is gradually making our homes smart. This occurrence is a reflection of the technological advancement of societies around the world. We predict that the future applications of WSN will incorporate smart textiles. These will appear in smart homes, as well as in commercial spaces, in automobile vehicles, in personal or business-owned clothing, and even toys. As the electronics become available to industry, smart textiles could be embedded with electronics capable of receiving and transmitting data packets. The implications are that soft furnishings or any surfaces with a textile have the potential capability of connecting to the Cloud. Considering future applications of smart textiles, whether for personal or commercial usage, we can predict data contents that would be stored in a WSN and discuss how to ensure safety and network stability.

1 Introduction

We live in an increasingly connected world, and the global impact of wireless sensor networks (WSNs) is a major contributing factor. Furthermore, societal connectivity is becoming critically dependent on the use of technology and WSNs, as the increasing number of people (and their objects) connected to the internet shape societal infrastructures [1]. As the number of ‘digital societies’ [2] continue to emerge, WSNs play an important role in the changes in the ways humans communicate and how inanimate objects are communicating.

The collective of inanimate objects that are able to communicate via WSNs are creating ‘connected’ homes—which we call smart homes. Objects exchanging or transferring data to the Cloud is ubiquitously known as the Internet of Things (IoTs), which relies on integrating these objects with sensors [3].

O. Ojuroye (✉) · R. Torah · S. Beeby · A. Wilde
University of Southampton, Southampton, UK
e-mail: oo2g12@soton.ac.uk

So far, objects connected to the IoT are typically electronic devices. Textile surfaces are yet to contribute to the IoT ecosystem despite their ubiquity. Smart textiles could have the capability to collect and supply data that can be analysed and re-distributed in the Cloud, if embedded with appropriate electronics and made compatible with WSNs. However, such smart textile products are not commercially available yet and the implications of their widespread use have yet to be questioned. At the time of writing, smart textiles that are functional (washable, stretchable, flexible, and sustainably disposable) are not commercially available. Smart textiles are traditional textiles with conductive properties due to metallic or electronic components. The project [4] this chapter is based on was a prototype for a three-part system involving a voice-controlled smart home hub operated by flexible wearable device. It is thought that the design of the flexible wearable device, of which an earlier prototype was made from polyimide with inkjet-printed conductive tracks, could be improved with developments in smart textiles. By assessing this option, this book chapter also offers an informed prediction of the future of the field. Additionally, considering the other industries that can benefit from and be used by smart textiles, the type of data submitted to a WSN can be defined. Consequently, we can speculate to what extent personal data will enrich WSNs and propose how that data could be protected.

With the rapid progression of smart textiles, considerations are necessary to be had as smart textiles that can communicate and exchange with WSNs become ubiquitous. Now is the time to consider those eventualities and protect the users and owners of the connected smart textiles as they enrich WSN data in the Cloud.

2 Benefits of Activities of Daily Living to Wireless Sensor Networks

2.1 Background

Activities of Daily Living (ADL) are recreational or occupational mundane tasks which include but are not limited to self-care, such as functional mobility and food preparation. Studying these gives us insights on how we interact with our environment [5]. ADL recognition has become a methodology to quantify, classify, and find patterns in human daily habits and routines in closed environments—a task originally used to monitor the wellbeing of the elderly [6]. ADL experiment participants can learn about their contextual framework, habits, behaviour and learn how to improve their lifestyles [5]. These closed environments have expanded beyond laboratory settings; ADL recognition has been experimented in homes [7] and even commercial spaces [8, 9]. Innovative technologies have allowed ADL research to be conducted outside laboratory settings. These technologies are used by participants in ADL research to remotely monitor their activity unobtrusively. Wearable sensors are useful in ADL research, as participants' movements and behaviour can be remotely and unobtrusively tracked. Hence, sensor-based human

activity recognition has improved through advancements in wearable sensors and wireless sensor networks (WSNs) [10]. However, research has shown the difficulty in monitoring and recognising the activities of multiple people through ADL [10]. Additionally, the desire has been expressed—to create a robust WSN platform with sufficient security and privacy of collected data for pervasive computing. In essence, this can enable ADL researchers to cultivate complex daily activity patterns [11].

Previously, smartphone battery-life problems have encouraged ADL researchers to find alternative portable, WSN compatible tools to collect data remotely [12]. This is due to battery-life problems causing interrupted data collection, making future pattern predictions unreliable. Recent alternatives include body-worn sensors, pressure sensors, passive infrared (PIR) sensors, and video monitoring which can allow long-term monitoring of habits and wellbeing [13]. However, these sensors must be wireless and light-weight for unobstrusive monitoring. Furthermore, the sensors must prevent skewed data caused by the sensors limiting mobility. Nef et al. [14] created a wireless sensor network addressing these issues. Specifically, a system was built to recognise overlapping ADL habits among many people using PIR wireless sensors and algorithms such as naïve Bayes (NB), support vector machines (SVM), and Random Forest. Although results showed that by combining PIR sensors with Random Forest algorithms gave the highest accuracy in activity recognition, one limitation was that collected data could not distinguish between activities performed by an individual or multiple people. Additionally, as the system was collecting raw data only, it could not reveal whether an individual or multiple people were producing the data. In this way, without the wireless network having contextual information about the environment and its inhabitants, activities of daily living can be recognised but the richness of the data that highlights the individual(s) behaviours are lost. Furthermore, as the PIR sensors were located around the walls in the experimented location, and the observed people were not uniquely tagged, the data gathered could not collect personalised activity. Therefore, by increasing the sensitivity of activities of daily living classification, we can enrich data in WSNs by giving specific information on the individuals performing the tasks, their locations, and whether multiple tasks are being performed simultaneously. This would overcome the limitation of data gathering within WSNs and instead reveal more trends in data—which can consequently train the network to handle data more personally to the individual or people it is serving.

2.2 Benefits ADL Can Offer WSNs

Any environment fitted with sensors can share information on the location, usage, and operators of the sensor-fitted device [15] for reporting behavioural patterns. Primary motivations are for the elderly, to provide a support care system that will allow elders to live as independent as they can through minimally invasive monitoring [16]. Research has shown how gathering activity of daily living data through

a wireless sensor network can improve the security and wellbeing of an environment's inhabitants. Gupta et al. [16] demonstrated this by building a wireless sensor network made from appliances in a smart home. In a smart home, if each appliance is connected to a sensor unit (SU) a WSN will be able to collect the appliances' ID, information on its current usage and duration, and their frequency of use. This information would enable the system to derive some rules for the smart home inhabitants on how often to use their appliances, and how long for, in order to minimise their energy usages. As each SU is a transceiver, the two-way communication allows for the appliances in the network to communicate with each other, in addition to the main central control unit (CCU)—that interrupts each appliance after a defined time interval to gather information from all the SUs. Once the system has established a pattern of the appliance usage then it can recognise when the pattern has broken. When a detected pattern deviates from that collected through continuous monitoring, it could be due to a malfunctioning appliance or when the health of an inhabitant degrades. Hence, using ADL data in the WSN could turn a smart home into an ambulatory monitoring environment which acts to secure the safety of its inhabitants [17].

Moreover, ADL monitoring can add contextual data to wireless sensor networks by creating an 'activity roadmap' through gathering data from human observation in an enclosed space [18]. A mechanism was proposed to use the contextual ADL data to make a WSN more robust. By using a Bayesian network fusion engine to collect the WSN data from multiple sensors within a defined space, the system could increase its confidence of when appliances were being used. Furthermore, this made its tolerance to noise and outlier data to increase which further increased the systems accuracy and ability to predict when appliances would be used again. To this effect, ADL can offer ambient intelligence to a WSN. However, it has been stressed that sensors should be as anonymous as possible for privacy reasons. Invasive activity tracking techniques, such as video recording, can reveal residential data which can threaten the security of the objects within and objects operators using the wireless sensor network. High-level recognition of the sensor objects in the wireless sensor network is needed to prevent residential ambient intelligence data being criminally accessed from outside the network.

However, in order to create a robust WSN based on ADL data we need to minimise the number of false prompts and ill-advised suggestions in behaviour [16]. Assisted living is considered a realistic application for wireless sensor networks [19]. Wireless Sensor Networks are often challenged with working in noisy environments that change over time. If a Wireless Sensor Network is incapable of recognising a false prompt, it will output false data making the system unreliable. The AlarmNet Assisted-Living and Remote Monitoring network [19] is an example WSN that aims to minimise false positives and false negatives. It unifies heterogeneous nodes in the network into a common architecture, and also compensates for sub-networks made from other sensors. An on-body wearable sensor network is mobile and based on the wearer's location. The on-body wearable network communicates with the main WSN via data streaming. This paper also highlights an issue with human-orientated WSNs, often used in smart homes: the necessary

grouping of personal data such as residential location, activity, and activity level. This emphasises the extent of data openness required to create a dynamic semantic WSN. Therefore, we need to be careful in how we carry information around a WSN holding personal data collecting in ADL research.

3 Case Study: Smart Home Hub WSN with Flexible Wearable Device Prototype

3.1 Motivation

Aforementioned, this book chapter uses previous work as a case study. That project [4] aimed to integrate a voice-controlled flexible wristband into a wireless sensor network in a smart home. It was motivated by the number of reported interrupted data collections during Activities of Daily Living (ADL) research, and aimed to counteract this occurrence by using a flexible wearable device to unobtrusively orchestrate the collection of data within a smart home and navigate streamed wireless data. The flexible attribute of the wearable device would increase its comfort, encouraging users of the system to wear the wearable device continuously.

The goals of the project were:

1. To establish efficiency of the voice recognition to control the wireless sensor network system.
2. To construct a flexible circuit that used conductive anisotropic adhesive printing technology that could communicate with a computer, showing this technology has the potential to make an unobtrusive wearable device that could collect ADL data.
3. To construct a wireless network that could control an external light to visually represent different smart home commands.

The outcome of the project evidenced a reliable and robust wireless sensor network that could be used to control a lighting system. The lighting system changed its visual appearance when a different smart home task was activated by the user.

3.2 Background

ADL research had primarily been based on smartphones to access activity information from their experiment participants; plausibly because of their familiarity and availability [20]. However, smartphones are ill-suited for ADL applications as their high-processing of data compromises battery life which can prevent the collection of continuous data collection [21]—essential for establishing reliable behavioural

patterns. A device with comparable computing power as smartphones, but portable and flexible enough to be ‘wearable’, would be a better alternative for ADL research. This, would offer an unobtrusive, reduced complexity interface [22]—which, if was controlled by voice, would increase engagement with our environment.

Smart home technologies are gaining intelligence through use of artificial intelligence [23] and becoming portable through wearable technologies [24, 25]. Nonetheless, for all data collected from these Home Informatics Technologies (HITs) how they are presented to the user will influence how often they are used. Factors include whether the user can understand the presented data [26], whether the data is considered useful [27] and whether behavioural changes resulting from computational analysis get the attention of the system user to change their habits [28].

Machine learning algorithms and methods [29] can aid for the correct classification voice commands which can expand the usage of the proposed WSN system to motor-impaired individuals whom could not use smartphones to control their environment [30].

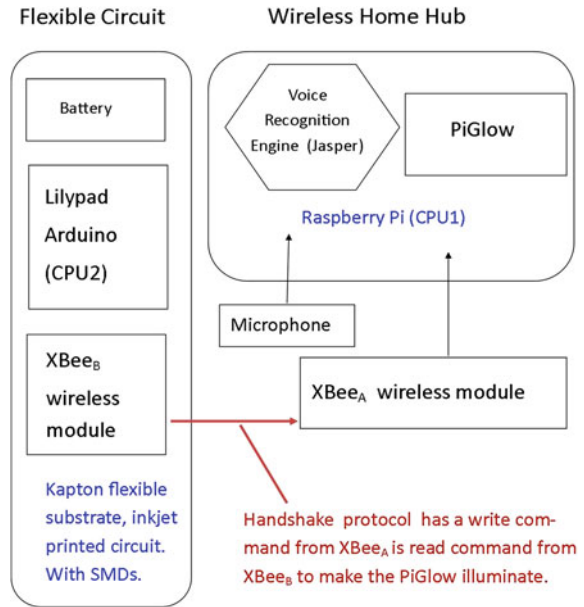
The above justified the requirement for the development of a screen-less interface to control a smart home environment and present behavioural data in an understandable way. The project approach involved creating a WSN that operates in a smart home environment. Additionally, the WSN includes a flexible wearable device as a human-computer interface that would allow remote monitoring of the system.

3.3 Prototype Discussion and Applications

Figure 1 shows the system architecture for the prototype. An essential part to the system architecture was the handshake protocol. The handshake protocol acted as a two-way acknowledgement infrastructure that ensured that the smart home hub system activated a task only when the task description matched the instruction set registered in the system central processing unit (CPU).

The wireless network was made from two Digi® [31] XBee Series 1 802.15.4 built-in antenna modules. One module was connected as a dongle to a Raspberry Pi and another module was connected to another computer system to be located on the flexible wearable device. The handshake protocol was configured using the CoolTerm App [32], a serial terminal software program. A Personal Area Network (PAN) ID was assigned to both Digi XBee Radio Frequency (RF) modules, each module was given a unique ATMY address so they can be addressed separately, and lastly each module was given interchangeable ATDL values so they can communicate only with each other. Successful matching of task with the registered executable commands between the two RF modules meant that the LED visual feedback, a PiGlow, could be controlled wirelessly. The PiGlow was attached to the

Fig. 1 System architecture diagram



GPIO pins of the Raspberry Pi and programmed in Python to recognise the executable tasks that can be communicated wirelessly to the smart home hub system.

Custom modules were programmed in Python for the PiGlow to recognise whether a light, locks, or personal notifications (email, weather, news) commands were given to the smart home hub to execute. The PiGlow would illuminate in red, blue, and green respectively to visually represent when a task was executed. This was done by addressing the appropriate LEDs on the PiGlow, shown in Fig. 1, using I2C communication and Pulse Width Modulation techniques.

The flexible wearable component was completed through inkjet printing conductive traces on polyimide. Furthermore, a LilyPad Arduino USB, LilyPad Arduino battery pack, a LilyPad Arduino XBee module chip, and surface mounted components (SMTs) such as LEDs and resistors were secured onto the polyimide using conductive anisotropic adhesive to replicate the PiGlow system attached onto the Raspberry Pi. An example of such SMT component can be seen in Fig. 2.

A Dimatix Materials Printer (DMP-2831) was used to print a circuit board layout using inkjet printing on the flexible polyimide substrate. This printed a silver conductive ink as tracks on the polyimide; the tracks outlining the circuit that would connect the Arduino hardware components together, as shown in Fig. 3.

The outcome of this project was a functioning wireless network comprised of the Raspberry Pi, PiGlow, and XBee Radio Frequency modules but not with the flexible wearable device. The project highlighted the problem of mounting relatively heavy and rigid hardware components onto a light-weight flexible substrate—a compromise on robustness, reliability, functionality, and comfort. However, the system did show potential of operating a wireless network that could control home utilities without

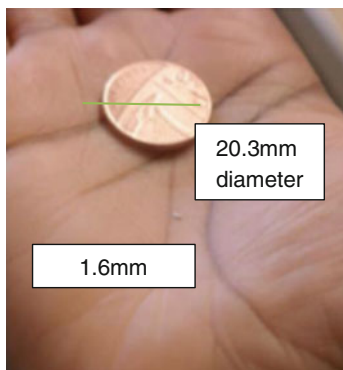


Fig. 2 KPGA-1602SURC-KA SMT LED component beside British 1p coin for comparison

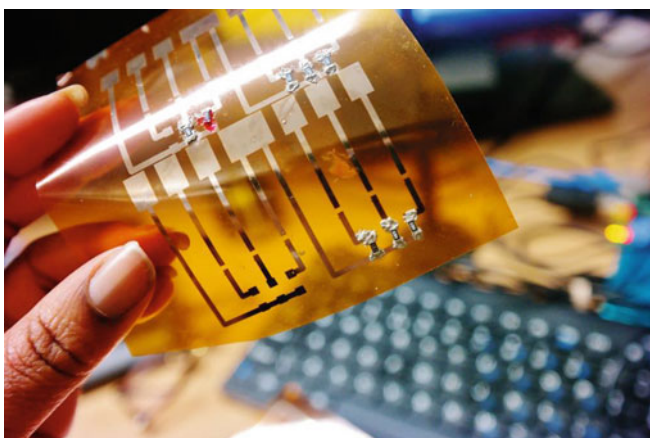


Fig. 3 Partial completion of surface mounted components on separate polyimide circuit

using a smartphone and using off-the-shelf, low-cost equipment and free software. The work showed that it was possible to print the conductive interconnects on to the flexible polyimide and create a complete system but it was not sufficiently robust to be wearable. Improved robustness of the conductive adhesives would allow all of the necessary components from the rigid PCB devices to be instead mounted directly on the printed circuit, thus improving overall flexibility.

Future extensions of such a system could include:

1. Utilising voice-recognition to recognise spoken commands to operating a light switch in a smart home despite the user being on a separate building level or distance away. The user gains feedback that the task was completed by the colour-changing wearable and the light illuminating.

2. Controlling locks remotely whilst the human system operator is engaged in another task.
3. Setting up the smart home sub system and accompanying wristband in an ordinary home, not already fitted with an integrated home informatics technology (HIT) system. Where each appliance is operated with a sensor connected to the wireless sensor network (WSN), this modular system makes an ordinary home smart.
4. Communicating with a microphone located on the smart home wristband can transmit packaged data to the smart home hub to give personal notifications like email, weather reports, and news. This allows the system user to control the smart home hub via voice remotely and additionally the relayed notification information can influence the user to change the utilities settings for improved energy usage.

3.4 Smart Textiles: Improving the Prototype

Polyimide has been used in other wearable technology prototypes in previous literature [33–36]. Polyimide has been used for its robustness, light-weight characteristics, and the ability to exhibit desirable chemical and electrical properties at a wide temperature range [37]. However, the project revealed that creating an entire wearable device predominately made from polyimide was not a feasible long-term solution. Compared to other projects, they reported use of smaller percentages of polyimide [38] or where the polyimide was either etched [39] or used as a layer of a complete wearable system [40] with smaller electronic components with more successful prototypes. Ideally, large polyimide surfaces should be avoided [41] due to potential for deformation and material distortion. However, if the wearable device in the smart home hub wireless sensor network project was made from a smart textile, improvements such as improved dexterity and stretch-ability can be achieved. Yet, there have been examples of smart textiles featuring polyimide. The PlaceIt FP7 EU project [42] developed organic field effect transistors to be located in the core of fibrous yarns. A metallic fibre has a polyimide layer on top—this becomes the gate of the structure. This layered approach, also applied to the drain and source of the transistor, is said to retain the flexibility of the yarn whilst still being soft against the skin.

An interesting trend is the production of smart textiles using traditional weaving and knitting techniques. This makes the smart textile stretchable and flexible, allowing this new ergonomic electronic interface to curve against the body and increase mobility [43]. For smart textile data to contribute to a wireless sensor network (WSN) it needs a textile-based antenna to implement sensing and localisation [44]. The choice of antenna topology depends on the surface and shape of the structure the smart textile will cover, and the how the structure will be used. The larger the surface area of the smart textile, the more antennas can be deployed

which can compensate body-shadowing or areas where the smart textile will be covered during use [44]. Maria et al. [45] have shown the feasibility of fabricating a smart textile sensor network for IoT applications. Textile-based panels were placed on the interior walls of a building for insulation purposes. It featured four sensors, a mainboard, a transceiver, and a low-power battery source was used to evaluate the thermal energy efficiency of a building. The applications of the smart textile version of the originally proposed wearable device would still act as a communication remote, wirelessly orchestrating the transfer for data in the WSN smart home system. Though, the wearable itself would need a textile wearable antenna to establish the wireless connection and a sensor tag to personalise the wearable devices' user and location in the home. This can be expressed as a wearable Radio Frequency Identification (RFID) tag which even can be embroidered onto the smart textile, further ensuring comfort whilst still being fully functional [46].

3.5 Smart Textiles to Enrich Activities of Daily Living Research Further

Smart textiles offer Activities of Daily Living (ADL) researchers access to previously inaccessible data. Lu et al. [18] suggest collecting activity of daily living data through a smart floor, which can wirelessly transmit and receive data about the locations of individuals in a monitored environment. Similarly, another proposition was the Smart-Surface [47] consisting of a matrix of pressure sensors capable of detecting large temporal and spatial patterns. The technology was applied to many furnishings found in a home e.g. sofas, yoga mat, carpet, table cloth, and outside the home—a car seat. The spatial pressure resolution matrix on the car seat (SmartSeat), with data mining, could detect different postures. The algorithm used, Random Forest Classifier, could detect different postures with 85 % accuracy and with this had the information to predict the driver's wellbeing, traffic conditions, and the driver's intentions. Hence, smart textiles with sensors that can wirelessly communicate with a WSN can provide information and further predictions that most of the current appliances are incapable of doing.

It is important that any smart textile capable of furthering ADL research still facilitates independent living and is not completely dependent on the IoT objects to function in their habitable space [48]. This is especially important for medical IoT spaces, where independent living of a growing population and urbanised society may help to relieve pressure upon doctors and resources in monitoring and caring for physiological symptoms [49]. In this light, wirelessly-connected smart textiles for ADL research may not benefit the research field alone, but also have greater implications such as helping us live more independently.

4 Smart Textiles and Their Contribution to Wireless Sensor Networks

4.1 Smart Textiles Are the Future of Wearable Devices

Textiles may be considered an unusual location to place electronics [50]. However, smart textiles have been predicted to be the future of wearable technologies for over a decade [50, 51]. Smart textiles used as the substrate for wearable devices can be called ‘wearable motion capture systems’. Applications could be wearable, display and sensory, haptic interfaces [51] which are skin-like. Challenges for smart textiles to become ubiquitous are industrially-scalable fabrication methods and interconnection lines. However, opportunities lie in creating electronic circuits using large-scale industrial looming and weaving machines which are used at a global level [50]. In the future, textiles are going to gain a new dimension of use—besides protection and aesthetics; they will also offer intelligence [52].

4.2 Smart Textiles Types and Uses in Wireless Sensor Networks (WSN)

Smart textiles can be categorised into passive, active, and intelligent [53]—each distinguishable by the extent at which they respond to environmental stimuli after detecting it. Active or intelligent textiles would be most suitable for a WSN since they can respond and adapt, respectfully, to their environment after gathering data from the WSN.

Google’s Project Jacquard [54] methodology can be used to create a textile wireless sensor network. Electronics or computational components can be embedded into textiles to gather data that can be processed in a WSN [55]. Thus far, we have considered how smart textiles can be used with WSNs, however, it is also necessary to understand their limitations. Current smart textiles lack the storage and energy capacity to become a wireless network in their own right. Therefore, ‘textile area networks’ (TANs) and the option of integrating a full computer system onto a smart textile are not yet possible. There are multiple options and associated terminologies to describe how wearable sensors can be used in WSNs [56]: wearable sensor network (WSN), body area sensor network (BASN) [57], and personal area network (PAN) as examples. However, since these systems will incorporate textiles, typically used in items of clothing—considered of personal use—other factors, not usually associated with WSN design, need to be taken into account, such as aesthetics, user-acceptance, ethics, privacy, safety, unobtrusiveness, and even legality [56].

A reported 15 % of individuals internationally have some form of disability [58]. WSNs used for Activities of Daily Living (ADL) purposes to monitor individuals with disabilities can benefit from BASNs. In this way, ADL supports the idea of digital inclusion by giving the same benefits of technological service to all types of

mobility and wellbeing. BASNs could also benefit the sports industry, by improving the feedback given to athletes to better their performance. Sensors located around athletes' bodies whilst training and performing can collect real-time data about posture, distance travelled, or time of workout and wirelessly communicate the results to the athlete and coach [59].

Overall, research has shown that smart textiles can benefit the wearable technology industry in offering applications for microelectronics and micromechanical components and integrating it into soft textile surfaces. The application, if these smart textiles were embedded with RFID tags, is the creation of on-body wearable sensor networks. These can potentially reveal more personal and sensitive data about the user and all individuals monitored by the WSN.

5 Applications of Smart Textiles and Types of Extractable Wireless Data

5.1 Fashion

For electronically fibrous smart textiles, the skill-set of the designers in the fashion industry would need an inherent understanding of technology to become creative with the material. Fabrics would be grouped by their technological function and not just their colours or patterns [60].

With wireless communication, smart textiles can produce garments capable of enhancing social interactivity at community events. Kan et al. [61] mention the rise of 'wearable social messaging' as way of using garments and accessories to make us more aware of the people around us, digitally brand the wearer, and create new social communities all done by socially messaging those in proximity. Placing Microelectronic Mechanical Systems (MEMS) near the skin by weaving them into textiles can allow us to extract real-time physiological data. Whether we use sensors in a two-to-one setup e.g. photodiodes and LEDs to enable near-infrared spectroscopy (NIRS), [62] or in a one-to-one setup e.g. a MEMS Radio Frequency (RF)-based transceiver capable of transmitting low-power wireless data [63], an input-output behaviour can be exhibited by smart textile fashion. The result, textiles with high level of functionality and with added intelligence could even complete tasks autonomously—increasing reliability and longevity [64].

5.2 Interior Design

If furnishings and surfaces are made from smart textiles they could contribute to the Internet of Things (IoTs).

Smart textiles could contribute to the independent living within buildings, at the moment provided by smart electronic devices connected to The Cloud [65]. As more smart textiles are found in homes, arguably the contents within the home become more personalised [66]. It could be possible, for a communication platform to be provided by these connected textiles. Either within the home, where smart textiles could collaborate with other electronic devices in the home, or between different homes where smart textiles could behave in synchronised ways to convey national information e.g. curtains illuminate red nationally to convey a national safety warning. For this to be feasible, smart textiles covering the whole surface or exist as patches [67] woven with traditional textiles. These smart textile surfaces can be interacted with passively e.g. by sitting or lying, or actively e.g. touching, tapping, gesturing. Active interaction would occur only when the user wants to share or gather information using the smart textile, and likely done in a more accurate manner [68]. Passive interaction would occur when the connected textile only aims to monitor and recorded data when interacted, the data simply being the ID of the person who interacted with the connected smart textile, interaction duration, and location [69].

5.3 *Automotive*

Textiles equate to 2 % of a car's average weight and nearly 45 m² of textile is used in a car's interior rim (seating, headlines, side panel, carpet, and trunk) [70]. Automotive textiles could be given Radio Frequency Interference/Electro Magnetic Interference (RF/EMI) shielding, light emitting, and anti-static qualities [71].

The benefits of smart textiles inside vehicles could include detecting physiological signals which indicate posture and stress levels of the driver and/or passengers. These sensors could be located in the car seats [72], or even in the steering wheel [73] which could detect more indirect driver behaviour such as drowsiness [74], emotions, and attentiveness to the road ahead. A wireless sensor network (WSN) could include this physiological data if these sensors were connected to the Cloud. The implication of this for self-driving cars could enable more intelligent decision making. Intelligence in future cars can respond to the data collected by the smart textile automotive interiors by alerting the drivers and passenger. The car could self-park itself in a safe place and call emergency services to attend to the driver.

5.4 *Medicine*

Wheelchairs for permanent and temporary usage can be upholstered with smart textiles to record physiological data. Postolache et al. [75] present its feasibility, by embedding a wheelchair's seat and arms with a combination of multifunctional I/O

modules, 3D MEMS accelerometers and an embedded PC to measure physiological signals related to stress. The data could be sent to the embedded computer and mobile software such as smartphones and tablets, allowing distant monitoring of the wheelchair user [75]. Distant monitoring of patients could be possible in the future due to smart medical textiles [76]. Clinical rehabilitation [77] and wound care can be optimised with smart textiles, allowing more medical care to be focused only on high-emergency cases and not on check-ups. Additionally, patients within the hospitals can also be tracked with smart textiles. Patients wearing hospital gowns made from smart textiles could have embedded RFID and with wireless communication can evaluate the transmission routes patients take around the ward. If each patient was categorised according to illness, information collected by these transmission patterns could reveal how infection spreads within a hospital [78].

5.5 *Sports*

Physiological data collected in real-time by sports textile uniforms [79] can detail athlete's levels of stress, emotional state, and even be used to predict injuries both in training and whilst performing. This data could help personalise different athletes' training or rehabilitation routine, or enhance the sports entertainment industry if viewers could receive physiological data of their favourite athletes and watch how this affects a match or competition. Pressure sensors embedded into sports uniforms could quantify forces exerted onto athletes' bodies due to physical contact [80]. In this way, smart textiles in sports could protect athletes from further injury as physiological problems can be detected earlier [81].

Smart textiles used in sports need to be comfortable and their sensors unobtrusive so they do not disturb the performance of the athlete [82]. In fact, if smart textiles can enhance the performance of the athlete, then the adoption of smart textiles in sport may become widely adopted futuristic sports teams and entertainment.

5.6 *Toys*

Wireless sensing networks integrating toys can involve smart textiles to create an engaging and safe human-computer interface for children and young adults. Children interact with toys for 'free play' and developing imagination [83] but they can also unobtrusively monitor their wellbeing if hospitalised using smart textiles. To aid psychotherapy, Rossi et al. [84] proposed three electronic-embedded dolls that use haptic feedback to non-verbally communicate with children. The intention was to make the child feel more at ease in a medical environment and subconsciously help to build a positive relationship between the hospitalised child, doctors, and medical staff [84]. The advantage of toys covered in smart textiles compared to wearable options, is that they can be shaped into any creative structure and they can

be designed to collect more specific information for the Cloud. The Sniff [85], a smart toy dog, had radio frequency identification (RFID) tags in its nose to identify different emotional states communicated from the Cloud. It translated this identification through different sounds and haptic feedback to the user, so that the user can learn the meaning of different emotions through multiple sensory engagements. It seems then, that smart textile toys can extract data about a child's emotional intelligence, wellbeing, and social knowledge.

Research on smart-textile wearable biomedical systems (ST-WBSs) [86] for infants, show that parents can remotely monitor the health of children under their care. Heartbeat, respiration, body temperature and sweat can be detected by ST-WBS in a vest format [87] or as infant textile shoes to monitor pulse oximetry and movement to prevent early deaths [88]. Furthermore, ST-WBs are said to be improved by microelectronics [89]. As toys can be used for short and long durations, the data transferred to WSNs will depend on the power supply, processing capacity, and storage capability of the node [89]. Still, consideration on the types and levels of radiation exposed to children and infants must be taken into account in the design of wirelessly-enabled smart textile toys [90].

6 Security Issues in Wearable Devices and Smart Textiles

6.1 *Wireless Sensor Networks with Smart Textiles*

Using Wireless Sensor Networks (WSNs) for human monitoring—whether focused on one building or several in a community—is beneficial to the whole society [91]. Concentrating in a smart home environment, all the sensors within it connected to the Cloud are clustered together in a WSN.

We can explore what happens when these smart textile sensor nodes are connected to a WSN by considering the surfaces they would be found on. For example, taking the idea of a smart textile rug embedded with a RFID sensor tag and a pressure sensor. This rug could be wirelessly connected to the smart home hub with the flexible wearable device system [4]. This smart textile rug is another sensor node in the WSN. As long as the sensor node is active, it is continuously or periodically sensing external stimuli from the smart home environment. The collected data may detail which individual is interacting with it, the time of interaction, and duration of interaction. Hence, the sensor node is measuring the parameters of the input. These measurements are transmitted to and received by the WSN where it can be shared with other neighbouring nodes, or transmitted into the Cloud for storage, or to another network provider for analysis.

One suggestion to counteract noise is an area-based noise measurement [92]. Area-based noise measurements can minimise the detrimental effects of noise upon WSNs. An algorithm in the WSN divides all the nodes in the network into groups, and noise measurement is scheduled between these groups and transferred to a

server [93]. The intention of other noise-defeating methods is to reduce the effects noise has upon the measured parameters observed by the sensor nodes. Once the noise effects are compensated for, the wireless protocol for smart textiles nodes in WSNs is to be established.

Arguably, the use of smart textiles in a smart home compared to other sensor appliances is more for extracting location and physiological data compared to encouraging energy-saving efficiency [94]. As a result, two different types of data—those which encourage energy-efficiency and those which encourage well-being—are being exchanged in a WSN and certain protocols may be more appropriate to use for facilitating this than others. Some protocols to consider include Wi-Fi, ZigBee, and Bluetooth. These protocols may be suitable for a monitoring a localised network, such as Local Area Network (LAN) and Personal Area Network (PAN), which may be desired if wanting to run a WSN at low cost [94]. The attraction of WSN is that they can be run at very low energy [95]. The pursuit of flexible battery systems and renewable energy solutions for powering smart textile objects has been intensely researched [96, 97]. Then, employing a WSN compared to other types of data sharing networks may be the best choice—as smart textiles get the benefits of wireless communication but are not depleted from energy through engaging with the WSN.

6.2 Protecting Smart Textile Data and Security Measures

Security is an important factor when setting up a Wireless Sensor Network (WSN) [95]. The whole network and each of the nodes within it are capable of external hacks, threats, and harmful links to outsiders. This can cause a leakage of personal data. Hence, it is important to protect system infrastructure, the individuals, and communities using the WSN. This can be done by giving entities (sensor units or separate WSNs) shared knowledge of a cryptographic ID; knowledge of this key acts as a security protocol [95]. Hence, wireless communication acts as the backbone [98] of implementing high-level integration of connected appliances and smart textile sensors in a smart home environment or even expanded to a smart city.

One of the most harmful data to leak out of a WSN is about location, especially if the node holding this data is a key node [99]. If a key node is attacked from outside the WSN, then all nodes connected onto it can also be infiltrated. Smart textiles will be collecting data about their location and maybe the individual interacting with it [100]—data which hackers can steal or misuse location or behavioural information. Therefore, users of the WSN are entrusting it with their local and global belongings, identity, and technological livelihood [101]. Enforcing a trust and reputation framework [102] among all sensor nodes in the WSN can ensure that data is only being exchanged when a threshold of data protection has been established. Yet, trust and reputation within a WSN can be threatened via a collusion attack—injecting false data into the WSN to reduce confidence and communication stability [101]. Therefore, there has been an effort to secure these

collection of sensor nodes that are collaborating together to provide a robust wireless communication network [103].

Sensor nodes, whether as an appliance or represented as smart textile structures, are expected to have drifting internal clocks. This is because their efficiency degrades with use [104]. Synchronising internal clocks of several nodes in a WSN could allow orchestration of data transmission to the key or source node simultaneously in a narrow time range. Hence, this orchestration can occur when an event within the WSN occurs. An event-based clock synchronisation has been proposed to increase communication efficiency [105]. If an event-based clock synchronisation was deployed when an interrupt was detected, and this interrupt was invoked when a potential threat was suspected, it could make the overall WSN more protected and robust.

7 Artificial Intelligence to Aid WSN Protection of Wearable Devices and Smart Textile Data

Machine learning (ML) strategies, a technique for artificial intelligence (AI) has proved effective in maintaining safe and robust wireless sensor networks (WSNs) [106]. As WSNs are dynamic, machine learning algorithms can learn from the changes and evolve the structure of the WSN to protect it from external attackers [107]. ML methods are used for either learning about systems' knowledge to improve their performance [108] or learning about systems' behavioural patterns to improve their performance [109]. For WSNs, either supervised, unsupervised, or reinforcement learning, ML algorithms can be used [110] to create prediction models of how information will be exchanged. Anomalies are detected in any prediction model when the integrity of the collected data [111] are challenged or when an attacker has harmed the WSN. Detecting and reducing the effects of anomalies is essential maintenance for single-hop and multi-hop WSN topologies. There are three types of anomalies that can be detected in a WSN thanks to ML algorithms. Anomalies can be found in a single measurement at sensor node, all measurements at a sensor node, or all sensor nodes in the WSN [112].

Estimating the location of nodes is essential in a WSN [113]. Sensor nodes may move around periodically or continuously within a short or long time period, for example if this node is furniture. Location information for a WSN can be collected using a Global Positioning System (GPS) or using range [114] or range-free [115] localisation techniques. Reducing localisation errors by detecting the distances between sensor nodes in a WSN will enable a more accurate collection of data from nodes [116].

Support Vector Machines (SVMs), machine learning classifier algorithms, are a versatile AI technique to use for WSN communication optimisation. SVM algorithms have been proposed to localise a wireless sensor network to estimate the geographic location of nodes [117]. Yet, SVM algorithms can also be used to detect outliers in WSNs [118]. The size, bandwidth, and communication between the

nodes in the WSN can affect the type of SVM algorithm applied. Distributed Support Vector Machines (DSVMs) are machine learning algorithms that could be used to manage communication between interconnected devices in WSNs [119]. Distributed types of algorithms are additionally becoming favourable to increase data privacy protection. The objective is to share data awareness among collaborative nodes within a WSN without sharing the contents of that knowledge with other nodes in the WSN to prevent external attackers accessing it easily [119]. The faster the SVM, the faster that global optimisation of the WSN is achieved. However, this depends on the number of SVM channels and the number of support vectors needed for each successful communication in the WSN. An alternative is an ad-hoc WSN, whereby the sensors communicate in a peer-to-peer (P2P) configuration and distributing the learning task between them [120].

To minimise global communication energy of the network, through distributed algorithms and localisation techniques, all ML algorithms used in WSNs [121] by making optimised data exchange decisions. This can help extend the life of WSNs, which are otherwise limited to the battery-life of the sensor nodes in the network [122]. There is a high-level of uncertainty within a WSN can be mathematically modelled using AI techniques, such as the Markov Decision Process (MDP) which organises the network so that future states are only dependent on the current state and not previous states [123]. This benefits the WSN by reducing wasteful energy usage or energy draining faster than desired when nodes communicate [124], maximising the number of nodes in a WSN [125], and allowing mobile nodes to be monitored in a WSN [126]. Yet, although SVMs have shown to be effective in WSNs, other machine learning techniques may be too computationally intensive to implement—especially when there is too much noise, limited knowledge to learn from, and limited storage in the WSN [127].

With the autonomy that machine learning techniques bring to WSNs, it may be possible for stochastic WSNs to become self-sustainable after a long period of time [128]. Hence, energy conservation becomes an important factor for self-sustainable WSNs and becomes imperative when they become highly dynamic and random—due the uncertainty in action and use from smart textile or wearable nodes. Nevertheless, artificial intelligence can help manage the increased complexity that smart textile sensor nodes and wearable nodes will introduce whilst also expanding the lifetime of the WSN [128].

8 Conclusions

This book chapter has exemplified how smart textiles can become a new and exciting human-computer interface for a wireless sensor network system. This is largely due to the increased functionality and reduced size of Microelectronic Mechanical Systems (MEMS), which can help transform wearable hardware devices into soft, flexible, and stretchable textile surfaces which can wirelessly communicate with the Cloud.

The intersection of electronics engineering, smart homes, activity of daily living (ADL), wireless communication, textiles and wearable technology featured in the project [4] is primarily what this chapter is based on. Furthermore, by improving the proposed system by replacing the wearable technology wristband with a smart textile-equivalent, it has been shown that more sensitive and personal data can be collected—which can enhance the pattern detection process and results. The types of data that can be collected from these smart textiles are contextually richer than that proposed in the original project. It has been hypothesised in this book chapter that the quantity and level of context this data contains can add to data already in WSNs. Hence, a new application of WSNs is using data extracted from sensory and interactive smart textiles to offer more personal data into The Cloud, which is anticipated to predict more behavioural patterns from our habits, locations, and interactions on an international scale.

However, as the data in the wireless sensor network (WSN) becomes contextually richer it becomes even more necessary to collect the data unobtrusively and provide more security. With the unprecedented opportunity to analyse data from textile surfaces and furnishings, new smart textile professions who design the circuitry within the textile—perhaps called ‘smart textile engineers’ or ‘electronic textile engineers’—and WSN designers need to facilitate how this information will be used to enrich the data already in the Cloud. Such implementation of the data collected from smart textiles and stored in the Cloud would be useful but it is important that users of the Cloud understand that this data contains personal information about their owners. Additionally, this means that threat towards this personal data also threatens the owners’ livelihood and privacy. Hence, perhaps adding smart textile data to wireless sensor networks will make the WSN infrastructure unstable. Though, this can be avoided by classifying the numerous ways that personal data extractable from smart textiles can be either hacked, attacked, and misused. Furthermore, to ensure that everyone has a chance to utilise the benefits of WSN-smart textiles, researchers and engineers need to consider digital inclusion. By reducing the number of physical restrictions and technical limitations on the sensor nodes of the network, the longer the components within the WSN can be used. Furthermore, we can increase confidence of the WSN retrieving and transmitting uninterrupted data.

The MEMS (or other electronic devices) within the smart textile will determine the data contents exchanged in the WSN. This chapter has highlighted the different applications that smart textiles can be used in, and subsequent examples of the wireless data that can be communicated. This shows the diverse ways that smart textiles can be used, such as improving wellbeing, monitoring physiological health, or even monitoring social intelligence.

There is optimism for artificial intelligence (AI) methods, especially machine learning (ML) algorithms protect data and maintain the WSNs efficiency in communicating data with minimal energy losses. Although several ML approaches can be used, the extensive choice can be implemented to enable a WSN with dynamic sensors—despite WSNs’ stochastic nature—to enable true smart home living in an increasingly urbanised society.

References

1. I. Thoma, L. Fedon, A. Jara, Y. Bocchi, Towards a human centric intelligent society: using cloud and the web of everything to facilitate new social infrastructures, in *2015 9th International Conference on Innovative Mobile and Internet Services in Ubiquitous Computing (IMIS)*. IEEE, (2015)
2. D. Ilišević, Mtel, B&H, B. Luka, Bosnia-Herzegovina, N. Banović-Ćurguz, Evolution toward digital society in B&H, in *2015 23rd Telecommunications Forum Telfor (TELFOR)*. IEEE, 2015
3. D. Bremner, *The IoT Tree of Life* (2015)
4. O. Ojuroye, A. Wilde, Prototyping a Voice-Controlled Smart Home Hub, Wirelessly Integrated with a Wearable Device, in *International Conference on Sensing Technology (ICST)*, 2015
5. D. Foti, J.S. Koketsu, Activities of daily living, in *Pedretti's Occupational Therapy: Practice Skills for Physical Dysfunction* (2008), pp. 157–232
6. S. Katz, Assessing self-maintenance: activities of daily living, mobility, and instrumental activities of daily living. *J. Am. Geriatr. Soc.* **31**(12), 721–727 (1983)
7. K. Avgerinakis, A. Briassouli, I. Kompatsiaris, Recognition of activities of daily living for smart home environments, in *2013 9th International Conference on Intelligent Environments (IE)*. IEEE, (2013)
8. P. Rashidi, D.J. Cook, Mining and monitoring patterns of daily routines for assisted living in real world settings, in *Proceedings of the 1st ACM International Health Informatics Symposium*. ACM, 2010
9. SMART CITIES, Trace analysis and mining for smart cities: issues, methods, and applications. *IEEE Commun. Mag.* **121** (2013)
10. L. Wang, T. Gu, X. Tao, H. Chen, J. Lu, Recognizing multi-user activities using wearable sensors in a smart home. *Pervasive Mob. Comput.* **7**(3), 287–298 (2011)
11. A. Wood, G. Virone, T. Doan, Q. Cao, L. Selavo, Y. Wu, L. Fang, Z. He, S. Lin, J. Stankovic, ALARM-NET: wireless sensor networks for assisted-living and residential monitoring, in *University of Virginia Computer Science Department Technical Report*, vol. 2 (2006)
12. A. Pathak, Y.C. Hu; M. Zhang, Where is the energy spent inside my app?: fine grained energy accounting on smartphones with eprof, in *Proceedings of the 7th ACM european conference on Computer Systems*, pp. 29–42. ACM (2012)
13. K.K. Peetoom, M.A. Lexis, M. Joore, C.D. Dirksen, L.P. De Witte, Literature review on monitoring technologies and their outcomes in independently living elderly people. *Disabil. Rehabil. Assistive Technol.* **10**(4), 271–294 (2015)
14. T. Nef, P. Urwyler, M. Büchler, I. Tarnanas, R. Stucki, D. Cazzoli, R. Müri, U. Mosimann, Evaluation of three state-of-the-art classifiers for recognition of activities of daily living from smart home ambient data. *Sensors* **15**(5), 11725–11740 (2015)
15. P. Augustyniak, E. Kantoč, Turning domestic appliances into a sensor network for monitoring of activities of daily living. *J. Med. Imaging Health Inform.* **5**(8), 1662–1667 (2015)
16. G. Sen Gupta, S.C. Mukhopadhyay, M. Sutherland, S. Demidenko, Wireless sensor network for selective activity monitoring in a home for the elderly, in *Instrumentation and Measurement Technology Conference Proceedings. IMTC, IEEE* (2007)
17. A. Dittmar, F. Axisa, G. Delhomme, C. Gehin, New concepts and technologies in home care and ambulatory monitoring. *Stud. Health Technol. Inform.* 9–35 (2004)
18. C-H. Lu, Y-C. Ho, L-C. Fu, Creating robust activity maps using wireless sensor network in a smart home, in *IEEE International Conference on Automation Science and Engineering, 2007. CASE 2007*. IEEE, 2007

19. J.A. Stankovic, A.D. Wood, T. He, Realistic applications for wireless sensor networks, in *Theoretical Aspects of Distributed Computing in Sensor Networks* (Springer Heidelberg, 2011), pp. 835–863
20. M. Meeker, Internet trends 2014-code conference. Retrieved 28 May 2014
21. A. Pathak, Y.C. Hu, M. Zhang, Where is the energy spent inside my app?: fine grained energy accounting on smartphones with eprof, in *Proceedings of the 7th ACM European Conference on Computer Systems*, pp. 29–42. ACM (2012, April)
22. H. Cheng, Z. Liu, L. Yang, X. Chen, Sparse representation and learning in visual recognition: theory and applications. *Sig. Process.* **93**(6), 1408–1425 (2013)
23. V.S. Gunge, P.S. Yalagi, *Smart Home Automation: A Literature Review* (2016), <http://research.ijcaonline.org/rtdm2016/number1/rtdm2568.pdf>. Accessed 23 Sep 2016
24. A.P.O.Y. Wrist, *Introducing The Samsung Galaxy Smartwatch*, by Joseph Milord, posted Sep. 4, 2013, elitedaily.com. 10, 1
25. D.J. Skiba, The connected age and wearable technology. *Nurs. Educ. Perspect.* **35**(5), 346–347 (2014)
26. L. Yang, S. Hanneke, Activized learning with uniform classification noise, in *Proceedings of The 30th International Conference on Machine Learning*, pp. 370–378 (2013)
27. S. Leppänen, M. Jokinen, Daily routines and means of communication in a smart home, in *Inside the Smart Home* (Springer, London, 2003), pp. 207–225
28. A.B. Lynggaard, M.G. Petersen, S. Hepworth, I had a dream and I built it: power and self-staging in ubiquitous high-end homes, in *CHI'12 Extended Abstracts on Human Factors in Computing Systems*, pp. 201–210. ACM (2012, May)
29. L. Rabiner, A tutorial on hidden Markov models and selected applications in speech recognition. *Proc. IEEE* **77**(2), 257–286 (1989)
30. R. Vipplerla, M. Wolters, K. Georgila, S. Renals, Speech input from older users in smart environments: challenges and perspectives, in *Universal Access in Human-Computer Interaction. Intelligent and Ubiquitous Interaction Environments* (Springer, Berlin, 2009), pp. 117–126
31. C. Bell, Tiny talking modules: an introduction to XBee wireless modules, in *Beginning Sensor Networks with Arduino and Raspberry Pi* (Apress, 2013), pp. 19–50
32. XBee/Xbee Pro OEM RF Modules: Product Manual v1.xEx802.15.4 Protocol, Digi International, Inc., (2009, Sept)
33. L. Francioso et al., Flexible thermoelectric generator for ambient assisted living wearable biometric sensors. *J. Power Sources* **196**(6), 3239–3243 (2011)
34. H.R. Khaleel, Design and Fabrication of Compact Inkjet Printed Antennas for Integration Within Flexible and Wearable Electronics. *Compon. Packag. Manuf. Technol. IEEE Trans.* **4**(10), 1722–1728 (2014)
35. Y. Li, et al., An all-inkjet printed flexible capacitor for wearable applications, in *2012 Symposium on Design, Test, Integration and Packaging of MEMS/MOEMS (DTIP)*. IEEE, 2012
36. L. Francioso, et al., PDMS/Kapton interface plasma treatment effects on the polymeric package for a wearable thermoelectric generator. *ACS Appl. Mater. Interfaces* **5**(14), 6586–6590 (2013)
37. L. Francioso, et al., Structural reliability and thermal insulation performance of flexible thermoelectric generator for wearable sensors, in *2013 IEEE SENSORS*. IEEE, 2013
38. J-H. Moon, et al., Wearable polyimide–PDMS electrodes for intrabody communication. *J. Micromech. Microeng.* **20**(2), 025032 (2010)
39. A. Arevalo, et al., A versatile multi-user polyimide surface micromachining process for MEMS applications, in *2015 IEEE 10th International Conference on Nano/Micro Engineered and Molecular Systems (NEMS)*. IEEE, 2015
40. S. Shibata, Y. Niimi, M. Shikida, Flexible thermal MEMS flow sensor based on Cu on polyimide substrate, in *2014 IEEE SENSORS*. IEEE, 2014

41. B. Plovie, et al., 2.5 D smart objects using thermoplastic stretchable interconnects, in *International Symposium on Microelectronics*. Vol. 2015. No. 1. International Microelectronics Assembly and Packaging Society, 2015
42. J. van den Brand, et al., Flexible and stretchable electronics for wearable healthcare, in *2014 44th European Solid State Device Research Conference (ESSDERC)*. IEEE, 2014
43. Y. Ahn, S. Song, K.-S. Yun, Woven flexible textile structure for wearable power-generating tactile sensor array. *Smart Mater. Struct.* **24**(7), 075002 (2015)
44. H. Rogier, Textile antenna systems: design, fabrication, and characterization, in *Handbook of Smart Textiles* (2015), pp. 433–458
45. A.R. Maria, P. Radu, Smart sensor grid networks for analyze the energy efficiency of the enveloped building by textile composites. *Rom. Rev. Precis. Mech. Opt. Mechatron.* **48**, 12 (2015)
46. K. Koski, et al., Electro-textiles—The enabling technology for wearable antennas in wireless body-centric systems, in *2015 IEEE International Symposium on Antennas and Propagation & USNC/URSI National Radio Science Meeting*. IEEE, 2015
47. J. Cheng, et al., Smart-surface: large scale textile pressure sensors arrays for activity recognition. *Pervasive Mob. Comput.* (2016)
48. N. Labonnote, K. Høyland, Smart home technologies that support independent living: challenges and opportunities for the building industry—a systematic mapping study, in *Intelligent Buildings International* (2015), pp. 1–26
49. S.C. Mukhopadhyay, Wearable sensors for human activity monitoring: a review. *Sens. J. IEEE* **15**(3), 1321–1330 (2015)
50. K. Cherenack, L. van Pieteron, Smart textiles: challenges and opportunities. *J. Appl. Phys.* **112**(9), 091301 (2012)
51. A. Mazzoldi et al., Smart textiles for wearable motion capture systems. *AUTEX Res. J.* **2**(4), 199–203 (2002)
52. S. Park, S. Jayaraman, Smart textiles: wearable electronic systems. *MRS Bull.* **28** (08), 585–591 (2003)
53. L. Van Langenhove, C. Hertleer, Smart clothing: a new life. *Int. J. Clothing Sci. Technol.* **16**, 63–72 (2004)
54. Project Jacquard, Google, <https://www.google.com/atap/project-jacquard/>. Last accessed 9 Feb 2016
55. D. Marculescu, et al., Electronic textiles: a platform for pervasive computing. *Proc. IEEE* **91** (12), 1995–2018 (2003)
56. M. Chan, et al., Smart wearable systems: current status and future challenges. *Artif. Intell. Med.* **56**(3), 137–156 (2012)
57. T. Dou, L. Yi, The development and trend of wireless body area networks in the smart clothing field (2015)
58. WHO, World report on disability, 2011
59. A. Nadeem, et al., Application specific study, analysis and classification of body area wireless sensor network applications. *Comput. Netw.* **83**, 363–380 (2015)
60. R. Pailles-Friedman, *Smart Textiles for Designers: Inventing the Future of Fashion* (2016)
61. V. Kan, et al., Social textiles: social affordances and icebreaking interactions through wearable social messaging, in *Proceedings of the Ninth International Conference on Tangible, Embedded, and Embodied Interaction*. ACM, 2015
62. C. Zysset, et al., Textile integrated sensors and actuators for near-infrared spectroscopy. *Opt. Expr.* **21**(3), 3213–3224 (2013)
63. K. Liang, *Transistor Circuits For A MEMS Based Transceiver* (2015)
64. S. Nihtianov, A. Luque (eds.), *Smart Sensors and MEMS: Intelligent Devices and Microsystems for Industrial Applications* (Woodhead Publishing, 2014)
65. N. Labonnote, K. Høyland, Smart home technologies that support independent living: challenges and opportunities for the building industry—a systematic mapping study. *Intell. Buildings Int.* 1–26 (2015)

66. L. Russell, R. Goubran, F. Kwamena, Personalization using sensors for preliminary human detection in an IoT environment, in *2015 International Conference on Distributed Computing in Sensor Systems (DCOSS)*. IEEE, 2015
67. J. Cheng, et al., Designing sensitive wearable capacitive sensors for activity recognition. *Sens. J. IEEE* **13**(10), 3935–3947 (2013)
68. H. Xia, T. Grossman, G. Fitzmaurice, NanoStylus: enhancing input on ultra-small displays with a finger-mounted stylus, in *Proceedings of the 28th Annual ACM Symposium on User Interface Software & Technology*. ACM, 2015
69. H. Kim, I. Kim, J. Kim, *Designing the Smart Foot Mat and Its Applications: as a User Identification Sensor for Smart Home Scenarios* (2015)
70. S. Parmar, T. Malik, *Application of Textiles in Automobiles*, www.fibre2fashion.com/industry-article/1807/application-of-textiles-in-automobile. Last accessed 23 Sep 2016
71. L. Jul, Adding values, upholstery concepts for automobiles using smart textiles (2007)
72. A. Braun, et al. CapSeat-capacitive proximity sensing for automotive activities recognition, in *Proceedings of the 7th International Conference on Automotive User Interfaces and Interactive Vehicular Applications*. ACM, 2015
73. J. Krajewski, et al., Steering wheel behavior based estimation of fatigue, in *Proceedings of the Fifth International Driving Symposium on Human Factors in Driver Assessment, Training and Vehicle Design*, 2009
74. A. Sahayadhas, K. Sundaraj, M. Murugappan, Detecting driver drowsiness based on sensors: a review. *Sensors* **12**(12), 16937–16953 (2012)
75. O. Postolache, et al., Toward developing a smart wheelchair for user physiological stress and physical activity monitoring, in *2014 IEEE International Symposium on Medical Measurements and Applications (MeMeA)*. IEEE, 2014
76. L. Lagenhove, *Advances in Smart Medical Textiles: Treatments and Health Monitoring* (Woodhead Publishing, 2015)
77. A. Fleury, M. Sugar, T. Chau, E-textiles in Clinical Rehabilitation: A Scoping Review. *Electronics* **4**(1), 173–203 (2015)
78. P. Vanhems, et al., Estimating potential infection transmission routes in hospital wards using wearable proximity sensors. *PloS One* **8**(9), e73970 (2013)
79. V. Ferraro, Smart textiles and wearable technologies for sportswear: a design approach, in *2nd International Electronic Conference on Sensors and Applications*. Multidisciplinary Digital Publishing Institute, 2015
80. J. McLoughlin, et al., *A Smart Textile for Measuring the Impact of Energy used in Competitive Contact Sports* (2013)
81. R. Shishoo, *Textiles for Sport* (Woodhead Publishing, 2015), ISBN: 978-1-78242-229-7
82. K. Förster, M. Bächlin, G. Tröster, Non-interrupting user interfaces for electronic body-worn swim devices, in *Proceedings of the 2nd International Conference on Pervasive Technologies Related to Assistive Environments*. ACM, 2009
83. L. Berglin, Spookies: combining smart materials and information technology in an interactive toy, in *Proceedings of the 2005 conference on Interaction design and children*. ACM, 2005
84. E. Rossi, G. Crampton-Smith, P. Tabor, I Mirabilia: taking care of the emotional life of hospitalized children. *Stud. Mater. Thinking* **7** (2012)
85. S. Johansson, Sniff, 2009. Available at www.nearfield.org/sniff
86. S. Park, S. Jayaraman, Smart textile-based wearable biomedical systems: a transition plan for research to reality. *Inf. Technol. Biomed. IEEE Trans.* **14**(1), 86–92 (2010)
87. C. Linti, H. Horter, P. Österreicher, H. Planck, Sensory baby vest for the monitoring of infants, in *Proceedings of the International Workshop on Wearable and Implantable Body Sensor Networks (BSN'06)*, Cambridge, MA, USA, 3–5 April 2006, pp. 3–137
88. Y. Rimet, et al., Surveillance of infants at risk of apparent life threatening events (ALTE) with the BBA bootee: a wearable multiparameter monitor, in *Engineering in Medicine and Biology Society, 2007. EMBS 2007. 29th Annual International Conference of the IEEE*. IEEE, 2007

89. Z. Zhu, et al. Wearable sensor systems for infants. *Sensors* **15**(2), 3721–3749 (2015)
90. A. Pantelopoulos, N.G. Bourbakis, A survey on wearable sensor-based systems for health monitoring and prognosis. *IEEE Trans. Syst.* **40**, 1–12 (2010)
91. A. Mainwaring, et al., Wireless sensor networks for habitat monitoring, in *Proceedings of the 1st ACM international workshop on Wireless sensor networks and applications*. ACM, 2002
92. I. Kivelä, I. Hakala, Area-based environmental noise measurements with a wireless sensor network (2015)
93. T.D.P. Mendes, et al., Smart home communication technologies and applications: Wireless protocol assessment for home area network resources. *Energies* **8**(7), 7279–7311 (2015)
94. B. Placzek, M. Bernaś, Uncertainty-based information extraction in wireless sensor networks for control applications. *Ad Hoc Netw.* **14**, 106–117 (2014)
95. D. Macedonio, M. Merro, A semantic analysis of key management protocols for wireless sensor networks. *Sci. Comput. Progr.* **81**, 53–78 (2014)
96. X. Pu, et al., A self-charging power unit by integration of a textile triboelectric nanogenerator and a flexible lithium-ion battery for wearable electronics. *Adv. Mater.* **27** (15), 2472–2478 (2015)
97. X. Pu, et al., Wearable self-charging power textile based on flexible yarn supercapacitors and fabric nanogenerators. *Adv. Mater.* **28**(1), 98–105 (2016)
98. T.D.P. Mendes, et al., Smart and energy-efficient home implementation: Wireless communication technologies role, in *2015 IEEE 5th International Conference on Power Engineering, Energy and Electrical Drives (POWERENG)*. IEEE, 2015
99. H. Ye, et al., *Research on Location Privacy Protection Methods of Wireless Sensor Network in Smart Grid* (2015)
100. G.M. Paul, et al., A smart textile based facial EMG and EOG computer interface. *Sens. J. IEEE* **14**(2), 393–400 (2014)
101. M. Rezvani, et al., Secure data aggregation technique for wireless sensor networks in the presence of collusion attacks. *Dependable Secure Comput. IEEE Trans.* **12**(1), 98–110 (2015)
102. R. Roman, C. Fernandez-Gago, J. Lopez, H.H. Chen, Trust and reputation systems for wireless sensor networks, in *Security and Privacy in Mobile and Wireless Networking*, ed. by S. Gritzalis, T. Karygiannis, C. Skianis (Troubador Publishing Ltd, Leicester, 2009), pp. 105–128
103. M. Conti, *Secure Wireless Sensor Networks* (Springer, 2015)
104. S. Gonzalez, *Improving Time Synchronization Protocols in Wireless Sensor Networks* (Diss. Colorado School of Mines, 2016)
105. Y. Kadowaki, H. Ishii, Event-based distributed clock synchronization for wireless sensor networks. *Autom. Control IEEE Trans.* **60**(8), 2266–2271 (2015)
106. T.O. Ayodele, Introduction to machine learning, in *New Advances in Machine Learning* (InTech, Rijeka, Croatia, 2010)
107. M. Abu Alsheikh et al., Machine learning in wireless sensor networks: algorithms, strategies, and applications. *Commun. Surv. Tutorials IEEE* **16**(4), 1996–2018 (2014)
108. A.H. Duffy, The ‘what’ and ‘how’ of learning in design. *IEEE Expert* **12**(3), 71–76 (1997)
109. P. Langley, H.A. Simon, Applications of machine learning and rule induction. *Commun. ACM* **38**(11), 54–64 (1995)
110. Y.S. Abu-Mostafa, M. Magdon-Ismail, H.-T. Lin, *Learning From Data* (2012)
111. S. Suthaharan, et al., Labelled data collection for anomaly detection in wireless sensor networks, in *2010 Sixth International Conference on Intelligent Sensors, Sensor Networks and Information Processing (ISSNIP)*. IEEE, 2010
112. S. Rajasegarar, C. Leckie, M. Palaniswami, R. Beyah, J. McNair, C. Corbett, *Security in Ad-hoc and Sensor Networks* (World Scientific Publishing, Inc, 2009), pp. 231–260
113. G. Mao, (ed.), *Localization Algorithms and Strategies for Wireless Sensor Networks: Monitoring and Surveillance Techniques for Target Tracking: Monitoring and Surveillance Techniques for Target Tracking* (IGI Global, 2009)

114. G. Han et al., Localization algorithms of wireless sensor networks: a survey. *Telecommun. Syst.* **52**(4), 2419–2436 (2013)
115. H.M. Ammari, The art of wireless sensor networks, in *Fundamentals*, vol. 1 (Springer, 2013)
116. X. Yan, et al., An improved multihop-based localization algorithm for wireless sensor network using learning approach. *Comput. Electr. Eng.* **48**, 247–257 (2015)
117. D.A. Tran, T. Nguyen, Localization in wireless sensor networks based on support vector machines. *Parallel Distrib. Syst. IEEE Trans.* **19**(7), 981–994 (2008)
118. H. Martins, et al., A support vector machine based technique for online detection of outliers in transient time series, in *2015 10th Asian Control Conference (ASCC)*. IEEE, 2015
119. D. Wang, Y. Zhou, Distributed support vector machines: An overview, in *2012 24th Chinese Control and Decision Conference (CCDC)*. IEEE, (2012)
120. J.B. Predd, S.R. Kulkarni, H.V. Poor, Distributed learning in wireless sensor networks. *IEEE Signal Process. Mag.* **23**(4), 56–69 (2006)
121. K. Fluri, B. Beferull-Lozano, P. Tsakalides, Optimal gossip algorithm for distributed consensus SVM training in wireless sensor networks, in *Proceedings of 16th international Conference on Digital Signal Processing*, Santorini-Hellas (2009)
122. K. Wu, Y. Gao, F. Li, Y. Xiao, Lightweight deployment-aware scheduling for wireless sensor networks. *Mob. Netw. Appl.* **10**(6), 837–852 (2005)
123. M. Abu Alsheikh et al., Markov decision processes with applications in wireless sensor networks: A survey. *Commun. Surv. Tutorials IEEE* **17**(3), 1239–1267 (2015)
124. A. Kobbane, M. Koulali, H. Tembine, M. Koutbi, J. Ben-Othman, Dynamic power control with energy constraint for multimedia wire-less sensor networks, in *Proceedings of IEEE International Conference on Communications*, pp. 518–522 (2012)
125. K. Etessami, M. Kwiatkowska, M. Y. Vardi, M. Yannakakis, Multi-objective model checking of Markov decision processes, in *Tools and Algorithms for the Construction and Analysis of Systems* (Springer, Berlin, 2007), pp. 50–65
126. M. Di Francesco, S.K. Das, G. Anastasi, Data collection in wireless sensor networks with mobile elements: a survey. *ACM Trans. Sens. Netw.* **8**(1), 7 (2011)
127. S. Rashid, U. Akram, S.A. Khan, WML: wireless sensor network based machine learning for leakage detection and size estimation. *Procedia Comput. Sci.* **63**, 171–176 (2015)
128. R. Daniel, K. Nageswara Rao, An optimal power conservation cluster based routing algorithm using Fuzzy Verdict Mechanism for Wireless Sensor Networks, in *2015 International Conference on Electrical, Electronics, Signals, Communication and Optimization (EESCO)*. IEEE, 2015

Smart Clothes for Rehabilitation Context: Technical and Technological Issues

Gabriela Postolache, Helder Carvalho, André Catarino
and Octavian Adrian Postolache

Abstract Smart clothes have the potential to improve rehabilitation processes by allowing clinicians to gather measures on patients' functional capacity, activity level, exercise compliance, the effectiveness of treatment, and the ability of patients to perform efficiently specific motor tasks at rehabilitation centers, at home or in community settings. The chapter provides an overview of smart clothing for health monitoring and healthcare, mainly for rehabilitation context. We present recent advances in the field of researches related smart clothes with capability of human body vital functions (i.e. heart beats, respiration) and activity monitoring, as well as several commercial smart clothes for rehabilitation context. Technical and technological issues related smart clothes design and development, and several directions for future research are also presented. Manufacturability, connectivity, integrations of things for smart clothing, durability, testing, wearability, maintainability and affordability of smart clothes are discussed.

1 Introduction

"It can feel your heartbeat ... look..." Sure enough there was a big red spot on the plastic shirt just over her heart, a spot that spread out into an expanding ring that moved on over her shoulders and down to her sleeves. Her heart beat again, and a new spot started - each beat of her heart started a new red splash in the blue heartshirt.

Source: Wetware, by Rudy Rucker, 1988.

G. Postolache (✉)

Instituto de Medicina Molecular, Universidade de Lisboa, Lisbon, Portugal

H. Carvalho · A. Catarino

Departamento de Engenharia Têxtil, Universidade de Minho, Guimarães, Portugal

O.A. Postolache (✉)

Instituto de Telecomunicações and ISCTE-IUL, Lisbon, Portugal

e-mail: opostolache@lx.it.pt

© Springer International Publishing AG 2017

O.A. Postolache et al. (eds.), *Sensors for Everyday Life*, Smart Sensors,
Measurement and Instrumentation 22, DOI 10.1007/978-3-319-47319-2_10

In 2010 Vivian Jang and Nick Lee from Cornell University designed and built a LED T-shirt [1] capable of displaying the heart rate of the wearer via a pulsing LED heart (see Fig. 1). The imagined T-shirt by the writer Rudy Rucker in his science fiction novel *Wetware*, published in 1988, is turned real. The photoplethysmography (PPG) technique (that recorded light absorption by a finger or ear lobe) and a technique proposed by Charlie Allen in early 1995 (at Maxim Integrated) for driving a multiplexed display (in which a microcontroller, with few I/O, was wired into T-shirt). The microcontroller was used for heart rate processing and driving of an LEDs' array. Heart beat signal is displayed in this T-shirt by a LEDs array producing a propagating effect. At that time, T-shirts that integrate technology for recording electrocardiogram (ECG) or plethysmogram were developed in several research projects, and also were commercialized in some countries (see Figs. 2, 3, 4 and 5). This was possible as a result of progress in development of sensors technology, miniaturization and increase in processing and communication capability of



Fig. 1 T-shirt with pulsing LED related with wearer heart beat

Clothing+ - Smart T-Shirt, Finland, 1998	WEALTHY EU Project, 2002-2005	Sensatex – Smart Shirt, U.S.A., 2003	SmartLife Technology – ECG Shirt, U.K., 2003	GEO View and FALKE KG - ECG-Shirt Germany, 2004	MagIC Smart Shirt, Italy, 2005
ECG T-Shirt, Sweden, 2007	Biodevice VitalJacket, Portugal, 2009	Philips Body Vest, Netherland, 2009	Nuubo – nECG, Spain, 2011	WearTech - GOW Smart T-Shirt, Spain, 2012	ECG Smart Shirt, U.S.A., 2014

Fig. 2 Smart T-shirt with capability of heart rate monitoring

Chronious, Smart Shirt, EU Project, Italy, 2012	Vivonoetics – LifeShirt, U.S.A., 2013	AiQ, BioMan Fabrics, Taiwan, 2013	OM Signal, Smart T-Shirt, Canada, 2014	Gymi, Smart T-Shirt, Australia, 2015
				

Fig. 3 Smart T-shirt with capability of heart rate, respiratory rate and activity recording








Bio-Shirt, Korea, 2006	Nuubo – UC3M, Spain, 2013	NTT Docomo – C3fit IN-pulse, Japan, 2014	Cityzen Sciences -Smoozi™, D Shirt™, France, 2014
			
Adidas - miCoach Training Shirt, Germany, 2014	Sensoria - T-shirt, U.S.A., 2016	Ralph Lauren - Polotech™, U.S.A., 2015	Samsung - Body Compass 2.0, Korea, 2016
			

Fig. 4 Smart T-shirt with capability of heart rate and activity recording

ECG, Respiration	HR, Activity	Respiration,	HR, Respiration, EMG, Activity	EMG, Activity
Biopac – BioNomadix BioShirt, U.S.A., 2016	Hexoskin, U.S.A., 2016		Swedish School of Textiles -High Tech Clothing, Sweden, 2008	Jabil Circuit – Peak +, Russia, 2015
				
				

Fig. 5 Smart T-shirt with capability of recording heart rate (HR), electrocardiography (ECG), respiration, electromyography (EMG)

wearable devices as well as increased awareness on the necessity of monitoring cardiac function for prevention, or better management of cardiovascular diseases—the main leading cause of mortality worldwide. Ageing population in many countries was also an important factor for development and use of wearable technology for fitness and clinical purposes.

In the last decades, demographic, social and economic changes as well as progress in *information and communication technologies* (ICT) have produced dramatic changes in healthcare provision. ICT promise: fast access to reliable information about illness and treatment options; attention to physical and environmental needs; participation in health care decision and service developments [2]. Technologies that allow health monitoring at home are now emerging as a distinct segment within the larger ICT market, forecasting the increase of consumers using home health technologies from 14.3 million worldwide in 2014 to 78.5 million by 2020 [3]. The terms *wearable technology*, *wearables*, *wearable device* or *wearable electronics* are used to refer to electronic technologies (i.e. ICT) that are worn as accessories or as clothes. The term *wearable technology* is sometimes used for implanted devices such as micro-chip or even smart tattoos. In the last decades a wealth of research was carried out in order to design and develop wearable systems with capability to automatically recognize the activity and the behavioral status of the user as well as of the situation around her/him, and to use this information to adjust the systems' configuration and functionality. Wearable technology includes some form of data acquisition and processing as well as communication capability. Examples of wearable devices are smart watches, glasses with image recording or data display capability or for recording eye movements, wearable strap for recording heart rate or respiratory rate, smart T-shirt, smart shoes. According to the International Data Corporation (IDC) report published in 2015 on the wearable devices market, total shipment volume for the quarter came to 18.1 million units, up 223.2 % from the 5.6 million units shipped in previous year [4]. IDC also projects this market to reach 155.4 million annual shipments by 2019, up from about 26.4 million last year. Rapid advances in ICT, increased the access to Internet for millions of peoples (82.1 % of European and 60 % American population has now Internet access at home). During the last years the increased development of mobile technologies, and increased access to mobile technologies (approximately 80 % of Europeans and Americans have active mobile broadband subscriptions) [5] have contributed to the fast growing wearable-tech market after 2014, faster than any other segment in the consumer-electronics market. Most of wearable devices are sold for fitness, entertainment and gaming purposes. However, wearable devices are nowadays viewed as important technology to promote preventive healthcare, patient engagement in healthcare and to achieve tailored treatment, better healthcare outcome and cost effective use of health services. Wearable devices can be divided into two categories:

1. garments (i.e. clothes) with embedded sensors and/or computation capability
2. body worn electronic accessories.

Because the humans prefer to wear textiles rather than “hard” or “heavy” “boxes”, most research on wearable products is related with e-textile and smart clothing. Generally, *smart clothes* are defined as clothes made or that include *e-textile* (electronic textile). E-textiles are textiles that include electronic components making these able to sense, communicate, compute and actuate. *Smart textiles* are defined as textile products such as fibers and filaments, yarns together with woven, knitted or non-woven structures, which can interact with the environment/user [6]. Also, the term is used when is referring to neat textile (free from dirt), clothes that fit well or is stylish. Many smart textiles with different functionality and behavior were created in the last decades by combining flexible materials—having different properties (i.e. conductivity, sensing volume change)—with computing structures. Its may be categorized into three subgroups be categorized into three subgroups [6]:

1. Passive smart textiles: only able to sense the environment/user, based on sensors;
2. Active smart textiles: reactive sensing to stimuli from the environment, integrating an actuator function and a sensing device;
3. Very smart textiles: able to sense, react and adapt their behavior to the given circumstances.

Big investment in research projects related to e-textile fabric and smart clothing for different healthcare needs have made possible the development of several commercial products based on e-textile. Great influence of these products on health monitoring and healthcare services is envisioned. Progress in smart clothes research made possible integration from a few isolated sensing and computing elements on the fabric (i.e. plethysmography based recording of heart rate) to a network of many sensing, actuating and computing elements distributed over the entire textile (i.e. Antelope, Vibe-ing smart clothes, Fig. 8) [7, 8]. Being close to the body, smart clothes might enable: monitoring of our activities or health; human-computer interaction; computer based context awareness. Smart clothes can provide biometric data inconspicuously and without intrusion to the user or healthcare service provider. Also, it is envisioned that they would possibly be the best support for people in rehabilitation process, by enabling improved sensing, in addition to actuation, both embedded in garments that might be worn at rehabilitations centers (for gathering information suitable to adjust the intensity and modality of the prescribed therapeutic exercises), as well as in—or outside home, during daily activities or therapeutic intervention.

This chapter provides an overview of smart clothing for health monitoring and healthcare, mainly for rehabilitation context. We present recent advances in the field of smart clothes with capability of vital signs and activity monitoring, as well as several commercial smart clothes for rehabilitation context (Sect. 2). Technical and technology issues related smart clothes design and development are discussed in Sect. 3. In this section, several directions for future research are also presented.

2 Smart Clothes for Rehabilitation

Various smart clothes were developed in the last years, worldwide, with potential on improving rehabilitation processes by allowing clinicians to gather measures on patients' functional capacity, activity level and exercise compliance, the effectiveness of treatment, and the ability of patients to perform efficiently specific motor tasks at rehabilitation centers, at home and in community settings. Available unobtrusive sensors based on e-textile allow clinical personnel to monitor patients' movements and physiological data such as heart rate, respiratory rate, etc. Sensors based on e-textile, mobile technology (i.e. smartphone, tablets) and the widespread access to Internet provide nowadays means to implement systems designed to remotely monitor patients' status and optimize interventions based on individual responses to different rehabilitation approaches.

The motor rehabilitation process is guided by clinical assessments of motor abilities, which are expected to improve over time in response to rehabilitation interventions. Assessing the impact of rehabilitation interventions on the individuals is a key element of the decision-making process for choosing rehabilitation strategy and for improving outcomes of rehabilitation process. In the past, therapists and physicians inferred the effectiveness of a given rehabilitation approach from observations performed in a clinical setting and self-reports by patients. Recent developments in wearable technology, particularly in smart clothing provide tools to complement the information gathered by health professionals. Smart clothes may contribute to functional ability assessment in the real life of patients receiving rehabilitation. Data gathered in the home and community settings are very useful to quantify impact of therapeutic on the performance of activities of daily living and quality of life, and to compare different rehabilitation intervention. It is envisioned that such data would allow health professionals to help patients achieve higher level of independence and better quality of life. Following some examples of smart clothes and their current or potential role in rehabilitation are presented.

2.1 *Vital Signs Monitoring*

Smart textiles were introduced in early 1990s. The first T-shirt with capacity of recording heart rate was presented in 1998, by Clothing+ (Clothing plus) company from Finland [9], and in 2002 the company started mass producing their heart rate sensor strap in their factory in China. Soon after, SmartLife Technology from U.K. [10], Sensatex from U.S.A [11] and GEO View and FALKE KG [12] (Fig. 2) began marketing their heart rate sensing T-shirt. A research team at Georgia Institute of Technology had an important role in pioneer work related to development of smart clothing. Funded initially in 1996 by the U.S Department of the Navy, the Georgia Tech Wearable Motherboard uses optical fibers to detect bullet wounds and special sensors and interconnects to monitor the body's vital signs

during combat conditions [13]. The Sensatex Smart Shirt is based on patented technology of Wearable Motherboard. This patent describes a T-shirt which incorporates optical fibers, a data bus, a microphone, various sensors (i.e. for heart rate, respiration rate, electrocardiogram, temperature, pulse oximetry), and a multifunction processor, all embedded in textile grid. The garment aimed to rescue soldiers by monitoring their health status in real time. The motherboard or “plug and play” concept means other sensors might be easily integrated into the structure. The sensors might be easily plugged and positioned on any location into Wearable Motherboard. The flexible bus integrated into the structure routes the information from the sensors to a smart shirt controller that is plugged into the shirt.

The controller can wirelessly transmit the monitored data to the desired display device (i.e. personal computer) via communication protocol (i.e. Bluetooth). The bus has also the role of transmitting information to the sensors. In Sensatex Smart Shirt that monitors heart rate, body temperature and motion of the trunk, data are transmitted to a pager-size device attached to the waist part of the shirt, from where it is sent via a wireless gateway to the Internet and routed to a data server where the data is processed. As the research progressed chips and processors were designed and developed to be plugged into Wearable Motherboard turning this into versatile framework for incorporation of sensing, monitoring, and information processing, to obtain the desired information. Several generations of the woven and knitted versions of the Wearable Motherboard have been produced. Following this pioneer work realized by the research team at Georgia Institute of Technology [14] several companies and research groups from U.S.A. pursued the development of garments with embedded sensors—i.e. the smart T-shirts developed by VivoMetrics (nowadays Vivonoetics) [15], Sensoria [16], Ralph Lauren [17], TruPosture [18], Athos [19], Hexoskin [20] (Figs. 3, 4, 5 and 6).













MEMSwear, Singapore, 2004	Kinesthetic System, Italy, 2004	Myontec – Mshorts, Finland, 2005	MIT wearable garment, U.S.A., 2005	ETH Zurich - Smash shirt, Switzerland, 2008	5DT Glove, U.S.A., 2011
					
Ohmatex and Danfoss PolyPower, Denmark, 2014	Sensoria – Smart Socks, U.S.A., 2015	Xenoma e-Skin, Japan, 2015	Lumo - Lumo Runs capri and shorts, U.S.A., 2015	BendCo – ElectricFoxyMove, U.S.A., 2015	TruPosture - Smart Shirt, U.S.A., 2016
					

Fig. 6 Smart T-shirt with capability of recording body motion

In Europe, EU funded research projects WEALTHY (Wearable Health Care System, 2002–2005), MYHEART (Fighting Cardio-Vascular Diseases by Preventive Lifestyle and Early Diagnosis, 2004–2007), MERMOTH (Medical Remote Monitoring of Clothes, 2003–2006), BIOTEX (Bio-Sensing Textiles to Support Health Management, 2006–2008), PROeTEX (PROtection e-TEXTile: Micro-Nanostructured fibre systems for Emergency-Disaster Wear, 2006–2010), CONTEX (Contact Less Sensors for Body Monitoring Incorporated in Textiles, 2006–2008), OFSETH (Optical Fibre Sensors Embedded into technical Textile for Healthcare, 2006–2009), STELLA (Stretchable Electronics for Large Area Applications, 2006–2010) contribute for development of smart T-shirts able to record body temperature, ECG signals, blood pressure, breath frequencies, acceleration for fall detection. The focus was on patients receiving cardiac rehabilitation and elderly people and the aim was development of a system that allow continuous monitoring of subject health, real-time alert on emergency event, telemedicine, telehealth, or telerehabilitation. Telerehabilitation (delivery of the rehabilitation services over telecommunications network or internet, also named e-rehabilitation) —has the potential to facilitate extending therapy and assessment capabilities beyond what can be achieved in a clinical setting. The information on EU funded project is in public domain (http://cordis.europa.eu/home_en.html).

The present commercial smart T-shirt developed in Europe is miCoach from Adidas [21] (Fig. 4). The T-shirt includes technology developed by Textronics company that is incorporated in the Adidas group as Adidas Wearable Sports. The company is specialized in wearable electronics and textile sensors with a certain focus on sports performance. Textronics T-shirt is based on four groups of components. The first is the textile sensors used to monitor heart or breathing rate. The second is a family of conductive elastic yarns, which are building blocks in sensors and interconnects. These sensors consist of conductive nano-composite elastomeric polymers that exhibit changes in electrical conductivity as the material is stretched. The last group of components is conductive ribbon that is attached to standard electronic connectors. MiCoach T-shirt that record heart beat, steps and position of body (through GPS) is mainly used for fitness purpose. However, it might be used in cardiac rehabilitation, for objective measurement of walking and impact of exercises on heart rate. Several other T-shirts commercially available nowadays may be used for activity monitoring in cardiac rehabilitation context (Figs. 2, 3, 4 and 5).

Work realized by a team from Harvard University [22] since 2003, proved that measurement of cumulative free-living physical activity with wearable technology in the patient's home environment, combined with physiological data collection (heart rate, respiratory rate, and oxygen saturation), can improve monitoring of patients with chronic obstructive pulmonary disease (COPD) and therapy outcomes. A smart wearable platform based on multi-parametric sensors data processing, for monitoring people suffering from Chronic Obstructive Pulmonary Disease (COPD) was developed in a European funded project—CHRONIOUS (2008–2012) (Fig. 3). The system is able to constantly monitor patients' health condition,

through sensors integrated in a T-shirt, or scattered in the living environment, and through ad hoc questionnaires on symptoms and lifestyle displayed on a smart device (touch screen PC or smart phone). The system generates alerts when health and behavior data lay outside the established patterns. A multi-parametric expert system was developed for the analysis of the collected data using intelligent algorithms and complex techniques. Collected data and alarms are used to notify the healthcare providers through a dedicated and secure web platform. The integrated platform provides real-time patient monitoring and supervision, both indoors and outdoors and represents a generic platform for the management of various chronic diseases. In addition, an ontological information retrieval system is being delivered satisfying the necessities for up-to-date clinical information. These works have great relevance for healthcare systems as COPD is a major public health problem in many countries and is currently the fourth leading cause of death in the world [23]. The CHRONIOUS platform was validated through clinical trials in several medical centers and patient's home environments around Europe with 100 patients in two stages.

2.2 Activity Monitoring

Several smart clothes were developed for tracking the activities of the user by using heart rate sensing textile (Fig. 4), electromyography sensing textile (Fig. 5) as well as textile-based sensors for monitoring deformation along textile, positions, **angles**, velocities and accelerations of body segments or **joints** during motion. Such smart clothes might be used for rehabilitation monitoring and training of movements. Following several techniques and technologies based on e-textile for activity monitoring are presented.

Many of smart T-shirt estimate activities of the user by analyzing **heart rate** signal (Figs. 4 and 5). For instance, Hexoskin app estimate resting condition (the lowest number of heart beats per minute when user wake up), maximum effort that the person can do—maximum heart rate (the highest heart rate that the person achieves during exercise), heart rate recovery (the difference between heart rate values at peak intensity exercise and after 60 s without exercising). The app also is able to estimate heart rate variability (time domain heart rate variability statistics). The app uses this data to inform user on training fatigue to avoid overtraining. Most of these measurements are not conforming to measurements established through evidence from physiology and clinical studies. Moreover, most of commercial fitness T-shirts that include electronics acquire heart beats signal at lower sampling frequency than the medical devices (thus reducing their capacity to accurately estimate clinical conditions). Therefore, for adoption of these smart T-shirts in rehabilitation context the characteristics of hardware and software should be comprehensively analyzed as well as validation studies of these smart clothes in clinical settings should be carried out.

Myontec [24] have developed and commercialized, since 2005, the MBody (Fig. 6) a e-textile based pants with capability of monitoring **electromyography** (EMG). Myontec is a company producing system for the monitoring physical performance and capacity of the muscles. The company portfolio consists of a system based on trousers and shirts integrated with sensors and different modules for the measurement and handling of measured data. The trousers are recording the big muscles such as quadriceps, hamstrings, gastrocnemius and gluteus. The Harry Asada team [25] at Massachusetts Institute of Technology (MIT) developed pants (Fig. 6) with conductive fibers incorporated into the fabric to measure lower body movements. The Athos [19] (Fig. 5) claim monitoring of muscle activity through stretch and electromyography sensors integrated in pants and T-shirt. In 2008 the Karlsson team [26] present a smart T-shirt with capability of recording heart rate, respiratory rate as well as muscle activity through electromyography (i.e. trapezius muscle), as result of many years of research developed in Swedish School in collaboration with Umea University Hospital, MedTech West and Chalmers University. Athos and Jabil Circuit company [27] (Figs. 5 and 6) commercialize nowadays sports suits with capability of recording muscle activity through electromyography. Reliability of EMG measurements with these two smart clothes should be analyzed. Also, clinical trials may give valuable information on the effectiveness of these garments in rehabilitation context.

Electrocardiography (ECG) and electromyography systems based on e-textiles were developed by our team [28, 29]. In Fig. 7 some example of the signals obtained with the developed system based on ECG and EMG integrating e-textile is presented. The shirt integrating ECG and EMG electrodes was developed as part of information system for physiotherapy [29]. ECG signal is used to infer on health and activities of patients during physiotherapy sessions in clinics or remotely monitoring of patients in rehabilitation. EMG electrodes integrated in shirtsleeve are used for monitoring muscle activity during flexion, pronation-supination of the upper limbs in motor rehabilitation.

Shape-sensitive fabrics can sense movement, and can be combined with EMG sensing to derive muscle fitness [30]. By measuring the **deformation along**

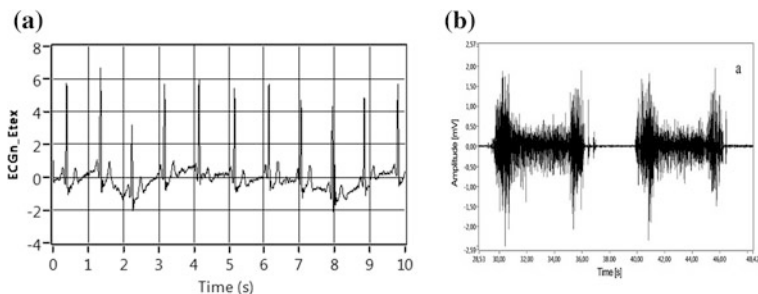


Fig. 7 ECG and EMG signals acquired with textile electrode. **a** Electrocardiogram **b** electromyogram from bicipital muscle

e-textile sensors the physical configuration of the user's body can be detected and information on body posture, balance and movements might be extracted (i.e. Xenoma e-Skin [31], TruPosture [18], Kinesthetic System [32], Fig. 6). In their pioneer work, the de Rossi group at University of Pisa [32] developed a Kinesthetic System that includes: skin like tactile sensors for fine-form discrimination and for incipient object slippage detection; and electroactive polymer based actuators, for producing flexion and extension in an active glove. Many, approaches of sensorized gloves are described in various websites. This type of gloves might be very useful in upper limb motor rehabilitation. The feasibility of using a sensorized glove to implement physiotherapy for motor retraining based on the use of video games was investigated [22]. In the study from Harvard University [22], the glove was used to implement grasp and release of objects in the video games. Processing data gathered from the data glove was used for a measure of "hand aperture" and estimating it. Calibration of the data glove was achieved by asking individuals to hold a wooden cone-shaped object with diameter ranging from 1 cm to 11.8 cm at different points of the cone corresponding to a known diameter. The output of the sensors on the glove was used to estimate the diameter of the section of the cone-shaped object corresponding to the position of the middle finger. Gloves developed by 5DT (Fifth Dimension Technologies Virtual Reality for Real World!) [33] (Fig. 6) might be used in upper limb rehabilitation by using driver for hand animation as well as for interaction with serious games. The Wearable Computing Lab. of ETH Zurich developed a matrix with several **capacitive pressure sensors** for integration into a piece of clothing. Applying this matrix on different body areas, more details on movements or for the detection of physical state of the muscles might be obtained [30]. In 2008 the Harms team [34] from Wearable Computing Lab., ETH Zurich has also presented a T-shirt with distributed sensing and processing architecture for posture classification. The group has been active in different EU-project, but has also carried out research on national levels. A SMASH (SMARt SHirt) integrates **acceleration sensors**. The classification performance was analyzed on data from overall 8 users, conducting 12 posture types, relevant for shoulder and elbow joint rehabilitation [34]. Body movements analysis based on integrated accelerometer into T-shirt (i.e. Nuubo Wearable Medical Technologies UC3 M [35], Fig. 4) or capri and shorts (i.e. Lumo Run Data [36], Fig. 6) was also presented.

2.3 *Smart Clothes for Physiotherapy*

Many wearable devices have been turned in valuable tools in physiotherapy interventions. In our knowledge clothes based on e-textile currently are not yet being used in physiotherapy practice. However, several smart clothes that are nowadays commercialized may be used in physiotherapy.

One example—the clothes based on e-textiles that record electromyography, might be used in neuromuscular reeducation (i.e. to assist patients in improving the

strength and voluntary control of muscle that are weak, unreliable and poorly controlled as a result of a stroke). Evidence from a small number of studies suggest that EMG *biofeedback* plus standard physiotherapy produces improvements in motor power, functional recovery and gait quality when compared to standard physiotherapy alone [37]. Smart clothes with EMG recording capability may contribute for clarifying the level of evidence on EMG biofeedback, allowing large data collection using the same and objective outcome measurements.

Smart clothes with capability on monitoring gait (i.e. including accelerometers, textile-based stretch or pressure sensors) as well as those providing biofeedback on gait or auditive, vibrotactile or visual cues may also benefit patients with Parkinson’s disease [38, 39].

EMS (Electrical muscle stimulation) devices are frequently used in physiotherapy practice. *Electrical muscle stimulation*, also known as *neuromuscular electrical stimulation* (NMES) or *electromyostimulation* use electric impulses to induce contraction of muscles. EMS has received increasing attention in the last few years because of its potential to serve as a strength training tool for healthy subjects or as a rehabilitation [40] and preventive tool for partially or totally immobilized patients.

Generally, the impulses are generated by a device and delivered through electrodes on the skin in direct proximity to the muscles to be stimulated. Antelope [7] suit (Fig. 8) commercialized by Wearable Life Science from Germany is based on the embedded EMS technology into a sport suit. The suit might be a valuable tool if would be adapted for patients receiving motor rehabilitation.

Smart clothes produced by WARMx [41] from Germany and COOLSHIRT SYSTEMS [42] from U.S.A. are other examples of clothes that might influence the way in which physiotherapy is provided. In physiotherapy practice *thermotherapy* (that consists of application of heat or cold for the purpose of changing the cutaneous, intra-articular and core temperature of soft tissue) is also frequently used with the intention of improving the symptoms of certain conditions. Cold therapy are useful adjuncts for the treatment of musculoskeletal injuries and soft tissue injuries. Using ice or heat as a therapeutic intervention decreases pain in joint and muscle as well as soft tissues. Also, heat or cold is used to change tissue metabolism, blood flow, inflammation, edema and connective tissue extensibility. Thermotherapy can be used in rehabilitation facilities or at home. Heated knitted



Fig. 8 Smart clothes for therapy

system is produced by WARMx GmbH (Fig. 8). The company has an own worldwide-patented technology for heating textiles called WARMx-technology as well as “know how” and partners in both textiles and electronics. The WARMx-undershirt is the classic in WARMx collection. The textiles knitted with silver coated fibers were adapted also for trunk and neck areas, for shoulder/neck area, knees, feet, or around the kidneys. The heating textile is supplied with power from a controller located in the side pocket, which closes the power circuit via pushbuttons. Li-ION batteries supply the power. Smart clothes for rehabilitation context may be developed also by including the technology by Thermotron of UNITIKA [43] (Japan). Thermotron is a particular fabric able to convert sun light into thermal energy while storing heat without wasting it. The inner layer of the fabric withholds the heat generated and prevents it from becoming lost. Inside the Thermotron there are microparticles of zirconium carbide which allow the fabric to absorb and filter sunlight. [43]. Clothes that function as cooling system were developed by COOLSHIRT SYSTEMS (Fig. 8). The company provides personal cooling systems for surgeons, race car drivers, football players, fire and emergency services, military and industrial workers. The invention that launched COOLSHIRT was a cooling vest for surgeons to use in the operating room. COOLSHIRT 6 Person Rehab Station—that incorporates a water port panel that allows for up to 6 connections, 6 Active Aqua Vests (sizes S-XXXL) and twelve 12' safety pull hoses—may allow cold therapy for 6 persons at the same time.

E-Textile are also developed and used for *vibration training*, also known as *vibration therapy*, *biomechanical stimulation* (BMS), and *biomechanical oscillation* (BMO), a training method that employ low amplitude, low frequency mechanical stimulation to exercise musculoskeletal structures for the improvement of muscle strength, power, and flexibility. Vibration training has been advocated as a therapeutic method in the treatment of osteoporosis, metabolic syndrome, stroke, neurodegenerative diseases (i.e. Parkinson) and is used in the fitness industry, professional sports, beauty and wellness applications [44]. Vibe-ing garment (Fig. 8) developed by partners from Eindhoven University of Technology, Mechatronics Engineering, the TextielMuseum, TextielLab Tilburg, was designed to stimulate the body by the vibration elements [8]. The garment includes several types of knitted areas, each of them according to the need of the specific function, and a certain amount of in-knit pockets situated in a specific way. In the pockets are 3D printed castings with one flat side and one structured side, to invite moving direction and stimulate the touched area more intensively. Small motor chips are included in castings. CRISP motor and vibration actuators have different programmes on them depending on the specific person's need for rehabilitation and vibration stimulation. They can react to the touch of the person (or therapist) or according to a specific programme tuned to the specific user. Also, the garment is designed to be worn in four different manners, which allow more body areas to be stimulated by the vibration elements with the use of minimal electronic components possible.

Therefore, the progress in e-textile and smart clothes might have great influence on the way the rehabilitation will be provided in the future. Nowadays, not many

smart clothes products are adopted by people for health monitoring or healthcare. Moreover, not many smart clothes can be seen in the streets today and only a few are integrated in the ready to wear clothing segment or are affordable. Quality of the products, problem with connectivity and durability of the smart clothes, power consumption and problems related power supply for continuous functioning, have been identified as barriers for adoption of these products [45]. Low level of population knowledge (particularly of engineers or health professionals) on smart textile or smart clothes also might contribute for less use of these products. Low production rates and costs are other barriers as well as safety and health constraints. There are also critical issues concerning the real need for smart textiles and the ethical issues of being monitored [45].

3 Technical and Technological Issues

Following we present several technical and technological issues related smart clothing for rehabilitation context. Information on conductive textile, type of textile/fabric manufacturing, sensors based on textile, textile as antenna, textile as actuator, textile as computer interface, circuit board into textile are presented and discussed. As an important challenge described by engineers on smart clothing is related with management of power supply, we present solutions described in the last years for power supply in smart clothing, particularly related energy harvesting. Connectivity, integration of things (i.e. integration of sensors, computing circuits, power supply) in smart clothing, wearability, maintainability, as well as issues related to design for durability and affordability of smart clothes are also discussed.

3.1 Manufacturability

The design of smart clothing involves the explorations of materials, structures, and manufacturing technologies. Electronic components for smart clothing should be designed in a functional, robust, small, unobtrusive and inexpensive way. As clothes should be designed for production in large quantities over different sizes of bodies, the manufacturability of smart clothing requires extensive research and comprehensive understanding of processes. By their nature, wearable e-textiles have a more complex form, structure and stress factors that should be considered in comparison with their non wearable e-textile and common textiles.

3.1.1 Conductive Textile

The conductive textile should be made from materials that should be robust to weaving, washing, and wearing stresses, should allow transmitting signals at high

Table 1 Electrical properties of metal monofilaments fibers

Conductivity [Sm/mm^2]								
Ag 99.99 %	Cu/Ag	AgCu1	Cu	Ms/Ag	Ms ^a 70	Bronze	Steel 304	Steel 316 L
62.5	58.5	57.5	58.5	16.0	16.0	7.5	1.4	1.3

^aGerman Milbe denomination, where Ms is accompanied by a number stating the composition in %Cu with respect to a Zn complement to 100 %

frequency with sufficient signal integrity and should be insulated to prevent shorts. The company Sprint Metal (Germany) [46] defined metal fibers and wires according to their diameter. A fine wire has a diameter between 30 μm and 1.4 mm, while a metal fiber possesses a diameter of 2–40 μm [47]. The advantages of metal fibers are their strength, composition, biological inertness and ready availability in textile form at low costs [6]. Due to its inertness some fibers are less sensitive to washing or sweating. The metal fibers are heavier than most textile fibers making homogeneous blends difficult to produce [48]. Moreover, they cannot provide uniform heating and their brittleness can damage spinning machinery over time. As the wired are not only characterized by their resistance, but also by wave effects depending on the line geometries and the surrounding material, the geometric structures that are created in the textile fabrication processes should also be carefully considered [49]. Moreover, the textiles that are used for smart clothing have to be made of fine and elastic fibers so that they are comfortable and lightweight.

According to the material used, conductive textiles with different electrical properties were developed. The products range from copper (Cu) and silver-plated copper (Cu/Ag) filaments, brass (Ms) and silver-plated brass (Ms/Ag) filaments, aluminum (Al) filaments to copper-clad aluminum (CCA) filaments [50]. In Table 1 electrical properties for various metal monofilaments [50] fibers are presented. The desired properties of the textile/fabric should be considered in choosing conductive filaments. Depending on the raw material used and the e-textile structure, different impedance behaviors could be obtained. Using the ‘conductive thread’ approach, no additional step after manufacturing of the fabric is required to establish conductivity. The conductivity of these conductive threads lies in the range of 10–500 Ω/m [51].

3.1.2 Types of Textile/Fabric Manufacturing

The integration of conductive yarns in a structure is a complex process. Different ways exist to produce electrically conductive fabrics. E-textiles might be produced by embroidering, sewing, non-woven textile, knitting, weaving, making a spinning, braiding, coating/laminating, printing and chemical treatments (Fig. 9) [6].

It should always be ensured that the electrically conductive fabric is comfortable to wear or soft in touch rather than hard and rigid. Embroidery offers advantages over knitting or weaving [6]. The image from Fig. 9 related embroidery technique represents a textile antenna realized at Ohio State University by embroidery process with a geometrical accuracy of 0.1 mm [52]. Embroidery technique allows

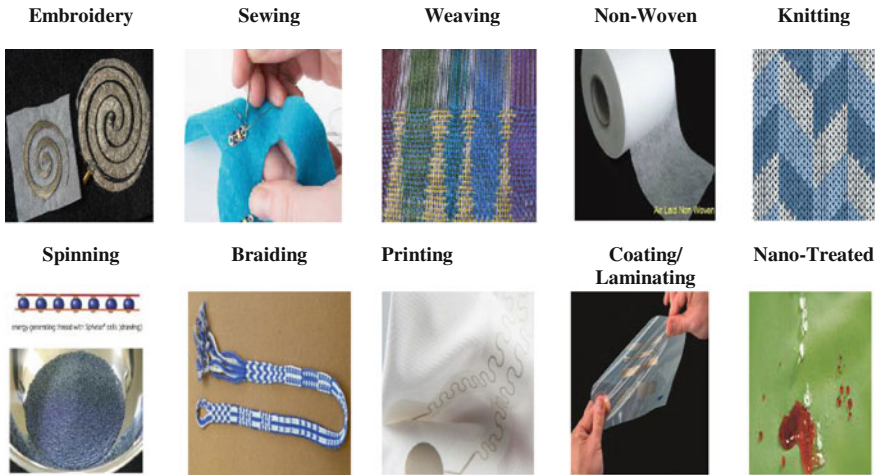


Fig. 9 Types of textile/fabric manufacturing

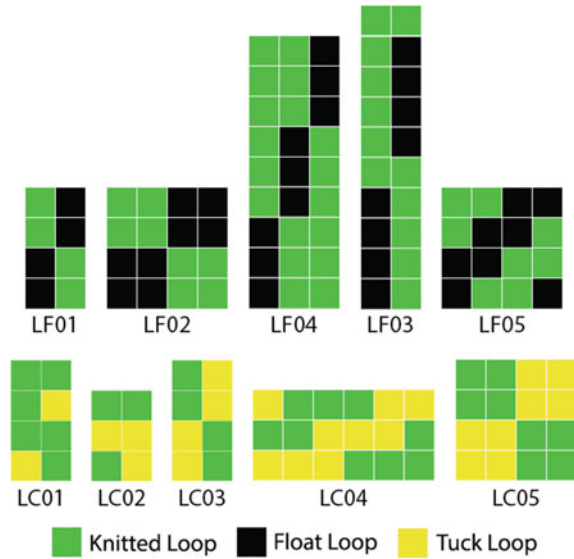
precisely specifying the circuit layout and stitching pattern in a computer-aided design (CAD) environment, from which any number of articles can be sewn under machine control. This process also allows control and integration of yarns with different electrical properties, for instance, different resistances. Conductive thread and yarn embroidery can be accomplished on single or multiple layers of fabric or can be applied on various types of textile and apparel products in one step [6]. The image from Fig. 9 related with spinning represents the production of thread by Spherical Power company [53] by alignment and connection of micro spherical solar cell. This thread is then used for textile-based energy harvesting. A group of researchers of Instituto Italiano di Tecnologia—Center for Space Human Robotics, Politecnico di Torino—Applied Science and Technology Department, in collaboration with a spin-off company, Politrónica Inkjet Printing (Italy), developed EMG sensor matrices by inkjet printing a silver nanoparticle-based ink on a polyimide flexible patch. Their results indicate good behavior and a base conductivity of 35 % with respect to traditional electrodes [6].

In Fig. 9 the image related with coating/laminating represents the stretchable material produced by DuPont Microcircuit Materials, Research Triangle Park, N.C., that was launched in 2014 [54]. The stretchable conductive inks and related materials produced by DuPont Microcircuit can be printed on a textile to produce smart active wear, health monitoring clothing and other smart textiles [54]. The silver-based conductive ink is applied to thin thermoplastic polyurethane (TPU) film that is then laminated onto the fabric. The company reports that the new materials provide a durable (the inks resist to repeated elongation and continue to show strong performance after 100 wash cycles), comfortable, flexible, cost-competitive, manufacturing-ready alternative to electronically conductive yarns, polymers and other materials. Nanotechnology contributes to development of

various textiles with great potential in development of smart clothes. Nano-treated textiles were developed with capability of self-cleaning, water repellent, anti-microbial function, fire retardation, etc. In Fig. 9 the image related with nano-treated textile represents one product developed by Swiss company—Schoeller [55]. By using 3XDRY technology the Schoeller produced a textile that on the outside is finished with water-repellent function whereas on the fabrics inside it absorbs perspiration.

Knitted electrodes for electrocardiography and electromyography [28, 29] were developed by our team. A study was conducted using several conductive raw materials, in the form of continuous filaments or staple yarns with the purpose of constructing single face weft-knitted structure and to investigate their electrical behavior. One of the key characteristics of weft knitted fabrics is their elasticity, very appreciated by the end user, which results in body fit and very comfortable pieces of garment. This kind of fabrics might be adequate to embed electrodes due to their capability to closely follow the human body and thus to provide an optimal contact between skin and electrode. Three distinct yarns were compared in our studies: Bekitex, which is a one-ply 80 % polyester/20 % stainless steel staple fiber yarn (Bekaert, Belgium [46]), Elitex silver coated polyamide multifilaments, with and without a core of bare elastane (Elitex, TITV-Greiz, Germany [56]) and Shieldex silver plated polyamide yarn (Statex, Germany [57]). Conductivity of the silver plated yarns is in the order of tens of Ω/m , whilst the much cheaper Bekitex yarn has a reference value for the resistance of 100 Ω/cm . A MERZ model MBS seamless jacquard knitting machine with a single needles system, located in the cylinder, was used. The disk is equipped with transferring jacks, knives and springs which allow a very flexible control of the yarn entry in the knitting zone. Being a jacquard machine, it is possible to obtain complex structures with localized variations, and to produce embedded electrodes. Different knitted structure were studied that may be categorized in two groups: (1) structures designed with knit and float loops and (2) structures designed with knit and tuck loops. A total of 40 structures were designed and divided into two groups of twenty, as stated above, according to the loops used [29]: (1) knit and float loops (LF's) and (2) knit and tuck loops (LC's) (Fig. 10). The design was done trying to produce smooth fabrics with the highest density technically possible. Using fabrics with smaller distances between conductive and non-conductive threads (that means between signal and ground line) would enable lower line impedance [49]. Materials with higher density have a better electrical conductivity and contact than the same material with a lower density [29]. Hence, the higher the structure's density, the better the performance is. Five structures of each of the groups were then produced in a Merz MBS circular knitting machine, with normal, non-conductive textile yarns. After fabricating the first samples, those that showed little mechanical strength or other technical problems from the textile point of view were replaced by new structures. The procedure was repeated until ten adequate structures were obtained. The repetition module of the selected structures is given in Fig. 10, where the rows represent knitted courses and the columns the number of needles used in this module. After the ten knitted structures were finally selected, the electrodes started to be fabricated

Fig. 10 Selected knitted structures LF: Float loop based, LC: Tuck loop based structure



with Bekitex yarn. All electrodes have 34 courses by 56 columns, resulting in a 2 cm side square. A line of 16 courses for 85 columns was also designed along with the electrode to provide the electrical connection to the conditioning circuit. The silver coated yarn, with or without bare elastane and with minor differences between the different structures have proved to be better yarn for knitted textile electrodes than Bekitex yarn [29]. Electrodes produced with one of the loop types produced better results than the others, namely the tuck loop used in the LC structures. Electrical insulation, if necessary, is achieved by coating with specific silicone compounds (Elastosil[®] from Wacker [58]). Elastosil silicone has been found to have a high adhesion capability, high electric isolation and stretch when compared with similar materials. The electrode area protrudes from the rest of the fabric, improving contact between the skin and the electrode. Electrodes based on silver coated yarn have proved more adequate for integration in T-shirt presenting better wearability and conductive properties than other tested electrodes. Electrodes based on Bekitex yarn presented good electrical characteristics, however, the resulting fabric cannot be used being too abrasive and unpleasant when in contact with skin and it was not able to recover its rest dimensions after stretching.

3.1.3 Textile as Sensors

Conductive textiles that change their electrical properties as a result of the environmental impact can be used as sensors. Most important for motor rehabilitation are the **strain gauge sensors**. Textiles acting as strain gauge sensors were developed with the purpose of monitoring respiration rate as well as for detection and monitoring posture, position of body segments and body motion. Textiles able to

acquire bio-potential (i.e. electrocardiography signal, electromyography signals) and smart T-shirts able to monitor **temperature** were also developed. Textiles that **react to deformations** have been used as pressure sensors, stretch sensors or as breathing sensors. Textile for **accelerometry** was also developed and included in smart clothing.

The most important progress in textile sensors for health monitoring is in the area of **heart beats sensing**. In European funded project WEALTHY coordinated by team from Italy, two types of sensors were developed for the integration in garments. The first sensor was a lycra based fabric coated with carbon black and rubber, for breathing rate recording. The other sensor was metal yarns based for heart rate monitoring. All sensors were integrated in a garment knitting process. Together with the textile development a miniaturized short-range wireless system was developed in order to transfer biophysiological signals from the garment to a computer or a mobile phone. In MYHEART project, a continuation of the WEALTHY project, two types of e-textile were created. One was a woven fabric with insulated copper wires, using the linear dependency of wires temperature and their resistance as a temperature sensing e-textile. Other types of textile sensors developed in this European project were a pressure sensing matrix and sensors for heart rate and muscle activity recording. The aim of the project was to gain knowledge on health status of a large group of people by continuous monitoring vital signs using flexible and wearable systems. In the last decade different textile based on various fabric processes were developed aiming heart beats signal acquisition [59–62]. Different yarns as well as different knitting structures were used in order to acquire changes in volume in measured body part (plethysmography) or electrical potential produced by heart (electrocardiography). A textile based system was developed by Lanata team, from Pisa University, for the area of cardiac monitoring and cardiac rehabilitation [63]. The heart and respiratory function is acquired through a textile based piezoelectric sensor (plethysmography) as well as with ultrasound (US) transceiver. The multimodal broadband piezoelectric transducer is based on polyvinylidene fluoride polymer integrated into a textile belt that might be wrapped around the chest. The system includes advanced electronic control unit, floating power supply, and wireless communication support. The multimodal transducer works either as an ultrasound transceiver or piezoelectric sensor. The US transceiver is enabled to work at high frequency, i.e., it is excited by suitable pulses to emit an ultrasonic wave, which penetrates the body and receives the echo signals bouncing off the biological interfaces having different acoustic impedances. The piezoelectric sensor works at low frequency and acquires both signals generated by heart apex movements and the mechanical movement of the chest induced by respiration. The smart clothes based on the Lanata system, beside heart rate and respiratory rate detection may give rich information on the cardiac and respiratory functions in clinical context.

Fabrics incorporating thermocouples can be used for **sensing temperature** [64]. Textiles able to monitor body temperature were developed [61] and nowadays T-shirts monitoring temperature in addition to other vital or body motion signals are commercialized (i.e. Cityzen Sciences [65] Fig. 4). The information on temperature

has great relevance in clinical context and smart clothes integrating temperature sensor are important for health monitoring and healthcare services.

The Meyer team [30] developed a **capacitive pressure sensor** for integration into clothing that might be used in rehabilitation, pressure-sore prevention or muscle activities monitoring. The developed sensor has spatial resolution of 2 times 2 cm and an average error below 4 percent within the measurement range 0–10 N/cm². Applied on the upper arm the textile pressure sensor determines the deflection of the forearm between 0 and 135° due to the muscle bending.

In EU funded project MICROFLEX (2008–2012) micro fabrication production technologies for MEMS on textile fabrics was investigated. The processes used are based on thick film printing, inkjet printing and sacrificial etching for the MEMS. These printing processes have many benefits including low-cost, repeatability, flexibility, suitability for high throughput production, relatively inexpensive equipment, short development time and the capability of depositing a wide range of materials. This technology is promising as it contributes for textile **accelerometer** development with application on smart clothes that might monitor both body motion as well as vital signs (i.e. heart rate, respiratory rate) at a lower price, therefore increasing affordability of smart clothes for rehabilitation context.

3.1.4 Textile as Antenna

An antenna is essential, if the purpose is to develop a wearable and autonomous system. It allows one to transfer information from the sensors hosted inside the garment to a control unit, or to monitor other electronic parameters. A wearable antenna is thus the bond that integrates clothes into the communication system, making electronic devices less obtrusive [6]. Fabric-based antennas are a relatively simple application of smart fabrics. Simple textile antennas are merely conductive yarns of specific lengths that can be stitched or woven into non-conducting fabrics [66]. Rapid progress on the fabrication of conductive textiles has produced significant development of wearable antennas, exploiting new flexible and conformable smart structures [67]. To achieve good results, wearable antennas have to be thin, lightweight, low maintenance, robust, inexpensive and easily integrated in radio frequency (RF) circuits. Stoppa and Chiolerio [6] indicated as main requirements for a correct antenna in a smart clothes project:

1. choosing the correct positioning of the textile antenna;
2. the textile antenna must be made with an accurate thickness stacking the different fabrics;
3. the geometrical dimensions of the patch must remain stable;
4. the connections between the layers must not affect the electrical properties and the connections with other parts of e-garments have to be stable and robust.

Planar structures, flexible conductive and dielectric materials are specific requirements for wearable antennas [68, 69]. Lowering the dielectric constant

increases spatial waves and hence increases the impedance bandwidth of the antenna [70]. The moisture can affect the dielectric behavior of textiles. In particular, when water is absorbed by the fibers, an increase of the dielectric constant and loss tangent occurs. A textile cover or superficial treatment may then provide a sufficient protection from the humidity and varying climatic conditions [71]. Another issue related to textile antenna integrated in smart clothes regards the movement of the body that can deform the spatial geometry of the antenna and affect its performance. When the textile fabric adapts to the surface topology it bends and deforms, causing changes to its electromagnetic properties and thus influencing the antenna performance [72]. Thus, a wearable FM antenna should be designed so as to be wider than the FM broadcast band (about 81–130 MHz) not to suffer from the detuning caused by the human body [73]. Patria (Finland) is a company with expertise in textile antenna design. It develops textile antennas composed by conventional or industrial fabrics, and typically conductive antenna parts are made out of modern conductive fibers [74]. Textile RFID (Radio-Frequency Identification) is a particular solution of antenna. In this sector TexTrace AG (Switzerland) provides the manufacturing line as well as the components for industrial in-house production of woven RFID labels. Integrating RFID and the label will provide added value for garment manufacturing, logistics, sales and after-sales management [75]. Textiles based RFID integrated in smart clothes might greatly contribute to management of the data for patients receiving rehabilitation in healthcare information system.

3.1.5 Textile as Actuator

Actuators respond to a signal and cause effects such as a color change in a textile, release of substances, change of shape, vibrate and others. One example of textile acting as actuator with potential use in rehabilitation is the electroluminescence materials that are light emitting materials where an applied voltage is the source of excitation. Light emitting diodes convert electrical potential to light and are often used as actuators in smart textile applications [76]. These materials may be used for providing biofeedback [77] in motor rehabilitation.

3.1.6 Textile as Human-Computer Interface

Human-computer interfaces based on e-textile can be grouped into two categories: input devices and annunciation or display devices. Input devices can include capacitive patches that function as push buttons [78], or shape-sensitive fabrics [79] based on motion or flexing, pressure, stretching or compression sensors. Annunciation and display devices may include e-textile based speakers [80], electroluminescent yarns [81], or yarns that are processed to contain arrays of organic light emitting diodes (OLEDs) [82]. Shirt developed by Xenoma e-Skin [31] (Fig. 6) from Japan allows subject interaction with virtual reality. Gloves

developed by 5DT—DataGlove™ VRLOGIC with hand flexion sensors based on fiber optic allows to take input from user's hand gestures. Four wires were used for each finger or tube to build up a circuit. The voltages coming out are varying depending on the finger position [33]. Gloves versions with 5 or 14 sensors detect the wearer's hand movements and allow better working with 3D modeling and animation software. The drivers allow for the animation of hands as well as using the glove as a puppeteering tool.

3.1.7 Power Supply in Smart Clothes

The most common power sources in smart clothes are AA batteries or lithium batteries. Great importance in smart clothing is nowadays given on energy harvesting (scavenging) and conservation. Energy harvesting and distributed power management are essential in design and development of smart clothes. The generation of electrical power from body movements and wearing mechanical stresses [83–88] body heat [89, 90], or solar cells [53, 91–95] have been demonstrated.

For example, Infineon claim a technology that might recover energy by body movements to feed MP3 players integrated in a jacket using piezoelectric materials [83]. In the U.K. the University of Bolton has developed a novel technology that integrates piezoelectric polymer substrate and photovoltaic coating system to create a film or fiber structure that is capable of harvesting energy from nature, including sun, rain, wind, wave and tide [85, 86]. Georgia Tech researchers have made a flexible fiber coated with zinc oxide nanowires that can convert mechanical energy into electricity [87]. A technology based on gold-plated zinc oxide nanowires with potential to harvest energy from many kind of vibration or motion for generation of electric current was developed. Gold-plated zinc oxide nanowires, each about 3.5 μm tall, are grown on a flexible polymer fiber and these nanowires brush against untreated nanowires, which flex and generate current [88].

Distributed batteries, possibly fuel cells or filament-type batteries woven into the fabric have already been demonstrated [49]. Photovoltaic is the most advanced way of providing electricity far from any mains supply. Integration of flexible solar cells into clothing can provide power for portable electronic devices. However, it might suffer from the limits of ambient light intensity. Nevertheless the energy demand of portable devices is now low enough that clothing-integrated solar cells are able to power most mobile electronics [92]. The European funded project Dephotex (2008–2011) explored and developed photovoltaic cells, in order to get flexible photovoltaic textiles based on fibers that turn solar radiation into energy. The research was based on fibers with conductive properties as substrate for flexible photovoltaic textiles. Spelhar Power Corporation developed an energy-harvesting textile where spherical solar cells are interweaved [53]. The ILLUM jacket is based on technologies including printed electroluminescent ink and printed photovoltaic technology. The functional parts are placed outside the jacket and into several ergonomic places at the front, and the photovoltaic e-textile at the shoulders and top of the back [95].

Unlike low-power systems that have a centralized power source like batteries, energy harvesting elements are distributed across the fabric, giving each processor access to local power. Because the local power supplies will be depleted and recharged at different rates, the task assignment service should predict and balance remaining power across the textile. The power requirements of the system can be reduced by optimal management of active sensors and processing units [49] as well as selecting communication protocols and architecture [96]. A stochastic approach to communication-based design, integrating wireless networks-on-chip (WNoC), voltage frequency island (VFI), and dynamic voltage/frequency (V/F) tuning in a synergistic manner, was proposed to achieve significant energy savings without paying a noticeable performance penalty [96].

3.1.8 Circuit Board into Textile

In addition to behaviour like sensing, reacting on and conducting electricity, the textile will be able to perform computational operations [97]. Most integrated circuits are made of silicon because of the semiconductor properties of this substance. Researches on materials for organic electronics allow development of circuits suitable for wearable application. These materials are flexible, lightweight, strong and have a low production cost, however the electronic properties of the conducting polymers do not match those of silicon [98]. The P-FCB [6] is one of the new technologies allowing implementation of a circuit board on a plain fabric patch for wearable electronics applications. It features a soft and flexible impression just as normal clothes.

3.2 Connectivity

Smart clothes typically contain just enough onboard computing to gather data and transmit it over a network. Communications may be a low-powered wireless local area network (WLAN) connection to a gateway, or a high-powered connection to the Internet via mobile technologies, like smartphone or tablet. The implementation of a high-level application programming interface for communication requires that the routing service know the embedding of the e-textile in three-space, and low-power, fault-tolerant communication [49]. In the event of a tear in the fabric, single leads running to one collection point could lead to significant rather than graceful degradation in performance. The smart clothes require multiple points at which analog data is converted to digital data; these conversion units, likely in the microcontroller or digital signal processor class, would need to communicate within a fault-tolerant network [49, 96]. The networks with multiple sensors should be designed so that the whole network continues to function even if individual nodes fail, or lose connectivity, though data may be lost. Attaching the leads of every

sensor/actuator to a single processing unit and power supply increase risk for data lost and fail in data communication.

Sensors from clothes together with embedded data communication and computation in smart clothes ensure mobility, ubiquitous connectivity or cloud based clinical decision support. While robust analytics and algorithms run at information system based on smart clothes, alert condition along with annotated data may be real time reported to the health professional on his/her mobile device allowing decision on optimal strategy for rehabilitation in a timely manner. In conjunction with the availability of textile embedded computing, the necessity of textile-based interconnectivity has also emerged. Internet of Clothes (term related with Internet of Things) may increase the quality of user experience. Unique identifier for smart clothes combined with communication capability and online presence pave the way for Internet of Clothes.

3.3 *Integration of Things for Smart Clothing*

Intelligent/smart clothes are characterized by optimal design, development and integration into textile of different things (i.e. yarns, textile, sensor(s), microchip(s), keypad(s), display(s), power supply, communication and control structure(s)).

In many smart clothing the computation is made *offline* (that is, on a separate system, connected to the fabric itself) or *onto* the fabric (on controllers attached onto the fabric) [49]. Generally, the computation is done in silicon, but with the advances in nanotechnology, molecular or polymer based technology, the possibility exists of having computation embedded into fibers (computation *into* the fabric) [97]. Better power efficiency might be achieved when communication among processing elements is wired with conductive textile in comparison with wireless communication. However, as textiles have generally low manufacturing costs the defect rate of the processing nodes and physical links might be higher than in the case of wireless network [49]. When many processing elements are connected in a textile area network, acquisition, processing, storage and communication capabilities shall be considered together with power consumption. For example, in smart clothing that includes electromyography elements together with other body motion or vital signals components, many technological aspects are challenging in terms of textile fabric as well as signal acquisition and processing. Sampling frequency of at least 250 Hz is necessary for the clothes that record surface EMG. The majority of the body sensor networks manage gathered data at a sampling rate of a 1–100 Hz per channel. Moreover, when requirements of being lightweight, comfortable, and at low cost is added, developing smart clothes that monitor muscle activity through EMG with accuracy necessary for assessment of impairment in clinical condition, remain a complex work and yet with many technological issues to be solved in the future. In our approach, Bluetooth communication sensor modules (Shimmer3ExG) were used as part of a wearable solution for surface EMG and ECG monitoring using smart clothes for physiotherapy context [29]. The

Shimmer3ExG module provides a configurable digital front-end, optimized for the measurement of physiological signals, for example 5-lead ECG or 2-channel EMG. The measurement channels of each sensor module were connected to the electrodes with metallic snaps. Using a desktop or mobile application the sensor modules were configured in order to perform the signal acquisition with a maximum of 1024 samples. To improve the SNR a second-order Butterworth high-pass filter at 10 Hz was used, thus the constant presence of signal fluctuation and some motion artefacts were removed.

In terms of intelligence, the smart system will require a central processing unit [99] that will receive, store and evaluate data from the different sensors and decide action on the basis of the results. The processing unit is a complex structure of electronic circuitry that executes stored program instructions. Included in this structure are; integrated circuits, secondary storages, power supply and communications technologies [98]. For better protection of the electronics and to increase durability some electronic components might be encapsulated in a robust package. Detachable structures should provide easily recharging and data transfer. Redundancy for both computation and interconnects, as well as energy sources was proposed [49] to ensure reliable operation in the presence of harsh or regular wear-and-tear environments.

3.4 Durability

Making smart clothes durable dictates that the system should: tolerate faults both permanent and transient, that are inherent in the manufacture and clothes use; have protection against various type of stress; be repairable; and that the system functionality should gracefully decline as components fail. For example, as textile material has viscoelastic behavior, inner tensions decrease over time and the geometry may change (especially in washing treatments) [49]. Damage of the components by washing processes and daily use shall be considered. Most solutions known so far require removal of complex electronics before starting the cleaning process. Several solutions for reducing impact of washing processes on e-textile were presented in the last years: (i) easy separation of electronic most influenced by washes; (ii) developing e-textile resistant to many washing cycles (i.e. NTT DoCoMo [100] shirt from Japan); (iii) developing textile resistant to dirt and with self-cleaning properties [101–103]. For example, WARMx underwear allow easily separation of the accumulator battery from the item of clothing without a problem thanks to the pushbuttons. Exhaustive testing has also proved that the conductivity remains even after a very high number of WARMx underwear washes. Treating a textile with a thin coating of titanium dioxide particle which measure just 20 nm in diameters, turn the textile able of self-cleaning [102] when is exposed to light. The surface of the textile material when exposed to light breaks down the impurities such as dirt, pollutants, and micro-organisms that come in contact with the fabric into carbon dioxide and oxygen, making possible cleaning of clothes only with light

[101, 102]. Other method presented for development of textile with potential of self-cleaning is based on synthesis of photo-active fabrics of silver and copper nanoparticles [103]. The hierarchical superstructure of these functional fabrics facilitates the access of reactants and visible light to the catalytically active sites of a localized surface plasmon resonance (LSPR)-active nano-metals. This improves the efficiency of redox processes under visible light photoexcitation. Mechanistic investigations reveal that light can dramatically influence the electron transfer processes in Ag@Cotton and Cu@Cotton that are critical for efficient redox reactions. The results of this work will be helpful in designing new multifunctional fabrics with the ability to absorb visible light and thereby enhance light-activated catalytic processes.

Other important concern related with durability is the connection between the conductive fibers and electronic components. In smart clothes with a large number of sensors and actuators simply attaching the leads of every sensor/actuator to a single processing unit and power supply would not meet the design goal of a durable e-textile. Redundancy for computation, interconnects, energy source [49] and design of the whole network so it would continue to function even if individual nodes fail, or lose connectivity, was proposed to ensure reliable operation in the presence of harsh or regular wear-and-tear environments.

To ensure durability and sustainability of smart clothing the design should also consider the potential environmental impact of manufacturing and services through the whole life cycle from raw-material acquisition, the production processes leading to products, transport processes, the product's use phase and its end-of-life stage [104].

3.5 *Testing*

Testing is necessary during smart clothes manufacturing process as well as for certification as medical device, or validation of their effectiveness on rehabilitation context. Among requirements for certification of smart clothes for medical use, data shall be included related to specifications, methods of manufacture, method of sterilization, results of risk analysis, results of calculations and test reports, reference to applicable harmonized standards, evidence that the essential requirements have been met [105]. Suitable quality system should be implemented in all relevant stages to ensure product performance and safety.

Various techniques for testing electrical properties of different textile and to optimize the fabrics and the signal line configurations are currently used. Time domain reflectometry, that measure the signal reflections along the transmission line, might be used for impedance measurement of e-textile. The textile with metal only in X direction have lower capacitance and inductance and, therefore, provide faster signal propagation than the textile with metal in XY direction [49]. Frequency characterization of the textile might be realized by using a network analyzer, to investigate textile transmission lines and transmission properties. Testing of digital

transmission should consider the line length, number of line and crosstalk effects from neighboring lines. Based on frequency characterizations, conclusions on possible line lengths, resulting losses, and usable bandwidth might be extracted [49].

In our work [28, 29] samples of knitted textiles developed by our team with different sizes were submitted to electrical characterization. The parameters under study were the sensor's dimension and the structure.

As thermal comfort when wearing smart clothes in rehabilitation sessions has great relevance for patient as well as for health professionals (taking into account that many patients might have impaired thermoregulation function) we proposed the use of thermography to investigate the effect of developed e-textile on body temperature during relatively long physical effort [29].

Confirmation of conformity with the requirements concerning characteristics and performances under normal conditions of use of the smart clothes and the evaluation of the undesirable side-effects must be based on 'clinical data' [105]. Several guidelines were deployed for assessment of the effectiveness of the medical devices in therapeutic processes. For example, the methodology guidelines for testing effectiveness of physiotherapy interventions are defined in PEDro (the Physiotherapy Evidence Database) [106]. We also proposed a methodology of rating quality of evidence related devices for health monitoring and healthcare based on RE-AIM (Reach, Effectiveness, Adoption, Implementation and Maintenance) and GRADE (Grading of Recommendations Assessment, Development and Evaluation) guidelines [107].

3.6 Wearability

Smart clothing should be lightweight, breathable, comfortable, easy to clean, easy to wear and take off. The wearer needs a comfortable touch in case the e-textile gets into direct contact with the skin. The textiles that are used for clothing have to be made of fine and elastic fibers to be comfortable and lightweight (a low weight per unit area, not more than 300 g/m²) [6]. Especially for clothing, tactile properties such as smoothness stretch, recovery, drape, shear and handle are quite important. These demands are inconsistent with the materials and geometries that are needed for a reasonable electrical conductivity, because the incorporation of elements such as metal fibers within textiles increases stiffness and reduces elasticity. However, in the last years various fibers, yarns, textile with conductive properties with high level of wearability were produced. Smooth surfaces are, in principle, more comfortable. They increase heat flow and the area of contact, which not only improves electrical conductivity, but also creates a cooler feeling [29]. However, they slide more easily over the skin, being thus more difficult to stabilize. These aspects are quite relevant in garments that are to be worn in sports, or in smart clothes that required fixed position of the sensors or electronic components necessary for communication and position detection. Moreover, it should be better that the design of smart clothes follows the principle of universal design. Universal design is a term coined by

R.L. Mace in [108], to describe the concept of designing all products and the built environment to be aesthetic and usable to the greatest extent possible by everyone, regardless of their age, ability, or status in life. Similar to ‘design for all’, rather than designing for certain disabilities, the approach aims to create a design solution that works for everybody, whether disabled or not. Universal design aims to make products usable in the broadest range of situations, whether the user is permanently disabled or not. The seven principles of universal design [108] can help with that.

Principle 1: Equitable use—The design is useful and marketable to people with diverse abilities.

Principle 2: Flexibility in Use—The design accommodates a wide range of individual preferences and abilities.

Principle 3: Simple and Intuitive Use—Use of the design is easy to understand, regardless of the users experience, knowledge, language skills, or current concentration level.

Principle 4: Perceptible Information—The design communication necessary information effectively to the users, regardless of ambient conditions or the user’s sensory abilities.

Principles 5: Tolerance for Error—The design minimizes hazards and the adverse consequences of accidental or unintended actions.

Principle 6: Low Physical Effort—the design can be used efficiently and comfortably and with a minimum of fatigue.

Principle 7: Size and Space for Approach and Use—appropriate size and space is provided for approach, reach, manipulation, and use regardless of user’s body size, posture, or mobility.

3.7 Maintainability

Maintainability is an important issue when wearable devices are deployed for health or healthcare purposes. Smart clothing should be designed and developed for easily cleaning, drying and repairing.

3.8 Affordability

Higher accessibility to rehabilitation services, convenience of home healthcare, enhanced and optimized care, reducing the needs for in clinic visits may increase affordability of smart clothes for patients in rehabilitation process. Wearable devices, particularly smart clothes may improve diagnostic and ensure time-sensitive intervention, increase patient participation and empowerment. Smart clothes can also create better conditions for patient rehabilitation interventions in the comfort of their homes. The patient receives the exercise and mobility

instructions from the health professionals (i.e. physician, physiotherapist, occupational therapist) and follows these instructions. The smart clothes record patient activity and transmit the data to the care provider in real time. After the analysis of the transmitted data, if it appears that the patient is deviating from the instructions, the therapist can initiate the corrections remotely and ensure that the prescribed treatment is followed accurately. These not only saves time and energy of the individuals in rehabilitation contexts, increase quality of care, reduce the need for in clinic visits, but also reduces the burden of the healthcare resources to a large extent. However, clinical staff as well as patients should be sufficiently trained on these technologies to make the best use of wearable system.

Low cost smart clothes with capacity for hardware and software upgrade as well as modular clothes are important to increase affordability. For example, smart clothes, as pants and shoes with capacity to monitor gait might be adopted by patient with Parkinson's disease or health professionals to improve diagnostic or outcome measurements. The patients or health professionals that achieve these smart clothes should have possibility to add other hardware (clothes or accessories) or software components, to monitor others parameters (i.e. balance, heart rate or heart rate variability) when are necessary and to combine and analyze all the acquired data. Therefore, interconnectivity and interoperability should be considered in the design of smart clothes for patients receiving rehabilitation. Also, upgrade with hardware and software for subject environment monitoring may provide a holistic non-invasive patient-centric health monitoring. Fair payment for healthcare services realized by using smart clothes and incentive for adoption of these technologies may also contribute to increase affordability.

4 Conclusions

Smart clothes can serve us in an unobtrusive and natural way. Current advances in textile technologies, new materials, nanotechnology and miniaturized electronics increase the smart clothes properties and features. Different smart clothes were developed and are nowadays commercialized, some with potential benefits for patients in cardiac, respiratory or motor rehabilitation.

Although, several smart clothes with capability of health monitoring or for healthcare have been brought to market with potential benefit for patients receiving rehabilitation services, in our knowledge their adoption in healthcare practice is non-existent or very low. The research projects in the area of e-textile are dominantly related with health monitoring and healthcare services while company activities are more represented in the sport and fashion areas. Low level of population awareness (particularly of health professionals) on available e-textile and smart clothes, and their potential benefits for health and healthcare might contribute to the gap between research, progress in smart clothes development and their adoption in healthcare services.

We discussed the technical and technological issues related with smart clothes designed for rehabilitation context. Information on conductive textile, type of textile/fabric manufacturing, sensors based on textile, textile as antenna, textile as actuator, textile as computer interface, circuit board into textile was presented and discussed. As an important challenge described by engineers on smart clothing is related with management of power supply, our study identified relevant progress in this domain, particularly on energy harvesting. Connectivity, integration of things in smart clothing, wearability, maintainability, as well as issues related to design for durability and affordability of smart clothes were also discussed. The data that we present on smart clothing for rehabilitation context underscore the requirement of multidisciplinary team, in which knowledge on human physiology and consumer behavior, rehabilitation techniques and technologies, textile fabric, sensors, electronic device deployment, telecommunications, computing, informatics, chemistry, physics should be integrated for design and development of tailored smart clothes, for subjects receiving rehabilitation.

Acknowledgments The work was supported by Fundação para a Ciência e Tecnologia project: TailorPhy—Smart Sensors and Tailored Environments for Physiotherapy PTDC/DTP-DES/6776/2014, by Instituto de Telecomunicações, and FEDER funds through the Competitvity Factors Operational Programme—COMPETE and by national funds through FCT-Foundation for Science and Technology within the scope of the project POCI-01-0145-FEDER-007136.

References

1. LED Shirt. Retrieved June 2016, from: <https://people.ece.cornell.edu/land/courses/ece4760/FinalProjects/s2010/vij2/LEDshirt/LEDshirt/>
2. A. Coulter, What do patients and the public want from primary care? *BMJ* **331**(7526), 1199–1201 (2005)
3. Tractica, Home health technologies, medical monitoring and management, remote consultations, eldercare, and health and wellness applications: Global market analysis and forecast (2015). Retrieved June 2016, from: <https://www.tractica.com/research/home-health-technologies/>
4. IDC Report. (2015) *Worldwide Quarterly Wearable Device Tracker* Retrieved June 2016, from: <http://www.idc.com/getdoc.jsp?containerId=prUS25872215>
5. ITU—International Telecommunication Union, *The World Telecommunication/ICT Indicators Database* (2015). Retrieved June 2016, from: <http://www.itu.int/en/ITU-D/Statistics/Pages/stat/default.aspx>
6. M. Stoppa, A. Chiolerio, Wearable electronics and smart textiles: a critical review. *Sensors* **14**, 11957–11992 (2014)
7. Antelope. Retrieved June 2016, from: <http://fitnessmodern.de/antelope-ems-sportbekleidung-mit-app-unterstuetzung/>
8. M.T. Bhömer, E. Jeon, K. Kuusk, Vibe-ing: designing a smart textile care tool for the treatment of osteoporosis, in *Proceeding of the 8th International Conference on Design and Semantics of Form and Movement (DeSForM)*, Wuxi, China, ed. by L.L. Chen, J. P. Djajadiningrat, L.M.G. Feijs, pp. 192–195, Sept 2013
9. Clothing plus. Retrieved June 2016, from: <http://www.clothingplus.com/>

10. SmartLife. Retrieved June 2016, from: <http://www.smartlife.co.uk/>
11. Sensatex. Retrieved June 2016, from: <http://www.sensatex.com/>
12. GEO View. Retrieved June 2016, from: <http://www.richardbanks.com/trends/2004/11/16/ecg-built-in/>
13. The Georgia Tech, *Wearable Motherboard: The Intelligent Garment for the 21st Century* (1998). Retrieved June 2016, from: <http://www.smartshirt.gatech.edu>
14. S. Park, C. Gopalsamy, R. Rajamanickam, S. Jayaraman, The Wearable Motherboard: a flexible information infrastructure or sensate liner for medical applications. *Stud. Health Technol. Inform.* **62**, 252–258 (1999)
15. Vivonoetics. Retrieved June 2016, from: <http://vivonoetics.com/>
16. Sensoria. Retrieved June 2016, from: <http://www.sensoriafitness.com/>
17. Ralph Lauren. Retrieved June 2016, from: <http://www.ralphlauren.com/product/index.jsp?productId=69917696>
18. TruPosture. Retrieved June 2016, from: <https://www.truposture.com/>
19. Athos. Retrieved from June 2016, from: <https://www.liveathos.com/>
20. Hexoskin. Retrieved from June 2016, from: <http://www.hexoskin.com/>
21. Adidas miCoach. Retrieved June 2016, from: <http://www.global.adidas.com/micoach>
22. P. Bonato, Advances in wearable technology for rehabilitation. *Stud. Health Technol. Rehabil.* **145**, 145–159 (2009)
23. WHO. *World Health Report*, Geneva, Switzerland, (2000)
24. Myontec. Retrieved June 2016, from: <http://www.myontec.com/en/>
25. P.T. Gibbs, H.H. Asada, Wearable conductive fiber sensors for multi-axis human joint angle measurements. *J. Neuroeng. Rehabil.* **2**(1), 7 (2005)
26. S. Karlsson, U. Wiklund, L. Berglin, N. Östlund, Wireless monitoring of heart rate and electromyographic signals using a smart T-shirt, in *5th International Workshop on Wearable Micro, and Nano Technologies for Personalised Health*, pHealth, pp. 1–5, 2008
27. Jabil. Retrieved June 2016, from: <http://www.clothingplus.com/peak-plus.php>
28. T. Pereira, H. Carvalho, A. Catarino, M.J. Dias, O. Postolache, P.S. Girão, Wearable biopotential measurement using the TI ADS1198 analog front-end and textile electrodes, in *IEEE International Symposium on Medical Measurements and Applications (MeMeA)*, pp. 325–330, 2013
29. A. Paiva, H. Carvalho, A. Catarino, O. Postolache, G. Postolache, Development of dry electrodes for electromyography: a comparison between knitted structures and conductive yarns, in *Proceeding of 9th International Conference on Sensing Technology, ICST*, pp. 447–451, 2015
30. J. Meyer, P. Lukowicz, G. Tröster, Textile pressure sensor for muscle activity and motion detection, in *Proceeding of the 10th IEEE International Symposium on Wearable Computers*, Montreux, Switzerland, pp. 11–14, Oct 2006
31. Xenoma e-skin. Retrieved June 2016, from: <https://xenoma.com/>
32. D. De Rossi, F. Lorussi, E.P. Scilingo, F. Carpi, A. Tognetti, M. Tesconi, Artificial kinesthetic systems for telerehabilitation. *Stud. Health Technol. Inform.* **108**, 209–213 (2004)
33. 5DT. Retrieved from June 2016, from: <http://www.5dt.com/products/pdataglove5u.html>
34. H. Harms, O. Amft, G. Troster, D. Roggen, SMASH: a distributed sensing and processing garment for the classification of upper body postures, in *Proceeding BodyNets '08 Proceedings of the ICST 3rd international conference on Body area network*. Art. 22, 2008
35. Nuubo. Retrieved June 2016, from: <http://www.nuubo.com/>
36. Lumo Run. Retrieved June 2016, from: <http://www.lumobodytech.com/lumo-run/>
37. H. Woodford, C. Price, EMG biofeedback for the recovery of motor function after stroke. *Cochrane Database Syst. Rev.* (2), CD004585 (2007)
38. M.R. van den Heuvel, G. Kwakkel, P.J. Beek, H.W. Berendse, A. Daffertshofer, E.E. van Wegen, Effects of augmented visual feedback during balance training in Parkinson's disease: a pilot randomized clinical trial. *Parkinsonism Relat. Disord.* **20**(12), 1352–1358 (2014)

39. B.C. Lee, T.A. Thrasher, S.P. Fisher, C.S. Layne, The effects of different sensory augmentation on weight-shifting balance exercises in Parkinson's disease and healthy elderly people: a proof-of-concept study. *J. Neuroeng. Rehabil.* **2**(12:75), 1–10 (2015)
40. T. Paillard, Combined application of neuromuscular electrical stimulation and voluntary muscular contractions. *Sports Med.* **38**(2), 161–177 (2008)
41. WARMx. Retrieved June 2016, from: <http://www.warmx.de/index.php/industry-and-research.html>
42. COOLSHIRT SYSTEMS. Retrieved June 2016, from: <http://coolshirt.com/>
43. UNITIKA. Retrieved June 2016, from: <http://www.unitika.co.jp/e/products/fbt-x-bis/clothes.html>
44. F.M. Lam, L.R. Liao, T.C. Kwok, M.Y. Pang, The effect of vertical whole-body vibration on lower limb muscle activation in elderly adults: influence of vibration frequency, amplitude and exercise. *Maturitas* **88**, 59–64 (2016)
45. A. Schwarz, L. van Langenhove, P. Guernonprez, D. Deguillemont, A roadmap on smart textiles. *Textile prog.* **42**(2), 99–180 (2010)
46. Sprint Metal. Retrieved June 2016, from: <http://sprintmetal.schmolz-bickenbach.com/home/>
47. UGITECH S.A. Retrieved June 2016, from: <http://www.sprintmetal.com>
48. Bekaert Fibre Technologies. Retrieved June 2016, from: <http://www.bekaert.com>
49. D. Marculescu, R. Marculescu, N.H. Zamora, P. Stanley-Marbell, P.K. Khosla, S. Park, S. Jayaraman, S. Jung, C. Lauterbach, W. Weber, T. Kirstein, D. Cottet, J. Grzyb, G. Troster, M. Jones, T. Martin, Z. Nakad, Electronic textiles: a platform for pervasive computing. *Proc. IEEE* **91**(12), 1995–2018 (2003)
50. Elektrisola Feindraht AG, *Textile wire ein Produkt*. Retrieved June 2016, from: www.textile-wire.com
51. I. Locher, T. Kirstein, G. Tröster, Routing methods adapted to e-textiles, in *Proceeding of the 37th International Symposium on Microelectronics (IMAPS)*, Long Beach, CA, USA, pp. 16–18, 2004
52. A. Kiourti, J.L. Volakis, High-accuracy conductive textiles for embroidered antennas and circuits, in *Proceeding IEEE International Symposium on Antennas and Propagation & USNC/URSI National Radio Science Meeting*, pp. 1194–1194, 2015
53. Sphelar Power. Retrieved June 2016, from: <http://sphelarpower.com/news/30>
54. Du Pont, *Smart and stretchable. Textile World*. Retrieved June 2016, from: <http://www.dupont.com/content/dam/dupont/products-and-services/electronic-and-electrical-materials/electronic-and-electrical-materials-landing/documents/Smart-and-Stretchable-Textile-World.pdf>
55. Schoeller Textile. Retrieved June 2016, from: <http://www.schoeller-textiles.com/>
56. Elitex. Retrieved June 2016, from: <http://www.titv-greiz.de/>
57. Statex. Retrieved June 2016, from: <http://statex.de/index.php/en/>
58. Elastosil. Retrieved June 2016, from: <http://www.wacker.com/cms/en/products/brands/elastosil/elastosil.jsp>
59. M.-H. Cheng, L.-C. Chen, Y.-C. Hung, C.M. Yang, T.L. Yang, A real-time heart-rate estimator from steel textile ECG Sensors in a wireless vital wearing system, in *Proceeding 2nd International Conference on Bioinformatics and Biomedical Engineering*, pp. 1339–1342, 2008
60. F. Chiarugi, I. Karatzanis, G. Zacharioudakis, P. Meriggi, F. Rizzo, M. Stratakis, S. Louloudakis, C. Biniaris, M. Valentini, M. Di Rienzo, G. Parati, Measurement of heart rate and respiratory rate using a textile-based wearable device in heart failure patients. *Comput. Cardiol.* 901–904 (2008)
61. D. Curone, E.L. Secco, A. Tognetti, G. Loriga, G. Dudnik, M. Risatti, R. Whyte, A. Bonfiglio, G. Magenes, Smart garments for emergency operators: the ProeTEX Project. *IEEE Trans. Inf Technol. Biomed.* **14**, 694–701 (2010)
62. X. Yang, Z. Chen, C.S.M. Elvin, L.H.Y. Janice, S.H. Ng, J.T. Teo, R. Wu, Textile fiber optic micro bend sensor used for heart beat and respiration monitoring. *IEEE Sens. J.* **15**(2), 757–761 (2015)

63. A. Lanata, E.P. Scilingo, D. De Rossi, A multimodal transducer for cardiopulmonary activity monitoring in emergency. *IEEE Trans. Inf Technol. Biomed.* **14**(3), 817–825 (2010)
64. M. Sibinski, M. Jakubowska, M. Sloma, Flexible temperature sensors on fibers. *Sensors* **10**, 7934–7946 (2010)
65. Cytizen Sciences. Retrieved June 2016, from: <http://www.cityzensciences.fr/en>
66. P. Salonen, L. Hurme, A novel fabric WLAN antenna for wearable applications, in *Proceeding of IEEE International Symposium on Antennas and Propagation Society*, Columbus, OH, USA, vol. 2, pp. 700–703, June 2003
67. H. Giddens, D.L. Paul, G.S. Hilton, J.P. McGeehan, Influence of body proximity on the efficiency of a wearable textile patch antenna, in *Proceeding of the 6th European Conference Antennas & Propagation (EuCAP)*, Prague, Czech, pp. 1353–1357, March 2012
68. L. Zhang, Z. Wang, D. Psychoudakis, J.L. Volakis, Flexible textile antennas for body-worn communication, in *Proceedings of IEEE International Workshop on Antenna Technology*, Tucson, ZA, USA, pp. 205–208, March 2012
69. B. Gupta, S. Sankaralingam, S. Dhar, Development of wearable and implantable antennas in the last decade: a review, in *Proceedings of Mediterranean Microwave Symposium (MMS)*, Guzelyurt, Turkey, pp. 251–267, August 2010
70. R. Salvado, C. Loss, R. Gonçalves, P. Pinho, Textile materials for the design of wearable antennas: a survey. *Sensors* **12**, 15841–15857 (2012)
71. C. Hertleer, A.V. Laere, H. Rogier, L.V. Langenhove, Influence of relative humidity on textile antenna performance. *Text. Res. J.* **80**, 177–183 (2009)
72. A. Moretti, Estudo do Brim Santista visando aplicações em antenas têxteis. MS.c. Thesis, Universidade Estadual de Campinas, Campinas, Brazil, 2011
73. J.-S. Roh, Y.-S. Chi, J.-H. Lee, Y. Tak, S. Nam, T.J. Kang, Embroidered wearable multiresonant folded dipole antenna for FM reception. *IEEE Antennas Wirel. Propag. Lett.* **9**, 803–806 (2010)
74. Patria. Retrieved June 2016, from: <http://patria.fi/en/media/news/patria-showcase-patria-amv-nemo-and-innovations-elint-systems-and-data-links-eurosatory>
75. TexTrace. Retrieve June 2016, from: <http://www.texttrace.com/en/rfid-brand-label/index.php>
76. L. Berglin, Smart textile and wearable technology—a study of smart textiles in fashion and clothing (2013). Retrieved June 2006, from: https://www.hb.se/Global/HB%20-%20student/utbildningsomr%C3%A5den/THS/BalticFashion_rapport_Smarttextiles.pdf
77. B.J. Munro, J.R. Steele, T.E. Campbell, G.G. Wallace, Wearable textile biofeedback systems: are they too intelligent for the wearer? in *Wearable eHealth Systems for Personalised Health Management: State of the Art and Future Challenges*, vol. 108, ed. by A. Lymberis, D. De Rossi (IOS Press—STM Publishing House: Amsterdam, The Netherlands, 2005), pp. 271–277
78. S. Gilliland, N. Komor, T. Starner, C. Zeagler, The textile interface swatchbook: creating graphical user interface-like widgets with conductive embroidery, in *Proceeding International Symposium on Wearable Computers (ISWC) 2010*, pp. 1–8, 2010
79. M. Pacelli, G. Loriga, N. Taccini, R. Paradiso, Sensing fabrics for monitoring physiological and biomechanical variables: e-textile solutions, in *Proceeding of the IEEE/EMBS International Summer School on Medical Devices and Biosensors*, St. Catharine's College, Cambridge, UK, pp. 1–4, August 2007
80. P.E. Edelman, Condenser loud-speaker with flexible electrodes. *Proc. Inst. Radio Eng.* **19**(2), 256–267 (2006)
81. T. Dias, Development and analysis of novel electroluminescent yarns and fabrics for localised automotive interior illumination: el yarns and fabrics. *Text. Res. J.* **82**, 1164–1176 (2012)
82. T. Dias, Development and analysis of novel electroluminescent yarns and fabrics for localised automotive interior illumination: el yarns and fabrics. *Text. Res. J.* **82**, 1164–1176 (2012)
83. S. Janietz, B. Gruber, S. Schattauer, K. Schulze, Integration of OLEDs in textiles. *Adv. Sci. Technol.* **80**, 14–21 (2012)

84. Infineon Technologies AG. Retrieved June 2016, from: <http://www.infineon.com/cms/en/product/>
85. Edmison, J., Jones, M., Nakad, Z., Martin, T. Using piezoelectric materials for wearable electronic textiles, in *Proceedings of the 6th International Symposium on Wearable Computers (ISWC)*, Seattle, WA, USA, pp. 41–48, October 2002
86. L.M. Swallow, J.K. Luo, E. Siores, I. Patel, D. Dodds, A piezoelectric fibre composite based energy harvesting device for potential wearable applications. *Smart Mater. Struct.* **17**(2) (2008)
87. S. Xu, Y. Qin, C. Xu, Y. Wei, R. Yang, R.L. Wang, Self-powered nanowire devices. *Nat. Nanotechnol.* **5**, 366–373 (2010)
88. S. Bai, L. Zhang, Q. Xu, Y. Zheng, Y. Qin, Z. Wang, Two dimensional woven nanogenerator. *Nano Energy* **2**, 1–5 (2013)
89. V. Leonov, Thermoelectric energy harvesting of human body heat for wearable sensors. *IEEE Sens. J.* **13**(6), 2284–2291 (2013)
90. T. Torfs, V. Leonov, C. van Hoof, B. Gyselinckx, Body-heat powered autonomous pulse oximeter, in *Proceeding 5th IEEE Conference on Sensors*, pp. 427–430, 2006
91. L.A. Samuelson, F.F. Bruno, J. Kumar, R.A. Gaudiana, P.M. Wormser, Conformal solar cells for the soldier, in *Proceeding International Interactive Textiles for the Warrior Conference*, Cambridge, MA, 2002
92. M.B. Schubert, J.H. Werner, Flexible solar cells for clothing. *Mater. Today* **9**, 42–50 (2006)
93. Y.-H. Lee, J.-S. Kim, J. Noh, I. Lee, H.J. Kim, S. Choi, J. Seo, S. Jeon, T.-S. Kim, J.-Y. Lee, J.-W. Choi, Wearable textile battery rechargeable by solar energy. *NanoLetters* **13**, 5753–5761 (2013)
94. R.C. Chiechi, R.W.A. Havenith, J.C. Hummelen, L.J.A. Koster, M.A. Loi, Modern plastic solar cells: materials, mechanisms and modeling. *Mater. Today* **16**, 281–289 (2013)
95. Consultancy Goose Design, *Illum Project Concept*, Retrieve June 2016, from: <http://www.goose.london/projects/illum/illum-concept/>
96. R.G. Kim, W. Choi, Z. Chen, P.P. Pande, D. Marculescu, R. Marculescu, Wireless NoC and dynamic VFI codesign: energy efficiency without performance penalty. *IEEE Trans. Very Large Scale Integr. VLSI Syst.* **24**(7), 2488–2501 (2016)
97. A. Afzali, S.H. Maghsoodlou, Modern application of nanotechnology in textile, in *Nanostructured Polymer Blends and Composites in Textiles*, ed. by M. Ciocoiu, S. Maamir (Apple Academic Press and CRC Press, 2016) pp. 41–85
98. X. Tao, *Wearable Electronics and Photonics* (Woodhead Publishing in Textiles, 2005)
99. K. Worden, W.A. Bullough, J. Haywood, *Smart Technologies* (World Scientific Publishing, Singapore, 2003)
100. NTT DoCoMo. Retrieved June 2016, from: https://www.nttdocomo.co.jp/english/info/media_center/pr/2014/0930_00.html
101. O. Berger, W.-J. Fisher, Photo-induced switchable TiO₂ thin films for decomposition of air pollutants and microorganisms, self-cleaning surfaces and biological application. *IEEE Sens.* **10**(8), 719–722 (2010)
102. S. Shahidi, M. Ahmadi, A. Rashidi, M. Ghoranneviss, Effect of plasma treatment on self-cleaning of textile fabric using titanium dioxide. *IET Micro Nano Lett.* **10**(8), 408–413 (2015)
103. S.R. Anderson, M. Mohammadtaheri, D. Kumar, A.P. O’Mullane, M.R. Field, R. Ramanathan, V. Bansal, Robust nanostructured silver and copper fabrics with localized surface plasmon resonance property for effective visible light induced reductive catalysis. *Adv. Mater. Interfaces* **3**(6) (2016)
104. N.M. van der Velden, K. Kuusk, A.E. Koehler, Life cycle assessment and eco-design of smart textile: the importance of material selection demonstrated through e-textile product redesign. *Mater. Des.* **84**, 313–324 (2015)
105. Basic Information about European Directive 93/42/EEC on medical devices. Retrieved June 2016, from: https://www.mdc-ce.de/fileadmin/user_upload/Downloads/mdc-Dokumente/Broschueren/040100_basic_info_93-42-EEC_06_e.pdf

106. PEDro, The PEDro scale (partitioned): guidelines and explanations. Retrieved June 2016, from: <http://www.otseeker.com/Info/pdf/PEDro-scale-partitioned-guidelines-jul2013.pdf>
107. G. Postolache, R. Oliveira, I. Moreira, O. Postolache, Why, what and when in-home physiotherapy? in *Transformative Healthcare Practice through Patient Engagement*, ed. by G. Graffigna (IGI Global, 2016) pp. 215–246
108. M.F. Story, J. Mueller, R.L. Mace, *Universal Design File: Designing for People of All Ages and Abilities* (NC State University, Center for Universal Design, 1998)

Wireless Sensing Systems for Body Area Networks

Xiaoyou Lin, Boon-Chong Seet and Frances Joseph

Abstract Body area networks (BANs) are a form of small-scale wireless sensor networks (WSNs) deployed on the human body. This technology embodies the convergence of wearable, sensing, and wireless communication techniques, with a focus mainly on health monitoring, human-machine interaction, and motion capturing applications. As the bridge between on-body circuits and their external application users, body-worn radio frequency (RF) structures operating at high frequencies have gained increasing attention in recent years, in particular RF structures fabricated with flexible or textile materials. Due to the flexibility of these RF structures to conform to human body for comfortable fit, they are well-suited for BAN applications. In addition, if the characteristics of these RF structures can naturally or technically be made to react to bodily phenomena such as temperature and humidity, the same structures (such as antennae) can also function as sensors. These RF structures with sensing capability could be referred to as *wireless sensing structures*. Besides, there also exist several techniques for the detection and the interpretation of the output signals of these sensing structures. For a system consisting of a wireless sensing structure and a data detection and interpretation circuit or device, we refer to it as a *wireless sensing system*. This chapter reviews the sensing mechanisms, data detection and interpretation methods and typical BAN applications of existing wireless sensing systems.

1 Introduction

Body area networks (BANs) have recently drawn increasing attention from researchers due to their wide-ranging applications in domains such as healthcare, sports, and entertainment [1]. It is a special form of wireless sensor network (WSN) that allow miniature sensors with intelligent and wireless communication functions to be placed around or inside the human body for the purpose of

X. Lin (✉) · B.-C. Seet · F. Joseph
Auckland University of Technology, Auckland, New Zealand
e-mail: Xiaoyou.lin@aut.ac.nz

monitoring physiological, environmental or other parameters such as human gestures and actions [1, 2].

Clothing is an obvious platform to embed the developed sensors in the near space around the human body. Some of these sensors may even need to be implanted inside skin or tissues [1–3]. To date, various types of sensors have been developed for use in BANs [3]. There are several requirements for these on/in-body sensor nodes. First, they should be capable of sensing physiological or other body-related parameters, processing the sensed data, and wirelessly reporting the processed results to the system. Besides, these nodes need a certain amount of energy to keep them running for the purpose of continuous monitoring. Furthermore, these nodes should be relatively small and flexible, so that they can be integrated within normal garments, adhered to or implanted inside human bodies [1, 2, 4]. However, so far, the realisation of highly integrated, ultra-low-power, lightweight, flexible and wearable sensors is still an ongoing research challenge [4, 5].

In order to realise such sensors and setup on-/off-body wireless channels, some basic techniques and algorithms from conventional WSNs can be adopted [4]. However, they are not well suited to meet the requirements of BANs. For example, one main requirement of conventional sensor nodes used in WSNs is the wiring between the sensor (i.e. data gathering element) and electronic circuitry (i.e. data processing and transmission unit), which may introduce extra system and operational complexity, thereby limiting the benefits of these sensor nodes in BANs [5]. Besides, since both the sensing element and the wireless unit require external power supply, the requirement of ultra-low power operation and the methods of supplying power are becoming critical in designing a promising BAN system [1, 2, 6].

Wearable RF structures/devices with sensing capability have been proposed to overcome the above shortages. In the existing research literature, some applications use antenna patches directly as the sensing structures, e.g. [7], and thus they are called sensing antennas. However, there exist other RF structures such as the LC tank circuits, which can be used for sensing signals [8]. Therefore, in order to distinguish them from conventional sensor nodes, in this chapter, we refer to these RF-based sensing structures as *wireless sensing structures*. Besides having the common compact and low-profile properties of body-worn RF, since the structure itself serves as both a sensing and transmission unit, the size of the sensor node can be further minimised [5]. Furthermore, such wireless sensing structures are mostly battery-free devices, thereby also minimising consumed energy and easing the system design. A system consisting of a wireless sensing structure and an external circuit or device for detecting and interpreting the output sensor signals can be defined as a wireless sensing system. Obviously, the sensing structure is an essential component in a wireless sensing system, which is the main topic of this chapter.

There are some challenges for designing a promising wireless sensing system. For one, as the performance of BAN systems relies on the stability of the data transmission and the reliability of the wireless link, the design of wearable RF structures needs to take into considerations the effects from human bodies and on-/off-body channel interferences [1, 2]. This is mainly because the human body is fluid-rich and characteristically has a high electromagnetic loss [9], thus the

parameters of RF structures, e.g. radiation performance, resonant frequency, bandwidth, will be considerably altered [6]. In addition, data analysis and interpretation are also another design challenge. For example, for a passive wireless sensing structure based on detecting changes in its resonant frequency, its power reflection coefficient (S_{11}) cannot be measured directly in real applications, and thus proper data analysis techniques, e.g. monitoring the impedance of the sensor as a function of frequency, have been developed.

The following sections will review the state-of-the-art designs of the existing wireless sensing structures used for BAN applications and briefly introduce two commonly used techniques for data detection and interpretation.

2 A Review of Wireless Sensing Systems

Wireless sensing techniques were initially developed based on surface acoustic wave (SAW) technique to sense pressure, temperature [10, 11], strain [12], etc. Later on, the sensing systems based on the RF technique were also investigated to overcome the shortages of low sensitivity and reliability of SAW-based systems. It is in industrial projects that such RF-based systems were firstly introduced, e.g. resonator used for detecting the temperature and gas properties in turbine engines in harsh environment [13]. With the increasing attention on health monitoring and human-machine interaction, wireless sensing systems were introduced in BANs and started to be investigated. They were firstly designed in small size and fabricated on conventional rigid printed circuit boards (PCBs) [14] due to lack of proper flexible materials as the substrates during the first few years of the investigation. However, with the intensive research on both the dielectric and electrical properties of textile and other flexible materials on microwave frequencies [15, 16], more wireless sensing systems are using flexible platforms made of materials such as flexible plastics, thin films and textiles [17].

It is firstly of interest to understand the state-of-the-art operating mechanism of classical sensors. With reference to Fig. 1, sensors are the electronic devices that can convert input stimulus such as physical, chemical, optical, and other information into, typically, electrical signals (pulsed or modulated signals) that can be interpreted by electrical circuits or devices [18].

The wireless sensing structures of wireless sensing systems also follow the above principle. More specifically, by relating the property of the input signal with one of the characteristics of the designed RF structures, a RF-based sensing structure can be designed. These characteristics may include:

- Resonant frequency (f_0): e.g. resonance-based wireless sensing structures;
- Receive signal parameters: e.g. time of arrival (ToA), angle of arrival (AoA), etc.;
- Radiating parameters: e.g. gain, backscattering, etc.

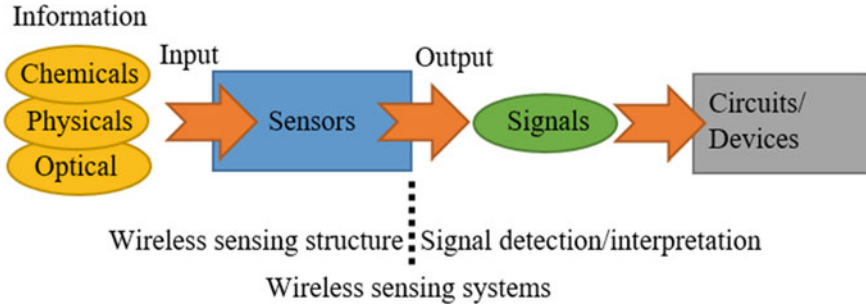


Fig. 1 Operating mechanism of sensors

There are two common designs for the RF-based sensing structures. The first design utilises an antenna, which shifts its resonant frequency (f_0) with the property of the sensed phenomenon, and works with other RF components, e.g. RF identification (RFID) tag chips or active RF transmitters, that can provide the RF signals [19]. Therefore, such systems could be a battery-free system (e.g. when working with a passive RFID tag integrated circuit). The second design utilises resonant circuits, e.g. a LC tank circuit, in conjunction with antennas, or just the LC circuit alone for short-range applications [20–22]. In the latter design, the resonant circuits are the sensing structures and can be designed to be a highly compactable structure, thereby further minimising their sizes.

This chapter will mainly focus on a discussion of the wireless sensing due to the variation of the resonant frequency (f_0) because this mechanism is the most popular approach and has been experimentally implemented for BAN applications. In addition, the chapter also introduces the wireless sensing systems for gesture monitoring, which operates on the basis of detecting differences in received signals from spatially distributed antennas deployed on a human body.

3 Wireless Sensing Antennas

3.1 General Working Principles

A wireless sensing antenna detects external physical phenomenon by modifying its resonant frequency (f_0). It is known that the resonant frequency of an RF structure is defined as the frequency point where minimum *return loss*, or *power reflection coefficient* (S_{11}), occurs. For RF structures used for radiating microwaves, i.e. antennas, or other RF structures embedded with antennas, the RF energy transmitted and/or reflected back by the antenna forms a peak at the receiver side [23]. Therefore, a RF-based sensing structure can be realised by relating the changing f_0 with the property of the sensed phenomenon.

Normally, there is an initial resonant frequency value for wireless sensing structures, which represents a state of ‘non-excitement’ of the sensing structure, i.e. no external phenomenon is applied to the sensing structure. If the variation of the resonant frequency has a relatively linear response to the sensed phenomenon (S), which is quite common for most current wireless sensing systems, then this response can be modelled as [19, 24]:

$$S(f_0) = \frac{|f_0 - f_0|_{S=0}|}{\frac{df}{dS}}, \quad (1)$$

where $S(f_0)$ is the measured value of the sensed phenomenon, $f_0|_{S=0}$ is the initial resonant frequency, f_0 is the resonant frequency after ‘excitation’ by the sensed phenomenon, and the $\frac{df}{dS}$ is the system sensitivity.

It is of interest to understand which parameters can affect the resonant frequency of antennas. Generally, for a simple microstrip antenna, f_0 depends on the geometry of the antenna patch and the permittivity (ϵ) of the substrate material [23]. Therefore, by relating the property of the sensed phenomenon with the variation of either geometrical dimension or permittivity value, a wireless sensing structure can be designed.

However, sometimes the above resonant-frequency-shifting effect is not significant due to the external phenomenon, e.g. temperature or pressure. Therefore, there are several approaches to assist or magnify this effect. The first approach is to cover the electrodes, e.g. antennas or LC tank circuits, with a sensitive layer such as cellulose acetate butyrate (CAB) which is sensitive to the humidity [25]. The second approach is to use the sensitive substrate directly which would bring down the design complexity [21]. This section will first present the theories of sensing by mechanical deformation and dielectric permittivity (ϵ) separately, and illustrate the use of both operating mechanisms with their typical applications.

3.2 Sensing by Mechanical Deformation

The easiest way to achieve the mechanical deformation is to change the geometrical dimensions of the sensing structures. This can be achieved by applying force to compress (Fig. 2a) or stretch (Fig. 2b) the wireless sensing structures, as they are applied to realise pressure sensors, and strain sensors, respectively.

Pressure sensors normally have a dielectric material sandwiched between two conductive patches [3, 10]. For example, if using patch antennas as the sensing structures, top side of the conductive patch is the radiation patch, while the patch on the other side is the ground plane. Because the electromagnetic (EM) field deciding the resonant frequency propagates only within dielectrics between two patches, the change of physical thickness (h) of the dielectric substrate leads to the redistribution of the EM field inside the substrate. This effect impacts the effective relative

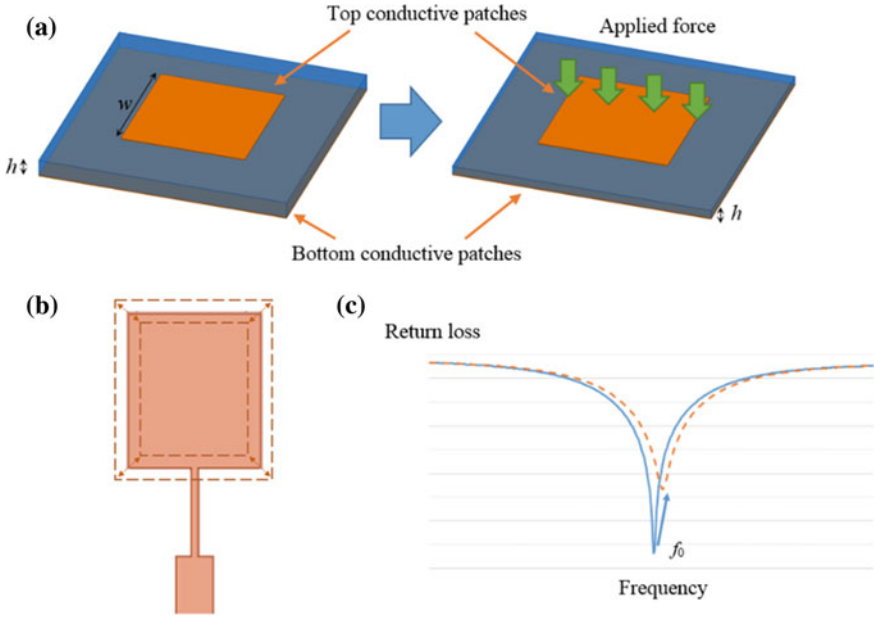


Fig. 2 The working principle of: **a** pressure sensor; **b** strain sensor; **c** a shift to the resonant frequency (f_0) due to the external force

permittivity ($\epsilon_{r,eff}$) of the antenna and results in a change of the resonant frequency (Fig. 2c). If the geometrical dimension of both conductive plates does not change when the forces are applied, then the resonant frequency of the RF system will increase with a decreasing thickness of the substrate [15, 23]:

$$f_0 \sim \frac{1}{h} \sim \frac{1}{\epsilon_{r,eff}}. \quad (2)$$

Therefore, the crucial part that affects the performance of a RF-based pressure sensor is the choice of a suitable deformable dielectric substrate.

The strain sensing antennas is based on the theory that the antenna resonates when its geometrical size is similar to that of the electrical length [23]:

$$l_e = \frac{l}{\lambda} = \frac{l \times f}{c}, \quad (3)$$

where l is the physical length, l_e is the electrical length, λ is the wavelength of operating frequency, and c is the speed of the light. As can be concluded from (3), the variation in the physical length l will definitely alter its resonant frequency f . The strain sensing has potential applications in measuring surface-deformation (e.g. skin ulceration and pregnancy), heart beats, blood pressure, etc. [26].

In [24], an ultra-small pressure sensing antenna was proposed for continuous intracranial pressure (ICP) and pulse monitoring. It adopted a layer of enhanced flexible micro-structured styrene-butadiene-styrene (SBS) elastomer with reduced viscoelastic behaviour as the dielectric materials. In addition to the thickness variation, the air between the pyramidal microstructures of the SBS elastomer (Fig. 3a) will be expelled when pressure is applied, which results in an improved sensitivity of the developed sensing structure. The resonant structure consists of two inductive spirals acting as antennas, each on one side of the SBS (Fig. 3b). The whole stacked structure acts as a resonant tank circuit. This system has a relatively linear frequency response (Δf_0) to the applied pressure under both in-air and in-saline conditions (Fig. 3c). In vivo experiments were carried out on a mouse for ICP monitoring and on the wrist for pulse monitoring (Fig. 3d). The response of the sensor to the pulse is shown in Fig. 3e.

Another application for strain sensing is a “smart fabric bellyband” [27] (Fig. 4a) in which a microstrip antenna pattern was knitted with silver-coated yarns (Fig. 4b). The knitting technique was used because it employs loose and interleaving structures during the fabrication process (Fig. 4c). Therefore, when the antenna pattern is stretched, its geometry will change according to the tension of the force, which leads to the change in the antenna’s resonant frequency (f_0) and radiation properties (e.g. gain) (Fig. 4d).

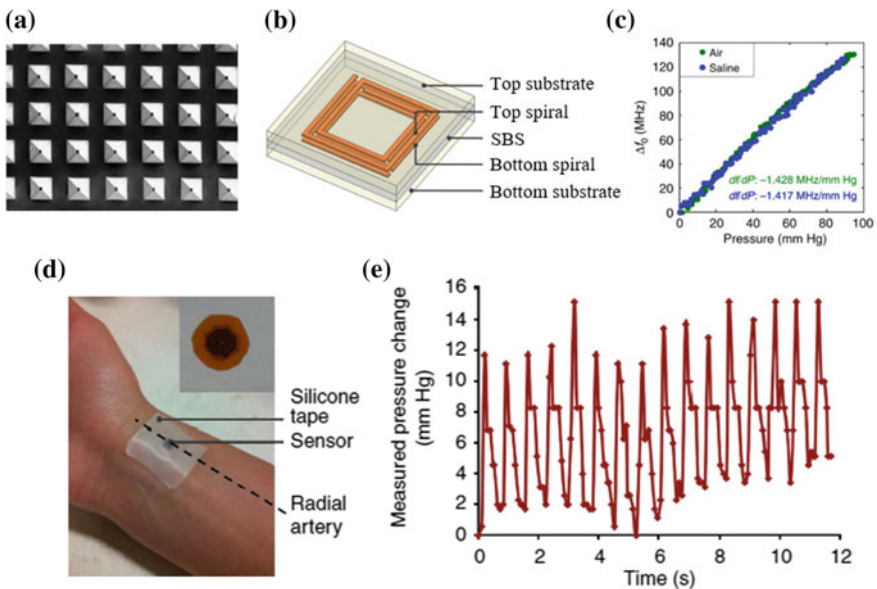


Fig. 3 An ultra-small pressure sensor for ICP and pulse monitoring: **a** sensor structure; **b** SBS structure under microscope; **c** frequency-pressure response in the air and in saline; **d** experiments for pulse monitoring; **e** sensor output for pulse monitoring (reproduced with the permission from Ref. [24])

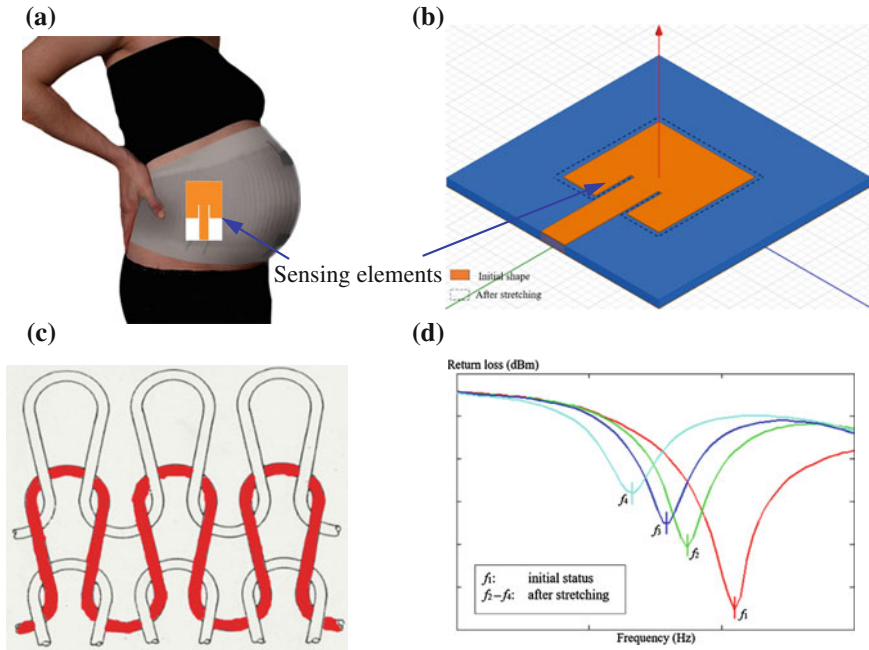


Fig. 4 **a** smart fabric bellyband; **b** stretching antenna sensor; **c** knitting structure; **d** the response of f_0 to the stretching force

3.3 Sensing by Electrical Permittivity (ϵ)

Beside the mechanical deformation to the physical geometry of sensing antennas, the electrical permittivity (ϵ) of the substrate material can also be made to change in response to the sensed phenomenon. Permittivity is the measure of the resistance encountered when forming an electric field in a medium [23]. It is defined as:

$$\epsilon = \epsilon_0 \epsilon_r, \quad (4)$$

where ϵ_0 is the permittivity of the air, which is unchangeable, and ϵ_r is the *relative permittivity*, or *dielectric constant* of the medium.

One important property of the relative permittivity ϵ_r is that it is *not a constant* for the same material under different conditions [28]. More specifically, for most dielectric substrates used in BANs or wearable applications, such as textiles and thin plastic film, their permittivity has a relationship with external environment, e.g. temperature and humidity, which, in turn, shifts the resonant frequency f_0 of the sensing structures. Previous researches find that the relative permittivity ϵ_r of certain solid flexible materials (e.g. textile and Kapton film) increases with a rising temperature or humidity [19, 28]. As mentioned in Sect. 3.1, the resonant frequency of the sensing antenna shifts with the permittivity of the substrate material [23]:

$$f = \frac{v_p}{\lambda} = \frac{c}{\lambda\sqrt{\epsilon_r}}, \tag{5}$$

Therefore, it is an ideal method to monitor the parameters of the ambient environment.

In [19], an inkjet-printed passive RFID antenna for sensing ambient humidity was fabricated (Fig. 5a). This system was intended for sensing ambient humidity within a sealed structure but also potentially be used as part of a wearable health-monitoring system [29]. The sensing system was printed on flexible Kapton film which has a linear humidity-permittivity response, and therefore no extra moisture-sensing layer is required. In order to effectively convert the variation of ϵ_r into a shifting resonant frequency, the arms of the antenna consists of multiple parallel printed conductive plates, thereby increasing the sensitivity of the capacitive sensing. A relatively linear response between the humidity and the lowest-power-on-tag frequency was characterised (Fig. 5b) and the achieved sensitivity is 171 kHz/%RH.

Another application is the body temperature sensor in [7]. A microstrip antenna operating at 38 GHz was designed and work close to the human skin as the sensing structure (Fig. 6a). Changes in the body temperature can be sensed because the dielectric permittivity of textile substrate monotonically increases with a rising temperature. Even though this permittivity variation is relatively weak, it still could be detected especially when the antenna is operating at the extremely-high frequency (EHF) band. This is because with an ultra-short wavelength at 38 GHz ($\lambda = 7.89$ mm) and tiny geometry of the designed antenna, a slight change of dielectric constant could magnify the frequency-shifting effect. The simulated results show that the performance of the proposed antenna has good selectivity at its resonant frequency point and is sufficiently sensitive to small temperature-induced

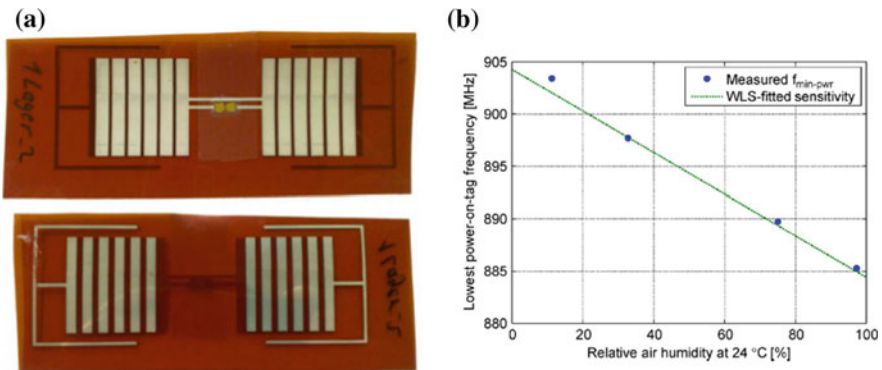


Fig. 5 Inkjet-printed wireless humidity sensor based on passive RFID tag: **a** antenna prototype; **b** lowest-power-on-tag frequency versus relative air humidity (reproduced with the permission from Ref. [19])

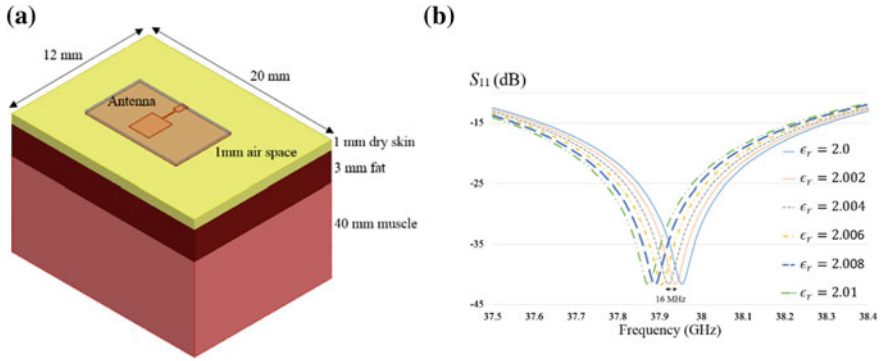


Fig. 6 Temperature sensor: **a** on the human-body phantom; **b** Reflection coefficient (S_{11}) for each dielectric constant value (ϵ_r) increased in steps of 0.002 for every 1 °C rise in temperature (reproduced with the permission from Ref. [7])

variations in the dielectric constant of the substrate to be usable as a human body temperature sensor (Fig. 6b).

4 Wireless Sensing LC Circuits

Apart from using antennas as the sensing structures, LC tank circuits are an attractive alternative, which can eliminate the need for RFID tag integrated circuit or other RF components. Therefore, the wireless sensing by LC tank circuits could further lower down the system profile and decrease the required energy. Another advantage of using LC tank circuits is that such sensing structures normally can achieve a higher quality factor (Q) at the resonant point than that of most antennas [30], which ensures better selectivity for the sensed phenomenon.

There are two main designs for LC sensing circuits as shown in Fig. 7a, b. Their main difference is the method of constructing capacitors. Type I consists of a series/parallel-connected capacitor and inductor (the dash line in Fig. 7a is used to divide these two components). Type II uses a parallel capacitor which is electrically connected with the spiral inductor by the via-hole. Type I has a coplanar structure, which makes it easier to fabricate as compared to Type II, which has a stacked structure although it is less complicated to design. The inductor L is normally fabricated as an inductive coil, and thus the designed circuit can be activated by external energy source. Generally, any LC-constructed sensing structure can be modelled as Fig. 7c, and its resonant frequency f_0 can be defined as:

$$f_0 = \frac{1}{2\pi\sqrt{LC}}, \quad (6)$$

where L is the inductance and C is the capacitance.

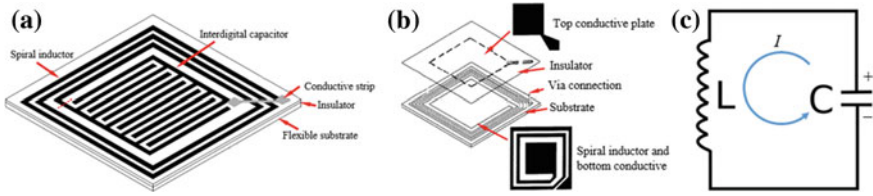


Fig. 7 LC sensing structure: **a** type I—interdigital capacitor; **b** type II—sandwiched capacitor; **c** LC tank circuit model

Between these two components, the inductor L is less sensitive to the permittivity of the substrate but is more suitable for sensing mechanical deformations as a strain sensor. This is because a closer distance between two turns leads to a higher inductance L , and thus lowering down the f_0 . On the other hand, the capacitor C is highly permittivity dependent. For an interdigital capacitor shown in Fig. 7a, its capacitance C can be defined as [31]:

$$C = \frac{(\epsilon_r \epsilon_0 + 1)}{d} l [A_1(n - 3) + A_2], \tag{7}$$

For a parallel capacitor shown in Fig. 7b, its capacitance can be defined as:

$$C = \frac{\epsilon_r \epsilon_0}{h} S, \tag{8}$$

where d is the distance between fingers, l is the finger length, A_1 and A_2 are the contribution of the interior and two exterior fingers, respectively, n is the number of fingers, h is the thickness of the insulator and S is effective area of the top and bottom conductive plates.

An implantable capsule-like sensor with etched LC tank circuits on silicon diaphragm were proposed for detecting abnormal pressures in anterior chambers [31]. A small vacuum cavity was designed as a capacitor and a spiral golden wire was connected to the capacitor as the inductor. The capacitance C changes with pressure-induced variations in the thickness of the vacuum cavity, and this effect in turn alters the resonant frequency of the designed LC sensing structure according to (8). A detector placed several millimetres away can wirelessly monitor the frequency variation. This is a typical application based on LC circuit for the medical area in its early research stage. A modified and enhanced version of the anterior-chamber-pressure monitoring system utilises LC tank circuit can be found in [32].

A strain sensor for long-term continuous skin monitoring (Fig. 8a) was proposed in [8]. A copper coil based on self-similar serpentine structure was designed and etched on stretchable polydimethylsiloxane (PDMS) substrate. The fractal serpentine structure of the coil itself also enhances the stretch-ability of the sensor. The capacitor is located at the centre of the sensor (Fig. 8a). The measured inductance

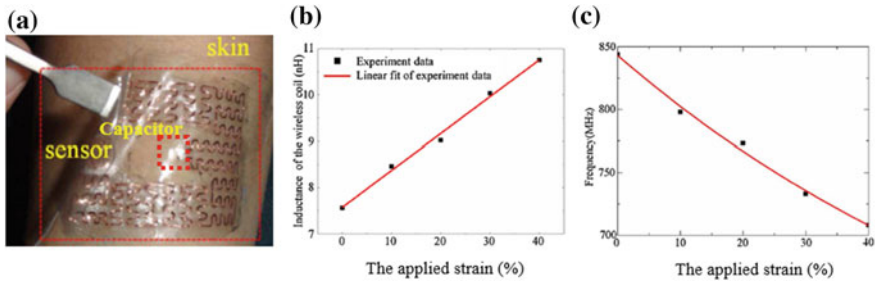


Fig. 8 Stretchable wireless strain sensor for skin monitoring: **a** fabricated inductive coil on the PDMS substrate; **b** inductance-strain response; **c** f_0 -strain response (reproduced with the permission from Ref. [8])

L of the coil has a linear response to the applied strain (Fig. 8b), thereby relating the resonant frequency (f_0) of the wireless sensing structure with the applied strain (Fig. 8c).

The above two applications utilised the force-induced mechanical deformation to change either the inductance or the capacitance to realise the sensing function. However, changing the permittivity of the medium surrounding the sensors is also another approach to realise a LC-based sensing structure. For example, in approximate sensing [33], a capacitive sensor was integrated with the inductive coil to form a LC tank circuit (Fig. 9a, b), and approaching or touching the sensor changes the capacitance and therefore shifting both the amplitude and resonant frequency of the tank circuit (Fig. 9c).

In [22], the LC circuit was fabricated on a piece of flexible and stretchable substrate to sense the existence of sweat on the skin surface. The microporous substrate can spontaneously absorb sweat released from the skin, and thus the dielectric property, i.e. ϵ_r , of the substrate changes, which in turn alters the frequency characteristics of the LC sensing circuit. Furthermore, by integrating functional microelectrodes inside the substrate, this LC sensing circuit is capable of identifying some specific chemical ions (e.g. OH^- and H^+) in the sweat as they introduce colorimetric effect in the substrate.

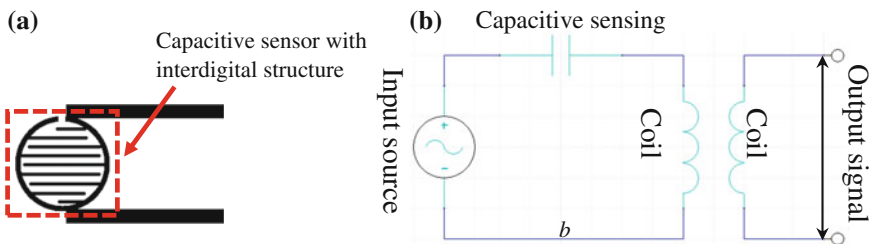


Fig. 9 Approximate sensing: **a** capacitive sensor; **b** LC tank circuit model

The drawback of LC-based sensing structures is that the monitoring antenna or the detector should operate near the sensing structures. Therefore, this type of LC sensing circuits sometimes is integrated with antennas to extend its detection range [34].

5 Gesture Monitoring for Bans

Wireless sensing systems have also been successfully applied to track the gestures of human activity [35, 36]. This technique is developed from indoor localisation systems [36], which rely on the individual wireless sensing structures deployed at different positions in the building (*reference nodes*, or *base stations*) and on human bodies (*targets* or *tags*). To achieve a sufficiently high resolution to capture the motion of bodily movements, gesture monitoring systems deploy more tags and base stations on human limbs/torso, and in the room, respectively. However, using more wireless sensing structures in the system will also lead to an increased system complexity, and thus, the trade-off between the number of sensors and the system resolution needs to be carefully considered before design the system [36].

Unlike the resonance-based wireless sensing structures which sense signals by changing their own physical (e.g. thickness) or electrical (e.g. permittivity ϵ) parameters accordingly, wireless sensing structures used for gesture monitoring are based on the fact that the parameters (e.g. ToA, AoA) of the signal received by the antennas attached on the human body from different base stations are also different. By developing suitable algorithms, the relative movement of body or limbs can be derived. As referred to Fig. 10, this process can be divided into two phases [35]:

Phase 1: The signals are transmitted between the target sensor nodes (tags) and the base stations. Useful signal parameters (e.g. ToA, AoA) are extracted in this phase;
Phase 2: The physical positions of each target will be calculated based on the parameters abstracted during Phase 1.

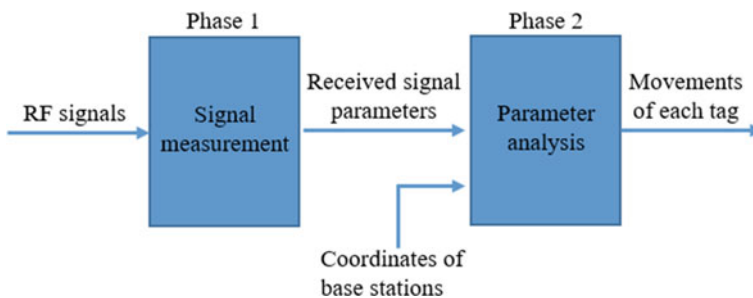


Fig. 10 Working principle of gesture monitoring systems

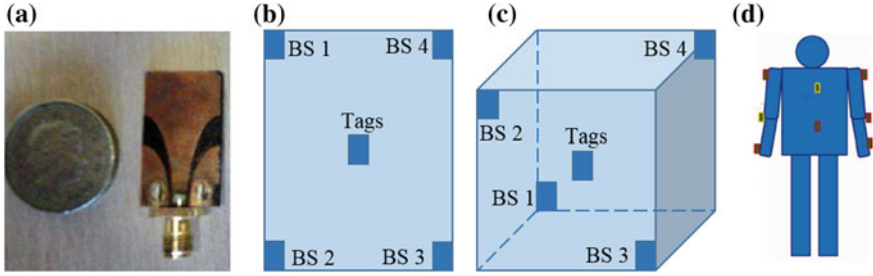


Fig. 11 **a** CPW-fed tapered antenna used for motion capturing; **b** top view of the cuboid shape configuration; **c** main view of the cuboid shape configuration; **d** tag locations on human body (reproduced with the permission from Ref. [36])

A number of algorithms have been developed for Phase 2, including time-based method, AoA method and the received signal strength (RSS) method [34], among which the time-based method is the first one to be implemented in BANs for health monitoring.

For tracking the motion of human body, the sensor tags are normally placed or bonded at the joints and ends of limbs. A time-based 3-dimensional (3D) monitoring system for tracking human daily movements was proposed in [36–38]. It utilised the ultra-wideband (UWB) technique that has relatively narrow pulses, so that sufficiently high resolution can be achieved for position and motion capturing. A type of CPW-fed tapered slot antenna (TSA) (see Fig. 11a) was used as the base stations and the tags. Four base stations were placed in a cuboid shape configuration (see Fig. 11b, c) and eight tags were worn by human (see Fig. 11d). The distance (r_i) between the tags and the base stations (BS $_i$) and the relative position of the tag (x_m, y_m, z_m) can be derived from [35, 36]:

$$r_i = t_{r,i} \times C, \quad (9)$$

$$r_i^2 = (x_i - x_m)^2 + (y_i - y_m)^2 + (z_i - z_m)^2, \quad (10)$$

where $t_{r,i}$ is the duration from the beginning of transmission by the tag to the reception of the transmitted signal by the i th base station, C is the speed of the light and (x_i, y_i, z_i) is the relative position of the i th base station. By applying the above algorithm, this 3D motion monitoring system can realise a system resolution of 1–3 cm, and thus could effectively capture human body movement in daily life.

6 Data Detection and Interpretation

As discussed above, the direct measurement of the sensors' output is impossible because it will increase the system complexity [5]. This section will briefly review the two most popular data detecting and interpreting methods: the power-on-tag

method for systems working with RFID tag antennas, and the impedance monitoring method for LC sensing circuits. The common advantage of these two methods is that they can wirelessly monitor the output signals.

6.1 Power-on-tag Method

This method is developed for wireless sensing systems with embedded RFID tags and was first implemented in [19] for ambient humidity sensing. However, it is also applicable for other similar sensing systems integrated with passive RFID tags or active RF source chips with minor modifications [39].

For RFID systems, the power transferring is realised by achieving the impedance matching between the tag chip (source) and the tag antenna (load). As discussed previously, any change in the permittivity, geometrical dimensions will alter the resonant frequency of an RF circuit, which, in turn, will affect the complex load impedance (Z_L). The power reflection coefficient Γ which defines the power transfer from a source to the load is given by:

$$\Gamma = \left| \frac{Z_L - Z_s^*}{Z_L + Z_s^*} \right|^2, \quad (11)$$

where Z_L is the load impedance, i.e. the impedance of the sensing structure; Z_S is the source impedance and Z_s^* is the conjugation of complex impedance Z_S . The power-on-tag P_{on-tag} is the minimal power required to activate a tag, and can be given by:

$$P_{on-tag} = L_{fwd} \times P_{TS} = \frac{P_{IC}}{G_{tag} \times (1 - \Gamma)}, \quad (12)$$

where L_{fwd} is the path loss in the forward link, i.e. the path from the reader to the tag, P_{TS} is the transmit power at the antenna port needed to activate the tag, P_{IC} is the sensitivity of the tag IC, and G_{tag} is the gain of the sensing structure. As can be noticed that, both Γ and P_{on-tag} are functions of the frequency, and thus they both also depend on the property of the sensed signal.

Figure 12 compares the variation of both simulated power reflection coefficient (S_{11}) and the P_{on-tag} with the changing relative permittivity (ϵ_r). It can be seen that the change of P_{on-tag} over different ϵ_r has a good agreement with that of S_{11} , and thus this method provides a wireless measurable approach for such sensing systems.

Apart from realising a wireless monitoring, another advantage of this power-on-tag method is that it considers the attenuations and reflections generated during the wave propagation and signal transmission, and thus it is robust enough to work under harsh environmental conditions, e.g. signal fading due to obstacles.

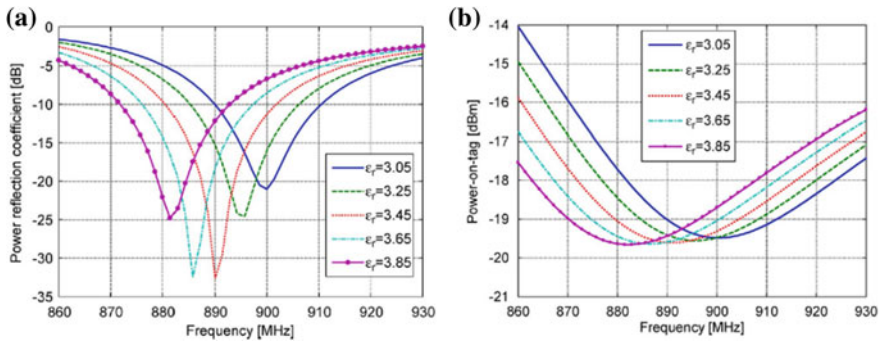


Fig. 12 **a** simulated power reflection coefficient (S_{11}); **b** simulated power-on-tag of the tag (reproduced with the permission from Ref. [19])

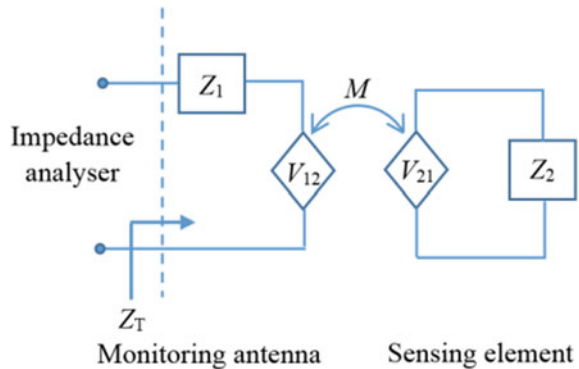
6.2 Impedance Monitoring Method

This method is useful when monitoring a purely passive sensing structure. The theory is based on the mutual inductance coupling between the monitoring antenna and the sensing structures. Specifically, an impedance analyser is used to monitor the impedance across the antenna, thereby deriving the ϵ_r -induced resonant frequency variation of the RF-based sensing structure. The operation process between the monitoring antenna and sensing structure can be illustrated by Fig. 13 and the following equation [32, 40]:

$$Z_T = \frac{\omega^2 M^2}{Z_2}, \tag{12}$$

where Z_T is the impedance across the monitoring antenna, Z_2 is the impedance of the sensing structure, M is the mutual inductance coupling coefficient and ω is the angular frequency. V_{12} and V_{21} are the coupling introduced voltage source for the

Fig. 13 Model of the impedance monitoring method



antenna and the sensing structure, respectively as shown in Fig. 13. Z_1 is the intrinsic impedance of the monitoring antenna, which can be eliminated by the background-abstraction routine presented in [41].

As can be seen from Eq. (12), the impedance of the monitoring antenna is proportional to the operating frequency (ω) and inversely proportional to the impedance of the sensing structure (Z_2), both of which are permittivity-dependent parameters. Therefore, by monitoring the change of Z_T at the antenna side, the permittivity values around the sensing structure can be derived.

7 Conclusion

Following extensive studies on microwave behaviours of both soft and flexible materials, wireless sensing systems have been proposed for BANs because they offer the advantages of tetherless operation and lower power consumption as compared to conventional sensor nodes. This chapter reviewed wireless sensing systems designed for the purpose of monitoring human physiological parameters and bodily movements. A typical wireless sensing system consists of a sensing structure which is a passive RF structure capable of the sensing, and a circuit or device for detecting or interpreting the signal output of the sensing structure. Wireless sensing systems have been widely used for the applications such as body temperature sensing, pressure/strain sensing, sweat analysis and gesture monitoring.

There exist several approaches to fabricate a RF-based sensing structure. Most of these existing structures are realised by relating the variation of the resonant frequency (f_0) of the designed RF structure with the properties of the sensed phenomenon. This is because this approach has relatively simple operating principles, and has been successfully implemented for sensing applications other than BANs. Normally the antennas and LC tank circuits are the common structures used as the sensing structures. Both types of structures can be fabricated, printed or etched on the dielectric substrates, and with the help of some special characteristics of the substrates, the sensing structures could be used to detect physical changes in their operating environments. Two data detection and interpretation techniques for RF-based sensing structures were also introduced.

Another commonly seen application of wireless sensing systems is the use of antennas as sensors to monitor human gestures or bodily movements. The received signal parameters such as TOA, can be used to detect the relative movements of human limbs with an accuracy of up to 2–3 cm.

However, most of the sensing structures developed thus far still rely on conventional rigid conductors (e.g. copper and aluminium) and fabrication methods (e.g. etching and milling). Future work may focus on soft conductive materials (e.g. conductive threads and inks), and their use in fabrication of soft wireless sensing systems using methods such as weaving and printing so that they could be easily integrated into wearable apparels for future BAN applications.

References

1. M. Chen, S. Gonzalez, A. Vasilakos, H. Cao, V.C. Leung, Body area networks: a survey. *Mob. Netw. Appl.* **16**(2), 171–193 (2011)
2. M.U. Talha, J. Ahmad, Body area networks (BANS)—an overview with smart sensors based telemedical monitoring system. *Int. J. Comput. Appl.* **84**(8), 20–23 (2013)
3. A.J. Martin, Sensors and computing systems in smart clothing, in *Smart Clothes and Wearable Technology*, ed. by J. McCann, D. Bryson (Elsevier, Ch, 2009), p. 9
4. M.A. Hanson, H.C. Powell Jr., A.T. Barth, K. Ringgenberg, B.H. Calhoun, J.H. Aylor, J. Lach, Body area sensor networks: challenges and opportunities. *Computer* **1**, 58–65 (2009)
5. H. Huang, Flexible wireless antenna sensor: a review. *IEEE Sens. J.* **13**(10), 3865–3872 (2013)
6. J. McCann, D. Bryson (eds.), *Smart Clothes and Wearable Technology* (Elsevier, 2009) (Chapter 9)
7. X. Lin, B.C. Seet, F. Joseph, Fabric antenna with body temperature sensing for BAN applications over 5G wireless systems, in *2015 9th International Conference on Sensing Technology (ICST)* (pp. 591–595). IEEE, 2015, Dec
8. Y. Huang, W. Dong, T. Huang, Y. Wang, L. Xiao, Y. Su, Z. Yin, Self-similar design for stretchable wireless LC strain sensors. *Sens. Actuators A* **224**, 36–42 (2015)
9. Z. Wang, L.Z. Lee, D. Psychoudakis, J.L. Volakis, Embroidered multiband body-worn antenna for GSM/PCS/WLAN communications. *Antennas Propag. IEEE Trans.* **62**(6), 3321–3329 (2014)
10. V.K. Varadan, P.T. Teo, K.A. Jose, V.V. Varadan, Design and development of a smart wireless system for passive temperature sensors. *Smart Mater. Struct.* **9**(4), 379 (2000)
11. W. Buff, S. Klett, M. Rusko, J. Ehrenpfordt, M. Goroli, Passive remote sensing for temperature and pressure using SAW resonator devices. *Ultrason. Ferroelectr. Freq. Control IEEE Trans.* **45**(5), 1388–1392 (1998)
12. J.R. Humphries, D.C. Malocha, Wireless SAW strain sensor using orthogonal frequency coding. *Sens. J IEEE* **15**(10), 5527–5534 (2015)
13. X. Ren, X. Gong, A wireless sensing technique using passive microwave resonators, in *Antennas and Propagation Society International Symposium, 2008. AP-S 2008*. IEEE (pp. 1–4). IEEE (2008, July)
14. R. Warty, M.R. Tofghi, U. Kawoos, A. Rosen, Characterization of implantable antennas for intracranial pressure monitoring: reflection by and transmission through a scalp phantom. *Microwave Theory Tech. IEEE Trans.* **56**(10), 2366–2376 (2008)
15. R. Salvado, C. Loss, R. Gonçalves, P. Pinho, Textile materials for the design of wearable antennas: a survey. *Sensors* **12**(11), 15841–15857 (2012)
16. Y. Ouyang, W.J. Chappell, High frequency properties of electro-textiles for wearable antenna applications. *Antennas Propag. IEEE Trans.* **56**(2), 381–389 (2008)
17. X. Huang, Y. Liu, K. Chen, W.J. Shin, C.J. Lu, G.W. Kong, et al., Stretchable, wireless sensors and functional substrates for epidermal characterization of sweat. *Small* **10**(15), 3083–3090 (2014)
18. H.A. Toprakci, T.K. Ghosh, Textile sensors, in *Handbook of Smart Textiles* (2015), pp. 357–379
19. J. Virtanen, L. Ukkonen, T. Björninen, A.Z. Elsherbeni, L. Sydanheimo, Inkjet-printed humidity sensor for passive UHF RFID systems. *Instrum. Meas. IEEE Trans.* **60**(8), 2768–2777 (2011)
20. K.G. Ong, *Design and Application of Planar Inductor–Capacitor Resonant-Circuit Remote Query Sensor*, Dissertation, University of Kentucky, 2000
21. J. Fernandez-Salmeron, A. Rivadeneyra, M.A. Carvajal Rodriguez, L.F. Capitan-Vallvey, A. J. Palma, HF RFID tag as humidity sensor: two different approaches. *Sens. J. IEEE* **15**(10), 5726–5733 (2015)

22. K.J. Loh, J.P. Lynch, N.A. Kotov, Inductively coupled nanocomposite wireless strain and pH sensors. *Smart Struct. Syst.* **4**(5), 531–548 (2008)
23. D.M. Pozar, *Microwave Engineering* (John Wiley & Sons, 2009) (Chapter 6)
24. L.Y. Chen, B.C.K. Tee, A.L. Chortos, G. Schwartz, V. Tse, D.J. Lipomi, et al., Continuous wireless pressure monitoring and mapping with ultra-small passive sensors for health monitoring and critical care. *Nat. Commun.* **5** (2014)
25. F. Molina-Lopez, D. Briand, N.F. De Rooij, All additive inkjet printed humidity sensors on plastic substrate. *Sens. Actuators B Chem.* **166**, 212–222 (2012)
26. A. Daliri, A. Galehdar, S. John, C.H. Wang, W.S. Rowe, K. Ghorbani, Wireless strain measurement using circular microstrip patch antennas. *Sens. Actuators A* **184**, 86–92 (2012)
27. Fabric Antenna Sensors, Sylvia Herbert, Sep 2016. Available at <http://sylviaherbert.com/fabric-antenna-sensors-1/>
28. J.W. Hearle, W.E. Morton, *Physical Properties of Textile Fibres* (Elsevier, 2008) (Chapter 21)
29. S. Amendola, R. Lodato, S. Manzari, C. Occhiuzzi, G. Marrocco, RFID technology for IoT-based personal healthcare in smart spaces. *Internet Things J. IEEE* **1**(2), 144–152 (2014)
30. L. Rosengren, P. Rangsten, Y. Bäcklund, B. Hök, B. Svedbergh, G. Selén, A system for passive implantable pressure sensors. *Sens. Actuators A* **43**(1), 55–58 (1994)
31. G.D. Alley, Interdigital capacitors and their application to lumped-element microwave integrated circuits. *Microwave Theory Tech. IEEE Trans.* **18**(12), 1028–1033 (1970)
32. K.G. Ong, C.A. Grimes, C.L. Robbins, R.S. Singh, Design and application of a wireless, passive, resonant-circuit environmental monitoring sensor. *Sens. Actuators A* **93**(1), 33–43 (2001)
33. W. Honda, S. Harada, T. Arie, S. Akita, K. Takei, Wearable, human-interactive, health-monitoring, wireless devices fabricated by macroscale printing techniques. *Adv. Funct. Mater.* **24**(22), 3299–3304 (2014)
34. J. Yoo, L. Yan, S. Lee, Y. Kim, H.J. Yoo, A 5.2 mw self-configured wearable body sensor network controller and a 12 w wirelessly powered sensor for a continuous health monitoring system. *Solid-State Circ. IEEE J.* **45**(1), 178–188 (2010)
35. D. Zhang, F. Xia, Z. Yang, L. Yao, W. Zhao, Localization technologies for indoor human tracking, in *2010 5th International Conference on Future Information Technology (FutureTech)* (pp. 1–6). IEEE (2010, May)
36. R. Bharadwaj, A. Alomainy, C. Parini, Numerical investigation of body-worn ultra wideband antenna localisation techniques for motion capture applications, in *Session 3A7b SC4: Body-centric Wireless Communications*, vol. 989 (2013)
37. R. Bharadwaj, C. Parini, A. Alomainy, Experimental investigation of 3-D human body localization using wearable ultra-wideband antennas. *Antennas Propag. IEEE Trans.* **63**(11), 5035–5044 (2015)
38. R. Bharadwaj, A. Alomainy, C. Parini, Study of Ultra wideband localisation techniques using various monitoring configurations, in *2012 6th European Conference on Antennas and Propagation (EUCAP)* (pp. 2035–2038). IEEE (2012, March)
39. C. Occhiuzzi, S. Caizzzone, G. Marrocco, Passive UHF RFID antennas for sensing applications: Principles, methods, and classifications. *Antennas Propag. Mag. IEEE* **55**(6), 14–34 (2013)
40. P.J. Chen, S. Saati, R. Varma, M.S. Humayun, Y.C. Tai, Wireless intraocular pressure sensing using microfabricated minimally invasive flexible-coiled LC sensor implant. *Microelectromech. Syst. J.* **19**(4), 721–734 (2010)
41. K.G. Ong, J.S. Bitler, C.A. Grimes, L.G. Puckett, L.G. Bachas, Remote query resonant-circuit sensors for monitoring of bacteria growth: application to food quality control. *Sensors* **2**(6), 219–232 (2002)

Radio Frequency Sensing for Assistive Monitoring

Yau Hee Kho

Abstract With the abundance of ubiquitous transmission of wireless signals nowadays due to the proliferation of wireless devices, these *man-made* radio frequency signals in the form of electromagnetic waves can be exploited in various forms, for example localization and tracking. Here, we describe how these signals can be used in sensing an object or human in the environment. We describe the design concept and implementation of an indoor *passive* tracking system that utilises an array of Wi-Fi transceivers, and without any electronic device or tag attached to the object being tracked. The sensing of an object or a person described here is made possible by exploiting the fundamental characteristic of signal attenuation due to blocking, i.e. shadowing, that is prevalent in a typical wireless communication system. By detecting significant signal attenuation in the system (i.e. by measuring the received signal strength value), it is possible to infer that an object is blocking the line-of-sight (LOS) link in a transceiver set and therefore transforming the existing hardware configuration into a proximity sensor network.

1 Introduction

Assistive technology such as location-based and location-aware services are increasingly gaining momentum due to the wide spread proliferation of smart mobile devices. Owing to this, wireless sensor networks (WSN) are becoming popular in sensor technology due to its ease of installation and flexibility in term of element placement [1]. Such networks are of particular use in object positioning and tracking—effective deployment of low cost and low energy sensing devices is attractive in the implementation of localization and ranging techniques [2]. Knowing such information is important in many fields, for example in military, security, medical, surveillance, etc. [3, 4].

Y.H. Kho (✉)
Nazarbayev University, Astana, Kazakhstan
e-mail: yauhee.kho@nu.edu.kz; yhkho@ieee.org

According to [5] and the references therein, localization of objects can be achieved in either physical or virtual domain, i.e. to determine the object position in the real or online world. The physical locations can be further categorized into the following types: descriptive, network and spatial locations [6].

The physical localization systems can be used for object positioning for both outdoor and indoor tracking. Probably one of the most well-known outdoor localization techniques is the Global Positioning System (GPS), which is widely implemented in modern mobile devices. Concurrently, numerous indoor localization techniques are being proposed, investigated and implemented as well [5]. While outdoor tracking using GPS technology is popular, the study on indoor tracking [7] remains as a challenge and largely conceptual due to significant attenuation of satellite signals caused by buildings, furniture, obstacles, etc.

These tracking systems can also be categorized as tag-based and tag-free (or quite similarly device-based and device-free). Systems such as GPS, radio frequency identification (RFID) and real-time location systems (RTLS) require a special device to be attached to or carried by an object to be tracked. On the other hand, the systems that do not require any device or tag to locate an object are called passive or device-free localization systems, abbreviated as DFL systems.

Indoor location tracking, contrary to an outdoor-based system, has two categories of research due to the nature of deployment limit that is confined to a closed site. The first category is the “active tracking strategy” that mostly mimic an outdoor tracking (e.g. GPS) where a subject/object is required to carry a device/tag that could either calculate its own position based on a series of signal detection from the surroundings or by transmitting signals that may be collected by some probing stations in the surroundings. One of the more prominent examples in this field is radio frequency identification (RFID) technology used in factory automation and integration, smart parking lot access, airline baggage identification, etc. The RADAR [8] and LANDMARC [9] projects are some of the efforts previously attempted in realising indoor tracking system using such configuration.

The other category of indoor tracking, which is the focus of this paper, is known as the “passive tracking strategy”. This strategy has an interesting feature where the emphasis is on a tagless (i.e. device-free) approach. Apart from that, the tracking system will be transparent to the subject being tracked, which means that the tracking activity will not be known to the subject a priori. Scenarios that make use of a passive approach are plentiful. Due to the anonymity in the tracking data, it is useful to deploy such a system in locations where the privacy of the subject cannot be violated, while at the same time, the observation is only required for monitoring purposes. Another advantage for this type of system is the convenience of deployment from the observer’s point of view because tracking tags/devices are not required.

Taking an example of customers in a departmental store, it is possible to monitor their visiting pattern in the store layout. The identity of the customers is not important but it could be useful to know the “hotspot” of the store so that relevant sales activities or try out events can be positioned at a more strategic location. This is possible without requiring the customers to carry some sort of awkward devices

when visiting and there is no issue of identity disclosure. Other possible deployment of a passive tracking system could be old folks home, museum, etc.

2 Sensors for Device-Free Localization

There are numerous types of wireless sensor networks that can be used for localization and tracking purposes. As was outlined by Wilson [10], positioning can be performed by employing various sensing technologies or a combination of some of them depending on the desired application, as shown in Fig. 1. A brief description of each technique is provided next.

Thermal Cameras: This type of sensing technology incorporates thermal sensor to detect the changes in temperature of the environment thus locating the object. Its main advantage is that it can detect and track the object in poor-visibility conditions, and the drawback is that thermal cameras are usually expensive, have limited view angles and require high bandwidth.

Optical Cameras: This technology is probably the most commonly used in the sensor networks to detect objects. It enables not only determining the location of an object, but also to visually observe its actual movement, thus ensuring high accuracy and efficiency. However, opaque obstructions of the line of sight of optical cameras or smoke, for example, severely undermine the effectiveness of systems implementing such kind of sensors. One way to overcome this is to use omnidirectional view sensors, where a 360° of field of view will be possible [11–13].

Infrared Cameras: These cameras work similarly to the optical cameras, but can sense a wider range of the light frequencies, namely infrared band frequencies that are invisible for optical cameras. Thus, employing such sensors enables night vision. However, similar drawbacks of the optical cameras such as considerable associated costs, limited view angle and bandwidth issues are characteristic to the infrared cameras.

Acoustic, Vibration and Ultrasound Sensors: Another sensing technique that can be implemented to perform DFL is based on the air pressure variation sensing. Acoustic sensor networks are able to detect the sound waves traveling in the space by installing series of microphones in an environment. Vibration sensor networks

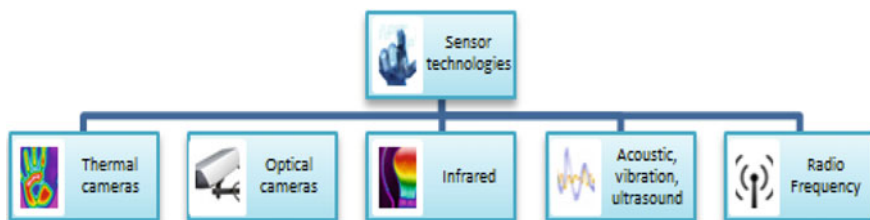


Fig. 1 Sensor technologies for device-free localisation

work similarly but consider vibration sensors. Finally, the ultrasound sensors are able to detect the sounds inaudible by a human ear by emitting an ultrasound wave and estimating various parameters of the received signal.

Radio Frequency: This type of sensing incorporates sensors working on radio frequency. It can be various wireless signals such as Bluetooth, ZigBee, WLAN, etc. According to [5] and the references stated therein, a human intruding the radio frequency wireless signal (which frequency is 2.4 GHz), attenuates it by absorbing part of the signal waveform, because the human body consists for more than 70 % of water which resonant frequency is 2.4 GHz as well. Thus, radio frequency sensing networks can be sufficient to perform localization and tracking of human objects. Various technologies are developed for this particular type of sensor networks; these would be described in more details in subsequent section.

3 Radio Frequency Based Techniques

Most of the literatures reviewed state that there are three main techniques developed thus far in this field: location fingerprinting (scene analysis), proximity and triangulation. These approaches will be described next.

Location Fingerprinting (Scene Analysis): Location fingerprinting method consists of two main parts known as offline and online stages. As [14] describes, “fingerprinting, pattern recognition or pattern matching” is performed during the first offline stage to create a map of monitored area using RSS reference values along wireless links. If any change is done to the static monitored environment, a new radio map should be created. During the online stage, real-time measurements of deteriorated RSS are compared to the radio map that was created. An object could be detected using various probabilistic frameworks, which correlate distance from receiver with signal strength and lessen the effect of random noise on the measured effect. As outlined in [7], there are at least five algorithms developed up to that time that implement fingerprinting: probabilistic methods, k-nearest-neighbour, neural networks, support vector machines, and smallest-vector polygon.

Proximity: The method of proximity estimation implies introducing a number of antennas each located at a known position. When an object enters the grid formed by these antennas, it will be closest to one of them (based on the signal received by the antenna from the mobile target)—thus the name ‘proximity’. Modern systems based on radio frequency methods such as Cell-ID often implement this simple technique.

Triangulation: “Triangulation uses the geometric properties of triangles to estimate the target location. It has two derivations: lateration and angulation” [7]. According to [2, 5, 7], the following metrics are used in this method (thus there are corresponding subdivisions of the technique):

- Received Signal Strength Indicator (RSSI),
- Time of Arrival (TOA)/Time Difference of Arrival (TDOA),
- Angle of Arrival (AOA) or Direction of Arrival (DOA)

A review of the RSSI method will be described here.

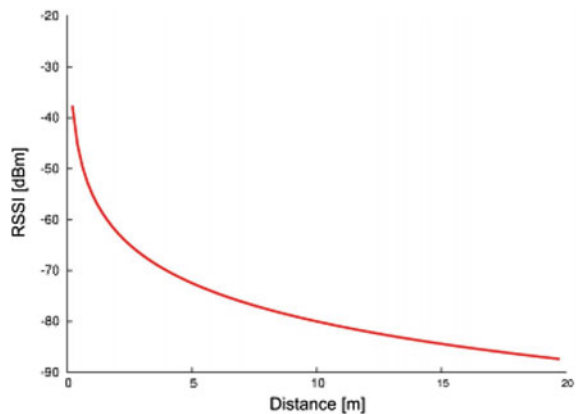
3.1 RSS-Based Method

The signal waveform has particular signal parameters when received at the destination node. One of such parameters is a power content, indicated by a value called RSS—Received Signal Strength. It also can be referred to as RSSI which stands for Received Signal Strength Indicator and, as the name suggests, indicates the relative value of the received signal strength. RSS is often a negative value expressed in dBm and it is the actual value of the received signal power. This parameter is intuitively simple for understanding: the larger the value of the RSS is, the stronger the signal received is (i.e. the power content is larger), and vice versa. The RSS values can be easily obtained from captured packets, thus this method requires no additional hardware. Various values of RSS and power are determined by the attenuation and fading a signal undergoes when traveling from the source port to the destination sink. Thus, it is logical to infer that a smaller RSS value implies a greater distance between a transmitter and a receiver.

According to the experimental measurements of the studies performed by Fang et al. [1], Heurtefeux and Valois [2], Hossen et al. [4] and many others, RSS values have logarithmic dependence on the distance between the receiver and transmitter. The graph illustrating the general expected trend of RSS with distance between transmitter and receiver is presented in Fig. 2.

The direct signal propagation for an indoor environment in Fig. 2 follows the free space model according to the Friis' transmission formula as shown in Eq. (1).

Fig. 2 The expected relationship between RSSI and distance [2]



$$P_R = \frac{P_T G_T G_R \lambda^2}{4\pi R^2} \quad (1)$$

where P_T and P_R are the transmit and receive power levels, G_T and G_R are the gains of the transmit and receive antennae, λ is the wavelength of the RF signal, and R is the distance between the transmit and receive antennae in meters.

Investigation by Hossen et al. [4] claim that human body's resonant frequency (due to its water content) is the same as RF signals frequency. Thus it is expected that the value of RSSI will vary when there is an object on the line of sight (LOS). When an object enters the path of wireless signal transmission, it creates additional factors that attenuate the signal—some of its power is absorbed by the object, some part of it is being reflected and thus amplified when superimposed with other signals in phase and canceled out or faded when superimposed out of phase. The effects contributing to the attenuated received signal are expressed mathematically in the following equation adapted from [10]:

$$Y(t) = P(t) - S(t) - F(t) - L - v(t) \quad (2)$$

where $Y(t)$ is the RSS in dBm, $P(t)$ is the undisturbed transmitted power in dBm, $S(t)$ is the shadowing loss in dBm due to objects, $F(t)$ is the fading loss in dBm that occurs from constructive and destructive interference of narrow-band signals in multipath environments, L is the static losses in dBm due to distance, antenna patterns, device inconsistencies, etc., and finally, $v(t)$ is the measurement noise.

Human body in the LOS of the link should theoretically increase shadowing losses significantly allowing the detection of the intruder. From this, it is assumed that basing on the values of RSS at the receiver the position of an object can be determined. The RSS-based method has gained popularity over the years due to its implementation and estimation simplicity, and energy and cost efficiency [3] and [15], but in recent years, this technique is being subject to constructive criticism for its drawbacks and instabilities. For example, the study by Heurtefeux and Valois [2] tested the efficiency and robustness of RSS-based localization method on three independent wireless networks and came to a conclusion that “RSSI-based localization in real environment and using standard sensors is not enough accurate” [2]. The study of these authors showed that “the localization error obtained with RSSI is close to 2 m when the localization error obtained with Euclidean distance is less than several centimeters” meaning that RSS-based method may not be the best localization algorithm due to its low accuracy.

There are several modern research works with the focus of study on improving the performance of RSS-based localization techniques. A recent research performed by Sahu et al. [3] proposes an alternative approach for object positioning using RSSI values—Dual RSSI Trend (DuRT) based localization. This technique considers the trend of RSSI values obtained from beacons to estimate the position of sensors. Two RSSI maximum points are estimated upon establishment of the RSSI-to-distance relationship enabling calculating the sensor position from

intersection point of the perpendiculars to the two maximum RSSI trajectories. As the authors state, this approach can significantly increase the accuracy of the RSSI-based localization.

The most recent research by Guo et al. [16] addresses the inconsistency and unpredictability issues in the change of RSS of the link due to the multipath interferences by developing the Exponential-Rayleigh model. As the name suggests it consists of two parts combined: large-scale exponential model and small-scale Rayleigh model. The latter part depicts the target-produced multipath components. One of the main findings of the group was that constructive fading noticed in the RSS values in the indoor environment is due to the reflection waves. The model proposed by the authors was experimentally justified to improve the performance of localization algorithm.

4 Radio Frequency Sensing

The technique proposed in this chapter uses Wi-Fi signal to achieve a passive tracking system [17, 18]. It exploits the phenomenon of radio frequency (RF) signal attenuation due to obstacle blockage [19, 20]. In particular, when an obstacle (e.g. a human) position itself between two Wi-Fi communication points (e.g. a router and a receiver), the attenuation in the received signal strength (RSS) value in the data packet will reflect the presence of the obstacle.

Wi-Fi signal that operates in the 2.4 GHz radio frequency band is a type of electromagnetic wave that interacts with the environment, and undergoes reflection, refraction and diffraction. From time to time, as it is blocked by objects in its transmission path, a phenomenon called shadowing will result in an attenuation of the received signal at the receiver's end. Such an occurrence, known as large-scale fading, is a critical issue in wireless telecommunication system as the effect is detrimental to the bit-error-rate (BER) performance of the system [21].

Another issue for an indoor environment is the small-scale fading that, for instance, resulted from multipath propagation which causes instantaneous fluctuations in the received signal level [21]. The multipath interferences could be either constructive or destructive to the main line-of-sight (LOS) component. Consequently, it may no longer be straightforward to observe a signal drop due to shadowing as compensations may come from those multipath propagations. Attempts on radio signal propagation modelling for an indoor environment is also a non-trivial work due to site-specific parameters such as floor layout, moving objects, and numerous reflecting surfaces [19, 22].

Wireless local area network (WLAN) operating in the Industrial, Scientific and Medical (ISM) band is a very common infrastructure found in public hotspots and enterprise location monitoring. Furthermore, as it has a dominant standard as outlined in the IEEE 802.11 specifications, it becomes appealing if existing WLAN infrastructure can be converted to support an indoor tracking system [7] as deployment cost can be kept to a reasonable, if not minimal, level.

The foundation of WLAN-based tracking and location estimation system relies mostly on the RSS value. The RADAR system [8] proposed by Microsoft research group was among the more significant work in the field of indoor position tracking research. In that proposal, 3 desktop computers were used as Wi-Fi access points (APs) and a laptop as a transceiver unit. The laptop was tracked as the target object in a typical indoor environment. Youssef et al. also [19] reported their research on tag less localisation using a wireless network. In their investigation on the variance of RSS value in a WLAN, an experiment was conducted with the purpose of detecting the motion of an object and subsequently its location using a manually trained look-up table.

On the other hand, our investigation on a passive indoor system relies on the fundamental concept of LOS link blocking as a proximity sensing in a WLAN as illustrated in Fig. 3. We also looked into the feasibility of our strategy in terms of object tracking.

5 Initial Measurement

The proposed concept was verified using two modem routers (TD-W8901G Wireless ADSL2+ Modem Router) that operate at a frequency of 2.4 GHz to function as transmitters, and a Wi-Fi USB adapter (TL-WN321G wireless USB Adapter) to function as a probing station.

The data was processed using a freeware called “inSSIDer” [23] installed on a Toshiba NB305 laptop. “inSSIDer” is a Wi-Fi data acquisition tool that is able to extract the RSS values from Wi-Fi data packets and present the data in graphs for easier visualisation. The configuration of the modem routers and the wireless USB adapter is shown in Fig. 4. All devices were placed at a height of 85 cm above the floor.

Fig. 3 Conceptual illustration of the proposed indoor location tracking technique

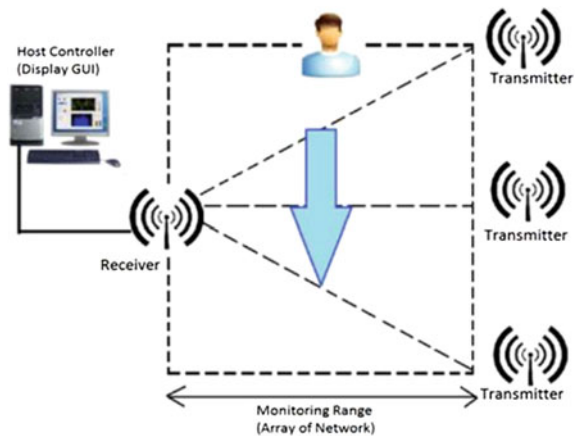
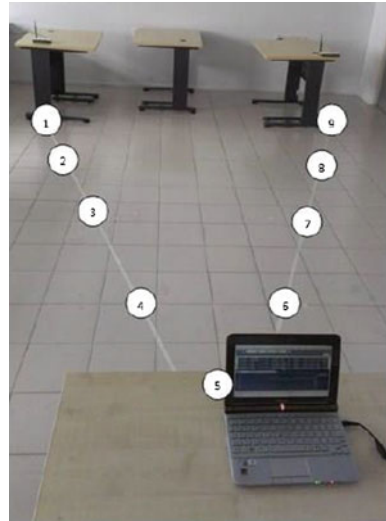


Fig. 4 Transceivers setup for testing and measurement



Observations on the signal attenuation on the transmission links between the modem routers and the Wi-Fi USB adapter were made by having two persons of different body sizes (see Table 1) standing on designated spots as shown in Fig. 4.

From the technical specifications of the modem routers, it is calculated that the theoretical unobstructed RSS value should be -33 dBm at a distance of 5 m. Table 2 shows that the theoretical calculations corresponded well with the measured values (between -33 dBm and -31 dBm). For the readers’ information, test spots 1–4 should block signal from the left router modem, test spots 6–9 block the right modem router whereas test spot 5 should block both.

Table 3 shows the signal attenuation calculated from the raw data shown in Table 2. It can be observed that the drop in RSS is at least 6 dB, with an average of 11.5 dB. Multipath propagation seems to have little effect in the test scenario which could mean that the compensation is less significant as compared to the signal loss incurred from a direct block of LOS. Apart from that, it also appeared that body size does not incur any significant observable difference in the attenuation level.

A screenshot of the “inSSIDer” software is shown in Fig. 5. It depicts a continuous observation on the RSS value where negative spikes indicate when a test subject was moving from test point 2 to 8. This condition confirms the feasibility of the proposed passive tracking system but nevertheless with limitation on the tracking speed. In any case if the test subject is moving faster than the scanning rate of the receiver/software, it is possible that the motion will not be detected by the system.

Table 1 Characteristics of the subject used in the testing

	Subject 1	Subject 2
Height (cm)	180	158
Size	Large	Medium

Table 2 Raw RSS value in dbm from modem router 1 and 2 when subject interferes at the various test spots as shown in Fig. 4

Test spot	Left router RSS (dBm)		Right router RSS (dBm)	
	Subject 1	Subject 2	Subject 1	Subject 2
1	-33	-33	-43	-47
2	-33	-31	-43	-47
3	-33	-31	-41	-45
4	-33	-30	-39	-45
5	-43	-47	-47	-47
6	-41	-45	-31	-31
7	-39	-43	-31	-33
8	-41	-43	-29	-33
9	-41	-43	-29	-33

Table 3 RSS attenuation in db from modem router 1 and 2 as deduced from Table 2

Test spot	Left router Att. (dB)		Right router Att. (dB)	
	Subject 1	Subject 2	Subject 1	Subject 2
1	0	0	12	14
2	0	0	12	14
3	0	0	10	12
4	0	0	8	12
5	10	16	16	14
6	8	14	0	-2
7	6	12	0	0
8	8	12	-2	0
9	8	12	-2	0

To determine the proposed system's sensitivity to detect a human's presence and motion, a person was walking through the midpoint of LOS of a single link at a speed of 1, 1.6 and 2 m/s. These particular paces were chosen as it was outlined in the study by Browning et al. [25], Levine and Norenzayan [26] that the average speed of walking at which people feel comfortable is 1.6 m/s, thus it was decided to refer to it as normal/medium, whereas for the speed of 1 m/s as low and for the speed of 2 m/s as fast walking speeds. It can be seen clearly from Fig. 6 that walking speed does indeed affect the length of deep attenuation period.

6 Prototype Development

The subsequent stage of the work was to produce a working prototype. After some review, it was found that with C Sharp (C#) programming language and the .NET framework [24], data from "inSSIDer" can be extracted directly. The relevant



Fig. 5 Screenshot of the “inSSIDer” showing 2 obvious drops in the signal strength level when the respective LOS was blocked by a test subject

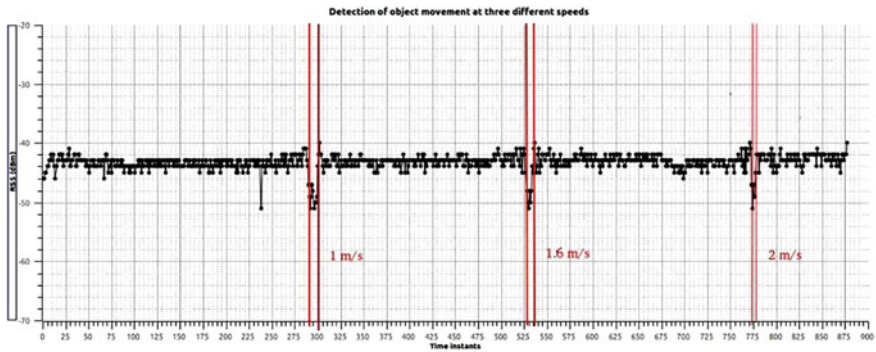


Fig. 6 Detection of object movement crossing single Tx-Rx link at three different speeds

development duration for a graphical user interface (GUI) was also relatively fast and convenient. For ease of testing, we fixed the positions of the modem routers and the Wi-Fi USB adapter as shown in Fig. 7.

The prototype GUI has an interface as shown in Fig. 8. The right panel has 8 squares corresponding to the actual environment in Fig. 7 where the relevant square will be highlighted whenever an obstacle moves into the LOS of the router modems. Prior to the commencement of the procedure, the proposed system will acquire the average RSS values from all router modems. This action is initiated by pressing the “get average” button. Subsequently, by using the average values and the empirical thresholds found in Sect. 3, as soon as one of the RSS values drops below

Fig. 7 Controlled environment for the prototype testing

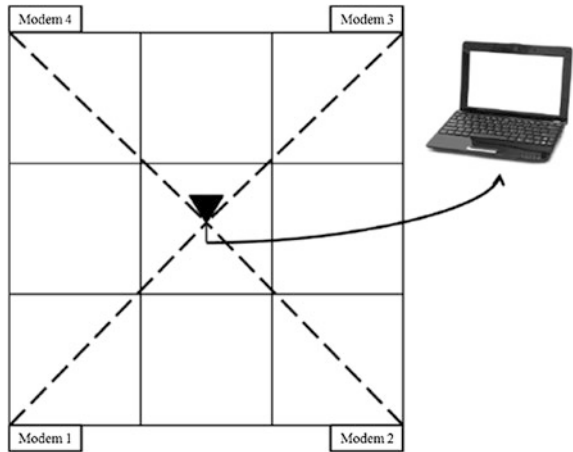
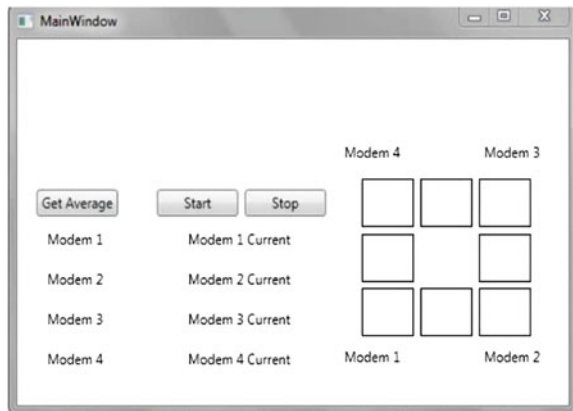


Fig. 8 GUI of the prototype software



5 dB from their average, the obstacle is considered to be detected and the relevant square gets highlighted accordingly. Figure 9 shows a demonstration on the working principle of the prototype.

The aforementioned prototype was a sandbox for the proof of concept but nevertheless suffered from several shortcomings. One of them is the refresh rate of “inSSIDer” that is at a mere 1 Hz. The other one being the observable random fluctuations that exist in the RSS values obtained. This condition is undesirable as the fluctuations may rapidly trigger on and off a detection while in actual fact a subject could be just standing idly on a LOS link. Finally, there is a lack of flexibility to reconfigure the position of each router modem. The GUI software needs to be recompiled every time the layout of the environment is changed, in order to reflect the new layout.

An improved implementation of the proposed passive tracking system is designed to address the aforementioned issues. We opted for a solution using

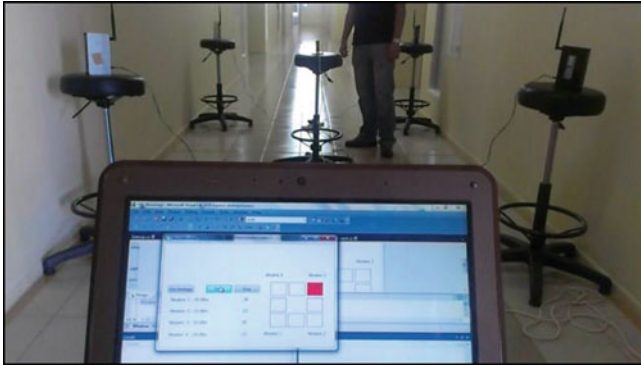


Fig. 9 A demonstration on the prototype GUI. As a subject passes through one of the LOS links, the corresponding square in the GUI gets highlighted

“nl80211” library [27] that works under GNU/Linux operating system. With “nl80211”, it is possible to have native communication to the wireless USB adapter without relying on another proprietary software such as “insider”. In addition, empirical observation has shown that the scanning rate can be increased to at least 3 Hz by requesting a restrained Wi-Fi frequency channel scanning via “nl80211”.

The false triggering due to random fluctuations in the RSS values is eliminated using a hysteresis triggering scheme similar to a Schmitt trigger in an electronic system.

In a simple definition, the threshold setting for both the on and off detection is configured at two different values so that when a subject is under detection, minor signal fluctuations will not cause the trigger that falsely indicates the subject is leaving. Figure 10 illustrates the operation of such a mechanism.

The final GUI of the proposed passive tracking system is depicted in Fig. 11. The interface can be basically split into three panels. The left panel is for setting the various configurations available to the tracking operation. The more significant settings being the refresh rate of scanning and the configuration for the router

Fig. 10 Small fluctuations can be remedied by having two different threshold values for on and off trigger

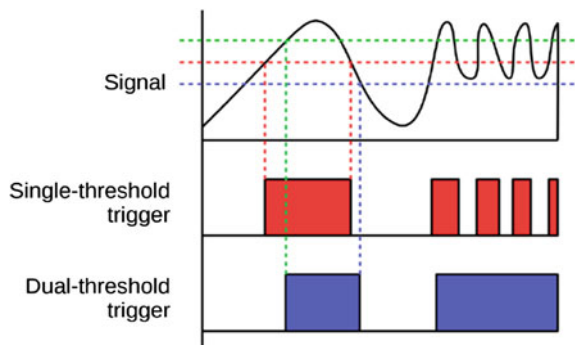
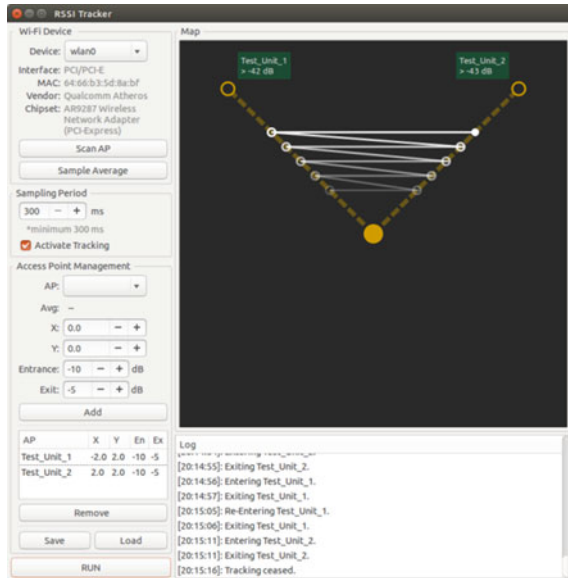


Fig. 11 The final GUI of the proposed passive tracking system



modem's positioning. As it has been stated about the inflexibility of the initial prototype, this final GUI allows user to configure the layout of the modems' position and sensing threshold of each router modem, and save it as a file for future use. The bottom right of the GUI features a log that records all the user's interaction to the GUI and all relevant tracking activity.

The most prominent feature of the GUI software is the map on the top right panel. The software will indicate the router modems as hollow circles and the probing station (e.g. the USB adapter) as a solid circle. Dashed lines are drawn from the USB adapter to the router modems to illustrate the LOS. A white dot will be displayed on the corresponding LOS as soon as a subject is detected. As time passes and the subject is found moving around, the accumulated tracking points will be shown as a white fading trail with the most opaque one being the latest position.

7 Discussion

The investigations have validated the feasibility in exploiting Wi-Fi signal as a proximity sensor. This can be used as a surveillance system to detect a human or moving object without requiring any a priori tag or device. Consequently, it alleviates any concern on privacy issues when, for example, a camera would have been used. As we have found out, the layout of the router modems is one of the major factors influencing the overall performance of the system. Although one of the advantages of the proposed system is to utilise the existing hardware, the effectiveness of sensing may be affected if a router modem is placed at a far-away

distance. More access points might be required in case the existing ones are not sufficient to provide sufficient tracking. These concerns will be further investigated in the future.

Although currently the refresh rate of scanning an object is three times faster than the initial prototype, a more rapid refresh rate is still desirable. At the current rate of 3 Hz, the system is likely to miss a detection if the subject is walking at a faster speed, e.g. brisk walking. Besides this, the refresh rate is also complicated by the number of access points to be processed where the processing time will be longer as the number of access points increase, which further slows down the refresh rate. However, with the use of “libnl”, the bottleneck now lies with the speed of the Wi-Fi USB adapter itself. Therefore, it may be necessary to design customised receivers for the proposed system.

The continuous tracking described in the proposed system is currently restricted to a single target. When more than one subject enters the monitored environment, they can still be detected although they may create confusion in tracking as their identities will not be known. In practice, it is still possible to track multiple targets simultaneously as long as the subjects are not too close to one another (e.g. not on the same LOS link). In such situation the system can still be used to count the number of people or estimate the concentration of people within the environment. In the subsequent phase of this project, statistical signal processing method using a probabilistic model will be employed to achieve better detection and tracking.

In general, several spatio-temporal aspects of object/human-sensing [28] can be analysed through the proposed radio frequency technique.

Presence: *is there at least an object or a person present?*

This is perhaps the most critical question to be answered for real-world monitoring purposes. Fluctuation in radio frequency signal in indoor environment is notoriously tricky due to multipath propagations. Even without a person, the RSS is constantly fluctuating randomly. In all the experiments, however, we can confidently demonstrate that the presence can be detected.

Count: *how many persons are there?*

This can be accomplished although at the moment the proposed system can only detect a group of people, rather than differentiating each individual.

Location: *where is each person?*

The localization ability depends on the density of the transmit and receive LOS pair; the more such LOS links there are, the higher the resolution of the localization. Alternately, probabilistic method using mathematical modelling and statistical signal processing can be used to enhance the localization capability.

Track: *where is this person going?*

This depends on the density of the LOS pair, as well as the speed of the person. As demonstrated, tracking is possible with normal walking speed. Beyond that, the refresh rate of the system needs to be increased to capture the RSS variation due to movement.

Identity: *who is this person?*

The proposed system is not able to identify the person because it is a device-free system. In order to enable identification, the person must carry a device that is in communication with the server. Alternately, perhaps a person can be identified through the disturbance of the RSS pattern of the overall system. As mentioned, water content in human body can affect the RSS, so different person may have a different disturbance pattern in the RSS.

There are a number of challenges to be solved in this radio frequency sensing in order to make the system more reliable and useful. For example:

Signal fluctuation: The propagation of wireless signal is inherently a random process, making the signal strength level unpredictable. Even without the presence of an object or human, the RSS level is constantly fluctuating. Hence, it is crucial to differentiate between random fluctuation and genuine attenuation.

Environment: Physical phenomena encountered by the signal while it is in flight, e.g. reflection, diffusion, diffraction etc., contribute to multipath propagation. This is further complicated by the environment in which the transmission occurs. Indoor environment, where there are more obstacles for example furniture, walls etc., is more prone to multipath propagation than outdoor environment, contributing to more severe signal level fluctuation. For a direct block on LOS link this effect may not be significant, however, it will be a challenge for detecting and tracking in between the LOS links. Furthermore, unexpected changes in the environment may contribute to errors in practical situation. Besides that, people can also behave unpredictably, moving in paths that may change on a whim, and thus present an enormous challenge to localization and tracking systems. In order to overcome these problems, statistical modelling such as using Kalman filter (and its variants) to predict the trajectory of the movement may be used.

8 Conclusion

This chapter has presented a proof of concept of a passive indoor tracking system that can be used to detect and track a subject that is moving within an environment monitored by an array of Wi-Fi router modems without carrying any device or tag. The system is implemented using GNU/Linux software “libnl”. The fundamental working principle of the system is based on signal attenuation that occurs as an object or human blocks a LOS between a router modem and a Wi-Fi receiver. Experimental results have suggested that multipath propagation that is typically present in an indoor environment has little effect on the attenuation caused by a direct block on the LOS link.

References

1. Z. Fang, Z. Zhao, D. Geng, Y. Xuan, D. Lidong, X. Cui. RSSI Variability characterization and calibration method in wireless sensor network. *In the proceedings of the 2010 IEEE International Conference on Information and Automation* (Harbin, China, 2010), pp. 20–23
2. Heurtefeux K. and Valois, F. Is RSSI a good choice for localization in wireless sensor network? *26th IEEE International Conference on Advanced Information Networking and Applications* (2012)
3. P.K. Sahu, E.H.-K. Wu, J. Sahoo, DuRT: Dual RSSI trend based localization for wireless sensor networks. *IEEE Sens. J.* **13**(8), 3115–3123 (2013)
4. M.S. Hossen, M.K.B. Kamal, M.S. Rahman (2012) Consistency analysis of RSSI measurement for distance estimation of wireless sensor nodes. *IEEE 15th International Conference on Computer and Information Technology (ICCIIT)* (2012), pp. 290–294
5. G. Deak, K. Curran, J. Condell (2010) Device-free passive localisation using RSSI-based wireless network nodes. *11th Annual Postgraduate Symposium on the Convergence of Telecommunications, Networking and Broadcasting* (PGNET 2010)
6. A. Küpper. *Location-Based Services: Fundamentals and Operation* (Wiley, New Jersey, 2005)
7. H. Liu, H. Darabi, P. Banerjee, J. Liu, Survey of wireless indoor positioning techniques and systems. *IEEE Trans. Sys. Man Cybern. Part C Appl. Rev.* **37**(6), 1067–1080 (2007)
8. P. Bahl, V.N. Padmanabhan. RADAR: an in-building RF-based user location and tracking system. *In the Proceedings of IEEE INFOCOM* (2000), vol. 2, pp. 775–784
9. L.M. Ni, Y. Liu, Y.C. Lau, A.P. Patil. LANDMARC: indoor location sensing using active RFID. *In the Proceedings of the First IEEE International Conference on Pervasive Computing and Communications (PerCom)* (2003), pp. 407–415
10. A.J. Wilson. *Device-Free Localization With Received Signal Strength Measurements In Wireless Networks* (PhD Dissertation, The University of Utah, 2010)
11. N.S. Chong, Y.H. Kho, M.L.D. Wong. A closed form unwrapping method for a spherical omnidirectional view sensor. *EURASIP J. Image Video Process.* **5** (2013)
12. N.S. Chong, M.L.D. Wong, Y.H. Kho. Closed form spherical omnidirectional image unwrapping. *In the proceeding of Image Processing (IPR 2012), IET Conference on* (2012), pp. 1–5
13. N.S. Chong, Y.H. Kho, M.L.D. Wong. Visual detection in omnidirectional view sensors. *SIViP* **9**(4), 923–940 (2015)
14. A. Bensusky. *Wireless positioning technologies and applications*. Artech House (2007)
15. P. Prasithsangaree, P. Krishnamurthy, P.K. Chrysanthis, On indoor position location with wireless LANs. *IEEE Int. Symp. Pers. Indoor Mob. Radio Commun.* **2**, 720–724 (2002)
16. Y. Guo, K. Huang, N. Jiang, X. Guo, Y. Li, G. Wang, An exponential-rayleigh model for RSS-based device-free localization and tracking. *IEEE Trans. Mob. Comput.* **14**(3), 484–494 (2015)
17. Y.H. Kho, N. Chong, G. Ellis, R. Kizilirmak. Exploiting RF signal attenuation for passive indoor tracking of an object. *In Proceedings of IEEE International Conference on Computer, Communication, and Control Technology, April 2015* (2015), pp. 152–156
18. Y.H. Kho, N. Chong, R. Kizilirmak. A passive wireless tracking system for indoor assistive monitoring. *In Proceedings of IEEE International Conference on Sensing Technology, December 2015* (2015), pp. 138–142
19. M. Youssef, M. Mah, A. Agrawala. Challenges: device-free passive localization for wireless environments. *In Proceedings of the 13th Annual ACM International Conference on Mobile Computing and Networking, ser. MobiCom '07, 2007* (2007), pp. 222–229
20. C. Xu, B. Firmer, Y. Zhang, R. Howard, J. Li. Exploiting human mobility trajectory information in indoor device-free passive tracking. *In proceedings of the 11th International Conference on Information Processing in Sensor Networks, ser. IPSN '12, 2012* (2012), pp. 121–122

21. A. Molisch. *Wireless Communications* (Wiley-IEEE Press, 2005)
22. K. Pahlavan, X. Li, J.-P. Makela, Indoor geolocation science and technology. *Commun. Mag. IEEE* **40**(2), 112–118 (2002)
23. Metageek, “inSIDDer,” <http://www.inssider.com/inssider4/>, version 4
24. Microsoft Corporation, .NET Framework, <http://www.microsoft.com/net>, version 4.5
25. R. Browning, E. Baker, J. Herron, R. Kram, Effects of obesity and sex on the energetic cost and preferred speed of walking. *J. Appl. Physiol.* **100**(2), 390398 (2006)
26. R. Levine, A. Norenzayan, The pace of life in 31 countries. *J. Cross Cult. Psychol.* **30**(2), 178205 (1999)
27. J. Berg. n180211, <https://wreless.wiki.kemel.mg/en/developen/> Documentation/n180211, version 3.18
28. T. Teixeira, G. Dublon, A. Savvides. *A Survey of Human-Sensing: Methods for Detecting Presence, Count, Location, Track, and Identity*. Available: http://www.eng.yale.edu/enalab/publications/human_sensing_enalabWIP.pdf

Efficient and High Speed FPGA Bump in the Wire Implementation for Data Integrity and Confidentiality Services in the IoT

Thomas Newe, Muzaffar Rao, Daniel Toal, Gerard Dooly, Edin Omerdic and Avijit Mathur

Abstract Data integrity is a term used when referring to the accuracy and reliability of data. It ensures that data is identically maintained during any operation, such as transfer, storage, or retrieval. Any changes to data, for example malicious intention, unpredicted hardware failure or human error would result in failure of data integrity. Cryptographic hash functions are generally used to provide for the verification of data integrity. The Internet of Things (IoT) is a world where billions of objects can sense, share information and communicate over interconnected public or private Internet Protocol (IP) networks. As the adoption of IoT becomes pervasive, the quantity of data that is captured and stored becomes larger. For many IoT applications, hardware implementations of cryptographic hash algorithms will be needed to provide high speed and near real time data integrity checking. ASICs and FPGAs are the two hardware platforms that can be used for these implementations. Currently FPGA is seen as the best leading platform of the modern era in terms of flexibility, reliability and re-configurability. In this chapter an efficient high speed FPGA implementation of the newly selected hash algorithm, SHA-3, is proposed. This high speed implementation can be used with IoT applications to provide near real time data integrity checks. In addition an efficient FPGA based implementation of the Advanced Encryption Standard (AES) is provided. The provision of these FPGA based implementations allows both data integrity and data confidentiality to be provided for high speed IoT applications in addition to enabling low cost Bump In The Wire (BITW) technology to be provided for Internet Protocol Security (IPSec) provision for all IoT applications.

T. Newe (✉) · M. Rao · D. Toal · G. Dooly · E. Omerdic · A. Mathur
University of Limerick, Limerick, Ireland
e-mail: thomas.newe@ul.ie

1 Introduction

In a public Internet Protocol (IP) [1–3] network data flow between IoT applications can be visible to any number of nodes on the network. Although data can be secured using encryption and data alteration on the network, whether the data is encrypted or not, can be detected using integrity checking, it is often the case that the facility/ability to offer these services is not available on the IoT device itself. This lack of available security makes IoT applications susceptible to various security attacks [4].

In order to address this security issue in networked communication systems the IPSec protocol [5] was developed. In IPSec, there are two protocols used to provide security services; a) Authentication header (AH) [6], and b) Encapsulating Security Payload (ESP) [7]. The AH protocol provides support for; (1) Data integrity of an IP datagram; because of the data integrity check, modification to an IP datagram in transit can be detected, (2) Authentication of an IP datagram; because of this feature the end system can verify the sender and prevent address spoofing attacks, (3) Replay protection; guards against old information being replayed on the network due to the use of sequence numbers in the AH header. The ESP protocol defines mechanisms for both data confidentiality and integrity. Both IPSec protocols (AH & ESP) support two modes of operation, (a) Transport mode and (b) Tunnel mode. In transport mode, only the upper-layer protocol data segment of the IP datagram is authenticated and it is typically used for end-to-end protection of IP datagram packets between two hosts. In tunnel mode, the entire original IP datagram is authenticated within a new outer IP header. Tunnel mode can be used between security gateways to create a VPN (virtual private network). The IPSec protocol is almost always embedded into the TCP/IP protocol stack via software in the OS (operating system), such as in Linux and NetBSD. However, IPSec has proven to be computationally intensive [8], which greatly affects the performance of the network it is implemented on. Data throughput in core routers has already achieved up to terabits per second, and line card interface speeds exceed 10 Gbps, yet high performance internet security device speeds are far behind these data throughputs. The main reason for this reduction in speed is that data processing requirements for security protocols is often complex and time consuming, so it is difficult for security devices to achieve equal performance when compared to internet devices. Given that software solutions to complex problems like IPSec generally suffer from low performance issues, when compared to hardware, it is necessary for high data throughput speeds that hardware implementations of IPSec are utilised. Some reported FPGA implementation of IPSec are [9–13].

Field Programmable Gate Array (FPGA) hardware implementations can often be the best available choice because of their architectural flexibility (parallelism, on-chip memory, etc.) and high performance features [14]. In addition a successful FPGA implementation can easily be transferred into a full-custom Application Specific Integrated Circuit (ASIC) to reduce cost for large scale device production. A possible implementation of an FPGA based IPSec core is suggested in Fig. 1.

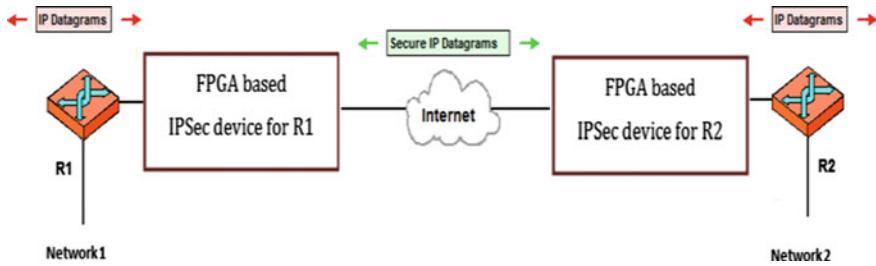


Fig. 1 FPGA based IPsec core implementation

This is a BITW architecture for IPsec. In Fig. 1 two networks that previously communicated using an insecure IP link with each other can now communicate securely by layering IPsec underneath regular IP using an FPGA based BITW IPsec hardware solution. This technique allows legacy IPv4 hardware to implement IPsec without having to replace expensive networking devices.

To provide IPsec it is necessary to implement the core symmetric cryptographic and hash functions required for its operation. In this work the AES (Advanced Encryption Standard) [15] and the SHA-3 (Secure Hash Algorithm-3) are implemented. The AES implementation [16] uses the BRAM (Block Memory) and LUT memory resources of the latest Xilinx FPGAs. The AES key generation scheme is instantiated as a separate module and it provides the round keys to the AES core for each respective round. For the complete implementation of AES only 56 clock cycles are required. To provide the data integrity security service, the cryptographic hash function, SHA-3 is implemented [17]. SHA-3 [18] is used as it is the newly selected and most secure [19, 20] cryptographic hash function available to date. Xilinx Xpower tool [21] is used to get power estimation for the proposed FPGA design.

This chapter discusses the implementation of the AES and the SHA-3 algorithms. This implementation is intended for use in BITW IPsec implementation for IoT applications.

2 Motivation

One of the challenges identified by the International Telecommunication Union (ITU) in their report on “The Internet of Things” [22] is that of privacy and security. When we start being surrounded by these smart objects that are moving around gathering information concerning our lives, behaviour or habits, there will be great concern regarding the security of that information. Currently a lot of IoT based devices do not have security as a main concern and indeed they do not even have the capability or processing power to implement this security. The European Parliament defines [23] network and information security as the ability of a network

or an information system to resist, at a given level of confidence, accidental events or unlawful or malicious actions that compromise the availability, authenticity, integrity and confidentiality of stored or transmitted data and the related services offered by or accessible via these networks and systems. Most books and papers discussing the subject will give a definition along similar lines, but what is needed here is how to provide security to existing deployments in the IoT domain.

The answer to this is to use BITW technology, where existing deployments need no hardware or software modifications. The solution proposed here can be attached to them to provide IPsec level security for traversing the internet through the provision of a VPN.

3 IPSEC Overview

IPsec is not a single protocol, but a set of protocols and services that provide a framework to implement a complete security solution for an IP network. An IPsec framework provides protection for any higher-layer TCP/IP application or protocol without the need for additional security methods. The security protection is provided by adding authentication and encryption functionality into the IP packet. The following protection services are provided by IPsec.

- **Connectionless Integrity:**

Connectionless integrity provides a guarantee that the message that is received is the exact one that was sent, and no tampering has occurred. Connectionless is because messages are sent from the sender to the receiver, but no attempt is made to ensure that they are received in order, or that any (or all) were in fact received. That task is left to one of the upper layer protocols.

- **Data Origin Authentication:**

A guarantee that the message actually was sent by the apparent originator of the message, and not by another user.

- **Replay Protection:**

Assurance that the same message is not delivered multiple times and that messages are not delivered totally out of order. This capability must be implemented by the sender, and the receiver may optionally enable its use.

- **Confidentiality or Privacy:**

A guarantee that, even if the message is “read” by an observer, the contents are not understandable, except to the authorized recipient.

- **Traffic analysis protection:**

An assurance that an eavesdropper cannot determine who is communicating with whom or determine the frequency and volume of communications between specific entities.

Above mentioned protections are possible by using the two core protocols of IPsec namely (AH & ESP). The AH protocol provides the security services of data

integrity, authentication and protection against replay attack, while the ESP provides privacy protection for the data and authentication (optional). AH and ESP are typically used independently, although it's possible (but uncommon) to use them both together. Both protocols provide protection by adding a header containing security information to an IP packet. IPSec also supports two modes of operation namely; Transport mode and Tunnel mode. In transport mode only the IP payload is authenticated or encrypted, this mode is used to provide end-to-end protection of an IP packet payload between two hosts, while tunnel mode adds a new IP header to provide protection for the entire IP packet and this mode is used to form a secure tunnel between two gateways across an untrusted internet i.e. VPN.

The purpose of IPSec is to provide various security services to traffic travelling between a source and destination, the destination/source may be a router or a host. The services may be applied to all packets, or only to specific types of traffic. Figure 2 (from [https://technet.microsoft.com/en-us/library/cc771593\(v=ws.10\).aspx](https://technet.microsoft.com/en-us/library/cc771593(v=ws.10).aspx)) below shows a VPN (Tunnel) connection provided by IPSec between two routers/gateways.

Figure 2 shows IPSec implemented on the path between two Routers as users data traverses the internet. There are different types of protection provided by IPSec and there are also different modes for IPSec to operate in as previously mentioned. Additionally IPSec can be configured so that it only operates on certain types of data while other data is transmitted on unprotected paths between routers. There may be separate IPSec protected links between the two routers and between Hosts and Routers. The security combinations available can be varied depending on the user's specific requirements.

IPSec protocols do not specify an exact mechanism used for encryption/authentication, which makes them flexible to work with a variety of algorithms. Authentication calculates an Integrity Check Value (ICV) over the packet's contents, and it is usually built on top of a cryptographic hash function such as MD5, SHA-1, SHA-2, SHA-3 etc. Encryption uses a secret key to encrypt the data before transmission and this hides the actual contents of the packet from eavesdroppers. Encryption algorithms include DES, 3DES, Blowfish, AES etc.

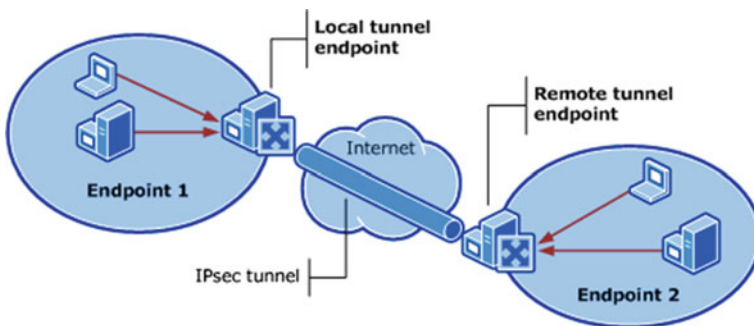


Fig. 2 Protection provided by an IPSec tunnel between two routers/gateways

Two devices which are exchanging encrypted information need to be able to share keys, security protocol to use, specific encryption/hashing algorithm and the mode of operation before the start of communications between them. There are two possibilities to perform this task (1) Manual configuration (2) IKE (Internet Key Exchange) protocol [24]. Manual configuration requires manual entry of the secret values on both ends, apparently conveyed by some out-of-band mechanism, and IKE is a sophisticated algorithm used to set up a security association (SA) between entities in IPSec to facilitate the sharing/specification of secret values and algorithms.

4 Hardware Implementation of Security Algorithms and FPGA

4.1 Hardware Implementation of Security Algorithms, Why?

Hardware solutions for security algorithms provide high speed and real time results for applications like data confidentiality, authentication and integrity. A hardware implementation needs both efficient and cost effective solutions on reconfigurable platforms. Generally hardware solutions of security algorithms are considered more physically secure by nature as they are located physically separate from the main system processor. They also provide better performance statistics than software solutions because of their dedicated type of operation. There are two major types of hardware platforms in use; 1) FPGA and 2) ASIC. The FPGA is considered the best leading representative of reconfigurable hardware devices of the modern era [25].

Generally the two most important design considerations for hardware solutions to security algorithms are area and throughput (speed). A trade-off is normally required between area and throughput for cost benefits. A cryptographic hash function has a wide range of applications and their area-throughput trade-offs may be different for different applications. For applications like smart cards, the area is of main concern, while Storage Area Networks (SANs) and VPNs require high performance and digital video recorders require best of throughput-area ratio.

4.2 Why Field Programmable Gate Array (FPGA)?

The flexible architecture and high performance features of FPGA make it particularly suitable to use for applications involving complex cryptographic algorithms. The FPGA is a family of reconfigurable hardware, where Field Programmable refers to the operation changing capability in the field, and Gate Array relates to the construction of the basic internal architecture of the device. These devices allow

digital computing tasks to be developed in software and compiled into a bitstream file. This bitstream file contains information about how the internal components should be wired together to perform the desired operation.

It can be said that FPGAs combine the best parts of ASICs and processor-based systems but are in fact parallel in nature. The advantage of using a software programmed processor is that software is very flexible to change while a disadvantage is that performance can suffer if the clock is not fast. The advantage of an ASIC is that it can provide very high performance because of its dedicated type of operation and its disadvantages are: 1) high cost to volume ratio; 2) extended delay between designs to end product; 3) incapability to include new changes after the system is fabricated and 4) difficulties in debugging errors. FPGAs fill the gap between hardware and software and offer numerous advantages [26] such as: (1) flexibility, (2) reliability, (3) low cost, (4) fast time-to-market and (5) long-term maintenance.

5 AES

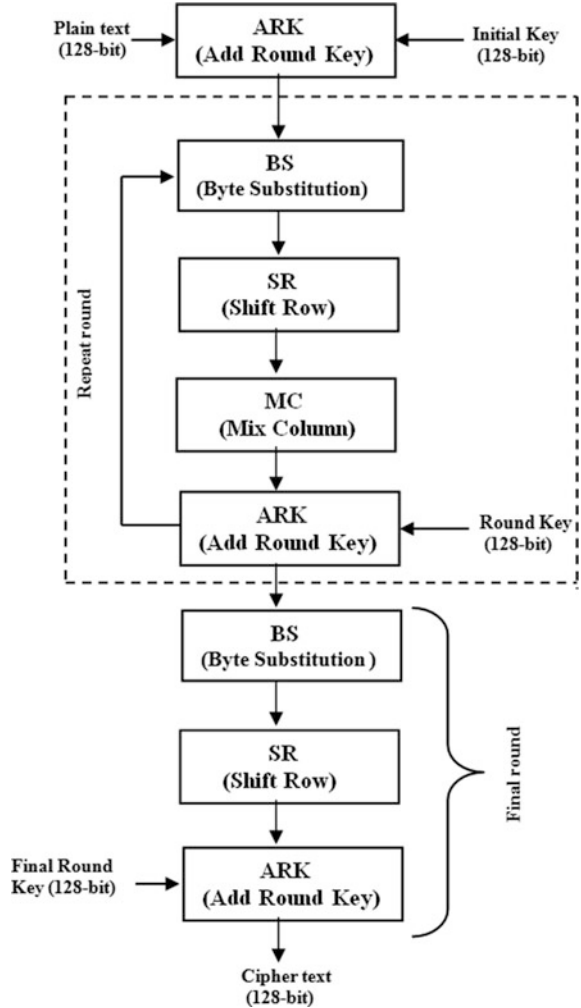
5.1 AES Overview

AES is a symmetric block cipher algorithm that processes data in 128-bit blocks. Block cipher means that the number of bytes that it encrypts is fixed i.e. 16 bytes.

It supports key sizes of 128, 192 and 256 bits with iterative rounds of 10, 12 and 14 respectively. The number of these rounds is chosen depending on the key size. A separate Key expansion unit is used to generate keys for each round of the AES algorithm. The bit series related to the input, the output and the cipher key are processed as arrays of bytes; called States. The State array consists of four rows of bytes and every row consists of 4 bytes. In each round of AES, a 128-bit data block is transformed by a sequence of operations as given in Fig. 3. These sequences of operations are given below.

- **Add round key (ARK):** The 16 bytes of the state are *XORed* with each of the 16 bytes of a portion of the expanded key for the current round as given in Fig. 4. There are three 'ARK' blocks in encryption scheme given in Fig. 3. In the first block, 128-bit plain text is *XORed* with 128-bit initial Key. Then this initial key goes to key generation/expansion scheme to generate a new key for each round. In the second block of 'ARK', each time, a new key (round key) is *XORed* with the updated 128-bit state. The round Key bytes are never reused. Similarly, the last block of 'ARK' uses 16-bytes of the last key generated from the key generation scheme.
- **Byte Substitution (BS):** This step replaces each byte of the 16 bytes updated state using the S-box lookup table value. The contents of an S-box is the multiplicative inverse in Galois Field (GF) (2^8), followed by an affine transformation. The 'BS' step is given in Fig. 5.

Fig. 3 Advanced encryption standard steps (encryption)



- Shift Row (SR): This step involves cyclic shifting to rows of the updated state. Each row is shifted 1, 2 or 3 spaces over to the right, depending on the row of the state. Although, the First row is never shifted as mentioned in Fig. 6.
- Mix Column (MC): The mix column transformation operates on each column individually, treating each column as a four term polynomial. The columns are considered as polynomials over GF (28) and multiplied modulo $x^4 + 1$ with a fixed polynomial given by: $\{03\}x^3 + \{01\}x^2 + \{01\}x + \{02\}$. In this way each byte of a column is mapped into a new value that is a function of all four bytes in that column. This MC step is mentioned in Fig. 7.

The AES decryption sequence is the same as that of encryption but each step performs an equivalent inverse operation as shown in Fig. 8. The key generation

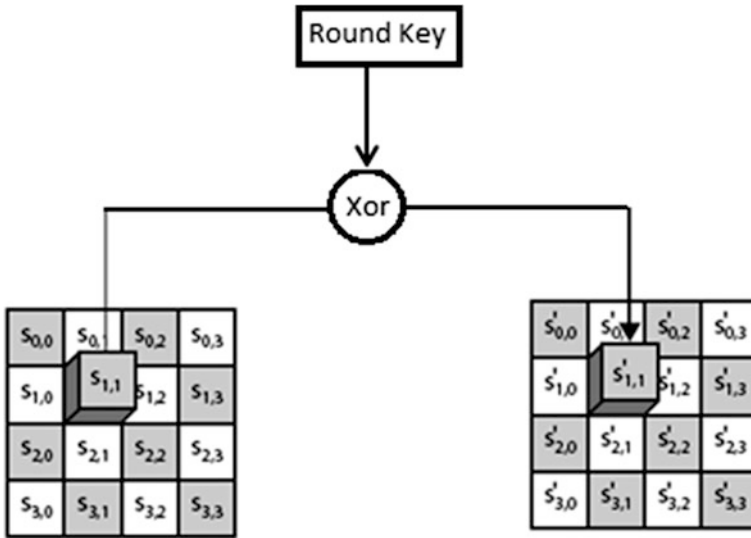


Fig. 4 Add round key step of AES

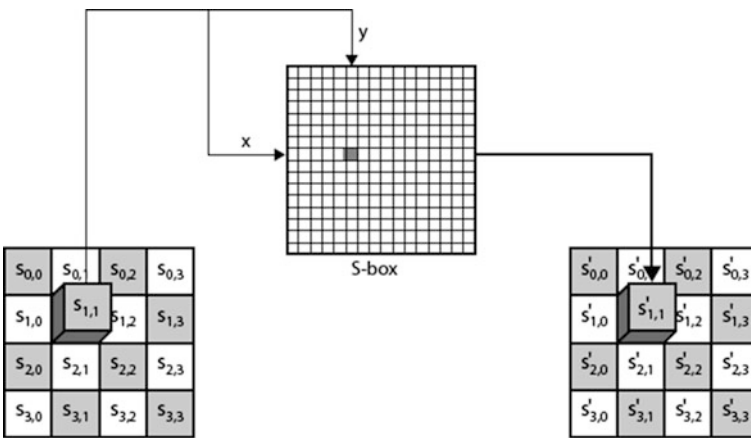


Fig. 5 Byte substitution step of AES

scheme is the same but the keys will be used in reverse sequence as compared to encryption. For example, the set of keys that are used in the final round of encryption will be used as an initial round key in decryption. In inverse BS step an inverse S-box is used to replace bytes, while in inverse SR all rows are shifted to the left with the same sequence as that of ‘SR’ step in encryption. In inverse MC a polynomial of $\{11\}x^3 + \{13\}x^2 + \{9\}x + \{14\}$ is used.

To implement the S-box step of AES, the Block RAM (BRAMs) facility of FPGA is used. The next section describes the BRAM feature of FPGAs.

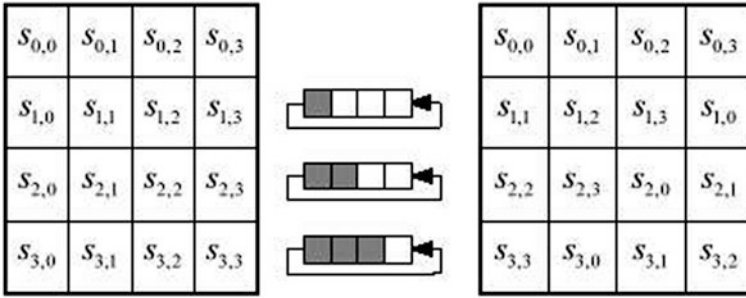


Fig. 6 Shift row step of AES

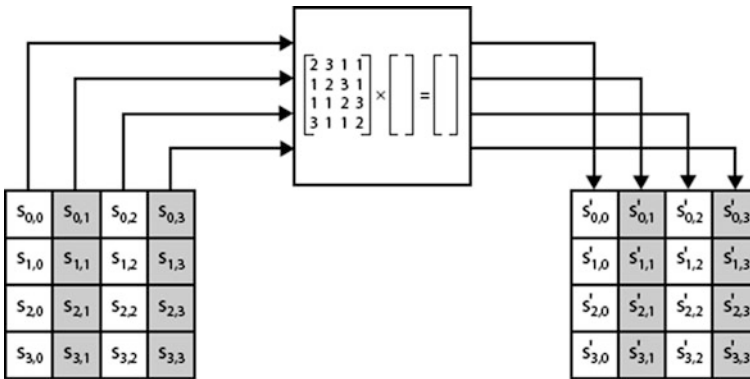


Fig. 7 Mix column step of AES

5.2 BRAM Feature of FPGA

Modern FPGAs are power packed with features to facilitate designers. Availability of features like huge block memory (BRAM), Digital Signal Processing (DSP) cores, and embedded CPU make an FPGA architecture more optimized with respect to area, speed and power. As mentioned previously to implement the S-box step of AES, we used the BRAM feature of modern FPGAs.

BRAMs [27] can be used in different configurations (Single port RAM, Simple dual port RAM, True dual port RAM, Single port ROM and Dual port ROM) for efficient data storage. Figure 9 shows the general block diagram of one port of a dual-port BRAM and shows that BRAM contains register to synchronize input data and address before accessing the memory array. The memory array is followed by a latch and an optional output register. The BRAM also contains several signals to control the use of output register or set/reset the value of the latch and output register.

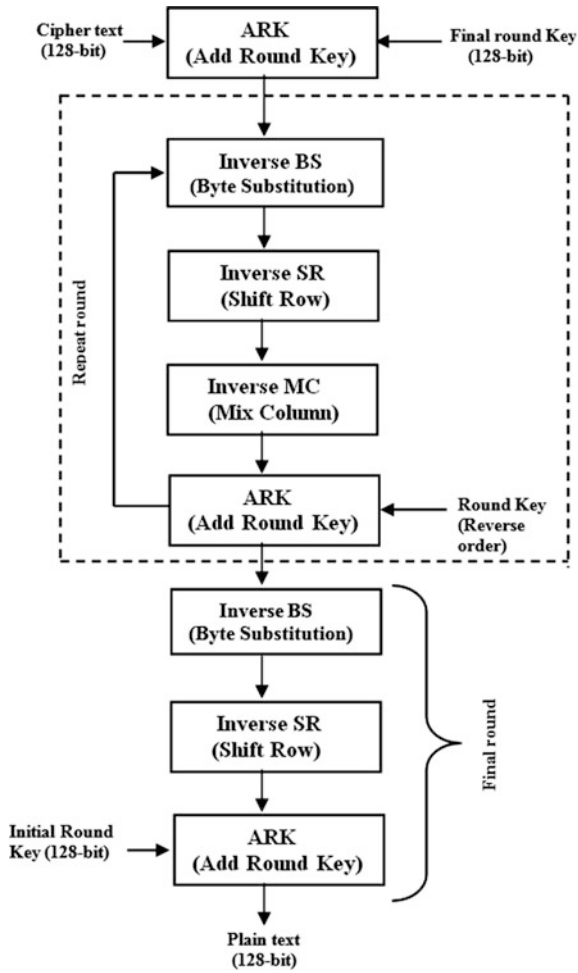


Fig. 8 Advanced encryption standard steps (decryption)

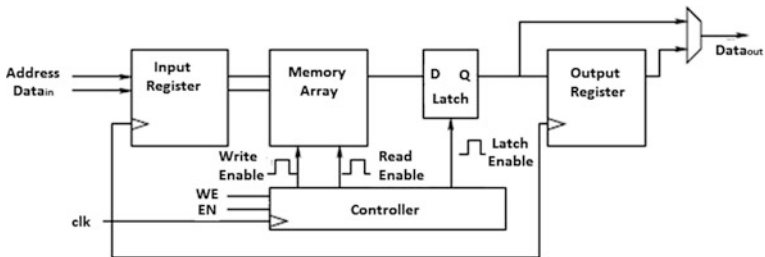


Fig. 9 BRAM port

In this implementation we have used the Dual port nature of BRAM. This feature of BRAM was first used by Drimer et al. in [28].

5.3 Proposed Implementation of AES

The proposed implementation of AES encryption is given in Fig. 10. This scheme provides a balance implementation with respect to low area, high throughput and low power consumption.

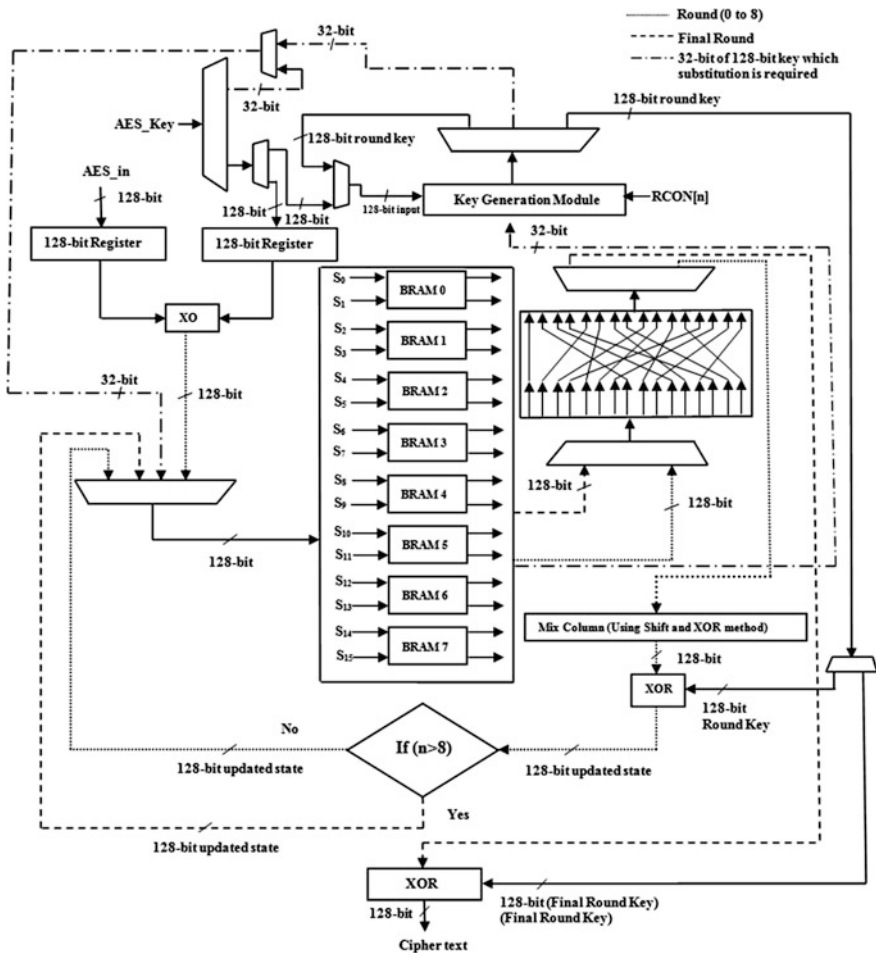


Fig. 10 Proposed architecture for AES implementation

In Fig. 10, plain text and the encryption key are represented by AES_in and AES_key signal and this data is stored in two different 128-bit registers, these two signals are *XORed* with each other to perform the initial ‘ARK’ step of AES before start of rounds. Meanwhile, the input key is also applied to the key generation module, with respective RCON value, to generate the round key.

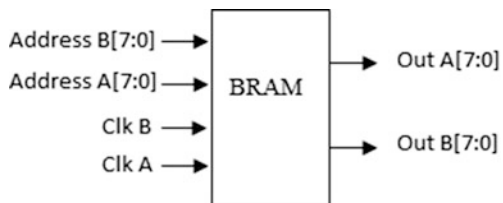
The 128-bit resultant state of the *XOR* operation data is saved into 16 intermediate registers, each of 8-bit (S_0 to S_{15}), these registers are updated whenever the intermediate 128-bit state is available. The data of these 16 registers is applied to an instantiated block, which is used to implement the ‘BS’ step of AES. The instantiated block consists of 08 BRAMs. These BRAMs are generated by using the Xilinx CORE Generator tool. All BRAMs are configured as Dual-Port ROM (Read Only Mode) to access the two 8-bit lookup values corresponding to the two 8-bit input addresses respectively, as shown in Fig. 10. The reason for using 08 dual port BRAMs is to get substitution output for all 16-bytes within a single clock cycle. This helps to get better throughput and also reduce the number of clock cycles. The S-box values are initialized in BRAMs using a coefficient (COE) file. The 16 intermediate registers are divided into pairs of two and each pair of two 8-bit registers become addresses of a single BRAM. In this way the data of all sixteen 8-bit registers becomes addresses of the BRAMs, while corresponding lookup values are taken from respective output ports of BRAMs. The dual port BRAM configuration is given in Fig. 11. Both ports of BRAMs are clocked with the same clock signal.

The ‘SR’ step of AES is implemented in a way that it does not utilize any hardware resources. All the resultant bytes of BRAMs are applied to the Mix Column step in such a way that these bytes fulfil the rotation bit requirement, as shown in Fig. 10. This technique helps to get better throughput and low area consumption.

The updated state of ‘SR’ step is multiplied with the multiplication matrix as shown below to implement the ‘MC’ step of AES. For multiplication a shift and *XOR* method is used.

$$\begin{pmatrix} S_0 & S_4 & S_8 & S_{12} \\ S_1 & S_5 & S_9 & S_{13} \\ S_2 & S_6 & S_{10} & S_{14} \\ S_3 & S_7 & S_{11} & S_{15} \end{pmatrix} \begin{pmatrix} 2 & 3 & 1 & 1 \\ 1 & 2 & 3 & 1 \\ 1 & 1 & 2 & 3 \\ 3 & 1 & 1 & 2 \end{pmatrix}$$

Fig. 11 BRAM dual port configuration



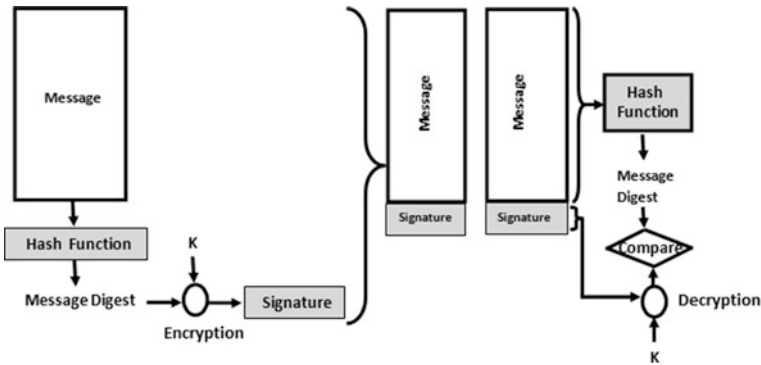


Fig. 12 Digital signature application using hash function

In the above expression, multiplication with ‘02’ is implemented by 1-bit left shift followed by a conditional bitwise XOR with (0001 1011). The conditional bitwise XOR is performed if the leftmost bit of the original value (before the shift) is 1. Similarly multiplication with 03 is implemented by using the same approach as that of multiplication with 02, in addition to XORing the multiplication resultant byte with the multiplying byte itself.

The updated bytes are XORed with the round key, which is generated from the round key generator function, to perform ‘ARK’ step. The key generation function is implemented as a separate block. The key generator module takes the previously generated key as the input key with respective RCON value. The substituted 32-bit of the ‘input key/round key’ are also applied to the key generation block. This is done to use the same BRAM resources. In this way a new set of key is generated for each round to use in ‘ARK’ operation.

The resultant bytes of ‘ARK’ step are stored in the previously used 16 intermediate registers and remaining rounds are completed using an iterative approach. The final round involves only Byte substitution, Shift Row and Add round key. As shown in Fig. 10, the same BRAM resources are again used to implement the byte substitution step of the final round.

Similarly, the decryption scheme of Fig. 8 is implemented. The only difference is that for ‘inverse MC’ step implementation, BRAMs are used. The lookup tables of multiply by 11, multiply by 13, multiply by 9 and multiply by 14 are saved in BRAMs to get the multiplication results. The key generated for encryption are stored in temporary registers to use for decryption.

5.4 Performance Results of AES Implementation

The proposed implementation was designed in Verilog HDL, and the design was synthesized, placed and routed in the Xilinx ISE 14.2 design suite. All the reported

Table 1 Performance results (encryption and decryption)

Device	Slices used/ slices available	BRAM used/ BRAM available	Frequency(MHz)
Artix-7(xc7a200t)	945/33,650	08 (Inverse SB)32 (Inverse MC)	229.6

results used a 64-bit wrapper. The generated cipher text is applied to the decryption scheme to get plain text, this gives results for combined implementation of the encryption and decryption scheme, as shown in Table 1.

Table 2 shows the results for encryption implementation only. Table 2 shows that Artix-7 FPGA consumes less power compared to all other Xilinx FPGAs and its TPA is also better. The Virtex devices are normally power hungry and so utilized more power.

6 Secure Hash Algorithm-3 (Sha-3)

6.1 Cryptographic Hash Functions

Cryptographic hash functions have many security based applications, particularly in the generation of message authentication codes (MACs), data integrity and digital signatures as shown in Fig. 12. Moreover, they can be used for digital fingerprinting, for data indexing in hash tables, to detect duplicate data or uniquely identify files and as a means to detect accidental data corruption during communication.

The most attractive property of a hash function is its input sensitivity, where an intended or unintended change to the message will change the entire hash value. This property makes hash functions an excellent choice for applications requiring data authenticity and/or integrity. An ideal cryptographic hash function has the following properties:

- It should be very difficult to find two inputs that produce the same message digest (collision free function).
- It should be easy to compute the hash value for any given message.
- It should be very hard (impossible) to recover a message from a given hash (one way function).
- It should be infeasible to modify a message without changing its hash.

Table 2 Performance results on Xilinx FPGAS (encryption)

Device	Slices used/ slices available	BRAM used/ BRAM available	Frequency (MHz)	Clock cycles	TP (Mbps)	TPA	Power consumption (Watt)
Artix-7(xc7a200t)	359/33,650	08/730	311.721	59	676.276	1.88	0.184
Virtex-7(xc7vx90t)	551/153,000	08/3000	308.642	59	669.59	1.21	0.463
Virtex-6(xc6vcx130t)	407/20,000	08/528	293.686	59	637.14	1.56	1.965
Virtex-5(xc5vix85t)	478/12,960	08/108	291.290	59	631.95	1.32	1.266
Virtex-4(xc4vix15)	1295/6144	08/48	287.105	59	622.87	0.48	0.641
Spartan-6(xc6s1x100t)	436/15,822	08/536	249.50	59	541.28	1.24	0.251

6.2 Secure Hash Algorithm-3 (SHA-3)

The National Institute of Standards and Technology (NIST) selected the ‘Keccak’ algorithm as the new hash function ‘SHA-3’, in October 2012 [29]. NIST issued a call for a new algorithm as previously used hash functions (SHA-0, SHA-1, RIPEMD and MD5) had vulnerabilities detected [30–32]. SHA-3 is a family of sponge functions [33] characterized by two parameters, the bitrate r and capacity c . The sum $(r + c)$ determines the width of the SHA-3 function permutation used in the sponge construction and is restricted to a total value of 1600. Selection of r and c depends on the desired hash output value. For ex.: for a 256-bit hash output $r = 1088$ and $c = 512$ and for a 512-bit hash output $r = 576$ and $c = 1024$ can be selected. The 1600-bits state of SHA-3 consists of 5x5 state matrix of 64-bit words as shown below in Fig. 13.

There are 24 rounds in the compression function (Core) of SHA-3 and each round consists of five steps/operations, $Theta(\theta)$, $Rho(\rho)$, $Pi(\pi)$, $Chi(\chi)$ and $Iota(i)$ as shown in Eqs. (1)–(6) below.

Theta (θ) Step:

$$C[x] = A[x, 0] \oplus A[x, 1] \oplus A[x, 2] \oplus A[x, 3] \oplus A[x, 4]; \tag{1}$$

$$D[x] = C[x-1] \oplus ROT(C[x+1], 1); \tag{2}$$

$$A[x, y] = A[x, y] \oplus D[x]; \tag{3}$$

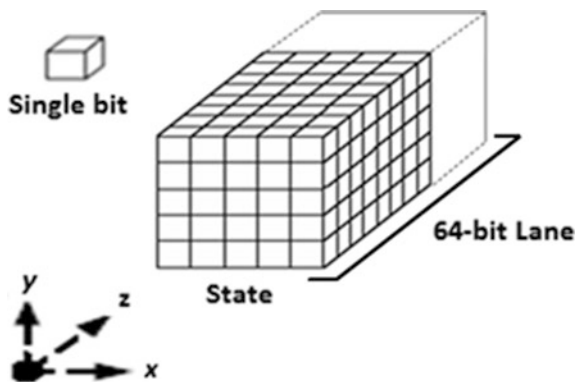
Rho (ρ) and Pi (π) Step:

$$B[y, 2x + 3y] = ROT(A[x, y], r[x, y]); \tag{4}$$

Chi (χ) Step:

$$A[x, y] = B[x, y] \oplus ((NOT B[x+1, y]) AND B[x+2, y]); \tag{5}$$

Fig. 13 State Matrix (A) of SHA-3



Iota (i):

$$A[0, 0] = A[0, 0] \oplus RC; \tag{6}$$

In the above equations all operations within indices are performed modulo 5. The complete permutation state array is denoted by (A) and $A[x, y]$ denotes a particular 64-bit word in that state. $B[x, y]$, $C[x]$ and $D[x]$ are intermediate variables. Other operations include bitwise *XOR*, *NOT* and *AND* logical operations. In Eq. (2) and (4) ROT is used to represent a bit-rotation operation. The constant $r[x, y]$ provides the rotation bit scheme for the updated bits of $A[x, y]$, and the RC is a 64-bit word that is unique for each round of the compression function. The details of $r[x, y]$ and RC is given in [18].

In Eq. (1) a 5-input *XOR* function is performed between the 64-bit word of each row of matrix (A) and the resultant bits are stored in an intermediate state $C[x]$. This *XOR* function detail is given in Fig. 14.

In Eq. (2), $C[x]$ position is rotated 1-time in a clock wise direction ($C[x + 1]$) and 1-time in an anti-clockwise direction ($C[x - 1]$). The bits of $C[x + 1]$ are also rotated one time. After this rotation operation, the 1-time rotated bits of $C[x + 1]$ are *XORed* with the bits of $C[x - 1]$ and the result is stored in an intermediate state $D[x]$ as shown in Fig. 15.

In Eq. (3) the 64-bit lane of $D[x]$ is *XORed* with each 64-bit lane of the input state matrix (A) and the entire state of 1600-bits is updated as given in Fig. 16.

Equation (4) involves the bit rotation of each 64-bit lane of the updated 1600-bit state of $A[x, y]$ according to the bit rotation scheme of $r[x, y]$. After the bit-rotation operation all the rotated bits are stored at the new lane position. This rotation operation and change in lane position is given in Figs. 17 and Fig. 18 respectively.

In Eq. (5) three logical operations (*XOR*, *NOT* and *AND*) are performed. Firstly the bits of $B[x + 1, y]$ are inverted by using the *NOT* logical operator. The *AND* logical operation is performed between $B[x + 2, y]$ and the inverted bits of $B[x + 1, y]$. The resultant 64-bits of this *AND* operation is *XORed* with each 64-bit lane of the 1600-bit state of $B[x, y]$ and the entire state of the 1600-bit state matrix (A) is updated. This is called *Chi (γ)* step and is shown in Fig. 19.

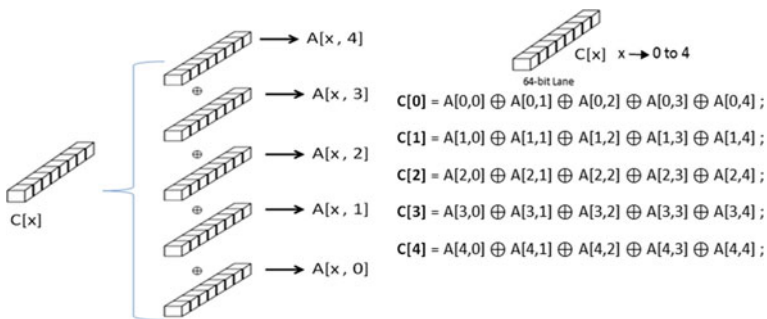


Fig. 14 XOR operation of Eq. (1)

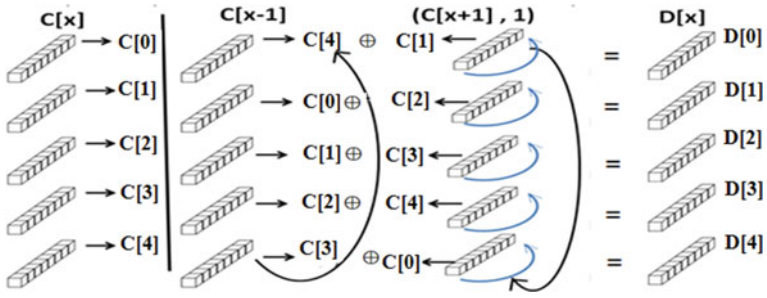


Fig. 15 Bit-rotation and XOR operation of Eq. (2)

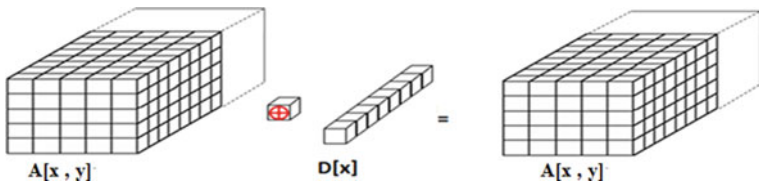


Fig. 16 XOR operation of Eq. (3)

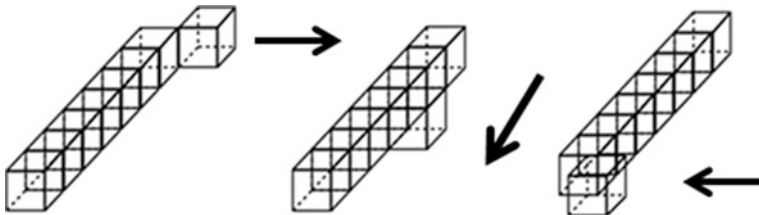


Fig. 17 Different phases of bit rotation

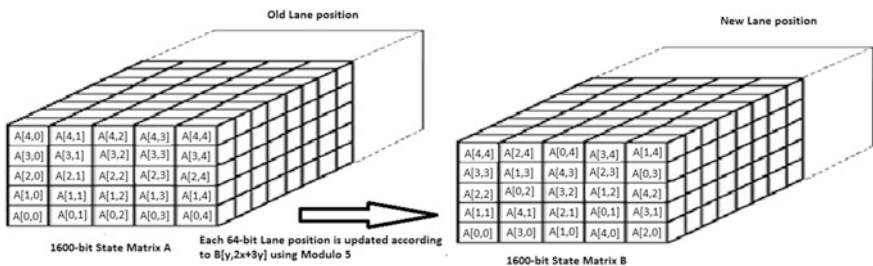


Fig. 18 Lane positions updated

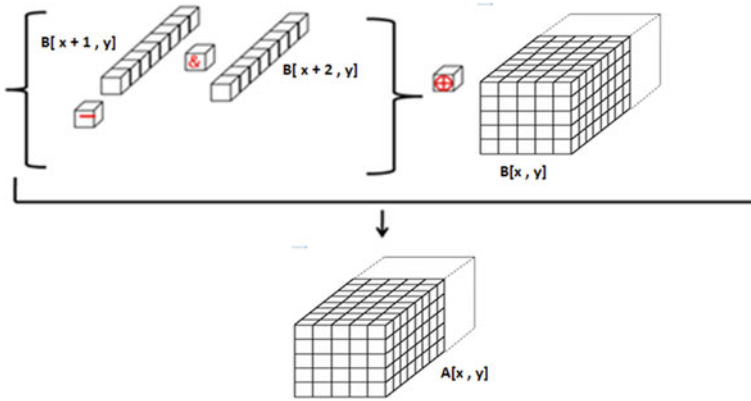


Fig. 19 Chi (χ) step

In Eq. (6) i.e. *iota* step, only the updated $A[0, 0]$ lane is *XORed* with a 64-bit round constant (RC) that is unique for each round of the compression function. This *XOR* operation is given in Fig. 20.

The SHA-3 hash function operation consists of three phases that include: initialization, absorbing and squeezing. Initialization is simply the initialization of state matrix (A) with all zeros. In the absorbing phase each r -bit (bitrate) wide block of the message is *XORed* with the current matrix state and 24 rounds of the SHA-3 compression function are performed. The initialization and absorbing phases are represented in Figs. 21 and Fig. 22 respectively.

Fig. 20 Iota (*i*) step

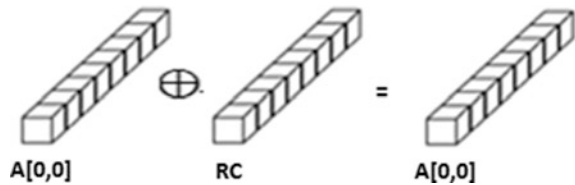
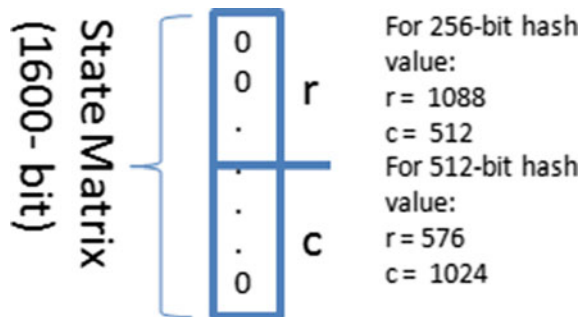


Fig. 21 Initialization phase of SHA-3



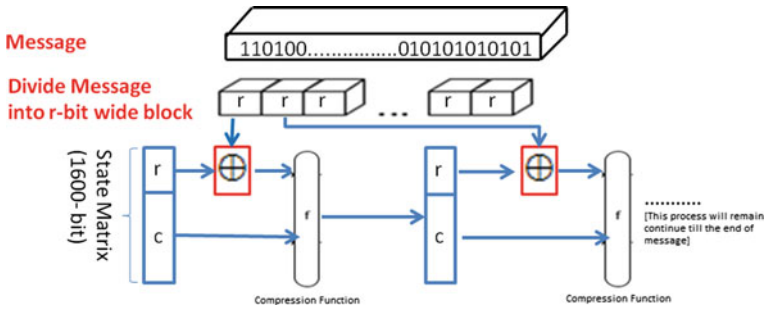


Fig. 22 Absorbing phase of SHA-3

After absorbing all blocks of the input message, the squeezing phase is utilised. In this phase the state matrix is simply truncated to the desired length of the output hash. If more than an r -bit hash value is required then more SHA-3 permutations are performed and their results are concatenated until the hash width reaches the desired length (generally 224, 256, 384, or 512 bits).

6.3 I/O Interface, Control and Data Paths

The I/O interface, control and data path implementation is given in Fig. 23. To ensure and control the availability of input data at each rising edge of the clock cycle the Load and acknowledgment signals are used. The length of input data to be loaded is a 64-bit word at each rising edge of the clock cycle. Similarly when the hash output is ready it is indicated by putting `hash_valid` signal to high and a 64-bit word (hash value) is available at each rising edge of the clock. The control path consists of a Finite State Machine, State register, clock and a counter.

The data path consists of an Input register Serial-In Parallel-Out (SIPO), a SHA-3 Core and an Output register Parallel-In Serial-Out (PISO). The state matrix (A) is stored in the 1600-bit register. The initialization phase initializes the state matrix (A) with all 0s. In the absorbing phase each r -bit wide block of the input message is XORed with the r -bit current state matrix and then Concatenation is used to combine r and c to form a new state and store it in the 1600-bit Register.

The input register of the data path is updated at each rising edge of the clock of the control path. The data path output register contains the resulting hash which is serially outputted. The 'counter' of the control path is used to count the rounds of SHA-3. The state registers of the control path are used to store the input message and also to manage the control signals like `Hash_en`, `hash_done` and `select`. The high logic of the 'Hash_en' signal informs the SHA-3 core to start the hash operation whenever the 1600-bit state is ready to use. At the end of the hash operation the 'Hash_done' signal becomes high. This indicates that the hash of the input message is calculated. 'select' is an extra signal that is used to select any round of SHA-3 for verification of the SHA-3 operations.

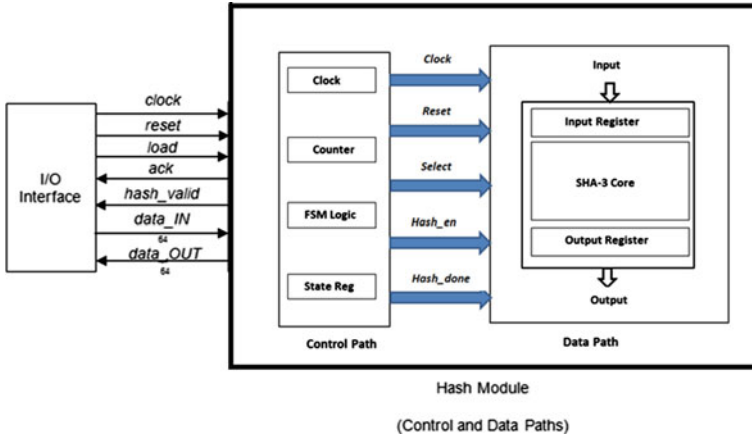


Fig. 23 I/O interface, control and data paths

The compression function is implemented in two phases; this includes the combining of the five steps from θ step to i step and implementation of the resultant equations using LUT primitives. The round constants (RC) are stored in ROM using a 24×64 bit distributed ROM. Respective round constants are addressed during each round using the round number as the ROM address. In the last phase of squeezing, the state matrix (A) is simply truncated to the desired length of the hash output. Further detail of the data path implementation of SHA-3 core is given in next section.

6.4 Proposed Implementation of SHA-3 Core

The proposed implementation used LUT-6 (Look UP Table) resources of FPGAs. LUTs are the basic logic building blocks of an FPGA and are used to implement most logic functions of a design. LUT_6 as shown in Fig. 24, is a 6-input, 1-output LUT that can either act as an asynchronous 64-bit ROM (with 6-bit addressing) or implement any 6-input logic function. The INIT parameter for the FPGA LUT primitive provides the logical value of the LUT and consists of a 64-bit Hexadecimal value.

It is obvious from the SHA-3 steps (*Theta, Rho, Phi, Chi and Iota*) given from Eqs. 1 to 6, that there are two types of logical operations throughout the compression function (a) XOR logic (b) χ (*chi*) logic. In this design we have stored the result of these logics manually in a single LUT_6 primitive as an INIT value. The MSB of the LUT_6 input is used as a control bit for the selection between XOR and χ logic. If the control bit is '0' then XOR logic is selected and in the case of the control bit being a '1', χ logic is selected. The INIT value of the LUT_6 primitive is 64'hD2D2D2D296696996. This is derived by using the truth table for all possible combinations of 6-input LUTs.

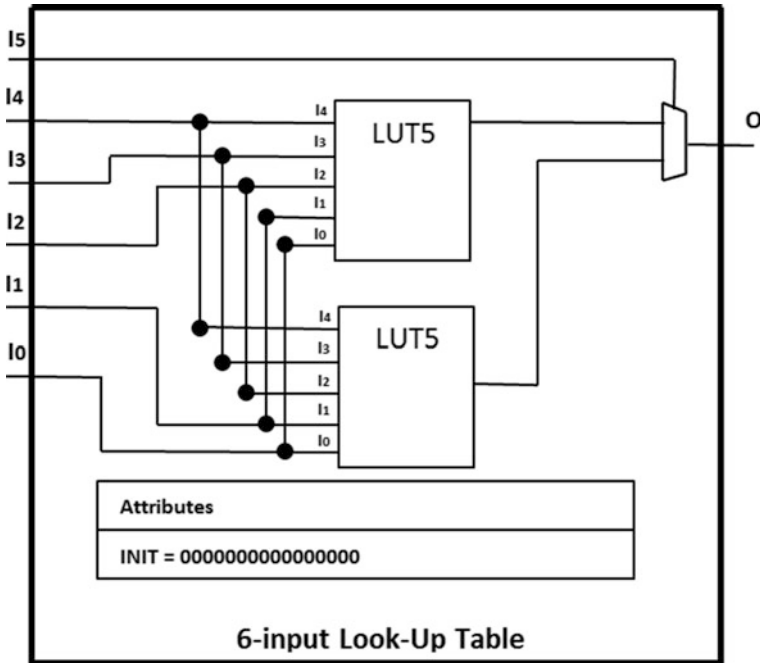


Fig. 24 LUT₆ primitive

The 1600- bits of the compression function are divided into a 5×5 matrix (A) of Fig. 13, in such a way that each position of the state matrix contains a 64-bit word. All the bitwise logical operations are performed between these 64-bit words. So, there should be 64 LUTs to perform bitwise logical operation between any 64-bit inputs at a time. Because of this, an architecture is proposed using 64 LUT-6 primitives with the same INIT value as shown in Fig. 25. In Fig. 25 all the input bits are arranged in a way so that this architecture can be used to perform bitwise logical operation of either XOR or chi logic between any five 64-bit inputs. As the maximum number of inputs in Eqs. (1)–(6) are five that’s why the Fig. 25 architecture is suitable for the implementation of these equations and the remaining input can be used as ‘control’ bit to select between XOR and chi logic.

In Eq. (1) a 5-input XOR function is performed between the 64-bit word of each row of state matrix (A) as given in Fig. 14. To implement Eq. (1) the architecture of Fig. 25 is instantiated 5 times with control bit equal to ‘0’ to select the XOR logic. The output of this XOR operation is stored in an intermediate register of C[x].

In Eq. (2), C[x] position is rotated 1-time in clock wise (C[x + 1]) and anti-clockwise (C[x - 1]) direction as given in Fig. 15. The 64-bits of C[x + 1] are also rotated one time. This rotation operation is implemented manually using concatenation operation. After this rotation operation, the rotated 64-bits of C[x + 1] and 64-bits of C[x - 1] are XORed. To perform this XOR operation, again

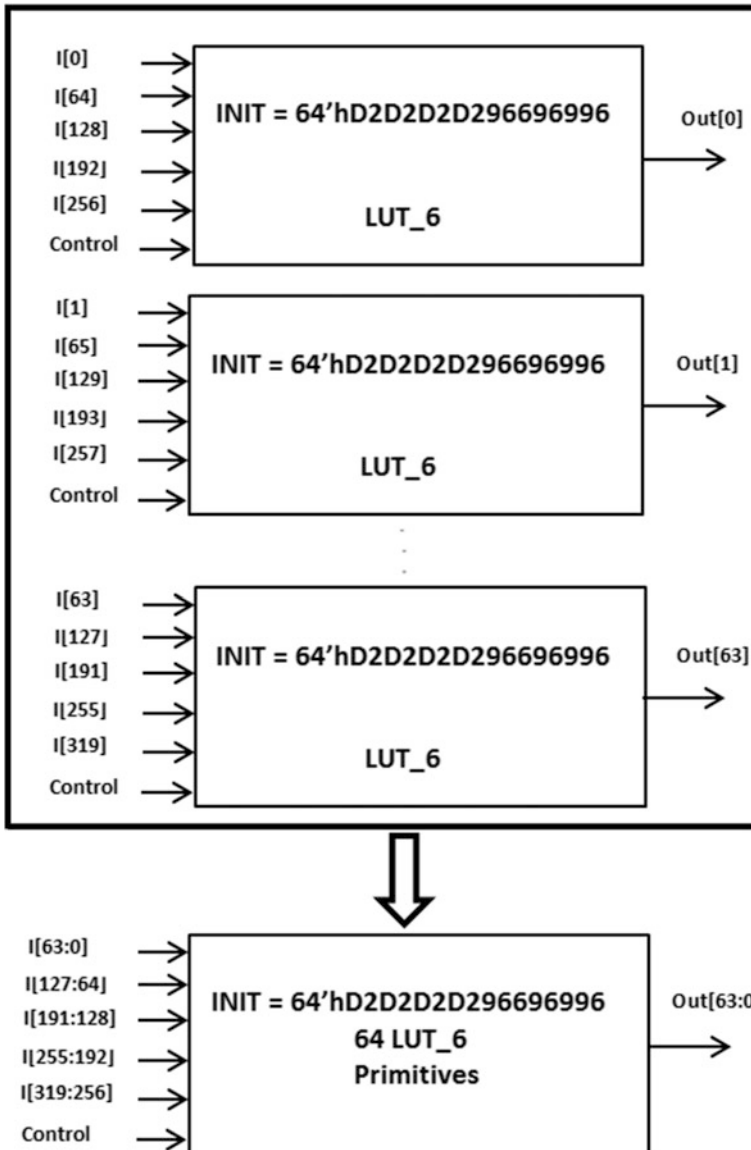


Fig. 25 64 LUT_6 architecture to implement SHA-3 Core

Fig. 25 architecture is instantiated 5 times with the control bit set to '0' and the output is stored in an intermediate register $D[x]$. This time only two inputs of Fig. 25 are used (excluding control bit) and the other inputs are grounded.

In Eq. (3), as shown in Fig. 16, the resultant $D[x]$ is *XORed* with each 64-bit row of input state matrix (A) and the entire state of 1600-bits is updated. There are 25

rows of 64-bits in state matrix (A). So, to implement this *XOR* function, Fig. 25 architecture is instantiated 25 times with the control bit set to '0'.

Equation (4) involves the bit rotation of each 64-bit row of the updated 1600-bit state of $A[x, y]$ according to the bit rotation scheme of $r[x, y]$. After the rotation operation all the rotated bits are stored at new position. This Eq. operation is given in Figs. 17 and 18. Here, the rotation operation is performed by using concatenation.

In Eq. (5) *chi* logic is used that consists of *XOR*, *NOT* & *AND* logical operation as given in Fig. 19. To implement this logic Fig. 25 architecture is instantiated 25 times and entire state of 1600-bit is updated. But now the control bit is set to '1' to select *chi* logic.

In Eq. (6) only 64-bit of updated $A[0, 0]$ are updated by *XORring* with 64-bit round constant (RC) as given in Fig. 20. To implement Eq. (6), Fig. 25 architecture is instantiated one time with the control logic set to '0'.

So, in this way one round of compression function is implemented in one clock cycle. The remaining 23 rounds of the SHA-3 compression functions are completed in the same way sequentially. Therefore, a total of 24 clock cycles are required for the complete implementation of the compression function.

6.5 Performance Results of SHA-3 Implementations Suitable for IoT Domain

Table 3 shows the implementation results in terms of area utilization, frequency of the implemented design, power consumption, throughput (TP) and TPA (throughput/area). The proposed architecture is implemented in all Xilinx FPGA platforms to show which platform is suitable for use in the IoT application environment.

The implementation results from Table 3 shows that the Artix-7 FPGA utilizes less power as compare to the other Xilinx FPGAs and also consumes less area. Virtex FPGAs are power hungry, but suitable for high speed implementation in IoT. The implementation on Spartan-6 consumes less power compared to Virtex-6 but the throughput is less when compared to other Xilinx FPGAs. The throughput result on Kintex FPGA is better but it utilizes more area making its TPA less attractive.

Table 3 Implementation results on Xilinx FPGAS

Device	Area (Slices)	Freq. (MHz)	Power (mW)	TP (Gbps)	TPA [TP(Mbps)/Area]
Artix-7	982	192.75	612	8.738	8.89
Virtex-6	1048	194.78	2026	8.830	8.45
Spartan-6	1162	111.73	823	5.065	4.35
Kintex-7	1185	213.17	629	9.660	8.15

7 Conclusion

This chapter discussed an FPGA implementation of the AES and SHA-3 security algorithms and also discusses the possible use of this proposed implementation for a BITW architecture suitable for use with IPsec. BITW technology is an implementation approach that places a network security mechanism outside of the system that is to be protected. Using BITW technology, security mechanisms can be implemented outboard, in a physically separate device so that the system that receives the protection does not need to be modified at all. Our proposed FPGA architectures for SHA-3 and AES are implemented on different Xilinx FPGA platforms. The proposed architecture can be used with any IoT application to provide up-to-date data integrity check and encryption security services using SHA-3 and AES. Results provided in Tables 2 and 3 can aid in selecting a suitable Xilinx FPGA for IoT applications by keeping in mind the area consumption, throughput and power utilization requirements of the IoT application in question.

Acknowledgments This work was supported by European Union EM STRoNGTieS Program and the Irish Research Council—Grant number IRCGOIPG/2013/1132 in collaboration with the SFI Centre for Marine Renewable Energy Ireland (MaREI) (Grant 12/RC/2302 and 14/SP/2740).

References

1. “RFC-791”, <http://www.ietf.org/rfc/rfc791.txt>
2. “RFC-1349”, <http://www.ietf.org/rfc/rfc1349.txt>
3. “RFC-2474”, <http://www.ietf.org/rfc/rfc2474.txt>
4. M. Healy, T. Newe, E. Lewis, Security for wireless sensor networks: a review. In: *IEEE Sensors Applications Symposium (IEEE SAS 2009)*. New Orleans, LA, USA. 17th–19th Feb 2009, pp. 80–85. ISBN: 978-1-4244-2787-1
5. S. Kent, R. Atkinson, Security architecture for the internet protocol. IETF network working group, RFC2401 (1998)
6. “RFC-4302”, <https://www.ietf.org/rfc/rfc4302.txt>
7. “RFC-4303”, <https://www.ietf.org/rfc/rfc4303.txt>
8. A. Ferrante, V. Piuri, J. Owen, IPsec hardware resource requirements evaluation. Next Generation Internet Networks (NGI 2005), Apr 2005. pp. 240–246. doi:10.1109/NGI.2005.1431672
9. Y. Niu, L. Wu, X. Zhang, An IPsec accelerator design for a 10Gbps in-line security network processor. *J. Comput.* 8(2), 319–325 (2013)
10. B. Driessen, T. Güneysu, E. Bilge Kavun, O. Mischke, C. Paar, T. Pöppelmann, IPSECCO: a lightweight and reconfigurable IPsec core. In: *International Conference on Reconfigurable Computing and FPGAs (ReConFig)* (2012). doi:10.1109/ReConFig.2012.6416757
11. A. Salman, M. Rogawski, J. Kaps, Efficient hardware accelerator for IPsec based on partial reconfiguration on Xilinx FPGAs. In: *International Conference on Reconfigurable Computing and FPGAs* (2011). doi:10.1109/ReConFig.2011.33
12. J. Lu, J. Lockwood, IPsec implementation on Xilinx Virtex-II Pro FPGA and its application. In: *19th IEEE International Parallel and Distributed Processing Symposium (IPDPS’05)* (2005). doi:10.1109/IPDPS.2005.262

13. M. McLoone, J. VMcCanny, A single-chip IPsec cryptographic processor. In: *IEEE Workshop on Signal Processing Systems* (2002). (SIPS'02). doi:[10.1109/SIPS.2002.1049698](https://doi.org/10.1109/SIPS.2002.1049698)
14. W. Vander, K. Benkrid, *High-Performance Computing Using FPGAs* (Springer book). ISBN: 978-1-4614-1790-3
15. NIST, Advanced encryption standard (aes), fips 197, November 2001. (Online). Available: <http://csrc.nist.gov/publications/fips/fips197/fips-197.pdf>
16. M. Rao, T. Newe, I. Grout, AES implementation on Xilinx FPGAs suitable for FPGA based WBSNs. In: *9th International Conference on Sensing Technology (ICST 2015)*. Auckland, NZ, 8–10 Dec 2015
17. M. Rao, T. Newe, I. Grout, Secure hash algorithm-3(SHA-3) implementation on Xilinx FPGAs, Suitable for IoT Applications. In: *8th International Conference on Sensing Technology (ICST 2014)*, Liverpool John Moores University, Liverpool, United Kingdom, 2–4 Sept 2014
18. NIST, SHA-3 standard: permutation-based hash and extendable-output functions,” Aug, 2015 (Online). Available: <http://nvlpubs.nist.gov/nistpubs/FIPS/NIST.FIPS.202.pdf>
19. P. Morawiecki, M. Srebrny, A SAT-based preimage analysis of reduced Keccak hash functions. Elsevier’s Info. Process. Lett. **113**(10–11), 392–397, May–June 2013
20. M. Taha, P. Schaumont, Side-channel analysis of MAC-Keccak. In: *IEEE International Symposium on Hardware-Oriented Security and Trust (HOST)*, June 2013, pp. 125–130
21. XPower Tutorial FPGA Design, (online). Available at: [ftp://xilinx.com/pub/documentation/tutorials/xpowerfpgatutorial.pdf](http://xilinx.com/pub/documentation/tutorials/xpowerfpgatutorial.pdf)
22. The internet of things. Technical report, International Telecommunication Union, 2005. ISBN: 92-61-11291-9
23. Regulation (EC) No 460/2004 of the European Parliament and of the Council of 10 March 2004 establishing the European Network and Information Security Agency
24. “RFC-4303”, <https://tools.ietf.org/html/rfc2409>
25. F. Rodriguez-Henrquez, N. Saqib, A. Daz-Prez, C. Koc, *Cryptographic Algorithms on Reconfigurable Hardware* (Springer), Nov 2006
26. National instruments. Introduction to FPGA technology: top five benefits. <http://zone.ni.com/devzone/cda/tut/p/id/6984>, Dec 2010
27. Xilinx, 7 Series FPGAs memory resources user Guide UG473_7
28. S. Drimer, T. G’uneysu, C. Paar, “DSPs, BRAMs and a pinch of logic: new recipes for the AES on FPGAs, in *IEEE Symposium on Field-Programmable Custom Computing Machines (FCCM)*, Apr 2008
29. National Institute of Standards and Technology (NIST): SHA-3 Winner announcement <http://www.nist.gov/itl/csd/sha-100212.cfm>
30. X. Wang, X.L. Feng, D. Yu, Collisions for hash functions MD4, MD5, HAVAL-128 and RIPEMD. Cryptology ePrint Archive, Report 2004/199, pp. 1–4 (2004), <http://eprint.iacr.org/2004/199>
31. M. Szydlo, SHA-1 collisions can be found in 263 operations. Crypto Bytes Technical Newsletter (2005)
32. M. Stevens, Fast collision attack on MD5. ePrint-2006-104, pp. 1–13, 2006. <http://eprint.iacr.org/2006/104.pdf>
33. G. Bertoni, J. Daemen, M. Peeters, G. Assche, Cryptographic sponge function. <http://sponge.nokeon.org/CSF-0.1.pdf>

Author Index

A

Afsarimanesh, N., [23](#)
Anumukonda, M., [121](#)
Arakawa, T., [45](#)
Arora, L., [1](#)

B

Beeby, S., [159](#)

C

Carvalho, H., [185](#)
Catarino, A., [185](#)
Chowdhury, S. R., [1](#), [121](#)

D

Dooly, G., [259](#)

F

Fujimoto, M., [67](#)

I

Ikezawa, S., [67](#)
Ishimitsu, S., [87](#)

J

Joseph, F., [221](#)

K

Kho, Y. H., [241](#)
Kitamura, C., [67](#)
Kosel, J., [135](#)
Kruger, M., [23](#)

L

Lin, X., [221](#)
Ling, Y., [103](#)

M

Mathur, A., [259](#)

Mitsubayashi, K., [45](#)

Mukhopadhyay, S. C., [23](#), [135](#)

N

Nag, A., [135](#)
Nakayama, M., [87](#)
Newe, T., [259](#)

O

Ojuroye, O., [159](#)
Omerdic, E., [259](#)

P

Postolache, Gabriela, [185](#)
Postolache, O., [185](#)

R

Ramasahayam, S., [1](#)
Rao, M., [259](#)

S

Seet, B. C., [221](#)
Shigekawa, N., [87](#)

T

Toal, D., [259](#)
Torah, R., [159](#)

U

Ueda, T., [67](#)

W

Wilde, A., [159](#)
Wong, L. J., [103](#)

Y

Yokouchi, T., [87](#)
Yoshii, S., [67](#)
Yu, P., [23](#)